AD-A126 948 LABORATORY DETERMINATION OF HORIZONTAL STRESS IN COHESIONLESS SOIL(U) AIR FORCE INST OF TECH WRIGHT-PATTERSON AFB OH S C BOYCE 1983 1/4

UNCLASSIFIED AFIT/CI/NR-83-4T F/G 8/13 NL

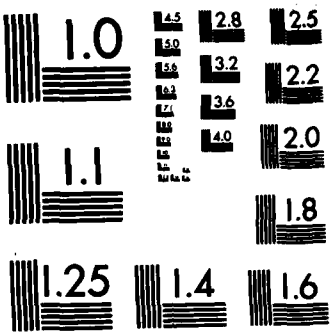

MICROCOPY RESOLUTION TEST CHART
NATIONAL BUREAU OF STANDARDS-1963-A

UNCLASS

SECURITY CLASSIFICATION OF THIS PAGE (When Data Entered)

AD A126948

REPORT DOCUMENTATION PAGE

READ INSTRUCTIONS BEFORE COMPLETING FORM

1. REPORT NUMBER
AFIT/CI/NR 83-4T

2. GOVT ACCESSION NO.

3. RECIPIENT'S CATALOG NUMBER

4. TITLE (and Subtitle)
Laboratory Determination of Horizontal Stress in Cohesionless Soil

5. TYPE OF REPORT & PERIOD COVERED
THESIS/DISSERTATION

6. PERFORMING ORG. REPORT NUMBER

7. AUTHOR(s)
Steven Craig Boyce

8. CONTRACT OR GRANT NUMBER(s)

9. PERFORMING ORGANIZATION NAME AND ADDRESS
AFIT STUDENT AT: Cornell University

10. PROGRAM ELEMENT, PROJECT, TASK AREA & WORK UNIT NUMBERS

11. CONTROLLING OFFICE NAME AND ADDRESS
AFIT/NR
WPAFB OH 45433

12. REPORT DATE
1983

13. NUMBER OF PAGES
310

14. MONITORING AGENCY NAME & ADDRESS(if different from Controlling Office)

15. SECURITY CLASS. (of this report)
UNCLASS

15a. DECLASSIFICATION/DOWNGRADING SCHEDULE

16. DISTRIBUTION STATEMENT (of this Report)
APPROVED FOR PUBLIC RELEASE; DISTRIBUTION UNLIMITED

17. DISTRIBUTION STATEMENT (of the abstract entered in Block 20, if different from Report)

18. SUPPLEMENTARY NOTES
APPROVED FOR PUBLIC RELEASE: IAW AFR 190-17

24 March 83

Lynn Wolaver
LYNN E. WOLAVER
Dean for Research and
Professional Development
AFIT, Wright-Patterson AFB OH

19. KEY WORDS (Continue on reverse side if necessary and identify by block number)

20. ABSTRACT (Continue on reverse side if necessary and identify by block number)
ATTACHED

DTIC

FILE COPY

DD FORM 1 JAN 73 1473 EDITION OF 1 NOV 65 IS OBSOLETE

UNCLASS

SECURITY CLASSIFICATION OF THIS PAGE (When Data Entered)

83 04 19 004

S-3-4

LABORATORY DETERMINATION OF HORIZONTAL STRESS IN COHESIONLESS SOIL

Steven Craig Boyce, Captain, USAF
Ph.D., Cornell University
1983, 310 pages

Three general approaches were used to investigate the problem of horizontal stress measurement in cohesionless soil: theoretical solutions, finite element modeling and laboratory testing. The best theoretical solution to represent a soil stress cell measuring lateral stress is that for a rigid ellipsoidal inclusion in an infinite, elastic, homogeneous, isotropic material. Finite element modeling of the Cornell Stress Cell using three-dimensional elements allowed the soil to be represented as a cross-anisotropic material which was not possible with the theoretical solution. Laboratory testing included air and soil calibrations of the stress cell, determination of the coefficient of horizontal soil stress at rest and constant volume direct shear tests.

The results of this study show that lateral stress measurements can be performed successfully with soil stress cells but the behavior of the cells is different from that of a cell oriented to measure vertical stress.

The use of soil stress cells to measure successfully the increases in lateral stress from dilation of dense sand during shear was demonstrated. This allowed the interpretation of the stress cell response during pullout tests of drilled shafts in dense sand conducted at Cornell. The pullout resistance of shafts in dense sand, prepared by vibration, was determined to be a function of the initial void ratio of the soil. The implication is that high horizontal stresses are not present in dense sands that have been prepared by vibration.

Accession For
NTIS GRA&I ☒
DTIC TAB ☐
Unannounced ☐
Justification
By
Dist
Dist
A

LABORATORY DETERMINATION OF HORIZONTAL STRESS IN COHESIONLESS SOIL

A Thesis

Presented to the Faculty of the Graduate School

of Cornell University

in Partial Fulfillment for the Degree of

Doctor of Philosophy

by

Steven Craig Boyce

January 1983

ACKNOWLEDGEMENTS

I would like to acknowledge those who have made a significant contribution toward my education and therefore have become contributors to this thesis. They include:

Colonel David Currin who first whetted my desire for studying soil mechanics.

Professor Charles C. Ladd of Massachusetts Institute of Technology who patiently helped me through my master's thesis and taught me much of my knowledge of soil mechanics.

Professor Fred H. Kulhawy who proposed this research topic, aided in its completion and served as a role model by his excellence in teaching.

Professors Thomas D. O'Rourke, Ta Liang and H. D. Conway who served on my committee and as role models by their excellence in teaching.

Fellow graduate students Charles Trautmann, Steve Pulley, Jay Beech, Priscilla Nelson, Jue-Yue Liu, Yih-Ping Huang, Edward Clukey, Craig Harris and William Burgess who offered their advice when asked and allowed me to express my thoughts and frustrations with remarkable patience.

The United States Air Force which has provided all the financial support for my graduate studies and the Air Force Academy for their sponsorship of my studies.

Finally, the most important contributor toward my success in graduate school, my wife, Pattie, who has allowed

me the time for studies which she and my daughters justly deserved.

To these and many others I owe a debt of gratitude.

TABLE OF CONTENTS

TITLE PAGE	i
BIOGRAPHICAL SKETCH	ii
ACKNOWLEDGEMENTS	iii
TABLE OF CONTENTS	v
LIST OF TABLES	viii
LIST OF FIGURES	ix
LIST OF SYMBOLS	xii
CHAPTER 1 INTRODUCTION	1
CHAPTER 2 REVIEW OF HORIZONTAL STRESS MEASUREMENTS WITH STRESS CELLS	6
2.1 BOUNDARY STRESS	7
2.2 FREE FIELD STRESS	11
2.3 CONCLUSIONS	17
CHAPTER 3 STRESS CELL THEORY	19
3.1 THEORETICAL METHODS	20
3.2 RIGID ELLIPSOIDAL INCLUSION	24
3.3 CONCLUSIONS	30
CHAPTER 4 FINITE ELEMENT MODELING OF STRESS CELLS	32
4.1 PREVIOUS MATHEMATICAL MODELS FOR STRESS CELLS	33
4.2 SOIL AS A CROSS-ANISOTROPIC MATERIAL	37
4.3 FINITE ELEMENT MODELING	41
4.4 FINITE ELEMENT RESULTS	49
4.4.1 Rigid Ellipsoid	50
4.4.2 Rigid Disc	53

4.4.3 Axisymmetrical Cornell Stress Cell 56

4.4.4 Three-Dimensional Cornell Stress Cell 69

4.5 CONCLUSIONS 79

CHAPTER 5 TESTING EQUIPMENT AND PROCEDURES 81

5.1 CORNELL STRESS CELL 82

5.2 AIR CALIBRATION 85

5.3 SOIL CALIBRATION 88

5.4 DATA ACQUISITION SYSTEM 96

5.5 DIRECT SHEAR AT CONSTANT VOLUME 97

5.6 CONCLUSIONS 99

CHAPTER 6 TIME EFFECTS OF THE CORNELL STRESS CELL 101

6.1 QUANTIFYING THE TIME EFFECT 104

6.2 POSSIBLE CAUSES OF TIME EFFECTS IN CSC 106

6.3 CAUSE OF TIME EFFECT IN CSC 115

6.4 SOLUTION TO ELIMINATE TIME EFFECTS 117

CHAPTER 7 LABORATORY TEST RESULTS 119

7.1 AIR CALIBRATION OF CORNELL STRESS CELLS. 120

7.2 K_o CONDITIONS IN FILTER SAND 124

7.3 SOIL CALIBRATION OF CORNELL STRESS CELLS 131

7.4 DIRECT SHEAR AT CONSTANT VOLUME 140

CHAPTER 8 GUIDELINES FOR MEASURING LATERAL STRESS WITH STRESS CELLS 149

CHAPTER 9 SUMMARY AND CONCLUSIONS 155

REFERENCES 158

APPENDIX A PHYSICAL PROPERTIES OF FILTER SAND 169

APPENDIX B SOIL CALIBRATION OF CORNELL STRESS CELLS 186

APPENDIX C K_o TESTING OF FILTER SAND 245

APPENDIX D CONSTANT VOLUME DIRECT SHEAR TESTS 267

APPENDIX E INTERPRETATION OF PULLOUT TESTS 284

APPENDIX F MEASUREMENT OF THE VARIATION IN UNIT WEIGHT BY FREEZING 306

LIST OF TABLES

Table Number	Title	Page Number
7.1	Calibration Constants for Cornell Stress Cells.	123
7.2	Results of K_o Soil Calibration Tests.	133
7.3	Results of Isotropic Soil Calibration Tests.	137
7.4	Results of Triaxial Soil Calibration Tests.	139
A.1	Petrographic Analysis of Filter Sand (Nelson, 1980).	173
A.2	Summary of Direct Shear Tests on Filter Sand.	176
B.1	Summary of K_o Soil Calibration Tests.	188
B.2	Summary of Isotropic Soil Calibration Tests.	191
B.3	Summary of Triaxial Soil Calibration Tests.	193
C.1	Summary of K_o Tests on Filter Sand.	247
D.1	Summary of Constant Volume Direct Shear Tests on Filter Sand.	268
E.1	Description of Shaft Pullout Tests.	285
F.1	Unit Weight of Filter Sand Determined from Frozen Samples.	309

LIST OF FIGURES

Figure Number	Title	Page Number
3.1	Normalized Vertical Stress on a Rigid Oblate Spheroid under K_o Conditions.	26
3.2	Normalized Lateral Stress on a Rigid Oblate Spheroid under K_o Conditions.	29
4.1	Finite Element Mesh for Rigid Ellipsoid.	43
4.2	2-D Finite Element Mesh for Cornell Stress Cell.	44
4.3	Finite Element Mesh for 3-D Cornell Stress Cell.	46
4.4	Vertical Stress Profile Across a Rigid Ellipsoid.	52
4.5	Vertical Stress Profile Across a Rigid Disc under Hydrostatic Stress.	54
4.6	Vertical Stress Profile Across a Rigid Disc under K_o Conditions.	55
4.7	Vertical Stress Profile Across the Cornell Stress Cell.	57
4.8	Effect of Soil Modulus on Measured Vertical Stress.	59
4.9	Effect of Cross-Anisotropy Ratio on Measured Vertical Stress.	61
4.10	Effect of Vertical Poisson's Ratio on Measured Vertical Stress.	63
4.11	Effect of Horizontal Poisson's Ratio on the Measured Vertical Stress.	65
4.12	Effect of Lateral Stress Ratio on the Measured Vertical Stress.	66
4.13	Comparison of Base Registration and Lateral Stress Rotation.	68
4.14	Comparison of 2-D and 3-D Finite Element Models.	70

Figure Number	Title	Page Number
4.15	Effect of Poisson's Ratio on Measured Lateral Stress.	72
4.16	Effect of Cross-Anisotropy Ratio on Measured Lateral Stress.	73
4.17	Effect of Vertical Poisson's Ratio on Measured Lateral Stress.	75
4.18	Effect of Horizontal Poisson's Ratio on Measured Lateral Stress.	76
4.19	Effect of Lateral Stress Ratio on the Measured Lateral Stress.	78
5.1	Cornell Stress Cell (Weiler and Kulhawy, 1978).	84
5.2	Air Calibration Chamber for Soil Stress Cells (Weiler and Kulhawy, 1978).	86
5.3	Soil Calibration Chamber for Stress Cells (Weiler and Kulhawy, 1978).	90
6.1	Time Effect of Cornell Stress Cell during Air Calibration Test.	102
6.2	Time Effect on Cornell Stress Cell with each Pressure Increment held Constant for Ten Minutes.	103
6.3	Stress Cell Variation with Time, Normalized by the Load Increment.	105
6.4	Percent Error per log Time for Time Effect of the Cornell Stress Cell.	107
6.5	Temperature Effects on the Cornell Stress Cell.	110
6.6	Comparison of Gage Creep and the Time Effect of Cornell Stress Cell.	113
6.7	Air Calibration for Cornell Stress Cell with Waterproofing Removed.	116
7.1	Air Calibration of Cornell Stress Cell #1.	122

Figure Number	Title	Page Number
7.2	K_o Values for Filter Sand.	126
7.3	Alpha Values for Filter Sand.	130
7.4	Critical Normal Stress for Constant Volume Direct Shear Test.	143
A.1	Grain Size Distribution of Filter Sand.	170
A.2	Grain Size Distribution Showing Lack of Degradation from Handling.	171
A.3	Standard Proctor Compaction Curve for Filter Sand.	174
A.4	Friction Angle Variation with Unit Weight.	175
A.5-A.13	Direct Shear Test on Filter Sand.	177-185
B.1-B.21	K_o Soil Calibration.	194-214
B.22-B.33	Isotropic Soil Calibration.	215-226
B.34-B.51	Triaxial Stress Path and Triaxial Soil Calibration.	227-244
C.1-C.17	K_o Testing of Filter Sand.	249-266
D.1-D.15	Constant Volume Direct Shear Test.	269-283
E.1-E.20	Stress Cell Response During Pullout Test.	286-305

LIST OF SYMBOLS

ENGLISH LETTERS

C	- Calibration constant for air calibration of stress cells.
	- Celsius temperature.
CSC	- Cornell Stress Cell.
D	- Diameter of stress cell = 2r.
E	- Elastic modulus.
F	- Fahrenheit temperature.
G	- Shear modulus.
	- Giga = 10^9.
GF	- Gage Factor for strain gage.
H	- Thickness of stress cell.
	- Horizontal.
K	- Lateral stress ratio, horizontal/vertical stress.
M	- Mega = 10^6.
N	- Newtons.
OCR	- OverConsolidation Ratio, maximum past pressure/ existing vertical stress.
Q4	- Four noded quadrilateral isoparametric elements.
Q8	- Eight noded quadrilateral isoparametric elements.
R	- Registration ratio.
	- Base registration.
V	- Vertical.
	- Volt.
d	- diameter of diaphragm.

g	- grams.
k	- kilo = 10^3.
m	- meter.
	- milli = 10^{-3}.
n	- Cross-anisotropy ratio = E_H/E_v.
p	- pressure.
pcf	- pounds per cubic foot.
ppm	- parts per million = 10^{-6}.
psi	- pounds per square inch.
r	- radius or radial direction.
t	- thickness of stress cell diaphragm.
x	- Horizontal direction.
y	- Vertical direction.
z	- Horizontal direction.

GREEK LETTERS

α	- Aspect ratio, thickness/diameter.
	- Slope of log K_o versus log OCR plot.
γ	- Shear strain.
δ	- Deflection.
ε	- Strain.
μ	- Lateral stress rotation.
	- Micro = 10^{-6}.
ν	- Poisson's ratio.
σ	- Normal stress.
	- Standard deviation.

τ - Shear stress.

ϕ - Angle of internal friction.

CHAPTER 1

INTRODUCTION

The purpose of this study is to determine a satisfactory method for the measurement and interpretation of lateral stresses in cohesionless soil in the laboratory environment. The instrument used throughout is a soil stress cell of the deflecting diaphragm type designed and constructed at Cornell University and known as the Cornell Stress Cell.

Soil stress cells serve several functions including: validation of theory, monitoring performance and warning of change in behavior of a structure. Stress cells have been used since the turn of the century to measure stresses against structures, abutments and tunnel linings; beneath foundations and pavements; in earth dams and embankments and to measure the dynamic stresses from traffic, compaction equipment and explosions. The performance of the stress cells in soil has been the subject of research and the topic of discussion for decades as is evident from the volume and variety of reports on the subject in the literature. Their use has met with mixed success and they have remained poorly understood among the practicing profession.

The performance of stress cells in soil is a function of the type of soil in which they are placed. Cells in cohesive material generally have much better performance

than the cells in granular material as noted from the following quotations from the literature on soil stress cells:

> "...the question has been raised as to the accuracy of this method (Goldbeck cells) of measuring pressures, particularly in granular and highly compacted materials." (Seaquist, 1934)

> "It was determined that the performance in the clay soil was very similar to that in air, but that in sand the cell behavior was erratic." (McMahon and Yoder, 1960)

> "The measurement of pressures in clay fills is likely to present far less difficulty than similar measurements in sands and gravels." (Trollope and Lee, 1961)

The orientation of stress cells in the soil also has an effect on their performance. Cells have usually been oriented to measure vertical stress in free field conditions or lateral stresses on retaining structures. When cells have been used to measure lateral stress in free field conditions they have met with mixed success.

> "...in some field installations of stress meters, faulty results had been obtained. In general, the trouble was mostly with meters oriented to measure stress in a direction other than the major pricipal one." (Carlson, 1978)

> "Both theory and experience have shown that the ratio between diameter and thickness must be greater than about five if the cell is installed for the purpose of measuring vertical pressure on a horizontal plane within a fill such as a dam. The same cell would lead to erroneous results if used to measure the horizontal pressure against a vertical plane, because the long vertical dimension of the cell would resist the vertical strain in the adjacent soil and radically change the state of stress." (Terzaghi and Peck, 1967)

Because of the difficulty experienced in the use of stress cells in granular material and the measurement of lateral stresses in particular, it was decided that this represented a suitable research topic. Specifically, the problem of lateral stress measurements in dense granular soil had been encountered by Stewart and Kulhawy (1981) during tests on the pullout resistance of concrete shafts in sand. In these tests, the lateral stress determined from the failure load on the shaft was an order of magnitude higher than the in situ stresses measured with the stress cells. Stewart and Kulhawy suggested possible causes of this error including stress induced anisotropy and the problem of vibratory compaction.

This study then started as an investigation into the problems of Cornell Stress Cells in measuring satisfactorily the lateral stress in dense sand. Three general approaches were taken in an effort to solve the problem: theoretical studies of stress cells, computer modeling of stress cells and laboratory testing and calibration.

Theoretical methods for representing stress cells in soil were evaluated to determine the effect of the soil parameters on the stress cell response. The best model found was that of a rigid ellipsoid embedded in an elastic, homogeneous and isotropic infinite solid by Askegaard (1963). His theoretical solution could be rotated to represent a cell measuring lateral stresses with good

results. The limiting factor in the solution was the use of isotropic soil conditions since the anisotropic properties of the soil were suspected of at least partially creating the problem encountered by Stewart and Kulhawy. The theoretical modeling of stress cell performance is discussed in Chapter 3.

Computer modeling of the stress cell was performed by using a three-dimensional finite element model which includes the anisotropic soil properties. A three-dimensional model was necessary to represent a cylindrical stress cell in a vertical plane. All previous finite element simulations were axisymmetical to model a stress cell in a horizontal plane. The finite element modeling is covered in Chapter 4.

Laboratory testing included the air and soil calibration of the stress cells under a variety of soil and stress conditions. During the air calibration phase, a time effect on the stress cell was discovered and had to be eliminated before proceeding. The time effect and its elimination is discussed in Chapter 6. Other laboratory tests included the determination of the lateral stress ratio for conditions of zero lateral strain in filter sand and constant volume direct shear tests. The procedures and equipment are described in Chapter 5, the test results included in the appendix and the test results summarized in Chapter 7.

Before beginning the investigation it was necessary to

do a literature search for the use of stress cells to measure lateral stress. Chapter 2 briefly summarizes previous attempts to use stress cells for this purpose. Several good summary papers on the general topic of stress cells are available, and they are referenced in this work to provide the requisite background for a treatment of lateral stress measurement.

CHAPTER 2

REVIEW OF HORIZONTAL STRESS MEASUREMENTS WITH STRESS CELLS

Among the very first applications of soil stress cells were measurements of horizontal stress. Perhaps the major driving force behind the development of soil stress cells was to determine the horizontal stresses and their distribution behind retaining structures. As a result of this emphasis, most applications for soil stress cells measuring lateral stresses are for boundary cells and only a fraction of the applications are for free field stresses. Nearly all the theoretical solutions applied to soil stress cells are based on models in which the cell is oriented to measure vertical stress as discussed in Chapter 3. Soil calibration of stress cells in the laboratory has usually been done for cells oriented only to measure vertical stress and the results were assumed to apply to cells measuring horizontal stress as well.

For all of the above reasons, it was necessary to review the literature on soil stress cells and determine what work had actually been done for stress cells measuring horizontal stress in free field stress conditions. This chapter is a summary of the literature found on the measurement of horizontal soil stresses with stress cells.

2.1 BOUNDARY STRESS

The earliest uses of soil stress cells to measure horizontal stresses were to determine the magnitude and distribution of lateral stress on retaining structures. These boundary cells were installed on or flush with the structure in an effort to determine the lateral stress. Mann (1913) used a hydraulic boundary cell read by the change in level in a capillary tube to measure the lateral stress on sand in a K_o condition. His small scale tests met with limited success because of the effects of friction on the sides of the soil retaining box. Hummel and Finnan (1921) used a carbon pile cell to measure lateral boundary stresses against a small wooden structure with variations in the slope of the sand backfill. The measured stresses followed the same trend as the theoretical solutions but were not precise enough to draw any conclusions.

McNary (1925) reports on the field use of Goldbeck pneumatic earth pressure cells to measure the stress distribution behind two bridge abutments. The 16th Street Bridge abutment in Washington, D.C. was backfilled with compacted clay-sand-gravel and the Bennings Bridge abutment, also in Washington, D.C., was backfilled with coarse random fill. The results of both tests were quite good and demonstrated the value of good field measurements. Goldbeck (1938) reported the results of the same two bridge abutments as McNary (1925), as well as the results of Goldbeck cells

installed on the abutment of the Skellet Fork Bridge in Illinois. In this application the total earth pressures were found to vary significantly with the variation in the water level and the location of weep holes in the abutment wall.

Sowers, et al. (1957) used deflecting diaphragm stress cells on a rigid concrete retaining wall to measure the residual lateral stress after compaction of both sand and clay backfill. The lateral stresses in the sand increased with compaction effort but were independent of water content and time after compaction. In the clay backfill the lateral stresses increased with compaction effort but decreased with increasing moisture and decreased with time after compaction.

Rowe and Peaker (1965) used a sophisticated movable retaining wall instrumented with eighteen hydraulic soil stress cells to determine the passive stress in both loose and dense sand. By integrating the stress cell results over the area of the wall, the resulting force was found to be within five percent of the applied horizontal load for excellent results. Kruse (1965) reports on the use of Carlson soil stress cells installed on the concrete core block of Oroville Dam to evaluate the performance of a clay zone used to distribute stresses. The trends of the results were correct but the magnitudes were quite erratic.

Scott and Kilgor (1967) installed ten Maihak vibrating wire stress cells on the concrete spillway of Wildwood Dam,

Ontario, Canada to monitor the change in soil stress with consolidation of the clay core. The results were quite erratic and affected by the location of the stress cells between counterforts of the spillway.

Jones (1973) used British Research Station stress cells to measure the lateral stress on cantilever retaining walls and bridge abutments. The measured stresses were higher than that predicted from earth pressure theory but matched very well with the results from finite element analyses.

Carder, Pocock and Murray (1977) used three different types of soil stress cells on a two meter square movable retaining wall to measure the lateral stress in sand. The instruments included hydraulic, pneumatic and strain gaged deflecting diaphragm cells. Stresses were measured after compaction and for both active and passive conditions in the soil with good results.

In addition to the relatively rigid structures just mentioned, boundary cells have been installed on more flexible sheet piles to measure the lateral stress as well. Øien (1958), Johannessen (1958), Kjaernsli (1958) and Bauer (1974) all report on the success of using a vibrating wire soil stress cell installed on a sheet pile prior to driving to measure the lateral stress in soft silty clay. The sheet piles were used for excavation support for the Oslo subway construction and the measurements of the lateral stresses contributed immensely to the understanding of stresses on

flexible retaining structures. Shelson (1958) reports on the use of soil stress cells on sheet piles used for a cofferdam. The cells were placed to determine the lateral stress from the soil used to fill the cellular cofferdam for the Saint Lawrence Power Project.

Rowe and Biggs (1961) determined the stress distribution on a braced sheet pile wall using soil stress cells. The integration of the stress cell results were within five percent of the applied load on the wall. Mead (1963) installed ten Goldbeck cells on sheet piles used as a tieback wall to determine the lateral stress distribution. His results for stress in the general fill were inconsistent and of little value. Scott, Wilson and Bauer (1972) had excellent results from the thirteen Geonor vibrating wire stress cells placed on sheet piles in fine dense sand despite the large deformations of the sheet piles.

Rigid retaining structures and flexible sheet piles have not been the only applications for boundary soil stress cells measuring lateral stress. Agarwal and Venkatesan (1965) placed stress cells in precast concrete piles to measure the lateral stresses on the pile. Although there were mechanical and electrical problems with their instruments, the results paralleled the expected stresses very well. Kenney (1967) used vibrating wire stress cells installed on a hollow steel pipe to measure the in situ lateral stress in quick clays with good results. This was

the first of what later developed into self-boring pressuremeters. Uff (1969) installed soil stress cells through slurry during construction of a concrete diaphragm wall. The results were erratic but the average values for all cells were very good.

Kasch, et al. (1977) used soil stress cells to measure the lateral stress on a drilled shaft. There was considerable difficulty in keeping the cells in contact with the soil throughout the test.

2.2 FREE FIELD STRESS

All of the works cited so far have been for the determination of lateral stress on a boundary. The determination of free field stresses by the use of soil stress cells is a more difficult problem. The following references are those in which the lateral stresses for a free field stress condition were measured. The disturbance of the free field stress by a soil stress cell is inevitable unless the stress-strain properties of the cell exactly match the stress-strain properties of the soil, which is highly unlikely.

Foster and Fergus (1951) reported on extensive tests performed by the Waterways Experiment Station on clayey silt. Stress cells at various orientations were used to evaluate the distribution of stress in the soil caused by surface loads. The measured stresses compared very well

with theoretical stresses for an elastic material with a Poisson's ratio of 0.5. Turnbull, Maxwell and Ahlvin (1961) summarize the results of Foster and Fergus (1951) as well as report on the results of additional tests performed on a sandy soil. The measured stresses in the sand compared well with the theoretical stress in an elastic material with a Poisson's ratio of 0.3.

McMahon and Yoder (1960) calibrated strain gaged deflecting diaphragm stress cells in clay and sand with excellent results for the cells in clay but with erratic results for the same cells in sand, independent of their orientation.

Buck (1961) used Redshaw stress cells oriented both vertically and horizontally in a nine inch (229 mm) diameter triaxial sample of sand. He found that the registration of the cells depended on their orientation with a vertical registration value of 1.08 and a lateral registration value of 0.91. Buck concluded that the difference in the registration values was caused by the cross-sensitivity of the cells.

Mackey (1966) used a unique cubic stress cell to measure both vertical and lateral soil stresses in dense sand. His cell was useful for measuring stresses only up to a maximum value of 1.0 psi (6.89 kN/m^2).

Reports by Kennard, Penman and Vaughan (1967) and by Thomas and Ward (1969) both describe the application of

vibrating wire soil stress cells in Balderhead Dam. This was the first use of stress cells in a dam in Britain and gave excellent results for the vertical and lateral stresses in the clay core of the dam.

Abbott, et al. (1967) calibrated rigid spool stress cells in Ottawa sand under K_o conditions with applied vertical stresses up to 800 psi (5.52 MN/m^2). The measured horizontal stress was compared to the theoretical K_o stress determined for Ottawa sand by Hendron (1963). The trend of the data was correct but with large differences in the magnitude. The differences were thought to be caused by placement difficulties for any orientation of the stress cell other than vertical.

Krivoritov (1969) measured lateral stress in a soil calibration chamber of sand subjected to surface plate loads. The measured lateral stresses were erratic, especially as the plate load approaches the bearing capacity of the soil.

Penman and Mitchell (1970) obtained good results from the vibrating wire stress cells installed to measure the lateral stresses in the clay core of Scammonden Dam.

Krizek, et al. (1974) reported detailed soil calibration, finite element modeling and field testing performance for stress cells. Unfortunately their work on lateral stress measurements was limited to a single cell in the soil calibration chamber which gave a coefficient of lateral

earth pressure consistent with the theoretical value.

Massarsch, et al. (1975) inserted a Gloetzl earth pressure cell into soft clay to measure the in place lateral stress. Although it took several days for the excess pore pressures generated by the disturbance to dissipate before accurate measurements could be made, the results were better for the stress cell than from those determined by hydraulic fracturing techniques.

Tavenas, et al. (1975) did a comparative study between the measured lateral stresses obtained from hydraulic fracturing, pressuremeters and stress cells. They recommended the use of stress cells in the soft sensitive clay used in the study to obtain the best results. The pressuremeter used was not the self-boring type which had an adverse impact on the results for that instrument and the results could have been improved by using the self-boring type of pressuremeter.

Weiler and Kulhawy (1978) calibrated a single Cornell Stress Cell measuring lateral stress in loose filter sand for a triaxial extension test. The response of the cell was consistent with the response for the same cell oriented vertically and no distinction between vertical and horizontal cell performance was noted.

Stewart and Kulhawy (1981) made extensive use of the Cornell Stress Cells to measure lateral stresses in large scale pullout tests of drilled shafts in filter sand.

The results for the soil stress cells measuring vertical stresses and for the stress cells measuring lateral stresses in loose and medium dense sand were consistent with measured loads on the shaft. The stress cells measuring lateral stresses in dense sand were as much as an order of magnitude lower than the stress determined from the pullout resistance of the shafts. This apparently poor performance for the Cornell Stress Cells in dense filter sand was the single most important factor in pursuing research on the determination of lateral stress by soil stress cells.

Stress cells have also been used in materials other than soil, such as concrete. Loh (1954) installed stress cells in concrete cylinders and found the cells oriented to measure lateral stresses were responding to uniaxial stress because of the cross-sensitivity of the cells. Carlson (1978) reports on stress cells installed in large, 30 inch (762 mm) diameter, cylindrical samples loaded in uniaxial (K = 0), triaxial (K = 0.22) and hydrostatic (K = 1.0) stress conditions. The cells measuring lateral stresses gave results with less than ten percent error for all stress conditions.

The determination of free field stresses subjected to dynamic loads have also been studied. Durelli and Riley (1961) embedded stress cells in urethane rubber cylinders and in cylinders of clay subjected to dynamic stresses using a ballistic pendulum. The cylinders were loaded in uniaxial

compression but with the stress cells at varying orientations. The measured stresses were consistent for all orientations of the cells.

Bernhard (1961) applied dynamic loads through a plate on sand and measured the stress in the sand. The stresses applied were only up to a magnitude of 0.5 psi (3.45 kN/m^2). His results matched the expected values very well.

Ingram (1965) did static and dynamic soil calibration tests in a K_o soil chamber with applied vertical stresses of 500 psi (3.45 MN/m^2). The measured horizontal stress in the dry sand decreased with depth of burial because of excessive sidewall friction in the chamber.

Sparrow and Tory (1966) varied the pulse times for loads on a typical road subgrade of silty clay known as Kueper Marl. Both vertical and horizontal stresses were measured but because of the high cross-sensitivity of their soil stress cells, the horizontal stress measurements were invalid. Brown and Pell (1967) continued these experiments by applying the pulse load to a layered soil system. The stresses agreed with theoretical predictions remarkably well but the horizontal stresses agreed less well than the other stresses. The cross-sensitivity was all but eliminated by rearranging the strain gages on the deflecting diaphragm.

D'Appolonia, Whitman and D'Appolonia (1969) used deflecting diaphragm stress cells to measure the stresses in sand caused by vibratory rollers. These full scale tests

measured the vertical and lateral stresses for variations in the frequency and number of passes of the rollers. The lateral stress ratio, K, was found to increase with frequency and number of passes to a maximum value of 2.0. The cells performed satisfactorily for orientations both vertically and horizontally.

2.3 CONCLUSIONS

A review of the stress cell literature has shown several trends for cells oriented to measure lateral stresses. Those stress cells installed to measure the lateral stress on a boundary such as retaining walls, bridge abutments and sheet piles have generally performed well. The best results were obtained when several measurements at the same stress level are averaged together rather than relying on the output of a single instrument. The successful performance of the boundary cells is independent of the soil type and installations in both sand and clay have performed well.

For stress cells used to determine the free field stresses, the vertical stress measurements are consistently better than the lateral stress measurements. For cells installed in soft clay soils the measurement of lateral stress is very good and agrees well with the theoretical values. For applications in laboratory soil calibration tests and field applications in the clay cores of earth dams

and in clay subgrades for pavements, the stress cells measuring lateral stresses have generally been excellent. Soil stress cells used to measure lateral stresses in sand have met with mixed success. The measured stresses as compared to expected values have varied from good (Turnbull, Maxwell and Ahlvin, 1961) to poor (McMahon and Yoder, 1960 and Stewart and Kulhawy, 1981).

The literature review for stress cell performance has demonstrated the necessity of laboratory calibration of the stress cells in the same material and under the same expected stress and boundary conditions as the field application. Without this calibration before field use, the stress cell output can only lead to confusion or misleading conclusions.

This chapter concentrates on the use of stress cells to measure lateral stress. Most laboratory calibration tests on stress cells and all the stress cell theories have been for cells oriented to measure vertical stress. Additional information on the performance and theory of stress cells can be obtained from the excellent review articles by Weiler and Kulhawy (1978, 1982), Brown (1977) and Hvorslev (1976).

CHAPTER 3

STRESS CELL THEORY

One possible method to determine the response of soil stress cells is to develop a theoretical solution. The value of the theoretical solution comes from a general closed-form solution to the problem in which the influence of each parameter is explicitly stated. The theoretical solution, if it can be obtained, would be the answer to the problem and only some laboratory verification of the solution would be required. The real difficulty is obtaining a theoretical solution in which the problem has not been oversimplified so that an adequate representation of the problem is obtained.

A stress cell in soil offers some real challenges for obtaining a theoretical solution. The soil is generally inelastic and anisotropic with a complex stress-strain-time-environment relationship. The Cornell Stress Cell is a nonhomogeneous disc consisting of titanium, silicone and stainless steel with a deflecting diaphragm. Obtaining a theoretical solution to such a complex problem is highly unlikely but, if some simplifying assumptions can reduce the problem to a manageable form, then a theoretical solution might be useful. Even with the simplifying assumptions, a closed-form solution could give indications of trends and relative influence of the parameters on the response of the

soil stress cell.

The first section of this chapter will briefly describe previous attempts to obtain theoretical solutions for the problem of stress cells in soil. This subject has been covered in depth by other reporters and extensive use of references will be done to avoid repeating their work. Those readers not familiar with the methods described should refer to the publications cited for additional information.

The second section of this chapter will describe in detail the derivation of a theoretical solution for the stress on the face of a rigid ellipsoid used to model a soil stress cell. The ellipsoid can be oriented to represent a stress cell measuring lateral stress as well as vertical stress. This was the best closed-form solution that could be found for representing soil stress cells and the results obtained from it are compared to the finite element modeling results in Chapter 4 and the laboratory test results in Chapter 7.

3.1 THEORETICAL METHODS

Through the years, many researchers have tried to apply theoretical solutions to the problem of soil stress cells. This section will only provide an overview to the methods and provide references for further information. There are several excellent articles which summarize the use of soil stress cells and their theoretical development. These

articles include work by Weiler and Kulhawy (1978, 1982), Brown (1977) and Hvorslev (1976), and are recommended for obtaining a background in soil stress cells. The detailed information on stress cell theory included in these four articles will not be repeated here and the interested reader is referred to them for details. The basic approaches for modeling stress cells are: rigid boundary cells, indentation theory, finite element modeling and rigid inclusions in an elastic medium.

Several theoretical solutions exist for modeling a stress cell placed on a rigid boundary. Terzaghi (1936, 1943) used a trap door analogy to obtain the stress on a portion of a rigid boundary as it moved away from or toward the soil. These results were used to determine the active and passive resistance, respectively, with the soil arching across the movable portion or the rigid boundary. McNulty (1965) did some trap door testing and verified Terzaghi's work. Kallstenius and Bergau (1956) analyzed the effect of deflection shape for a circular stress cell on a rigid boundary and compared a rigid piston cell to a deflecting diaphragm cell. This method for modeling stress cell performance does not include lateral stress effects between cell and soil.

Indentation theory has been used by several researchers in modeling soil stress cells. The most frequently referenced work for indentation theory in stress cell literature

was that done by Taylor (1945, 1947) for the United States Army Engineer Waterways Experiment Station. Others who have applied indentation theory include: Hast (1943), Coutinho (1949) and Peattie and Sparrow (1954). The indentation theory assumes a thin cylindrical stress cell with uniform axial compressibility on a homogeneous, elastic, halfspace. Boussinesq's (1885) solution for a surface load is applied to obtain the stress cell response, neglecting the radial compressibility of the disc, shear stresses, lateral stress rotation and cross-sensitivity. The major conclusions from this theory are: the cell response is proportional to the aspect ratio of the cell and inversely proportional to Poisson's ratio of the soil and the effect of soil/cell stiffness becomes nearly constant when the stiffness of the cell is greater than ten times the stiffness of the soil. These were significant findings which have been used for stress cell design ever since Taylor proposed them in 1945. However the assumptions used in the indentation theory do not apply for stress cells oriented to measure lateral stresses.

Finite annular elements were used by Monfore (1950) to model a soil stress cell and Bates (1969) used finite element methods to model stress cells. The results of these and other applications of finite element modeling of soil stress cells are included in Chapter 4. Although a very powerful tool, the finite element method gives a solution to

a single problem in which the material properties, applied stresses and boundary conditions must by specified. To determine the relative effect of a single parameter, several solutions must be made while holding all the other parameters constant. The finite element method is a mathematical procedure to obtain a single solution and is not a true theoretical solution in that a closed-form solution is not obtained.

The modeling of a soil stress cell as a solid inclusion in an elastic material has met with some success. Theoretical solutions for the stress concentrations around spherical and long cylindrical solid inclusions in an infinite, homogeneous, isotropic elastic space were first derived by Goodier (1933). Additional work on the solution of a solid ellipsoidal inclusion was done by Edwards (1951) and Eschelby (1957). Askegaard (1963) applied the solution derived by Eschelby to a rigid oblate spheroidal inclusion and showed that the aspect ratio of the inclusion and Poisson's ratio of the soil have a significant effect on the vertical stress on the face of the inclusion. Collins, et al. (1972) derived the same conclusions from Edward's and Eschelby's solutions, independently of Askegaard's work. The experimental work done by Askegaard (1963), Collins, et al. (1972) and the finite element modeling by Weiler and Kulhawy (1978) all confirm the use of the theoretical solution of a rigid ellipsoid to model a stress cell.

However, all the theoretical solutions and experimental work were for ellipsoids oriented as if the cells they were modeling were measuring vertical stress. For conditions of hydrostatic stress, the theoretical solution is the same for ellipsoids oriented either vertically or horizontally. A cell oriented to measure lateral stresses would respond differently under any stress conditions other than hydrostatic as compared to the same cell oriented to measure vertical stress. The following section describes the results of the theoretical solution obtained for a rigid ellipsoid oriented as if measuring lateral stress.

3.2 RIGID ELLIPSOIDAL INCLUSION

The theoretical solution for stress on a rigid ellipsoid in an infinite, elastic, homogeneous, isotropic material was used by Askegaard (1963) to model a disc-like stress cell oriented to measure vertical stress. The best ellipsoidal representation for a typical soil stress cell is an oblate spheroid with the two long axes of the ellipsoid being equal. The ratio of the length of the short axis to the length of the long axes is the aspect ratio of the oblate spheroid. The theoretical solution gave the stress at the center on the face of the oblate spheroid which was normalized by dividing it by the magnitude of the applied vertical stress. The theoretical results for the normalized vertical stress are dependent on only three parameters: the

aspect ratio of the ellipsoid (α), Poisson's ratio of the material (ν) and the ratio of lateral to vertical applied stress (K) as shown in Equation 3.1.

$$\frac{\sigma_{face}}{\sigma_{vert}} = \frac{1-\nu}{1+\nu}\left[\frac{4\alpha^2(1+2K) + 4IK(\nu-\alpha^2-\nu\alpha^2) - I(3+2K)}{I^2(1-\alpha^2)(1-2\nu) - I(3-4\nu(1-\alpha^2)) + 4\alpha^2}\right]$$

$$\text{Where} \qquad I = \frac{2\alpha}{(1-\alpha^2)^{1.5}}\left[\cos^{-1}\alpha - \alpha(1-\alpha^2)^{\frac{1}{2}}\right] \tag{3.1}$$

The coefficient, I, is dependent only on the aspect ratio of the ellipsoid and is a constant for a given value of the aspect ratio. The lateral stress ratio, K, can be varied from zero for uniaxial stress through hydrostatic stress with K = 1.0 and beyond. Poisson's ratio becomes very important and the results of Equation 3.1 are discussed by Askegaard (1963) and Weiler and Kulhawy (1978).

The results of Equation 3.1 are shown in Figure 3.1 for the K_o condition of zero lateral strain. When the aspect ratio is zero, the results are a constant value of 1.00 over the range of Poisson's ratio from zero to one half. As the aspect ratio increases the deviation from the applied stress increases dramatically for low values of Poisson's ratio, as much as 223 percent for an aspect ratio of one. This means that an ellipsoid with a small aspect ratio (large width to thickness) has a negligible effect on the stress at the

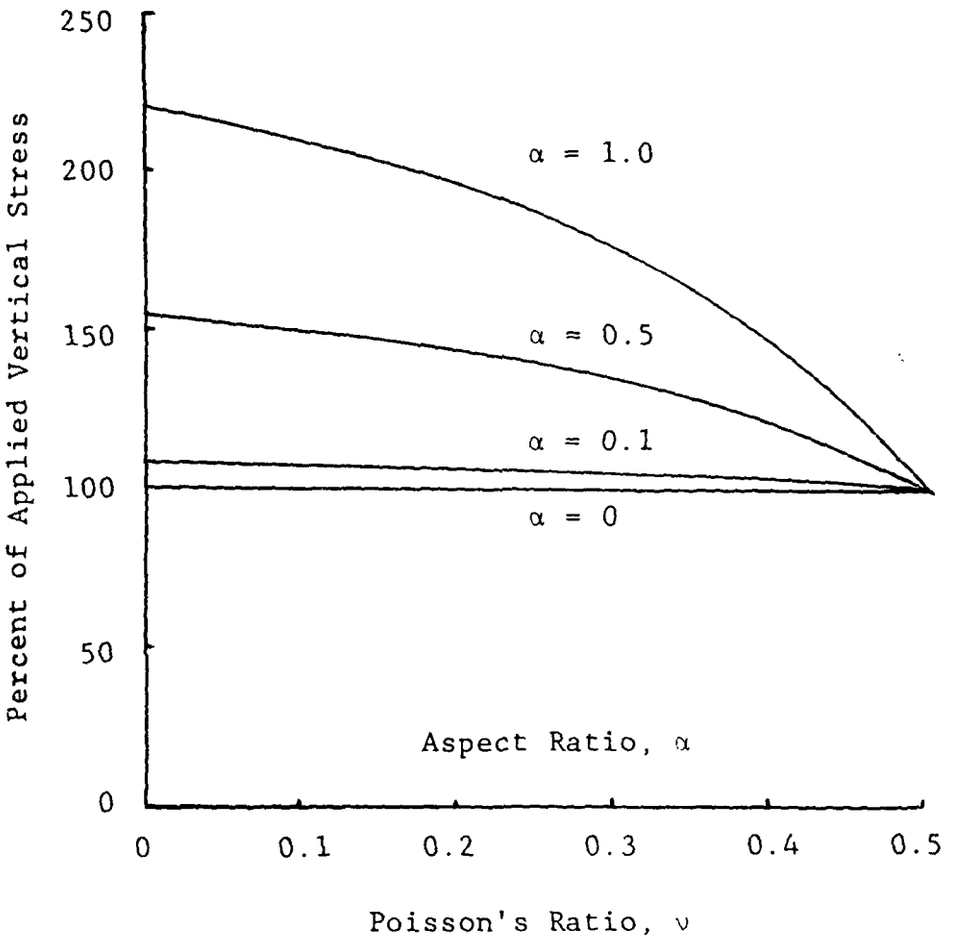

Figure 3.1 Normalized Vertical Stress on a Rigid Oblate Spheroid under K_o Conditions.

center of the face. The effect of aspect ratio on the response of a stress cell measuring vertical stress was recognized prior to Askegaard's (1963) work by Taylor (1945) who quantified the effect of aspect ratio using indentation theory. Soil stress cells have been generally designed to have a small aspect ratio to avoid this large error.

Because of the success of representing the soil stress cell oriented to measure vertical stresses by a rigid ellipsoid, the theoretical solution for an ellipsoid oriented for lateral stress was desired. It was possible through a rotation of coordinates to obtain the stress on the center of the face of the oblate spheroid oriented to represent a stress cell measuring lateral stress. The stress on the rigid ellipsoid was again normalized by the applied vertical stress. The resulting lateral stress is:

$$\frac{\sigma_{face}}{\sigma_{vert}} = \frac{1-\nu}{1+\nu}\left[\frac{4\alpha^2(1+2K) + 2I(1+K)(\nu-\alpha^2-\nu\alpha^2) - I(1+4K)}{I^2(1-\alpha^2)(1-2\nu) - I(3-4\nu(1-\alpha^2)) + 4\alpha^2}\right] \tag{3.2}$$

with the coefficient, I, as defined in Equation 3.1.

For an aspect ratio of one, representing a sphere and under hydrostatic stress conditions, K = 1.0, Equations 3.1 and 3.2 give identical results as would be expected. For the special case of zero lateral strain where $K = K_o$, the

coefficient of lateral earth pressure at rest, the value of K_o can be expressed as a function of Poisson's ratio (See Equation 4.11.). The results of Equation 3.2 for the K_o condition are shown in Figure 3.2 for variation in the range of Poisson's ratio from zero to one half and the range of aspect ratio from zero to one. The theoretical lateral stress ratio for free field conditions is also shown for comparison. The results of Equation 3.2 do not match the free field results for low values of Poisson's ratio but merge to the free field values at Poisson's ratio of one half. The differences between aspect ratios are small (less than six percent of the range) compared to the differences (as much as 39 percent) between the values of stress on the rigid ellipsoid and the free field stress.

One conclusion drawn from Figure 3.2 is the insensitivity to the variation in aspect raio for a rigid ellipsoid oriented as if measuring lateral stress under conditions of zero lateral strain. The stress on the face of the oblate spheroid is significantly different than the free field stress but relatively constant for variations in the aspect ratio. This behavior is contrasted with the inclusion oriented to measure vertical stress which is very sensitive to the value of the aspect ratio. A stress cell designed to measure vertical stress should be as thin as practical to minimize the error in the measured stress. A stress cell used to measure lateral stress has an error that is insen-

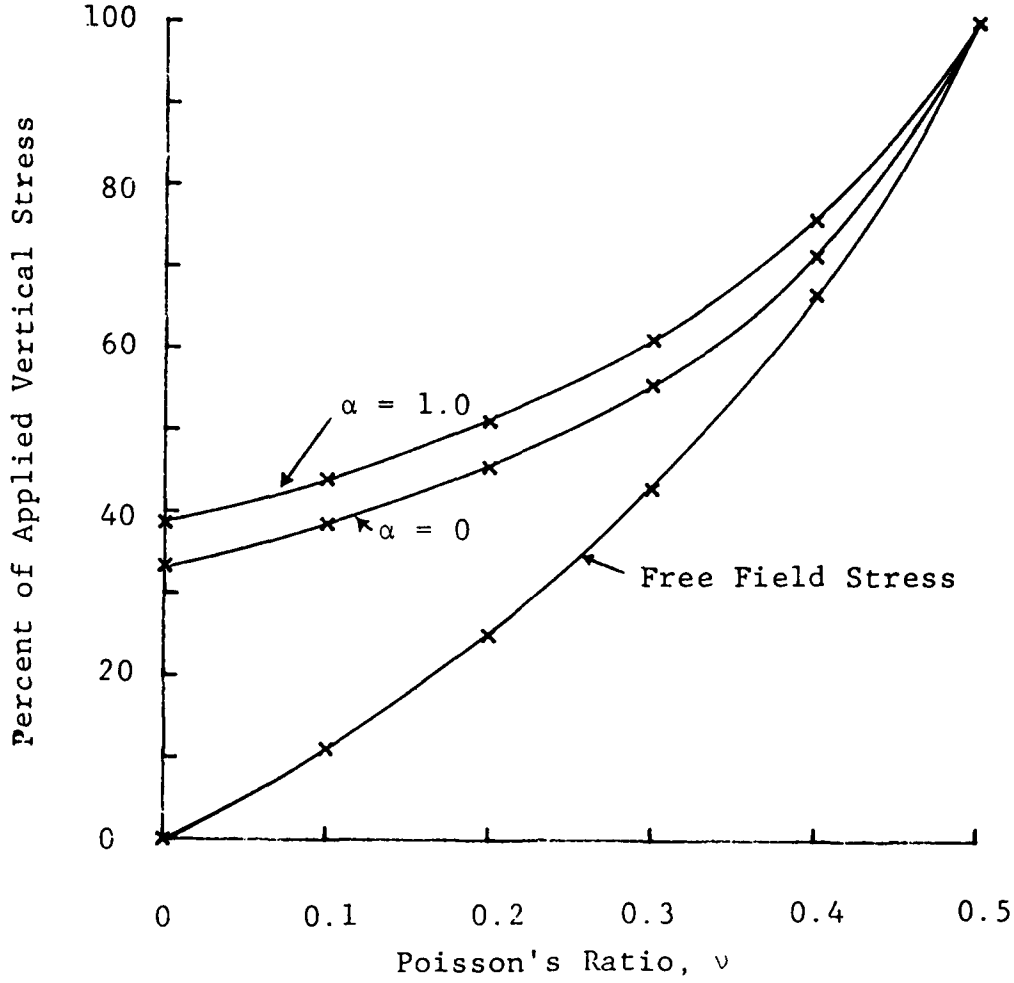

Figure 3.2 Normalized Lateral Stress on a Rigid Oblate Spheroid under K_o Conditions.

sitive to the aspect ratio of the cell for conditions of zero lateral strain.

Another conclusion that can be drawn from Figures 3.1 and 3.2 is about the effect of Poisson's ratio on the stress on the face of the inclusion. The stress approaches the free field stress for the K_o conditions as Poisson's ratio approaches one half. This occurs whether the inclusion is oriented vertically or horizontally and for any value of the aspect ratio. This behavior would explain the successful application of stress cells in saturated clays discussed in Chapter 2. The value of Poisson's ratio for saturated clays is nearly one half and the measured stress in this type of soil has been found to be much closer to the expected free field stress than for any other type of soil. The results for the stress on a rigid ellipsoidal inclusion help to explain why stress cells have performed well in soils with a high value of Poisson's ratio such as saturated clays.

3.3 CONCLUSIONS

A review of the theoretical solutions for modeling soil stress cells has shown the best theoretical model to be that of a rigid ellipsoid. Askegaard's solution for a rigid oblate spheroid in an infinite, elastic, homogeneous and isotropic material has been transformed to allow the representation of a stress cell measuring lateral stress as well as vertical stress. The results show that for the K_o

conditions of zero lateral strain, the measured lateral stress is relatively insensitive to the aspect ratio of the cell and very sensitive to changes in the Poisson's ratio of the material.

CHAPTER 4

FINITE ELEMENT MODELING OF STRESS CELLS

There are three general approaches to solve the problem of stress cell response in soil: theoretical solutions, laboratory testing and mathemetical modeling. This chapter deals with the latter approach, mathematical modeling of stress cells.

The first section covers previous attempts to model stress cells. Common to all the earlier mathematical models by other researchers was the use of axisymmetric models with isotropic soil properties. One of the purposes of this investigation was to determine the response of stress cells measuring horizontal stress in cross-anisotropic soil. This requires three-dimensional modeling and the use of anisotropic soil properties.

Soil as a cross-anisotropic material is treated in the second section. Cross-anisotropy is an improved model for soil behavior in which the soil can be described by five independent elastic parameters with any vertical axis being an axis of symmetry. Most soils created in a sedimentary environment exhibit the characteristics of cross-anisotropy. The effect of cross-anisotropy on the response of stress cells in finite element models is the desired result.

Four separate finite element models are used in the analysis and are described in the third section. The four

models are: axisymmetric models of a rigid ellipsoid, a rigid disc and the Cornell Stress Cell, and a three-dimensional model of the Cornell Stress Cell. The effects of inclusion shape, soil modulus, cross-anisotropy, Poisson's ratio and lateral stress ratio are investigated using these four models. The results of the finite element analysis are discussed in the fourth section by taking each model separately and comparing the results to other known solutions.

The fifth and final section of the chapter summarizes the chapter and includes the conclusions reached during the finite element modeling of the stress cell.

4.1 PREVIOUS MATHEMATICAL MODELS FOR STRESS CELLS

The earliest known attempt to model stress cell performance mathematically was by Monfore (1950) who used finite annular rings to determine the distribution of stress across the face of an elastic disc. Monfore assumed that a plane parallel to the face and through the center of a rigid disc embedded in an elastic material would remain plane when the elastic material was subject to a uniform uniaxial stress normal to the rigid disc. This assumption allowed him to use the center plane as a plane of symmetry and to model only half the disc on the surface of an elastic half space. Boussinesq's solution for surface loading on an elastic half space was then applied to determine the load on concentric annular rings necessary to keep the surface

plane. The stresses from the load on each annular ring were then superimposed to determine the stress distribution across the face of the rigid disc. This pioneering work on stress cells was limited by the use of a solid elastic disc to model the stress cell and it ignored the effects of lateral stress on the disc and shear stress on the center plane.

The first use of the finite element method for modeling stress cells was by Bates (1969) who did plane stress and axisymmetric modeling of the SMRL, Spokane Mining Research Laboratory, deflecting diaphragm strain gaged cell. The results showed nearly constant overregistration in soft soils and he recommended that cells be constructed to be much stiffer than the soil they are embedded in. The major principal stress was also applied laterally to the cell and although the results clearly show the effect of lateral stress rotation, it was not identified by Bates.

Both diaphragm and rigid spool cells were modeled as axisymmetric problems by Fossberg (1970) to obtain the stress distribution across the cell face. Radial tension in the soil elements near the edge of the cell was identified for cells in uniaxial compression. Only cells measuring vertical stress were modeled and although lateral stress rotation was evident in the results, it was not identified by Fossberg.

Forsyth and Jackura (1974) modeled stress cells as a

solid elastic disc using axisymmetric conditions with the major principal stress both normal and parallel to the cell. They investigated the effects of soft and stiff annular rings as well as variations in the edge shape for a solid disc-like cell. They concluded that cell geometry is the single most important physical property associated with minimizing registration error and failed to recognize lateral stress rotation and the effects of Poisson's ratio on the registration values.

Krizek, et al. (1974) used the finite element method to model their soil calibration chamber to determine the theoretical stress cell response. Their investigation included variations in the stiffness and Poisson's ratio of both the cell and the soil, as well as the boundary conditions of their calibration chamber. All thirty-one of their finite element solutions were for vertical stresses in axisymmetric models. The stress cell used was a fluid filled deflecting diaphragm modeled as an elastic disc with a stiffer outer ring. The results indicated only a small deviation in the free field stress caused by a stress cell measuring vertical stress. Therefore they assumed little or no disturbance in the free field stress for a stress cell measuring horizontal stress, although this was not modeled.

Audibert and Tavenas (1975) report on modeling pocket action on the response of a stress cell using a nonlinear stress-dependent elastic model. The cell was modeled as a

rigid disc in this axisymmetric problem. No mention of the imposed lateral stress or lateral strain conditions were given in their report.

A rigid piston boundary cell was modeled by Carder (1976) using isotropic stress on an axisymmetric model. He concluded that the amount of friction along the rigid boundary was very important to the registration value of the cell.

Weiler and Kulhawy (1978) modeled the Cornell Stress Cell as a deflecting diaphragm cell with both soft silicone and rigid stainless steel annular rings. Their analysis included uniaxial stress, lateral stress only and zero lateral strain, K_o, conditions to quantify the lateral stress rotation effects. They clearly separated the cross-sensitivity and lateral stress rotation effects which had been so long confused and mislabeled in the literature. Their model was axisymmetric for modeling only stress cells oriented to measure vertical stresses.

All of the above researchers modeled the stress cell problem using: an axisymmetric model representing a cell measuring vertical stress; linear elastic soil properties (except for Audibert and Tavenas, 1975); and isotropic soil properties. The purpose of the finite element modeling done for this study was to determine the effects of anisotropic soil properties, specifically cross-anisotropy, and to model a stress cell oriented to measure horizontal stresses.

This required a finite element program that would include both anisotropic material properties and three dimensional elements.

4.2 SOIL AS A CROSS-ANISOTROPIC MATERIAL

Mathematical models usually treat soil as a homogeneous, isotropic, elastic medium, often with acceptable results such as the popular Boussinesq solution. However it is well known that soil is not homogeneous, isotropic or elastic and it has an extremely complex stress-strain-time behavior. To treat soil as a general anisotropic material would require the determination of nine independent elastic parameters: three elastic moduli, three Poisson's ratios and three shear moduli as shown in Equation 4.1.

$$\begin{Bmatrix} \varepsilon_x \\ \varepsilon_y \\ \varepsilon_z \\ \gamma_{xy} \\ \gamma_{yz} \\ \gamma_{xz} \end{Bmatrix} = \begin{bmatrix} 1/E_x & -\nu_{xy}/E_y & -\nu_{xz}/E_z & 0 & 0 & 0 \\ & 1/E_y & -\nu_{yz}/E_z & 0 & 0 & 0 \\ & & 1/E_z & 0 & 0 & 0 \\ & & & 1/G_{xy} & 0 & 0 \\ & \text{Symmetrical} & & & 1/G_{yz} & 0 \\ & & & & & 1/G_{xz} \end{bmatrix} \begin{Bmatrix} \sigma_x \\ \sigma_y \\ \sigma_z \\ \tau_{xy} \\ \tau_{yz} \\ \tau_{xz} \end{Bmatrix} \tag{4.1}$$

Because of the difficulty in determining these nine independent parameters, general anisotropic material properties are seldom used to model soil. Since soil is often

deposited in a sedimentary environment where the soil is uniform over a large lateral extent, it has been proposed that a cross-anisotropic elastic material is an improved mathematical model for soil as compared to the isotropic model.

A material with no preferred orientation in the horizontal plane has elastic properites that are symmetrical about any vertical axis. This material is known as transversely isotropic or cross-anisotropic and is the same as the crystals of a hexagonal system described by Love (1892). Love showed that a cross-anisotropic material can be described by only five independent elatic parameters: E_x, E_y, ν_{xz}, ν_{xy}, and G_{xy} assuming a coordinate system with the xz plane being horizontal and the y axis the vertical direction. The four remaining dependent parameters are:

$$E_z = E_x \tag{4.2}$$

$$G_{yz} = G_{xy} \tag{4.3}$$

$$\nu_{yz} = n(\nu_{xy}) \qquad \text{where } n = E_x/E_y \tag{4.4}$$

$$G_{xz} = \frac{nE}{2(1+\nu_{xz})} \qquad \text{where } E = E_y \tag{4.5}$$

By substituting these parameters back into Equation 4.1, the stress-strain relationship for a cross-anisotropic material

is obtained:

$$\begin{Bmatrix} \varepsilon_x \\ \varepsilon_y \\ \varepsilon_z \\ \gamma_{xy} \\ \gamma_{yz} \\ \gamma_{xz} \end{Bmatrix} = \begin{bmatrix} \frac{1}{nE} & \frac{-\nu_{xy}}{E} & \frac{-\nu_{xz}}{nE} & 0 & 0 & 0 \\ & \frac{1}{E} & \frac{-\nu_{xy}}{E} & 0 & 0 & 0 \\ & & \frac{1}{nE} & 0 & 0 & 0 \\ & & & \frac{1}{G_{xy}} & 0 & 0 \\ \text{Symmetrical} & & & & \frac{1}{G_{xy}} & 0 \\ & & & & & \frac{2(1+\nu_{xz})}{nE} \end{bmatrix} \begin{Bmatrix} \sigma_x \\ \sigma_y \\ \sigma_z \\ \tau_{xy} \\ \tau_{yz} \\ \tau_{xz} \end{Bmatrix} \tag{4.6}$$

Wolf (1935) is generally accepted as the first to apply cross-anisotropy to a soil (Barden, 1963). However, Wolf assumed that all Poisson's ratio values were zero and therefore used only three independent parameters: E_x, E_y and G_{xy}. This does not meet the requirements of Equation 4.4 derived by Love (1892) and is theoretically unsound.

Barden (1963) correctly applied cross-anisotropy to describe soil behavior and derived exact expressions for the vertical normal and shear stresses and approximate expressions for the horizontal normal stresses. Barden states, "The exact expression for the horizontal stresses σ_r and σ_θ are, however, greatly affected by the values of Poisson's ratio, and so are of little interest in soil mechanics".

Pickering (1970) applied the requirement that the strain energy of an elastic material should always be

positive for a cross-anisotropic material and defined the limits for the five independent parameters:

$$E_x > 0;\ E_y > 0;\ G_{xy} > 0 \qquad (4.7a,b,c)$$

$$-1 < \nu_{xz} < 1 \qquad (4.8)$$

$$n(1-\nu_{xz})-2\nu_{xy}^{2} > 0 \qquad (4.9)$$

These limits allow the material to undergo either a positive or negative volume change when subjected to a compresssive stress. Morgan and Gerrard (1973) tested samples of a medium fine sand, porosity = 0.53, and found that the modulus decreased with stress level and Poisson's ratio increased with stress level, but stayed within the limits defined by Pickering.

Dolezalovå (1974) used the stress-strain relationship for a cross-anisotropic material, Equation 4.6, to obtain the expression for K_o, the lateral stress ratio for zero lateral strain:

$$K_o = \frac{n\nu_{xy}}{1-\nu_{xz}} = \frac{\nu_{yz}}{1-\nu_{xz}} \qquad (4.10)$$

For an isotropic material the expression for the lateral stress ratio for zero lateral strain, also known as the coefficient of horizontal soil stress at rest, is:

$$K_o = \frac{\nu}{1-\nu} \tag{4.11}$$

Equation 4.10 clearly demonstrates the effect of cross-anisotropy on the magnitude of the lateral stress.

The value of n, which is the measure of cross-anisotropy in soil, has been measured by many researchers as summarized by Ladd, et al. (1977). For loose sands pluviated through either air or water, n values are typically 0.5. As the sands are densified by vibration, the n value increases and vibrated dense sands are nearly isotropic with n values equal to one. Overconsolidated clays may have n values in excess of three but clays were not used in this investigation. The range of interest for the n values in vibrated sands would be between 0.5 and 1.0.

4.3 FINITE ELEMENT MODELING

To perform a finite element analysis of the Cornell Stress Cell, CSC, in a cross-anisotropic medium oriented to measure horizontal stresses, it was necessary to use a program capable of handling anisotropic material properties and three dimensional elements. ANSYS, a multi-purpose finite element program developed by Swanson Analysis Systems Inc. of Houston, Pennsylvania was used in this study. The program has interactive preprocessing which vastly simplifies the data input and eliminates all card punching. Postprocessing can also be done interactively to reduce the

large volume of possible output into easily manageable form and allows graphic displays of solution values.

The first step in the finite element modeling was to model a rigid ellipsoidal inclusion with an aspect ratio of 0.129, the same as the Cornell Stress Cell. The axisymmetric mesh shown in Figure 4.1 is composed of four noded isoparametric elements. The axisymmetric model allowed no horizontal displacements along the axis, centerline or surface of the ellipsoid, no vertical displacements along the plane of symmetry or surface of the ellipsoid and either specified surface pressures for the isotropic stresses or both specified surface pressures and specified boundary displacements for the K_o conditions. This model was used to compare the finite element results with the theoretical solution derived by Askegaard (1963) and discussed in Section 3.2. A comparison of the results follows in Section 4.4.

The mesh shown in Figure 4.1 was then modified to model a rigid disc with the same aspect ratio. This allowed a comparison between the rigid ellipsoid and rigid disc to evaluate the influence of geometry and to compare the results with those of Monfore (1950).

The third step in the finite element modeling was to replace the rigid disc with the Cornell Stress Cell described in Section 5.1 and shown in Figure 5.1. This axisymmetrical mesh, Figure 4.2, is composed of eight noded

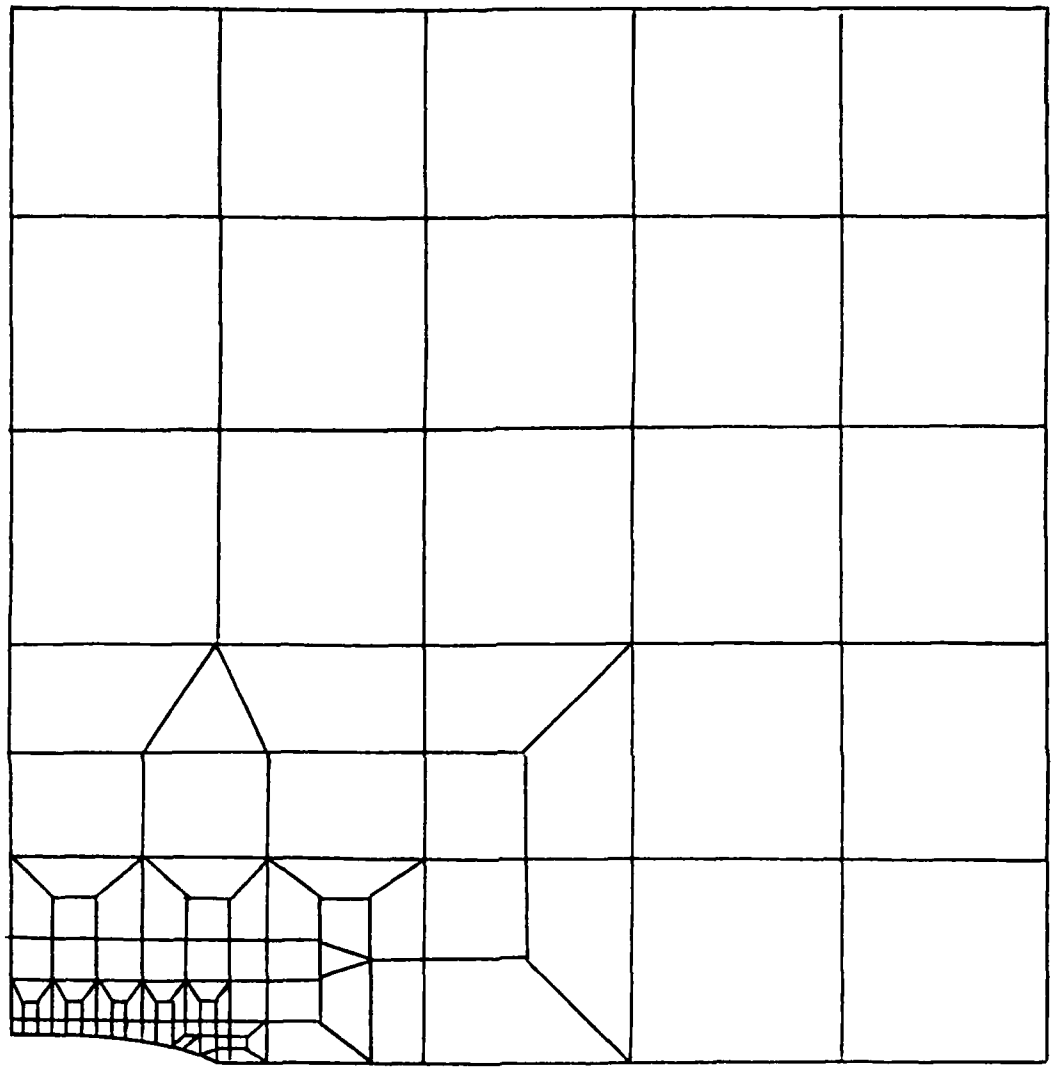

Q4 elements (101 elements)
Axisymmetric
Aspect Ratio = 0.129

Figure 4.1 Finite Element Mesh for Rigid Ellipsoid.

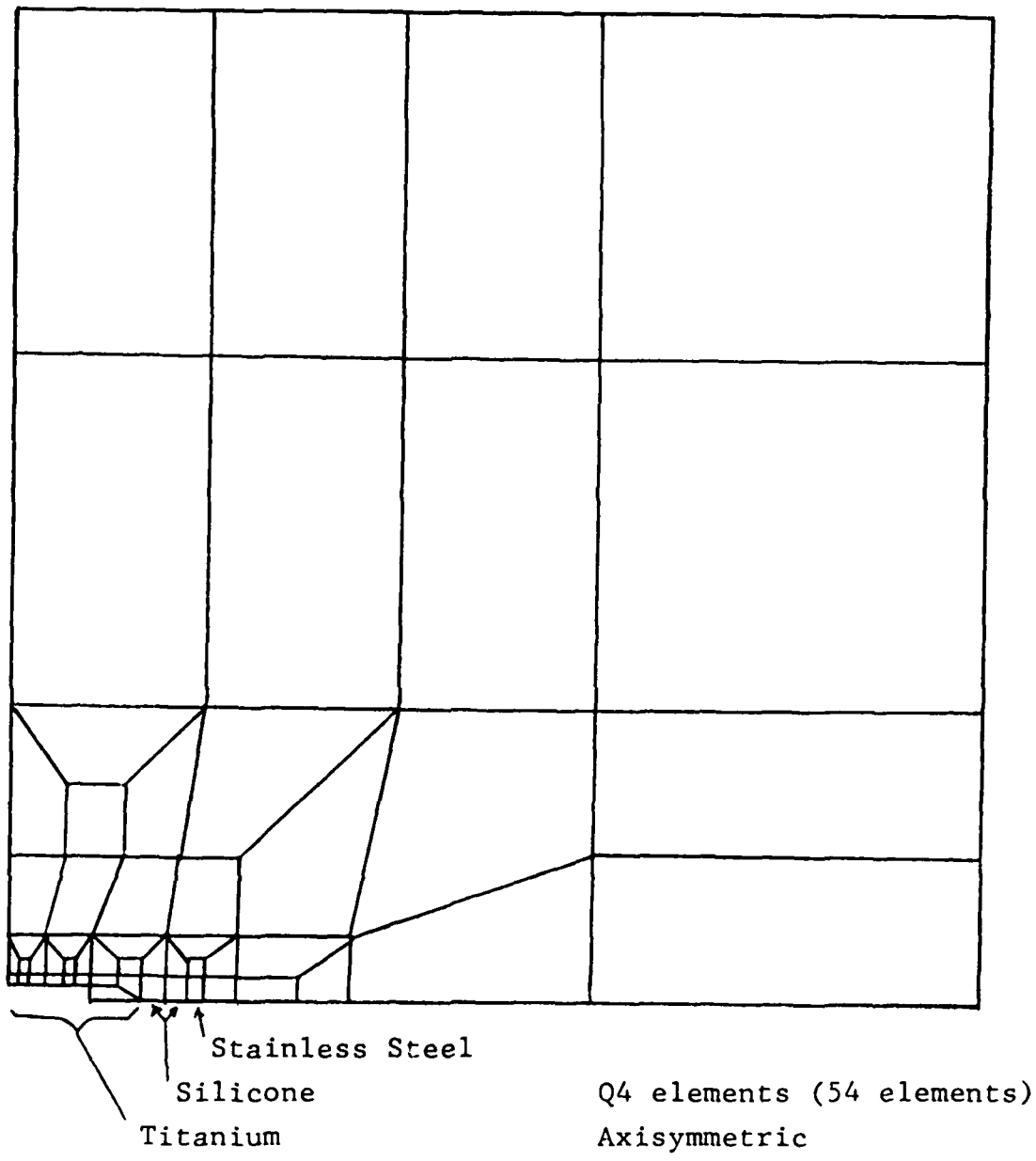

Figure 4.2 2-D Finite Element Mesh for Cornell Stress Cell.

isoparametric elements which are necessary to simulate successfully the bending action of the diaphragm. The deflection at the center of the diaphragm from an applied uniform normal stress was 1.63×10^{-5} inches/psi (6.00×10^{-11} m/N/m^2) as compared to 1.38×10^{-5} inches/psi (5.08×10^{-11} m/N/m^2) for a fixed edge diaphragm of the same thickness, 0.025 inches (0.635mm), as calculated from equations defined by Timoshenko (1955). The increased deflection of the model is caused by the distortion allowed at the outer edge of the diaphragm in the finite element model which is not present in the fixed edge analysis of Timoshenko. It was assumed that a horizontal plane through the center of the cell was a plane of symmetry which is not exactly correct but is thought to be a close approximation. This axisymmetric model was used to study the effects of soil modulus, Poisson's ratio and soil anisotropy on the distribution of vertical stress across the face of the stress cell.

To model the measurement of horizontal stress by a stress cell, it was necessary to use a three-dimensional model. By again assuming that a plane through the center of the stress cell, parallel with the diaphragm face, is a plane of symmetry there exist three orthogonal planes of symmetry. The stress cell can then be modeled by representing only one eighth of the cell as shown in Figure 4.3. The three-dimensional model is composed of twenty noded isoparametric brick elements. No displacements were allowed

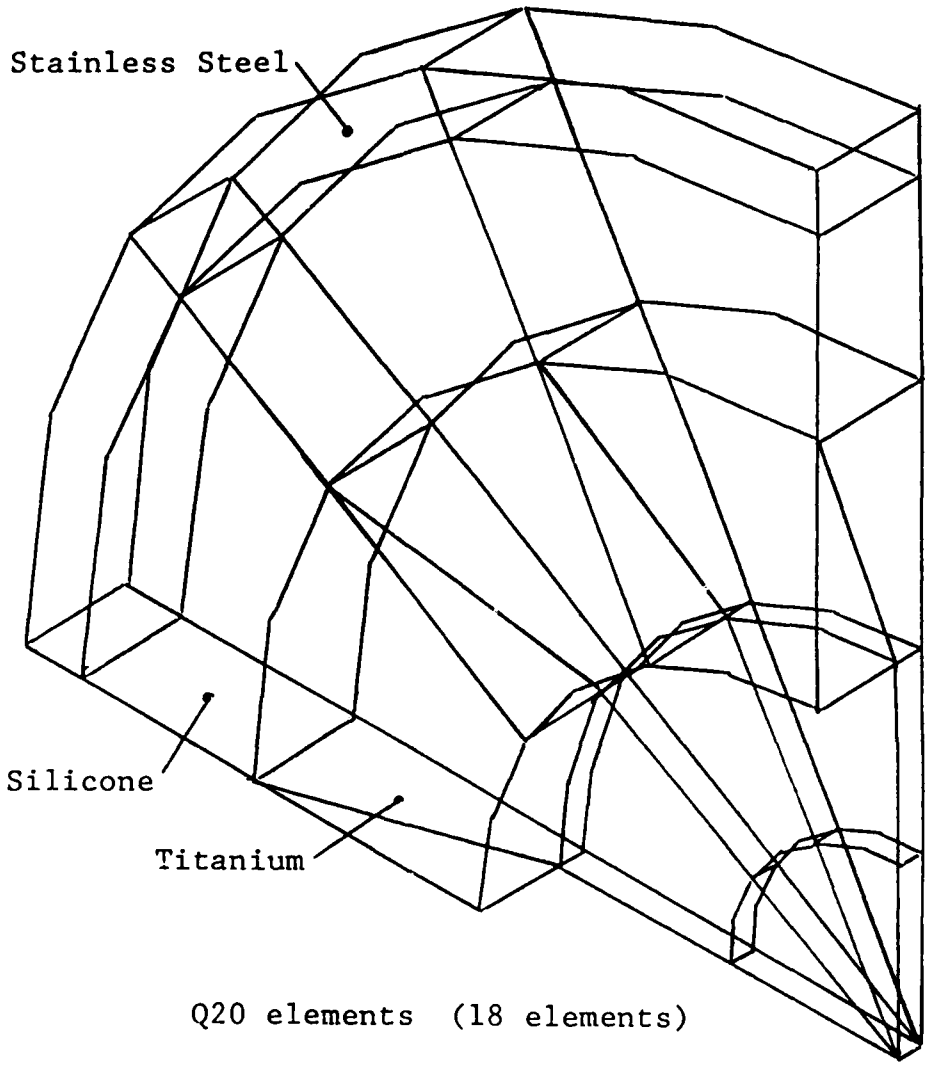

Figure 4.3 Finite Element Mesh for 3-D Cornell Stress Cell.

normal to and occurring on any of the three planes of symmetry. Because of the rapid increase in computational effort required with increasing element sophistication, the diaphragm was modeled with only six elements. This prevents direct rumerical comparisons of the results between the axisymmetric and three-dimensional models. However the trends in the stress cell performance should be similar and modeling for exact results between the two stress cell models was not considered essential. The post processor for ANSYS calculates the nodal point stresses from the 3x3x3 array of Gaussian points but only for the eight corner nodes. This did not allow for as smooth a depiction of normal stress across the face of the cell as did the axisymmetric models.

The material properties used for the Cornell Stress Cell in all models are:

Titanium	$E = 16.8 \times 10^6$ psi (116 GN/m^2)
	$\nu = 0.30$
Silicone	$E = 227$ psi (1.56 MN/m^2)
	$\nu = 0.45$
Stainless Steel	$E = 30 \times 10^6$ psi (207 GN/m^2)
	$\nu = 0.30$

The material properties for the soil were varied to investigate the influence of modulus, Poisson's ratio and cross-anisotropy.

To input the properties for a cross-anisotropic

material it was necessary to match the stress-strain relationship used in the element formulation of ANSYS (Kohnke, 1977), Equation 4.12, with that in Equation 4.6.

$$\begin{Bmatrix} \varepsilon_x \\ \varepsilon_y \\ \varepsilon_z \\ \gamma_{xy} \\ \gamma_{yz} \\ \gamma_{xz} \end{Bmatrix} = \begin{bmatrix} \frac{1}{E_x} & \frac{-NUXY}{E_y} & \frac{-NUXZ}{E_z} & 0 & 0 & 0 \\ & \frac{1}{E_y} & \frac{-NUYZ}{E_z} & 0 & 0 & 0 \\ & & \frac{1}{E_z} & 0 & 0 & 0 \\ & & & \frac{1}{G_{xy}} & 0 & 0 \\ \text{Symmetrical} & & & & \frac{1}{G_{yz}} & 0 \\ & & & & & \frac{1}{G_{xz}} \end{bmatrix} \begin{Bmatrix} \sigma_x \\ \sigma_y \\ \sigma_z \\ \tau_{xy} \\ \tau_{yz} \\ \tau_{xz} \end{Bmatrix} \tag{4.12}$$

This requires the nine input parameters of Equation 4.12 be related to those of Equation 4.6 by the following:

$$E_x = E_z = nE$$

$$E_y = E$$

$$G_{xy} = G_{yz}$$

$$G_{xz} = \frac{nE}{2(1+\nu_{xz})}$$

$$NUXY = \nu_{xy}$$

$$NUYZ = n\nu_{xy}$$

$$NUXZ = \nu_{xz}$$

which allows all nine input parameters to be expressed in terms of five independent elastic constants: n, E, G_{xy}, ν_{xy}, and ν_{xz}.

4.4 FINITE ELEMENT RESULTS

In this section the results of the four step finite element analysis performed in this study are discussed. The models used in the four step approach are: axisymmetric rigid ellipsoid, rigid disc and Cornell Stress Cell analyses and the three-dimensional Cornell Stress Cell which are described in Section 4.3.

It was decided that the magnitude of the soil stress normal to the face, at the centerline, of the inclusion or stress cell would be used for comparisons between the four different models. It was not considered appropriate to try to determine an average or equivalent stress across some portion of the inclusion or stress cell. To do so would require additional assumptions concerning edge conditions of

the diaphragm and an arbitrary selection of the sensitive portion.

Weiler and Kulhawy (1978) determined the equivalent uniform stress on a fixed edge diaphragm necessary to produce a displacement similar to the displacement of the diaphragm on the Cornell Stress Cell. In every case, the equivalent uniform load exceeded the stress determined from their finite element analysis. The additional displacement in the finite element analysis was attributed to the presence of shear stresses across the face of the cell. Another likely source of the additional displacement in the finite element analysis is the nonfixity of the edge of the diaphragm which allows small rotations and displacements in the model that are not present in the equivalent uniform stress on a fixed edge diaphragm.

Fixed edge diaphragms are more sensitive to applied pressures near the center than near the edge so that a uniform pressure determined from an average value of pressure over the face would not necessarily match the actual displacement shape of the diaphragm. Only the normal stress in the soil on the axis of symmetry of the cell or inclusion is used for comparisons in this study for both simplicity and accuracy.

4.4.1 Rigid Ellipsoid

In the first step of the finite element analysis a rigid ellipsoid with an aspect ratio equal to that of the

Cornell Stress Cell was modeled. The vertical stress profile is shown in Figure 4.4 for the conditions of hydrostatic stress, isotropic soil properties and a Poisson's ratio of 0.3. The stress normal to the surface of the inclusion and along the plane of symmetry of the ellipsoid is normalized by the vertical stress applied on the soil at the boundary so that the results could be expressed in percent. The stress was normalized in all four steps of the analysis to allow a more convenient method of comparison. Since the material properties in all cases were elastic, the magnitude of the applied stress is not important in the discussion of the results. The ratio of the applied horizontal to vertical stress, K, is reported for each analysis along with the value of Poisson's ratio and the ratio of horizontal to vertical moduli, n.

It can be seen in Figure 4.4 that the normal stress is nearly constant at 109 percent of the applied stress across the rigid ellipsoid except at the outer edge where it is lower than the applied stress. At a distance greater than two radii from the centerline there is very little change in the free field stress due to the presence of the rigid ellipsoid.

The normal stress on the centerline of the rigid ellipsoid as determined by the finite element method is 109.3 percent of the applied strress. For the same conditions of Poisson's ratio, stress ratio and isotropy, the

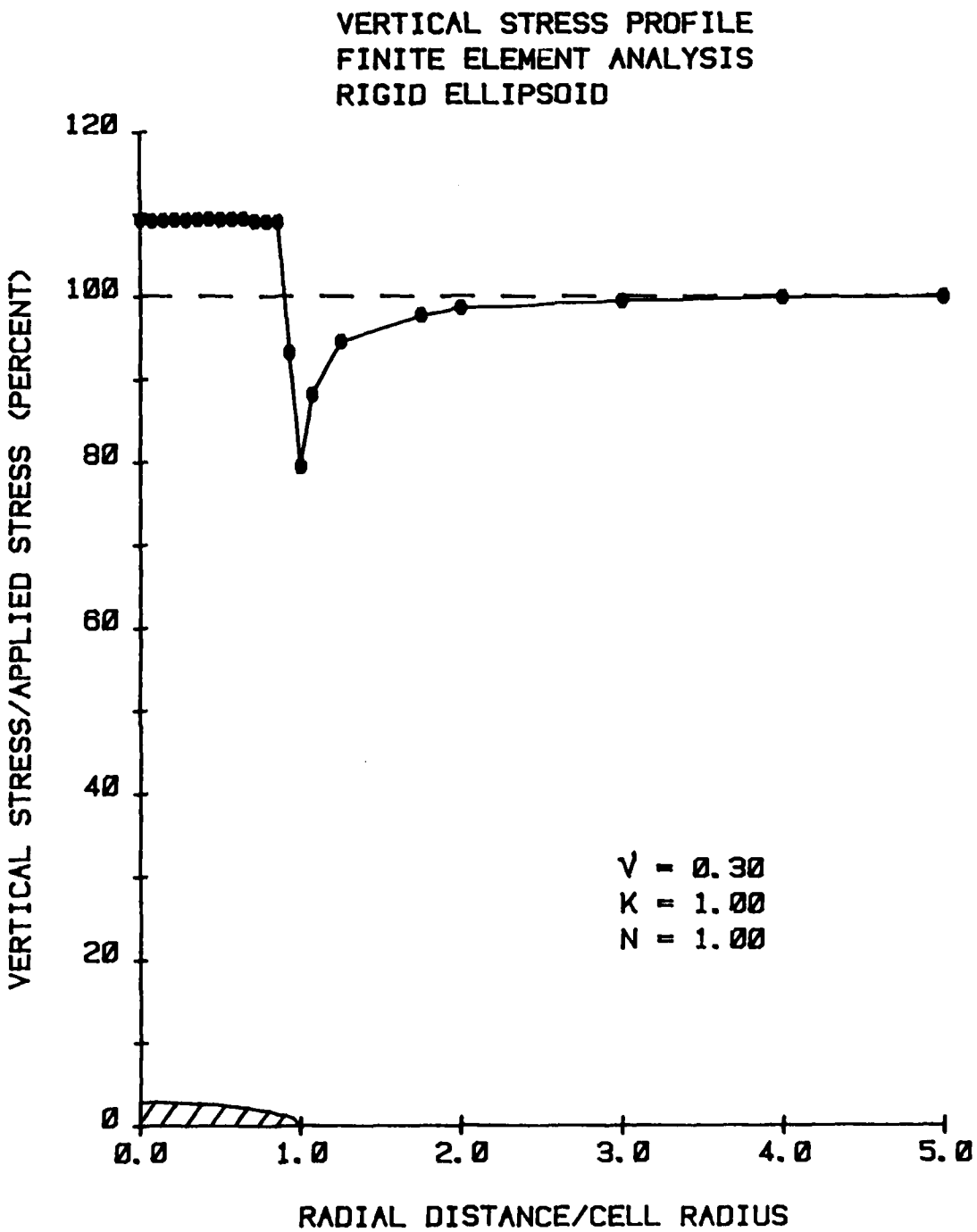

Figure 4.4 Vertical Stress Profile Across a Rigid Ellipsoid.

theoretical solution of Askegaard (1963) gave 109.1 percent. This excellent agreement offered evidence that both the model and the finite element program were capable of producing correct solutions.

4.4.2 Rigid Disc

In the second step of the finite element analysis a rigid disc with an aspect ratio of 0.129 was modeled. The normal stress across the face of the disc and the plane of symmetry is shown in Figure 4.5 for the conditons of Poisson's ratio of 0.3, hydrostatic stress and isotropic soil. The stress profile is very similar to that of a rigid ellipsoid with the same conditions shown in Figure 4.4. The discontinuity occurs at the outer edge of the disc as the reported stress switches from the face of the disc to the plane of symmetry.

The normal stress at the centerline of the rigid disc is 112.1 percent of the applied stress compared to 109.3 percent obtained for the rigid ellipsoid. This close agreement between the two different shapes of rigid inclusion supports the use of Askegaard's 1963 solution for rigid ellipsoids when modeling stress cells that are disc-like in shape.

When the applied stress conditions were changed from hydrostatic, $K = 1.0$, to at rest, $K = K_o$, the vertical stress profile, Figure 4.6, changed significantly. The normal stress now increases from a value of 105.1 percent at

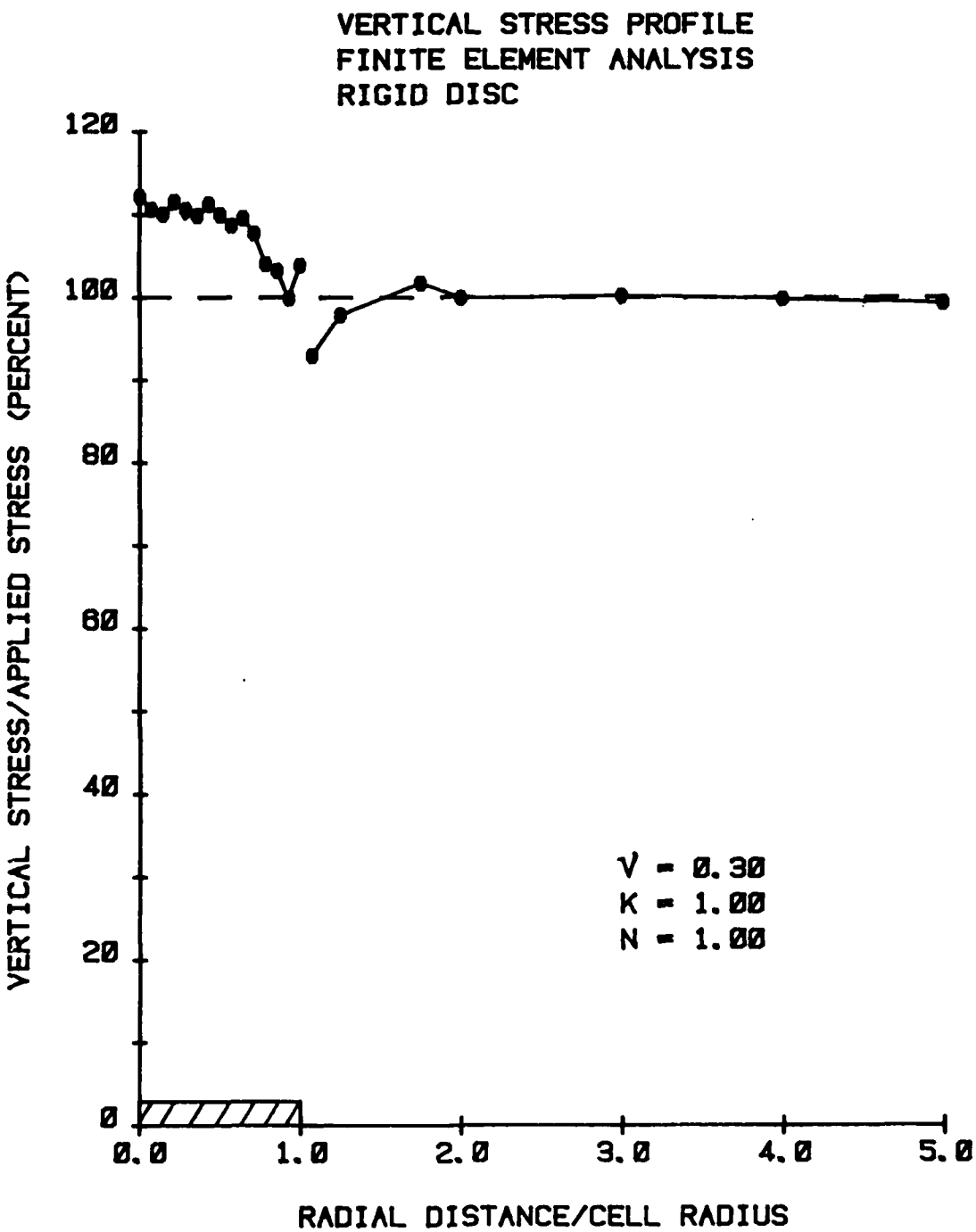

Figure 4.5 Vertical Stress Profile Across a Rigid Disc under Hydrostatic Stress.

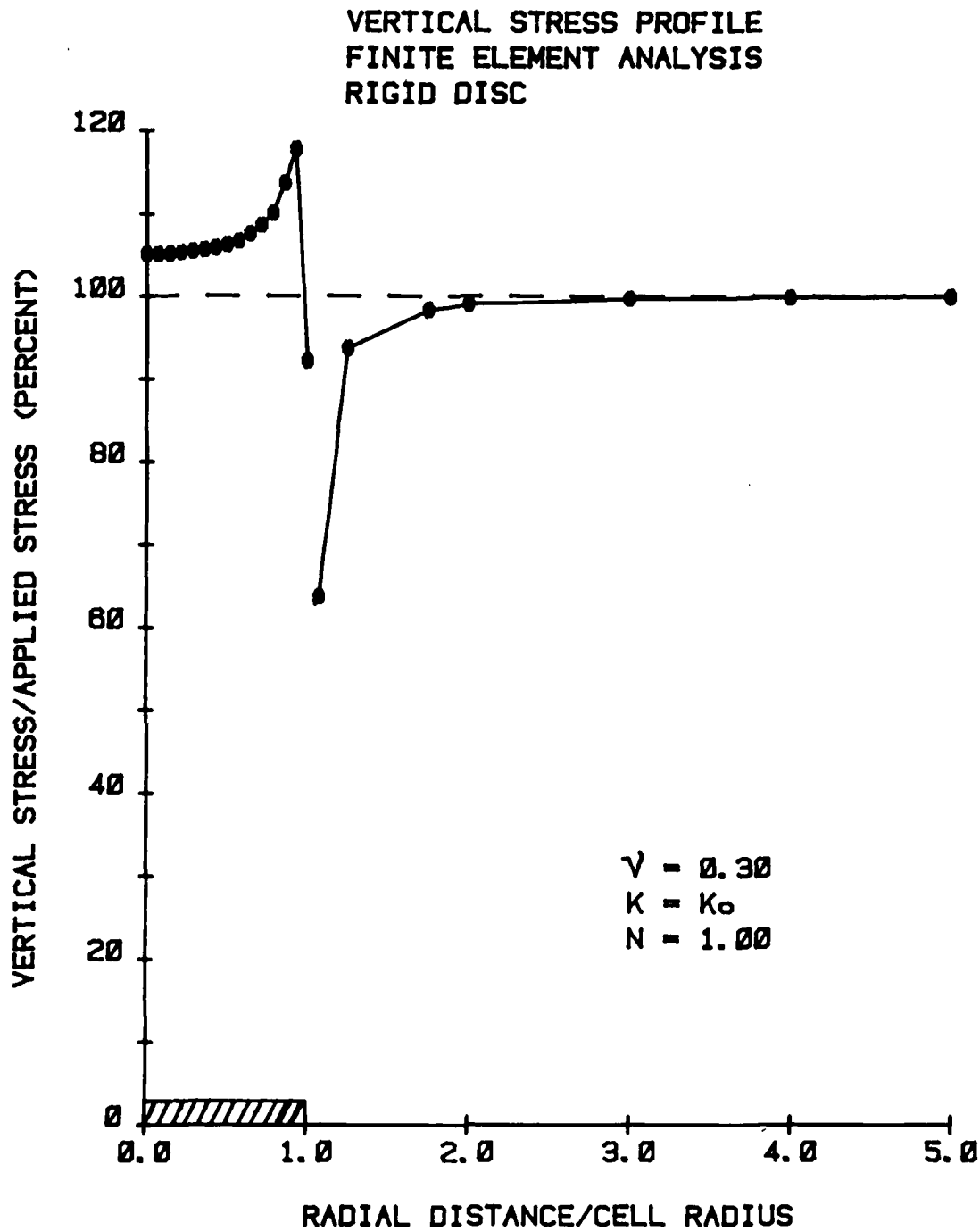

Figure 4.6 Vertical Stress Profile Across a Rigid Disc under K_o Conditions.

the centerline to 117.9 percent near the outer edge of the disc. This result is very similar in form to Monfore's (1950) stress distribution calculated using finite annular rings, discussed in Section 4.1.

A finite element analysis was also performed where horizontal displacements of the nodes on the surface of the rigid disc were not permitted. This was done to check on the sensitivity of the surface conditions, smooth being modeled by allowing displacements and rough being modeled by not allowing displacements along the interface. The results varied by less than two tenths of a percent for isotropic conditions, at rest stress ratio and Poisson's ratio of 0.3. On all subsequent analyses, the surface of the cell was considered rough and no displacements were allowed along the interface.

As with the rigid ellipsoid, the stress field at a distance greater than two radii from the centerline of the rigid disc is barely affected by the presence of the inclusion.

4.4.3 Axisymmetrical Cornell Stress Cell

The third step in the finite element analysis was to replace the rigid disc with a three material model of the Cornell Stress Cell. The vertical stress distribution across the face of the stress cell and the plane of symmetry for the conditions of Poisson's ratio of 0.3, at rest stress ratio and isotropic material is shown in Figure 4.7. The

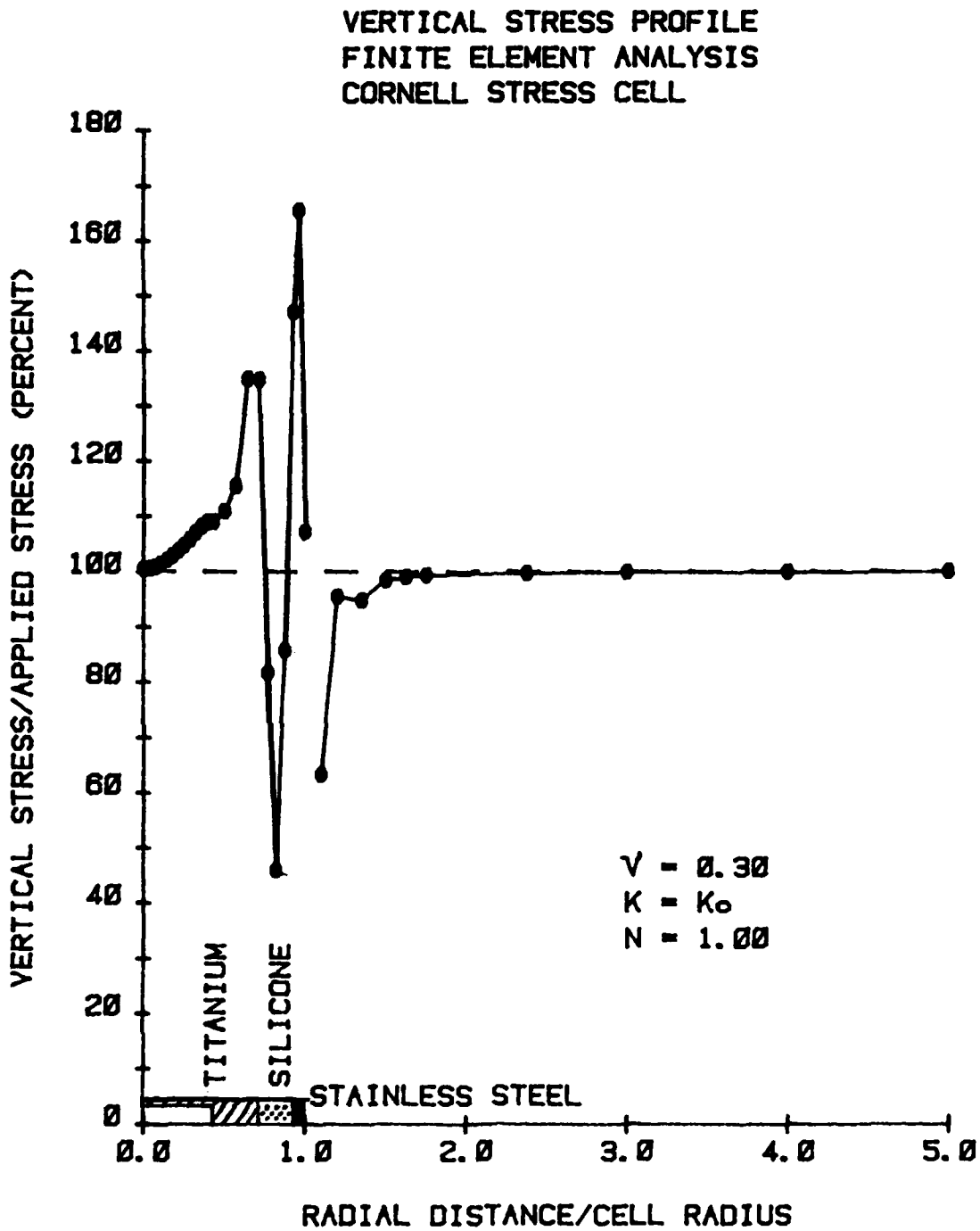

Figure 4.7 Vertical Stress Profile Across the Cornell Stress Cell.

results should be compared to those of the rigid disc subject to the same conditions shown in Figure 4.6. Although the basic form of increasing stress toward the outer edge with a rapid drop in stresss at the edge is similar, there are some major differences. Because the diaphragm of the Cornell Stress Cell deflects under load, the resulting stress on the diaphragm is lower than that of the non-yielding rigid disc. The stress on the centerline of the stress cell is 100.4 percent compared to that of the rigid disc with 105.1 percent. For the same reason the stress on the relatively soft silicone is very low compared to the non-yielding rigid disc. Because of the deflection and resulting decrease in stress over the deflecting diaphragm and soft silicone annulus, the stress on the relatively rigid titanium annulus and stainless steel is higher than that of a disc of uniform stiffness.

Figure 4.8 shows the effects of soil modulus on the response of the Cornell Stress Cell. Isotropic soil properties and Poisson's ratio of 0.3 were used for two different stress conditions, hydrostatic and at rest. The stress on the centerline of the diaphragm, normalized by the applied vertical stress, decreases slightly as the modulus of the soil is increased from 100 to 2000 psi (689 kN/m^2 to 13.8 MN/m^2). This behavior is consistent with the the oretical response (Peattie and Sparrow, 1954) when the cell is much stiffer than the soil. The modulus of dense

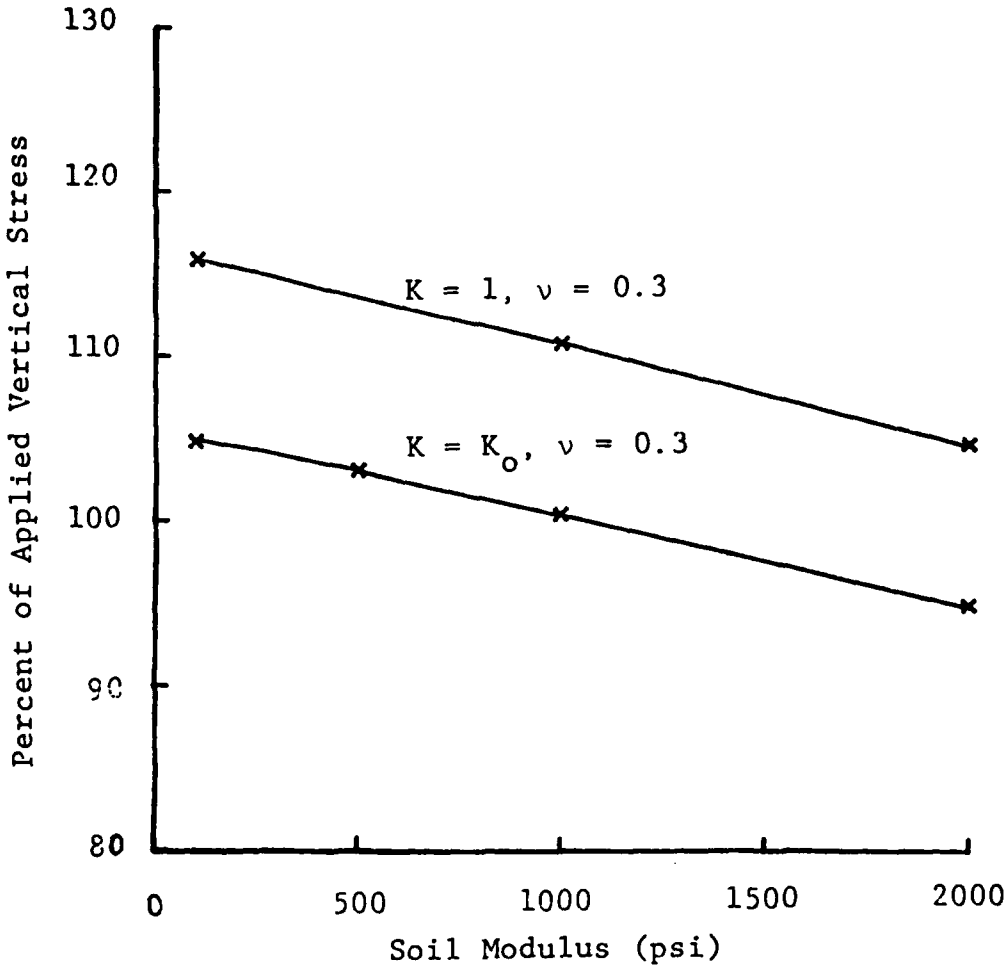

Note: 1 psi = 6.89 kN/m^2

Figure 4.8 Effect of Soil Modulus on Measured Vertical Stress.

filter sand as determined from shaft pullout tests by Stewart and Kulhawy (1981) is 1100 psi (7.58 MN/m^2). Since the modulus of sand increases with density and dense tests in the filter sand created the largest problems in evaluating stress cell response for Stewart and Kulhawy, a soil modulus value of 1000 psi (6.89 MN/m^2) was selected for all subsequent finite element analyses. The effect of variation in the soil modulus was not considered significant for the range of values studied.

To determine the effect of cross-anisotropic soil properties on the response of the Cornell Stess Cell, several finite element analyses were performed with results shown in Figure 4.9. For varying values of Poisson's ratio in both the horizontal and vertical planes and for hydrostatic as well as at rest stress conditions, there are only small changes in the stress cell response as the cross-anisotropy ratio ranges from 0.5 to 2.0. The range of normalized stress is much larger between different values of Poisson's ratio and lateral stress ratio than for the variations in the cross-anisotropy. In all cases in Figure 4.9 the vertical modulus is 1000 psi (6.89 MN/m^2) and the horizontal modulus is varied to obtain the different n values. The response of the Cornell Stress Cell is insensitive to changes in the cross-anisotropy of the soil for measurement of vertical stresses.

The results of the finite element modeling for stress

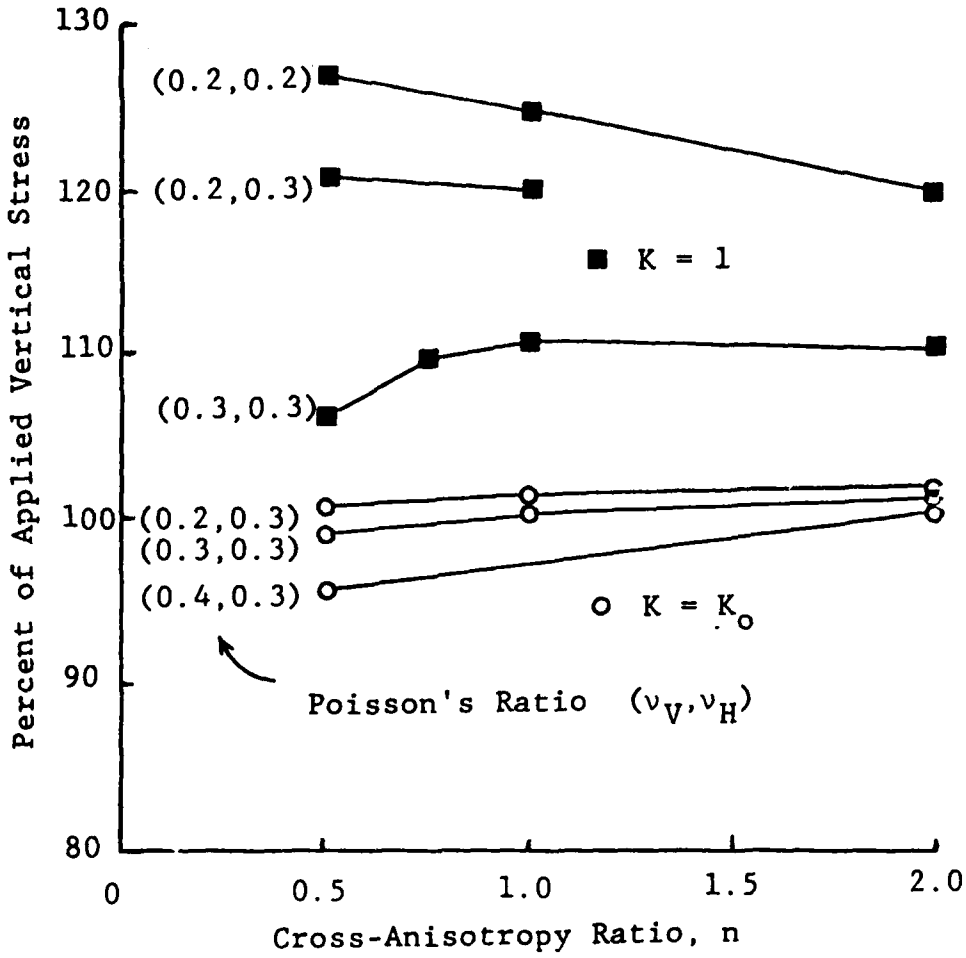

Figure 4.9 Effect of Cross-Anisotropy Ratio on Measured Vertical Stress.

cells oriented to measure vetical stress are shown in Figure 4.10 for variations of Poisson's ratio in the vertical plane. The K_o condition of zero lateral strain with values of cross-anisotropy varying from 0.5 to 2.0 show very little sensitivity to the value of Poisson's ratio in the vertical plane. The value of Poisson's ratio on the horizontal plane is 0.3 for all results in Figure 4.10. For hydrostatic stress conditions the cell response is very sensitive to changes in Poisson's ratio in the vertical plane, especially at low values of Poisson's ratio. For decreasing values of Poisson's ratio in the vertical plane the lateral stress required for K_o strain conditions also decreases as determined from Equation 4.10. Weiler and Kulhawy (1978) and Askegaard (1963) both showed that the effect of lateral stress on the face of a cell increased with decreasing Poisson's ratio. These two counteracting trends of decreasing lateral stress and increasing lateral stress rotation that occur with decreasing Poisson's ratio result in a fortuitous cancellation for the K_o condition. With decreasing Poisson's ratio, the lateral stress is reduced, but a larger portion of that stress is rotated onto the face of the cell resulting in nearly constant stress, independent of the value of Poisson's ratio. Under hydrostatic stress conditions the lateral stress is constant and as a larger portion of the lateral stress is rotated to the face of the cell with decreasing values of the Poisson's ratio,

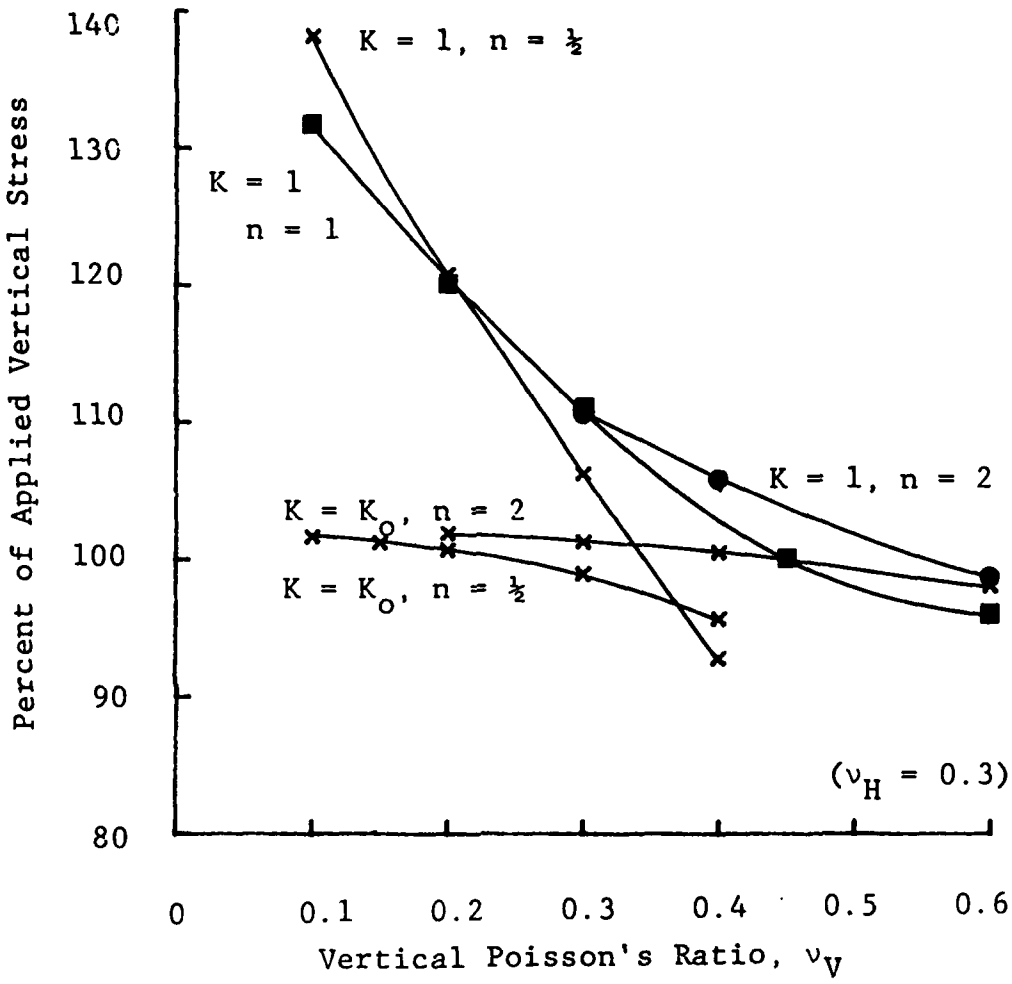

Figure 4.10 Effect of Vertical Poisson's Ratio on Measured Vertical Stress.

the response of the cell increases dramatically.

The effect of Poisson's ratio in the horizontal plane on the response of a stress cell measuring vertical stress is shown in Figure 4.11. For K_o stress conditions there appears to be little effect, just as was shown for Poisson's ratio in the vertical plane, Figure 4.10. Under hydrostatic stress the stress cell response increases with decreases in the Poisson's ratio in the horizontal plane. The amount of change in the stress cell response increases with decreasing values of Poisson's ratio. Therefore a decrease in the Poisson's ratio in either the horizontal or vertical plane will result in an increased response of the stress cell measuring vertical stress.

Figure 4.12 shows the effect of lateral stress on the response of stress cells oriented to measure vertical stress. The stress cell response increases linearly with lateral stress and the rate of increase of the lateral stress rotation changes inversely with Poisson's ratio. As the applied horizontal stress increases, the vertical response of the stress cell changes proportionally. The slope of the plot in Figure 4.11 is very sensitive to the value of Poisson's ratio, with the larger variation in cell response occurring with lower values of Poisson's ratio.

Weiler and Kulhawy (1978) express the measured vertical stress on a stress cell in the form:

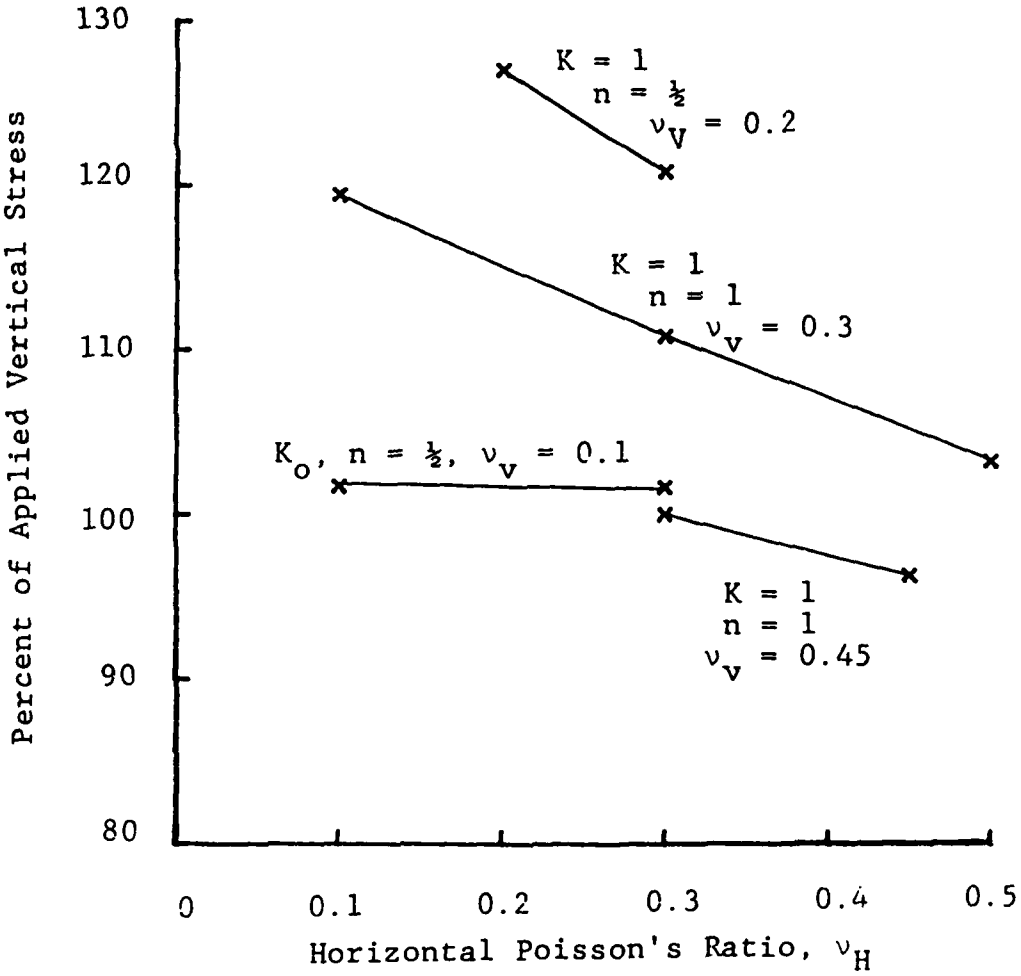

Figure 4.11 Effect of Horizontal Poisson's Ratio on the Measured Vertical Stress.

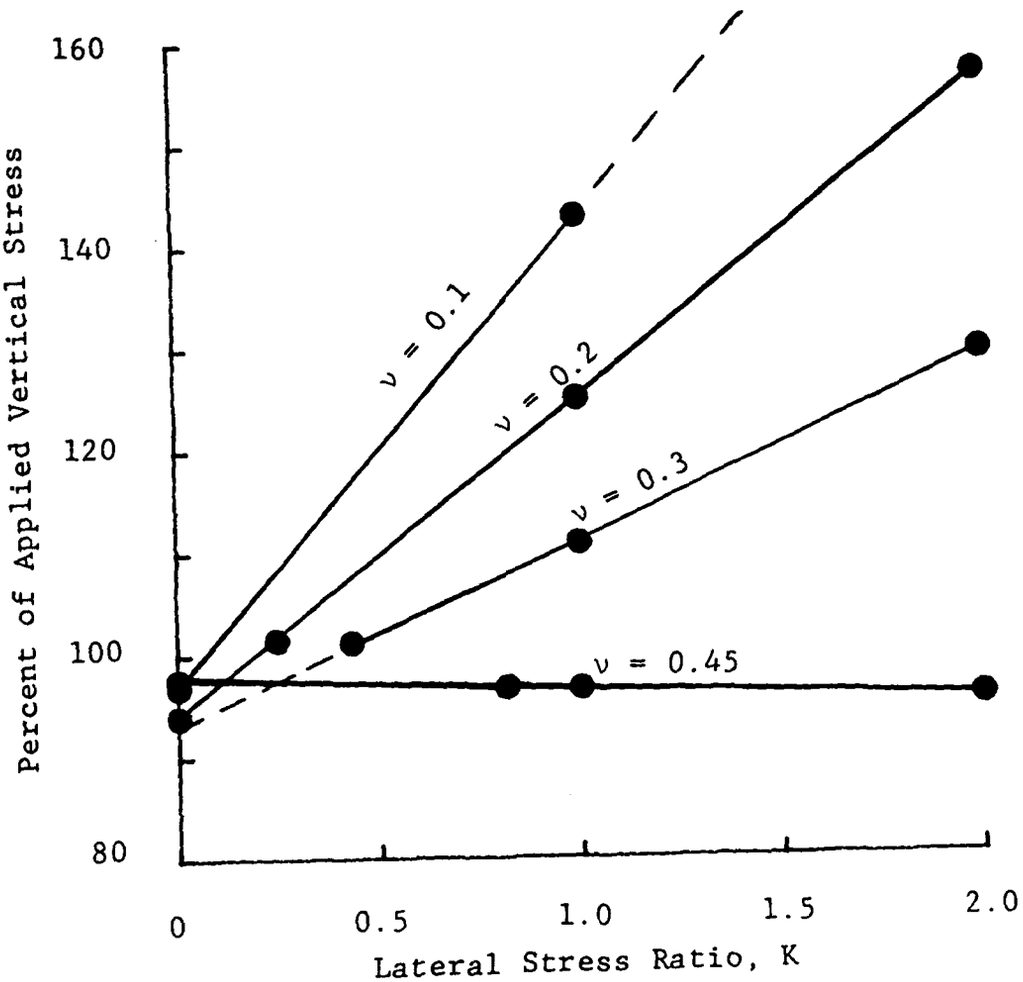

Figure 4.12 Effect of Lateral Stress Ratio on the Measured Vertical Stress.

$$\sigma_{measured} = \sigma_{applied} (R + \mu K) \qquad (4.13)$$

where R is the base registration or cell response in uniaxial stress, K is the lateral stress ratio, and μ is the magnitude of the lateral stress rotation which is a function of Poisson's ratio. From their test results, the base registration was a constant 0.82 and the lateral stress rotation was:

$$\mu = 0.684 - 1.657\nu \qquad (4.14)$$

Expressing the finite element results shown in Figure 4.12 in the same format as Equation 4.13, the base registration value varies slightly with Poisson's ratio and the magnitude of the lateral stress rotation is:

$$\mu = 0.584 - 1.334\nu \qquad (4.15)$$

The base registration is intermediate between the values of Weiler and Kulhawy (1978) for the Cornell Stress Cell and those of Askegaard (1963) for a rigid ellipsoid while the magnitude of the lateral stress rotation is comparable with both as shown in Figure 4.13.

The differences in the base registration values between Weiler and Kulhawy (1978) and this study could be from the

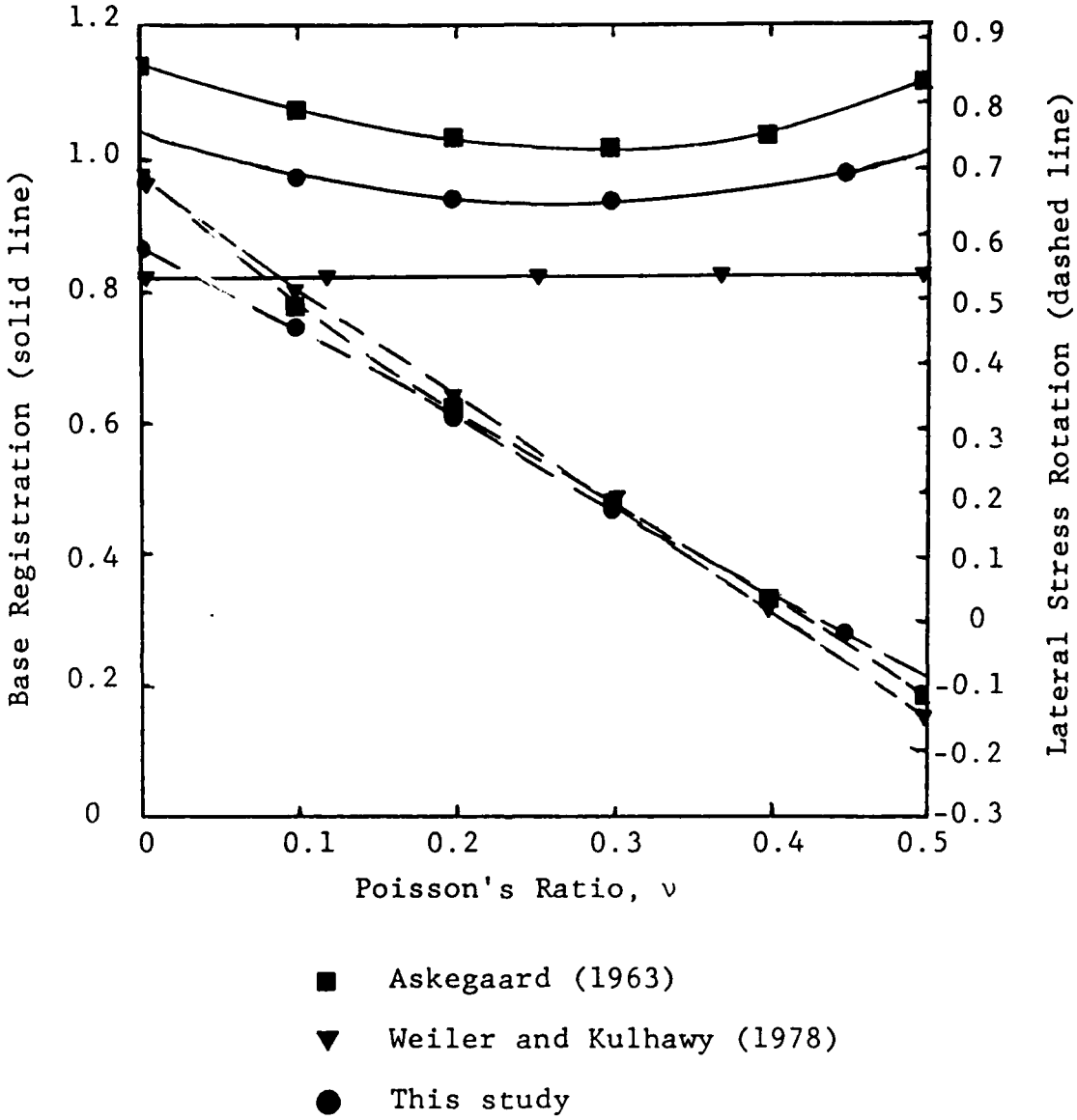

Figure 4.13 Comparison of Base Registration and Lateral Stress Rotation.

values of soil modulus used in the models and/or the method of determining the stress cell response from the finite element results. Weiler and Kulhawy used a soil modulus of 100 psi (689 kN/m^2) and the soil modulus used in this study was 1000 psi (6.89 MN/m^2). The response of the Cornell Stress Cell determined by Weiler and Kulhawy was based on an equivalent uniform pressure necessary to produce a similar diaphragm deflection on a fixed edge diaphragm while this study used the normal stress on the centerline of the diaphragm without any modification or averaging technique applied.

4.4.4 Three-Dimensional Cornell Stress Cell

The fourth and final step in the finite element analysis was to model the Cornell Stress Cell oriented to measure lateral stress. Two vertical and one horizontal planes of symmetry through the center of the cell allowed the cell to be modeled as shown in Figure 4.3. A comparison of the results for hydrostatic stress and isotropic soil properties between the axisymmetric model and the three-dimensional model is shown in Figure 4.14. Although the numerical values are not the same, the behavior is quite similar between the two different models. The axisymmetric model used six, eight noded, isoparametric elements along the radius of the diaphragm while the three-dimensional model used only two, twenty noded, isoparametric elements along the radius of the diaphragm. When the ANSYS postprocesser

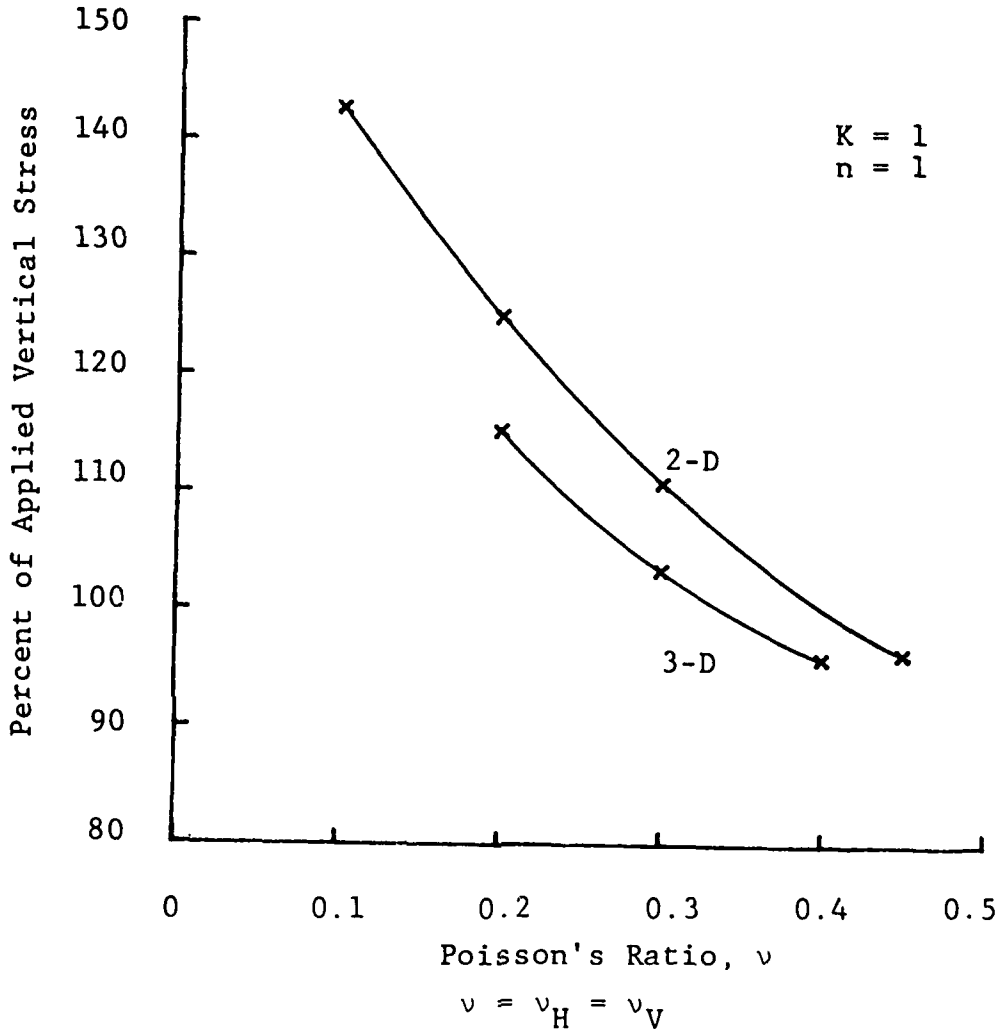

Figure 4.14 Comparison of 2-D and 3-D Finite Element Models.

determined stresses for the two-dimensional model it gives values at each node, or thirteen stress values across the radius of the diaphragm. For the three-dimensional model, ANSYS determines only the stresses at the corner nodes of each element or three stress values across the radius of the diaphragm. These differences between the models could account for the difference in the results shown in Figure 4.14.

The three-dimensional finite element model allows a comparison of the horizontal stress response of the stress cell in the at rest condition with that derived from theory in Chapter 3 for a rigid ellipsoid. The lateral stress expressed as a percent of the applied vertical stress is shown in Figure 4.15 for variation in Poisson's ratio. For three different values of cross-anisotropy the stress cell response parallels the theoretical solution for the rigid ellipsoid. Again the theoretical solution for a rigid ellipsoid is found to be valid for representing trends in the stress cell response.

The results in Figure 4.15 are replotted in Figure 4.16 to show the effect of the cross-anisotropy ratio, n, on the response of the stress cell. The measured lateral stress is seen to increase with increasing cross-anisotropy or as the lateral soil modulus increases since the vertical soil modulus was held constant at 1000 psi (6.89 MN/m^2) for all the three-dimensional analyses. Stress cells measuring

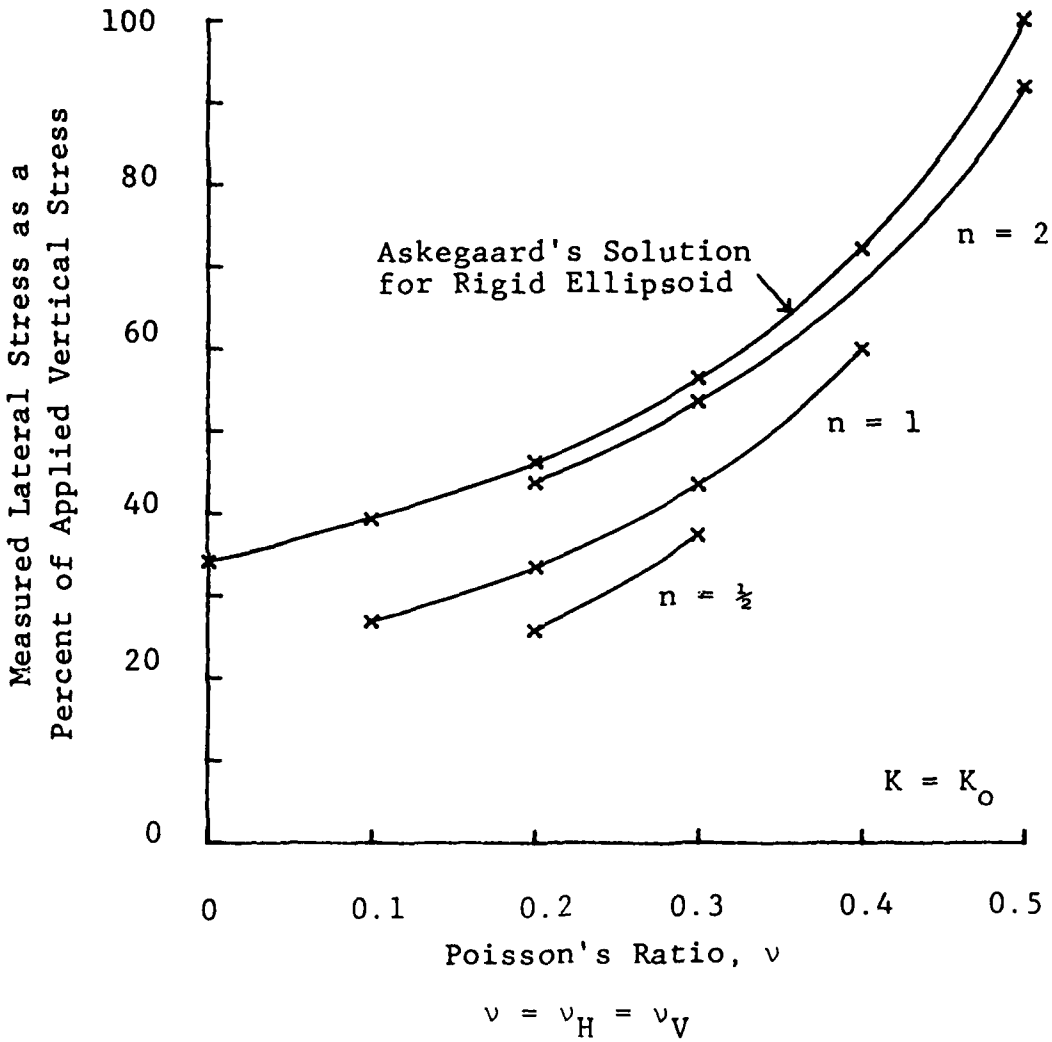

Figure 4.15 Effect of Poisson's Ratio on Measured Lateral Stress.

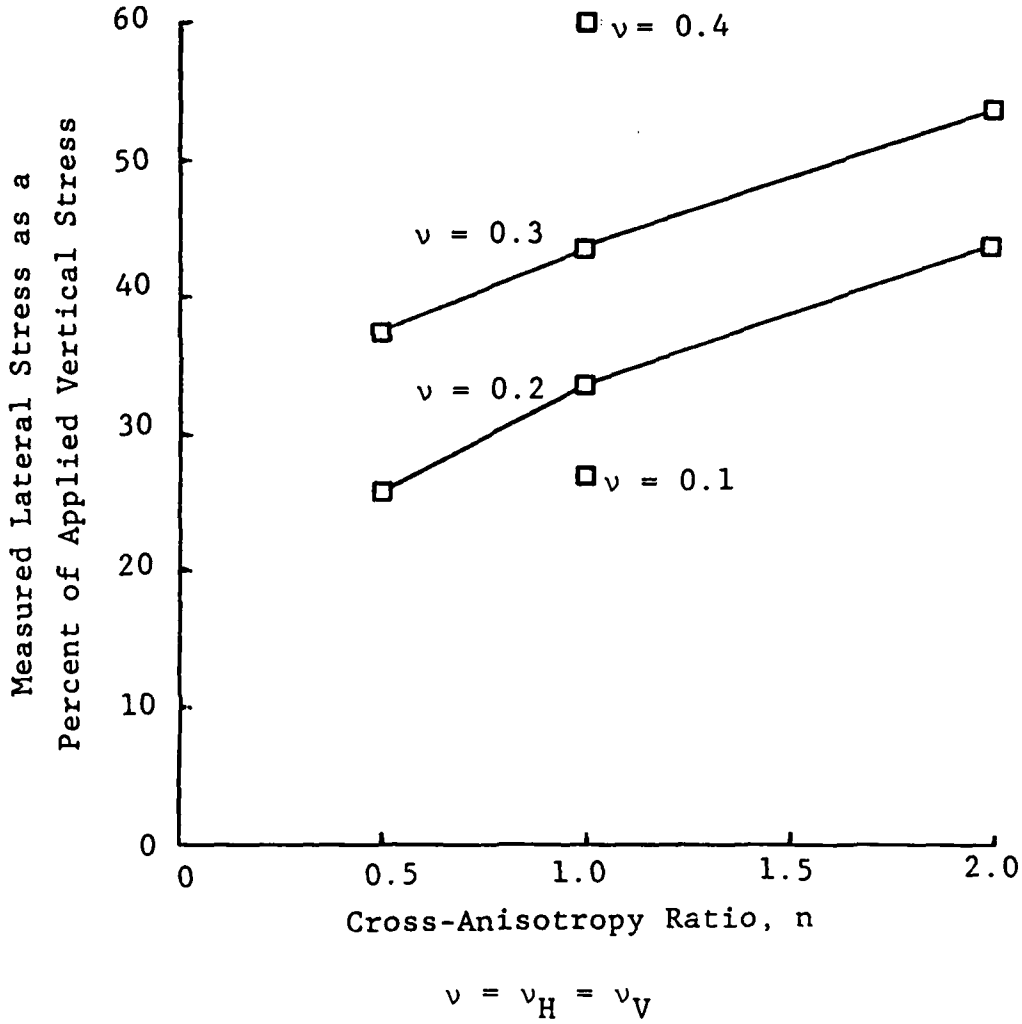

Figure 4.16 Effect of Cross-Anisotropy Ratio on Measured Lateral Stress.

lateral stress are affected by the cross-anisotropic properties of the soil while stress cells measuring vertical stress, Figure 4.9, are insensitive to cross-anisotropy. Loose sand may be characterized by a cross-anisotropic ratio of 0.5 and the value increases to 1.0 as the sand is densified. The response of a stress cell measuring lateral stress to this increse in cross-anisotropy would be to increase also. Stewart and Kulhawy (1981) speculated that a change in the cross-anisotropic ratio, n, might account for part of the reduced response of the stress cell in dense sand. This is not consistent with the pattern of response shown in Figure 4.16. With increasing density of sand the cross-anisotropic ratio increases and with it the response of the stress cell measuring lateral stress.

Although the cross-anisotropic ratio affects the response of the stress cell measuring lateral stress, the Poisson's ratio of the soil has a larger effect. To determine which Poisson's ratio, the horizontal or vertical, has the greater influence on the stress cell response, one value of Poisson's ratio was held constant while the other was varied. The response of the stress cell when the vertical Poisson's ratio was varied is plotted in Figure 4.17. The results are very similar to those when both values of Poisson's ratio were varied together as shown in Figure 4.15. With Poisson's ratio in the horizontal plane varied, the stress cell response is shown in Figure 4.18. This plot

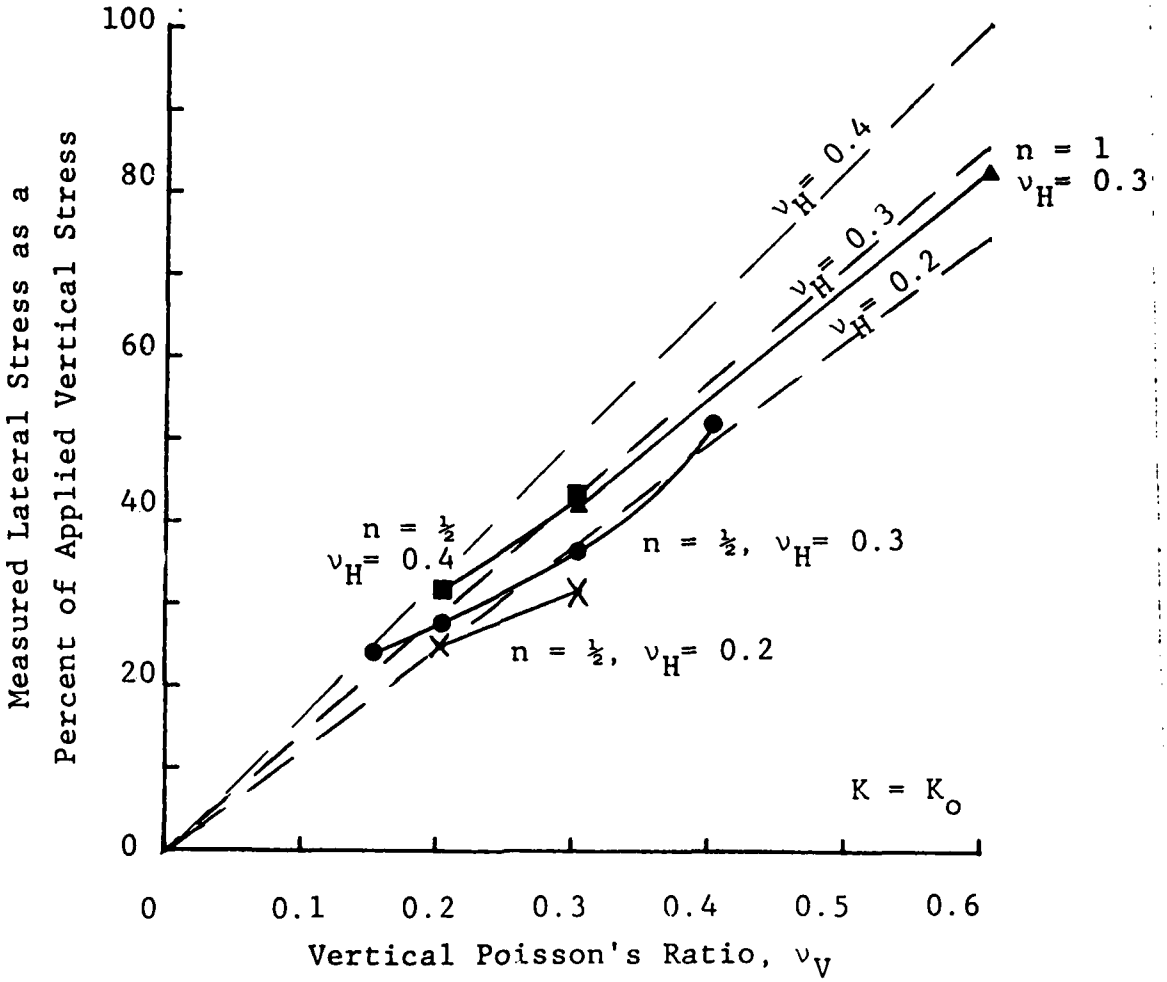

Figure 4.17 Effect of Vertical Poisson's Ratio on Measured Lateral Stress.

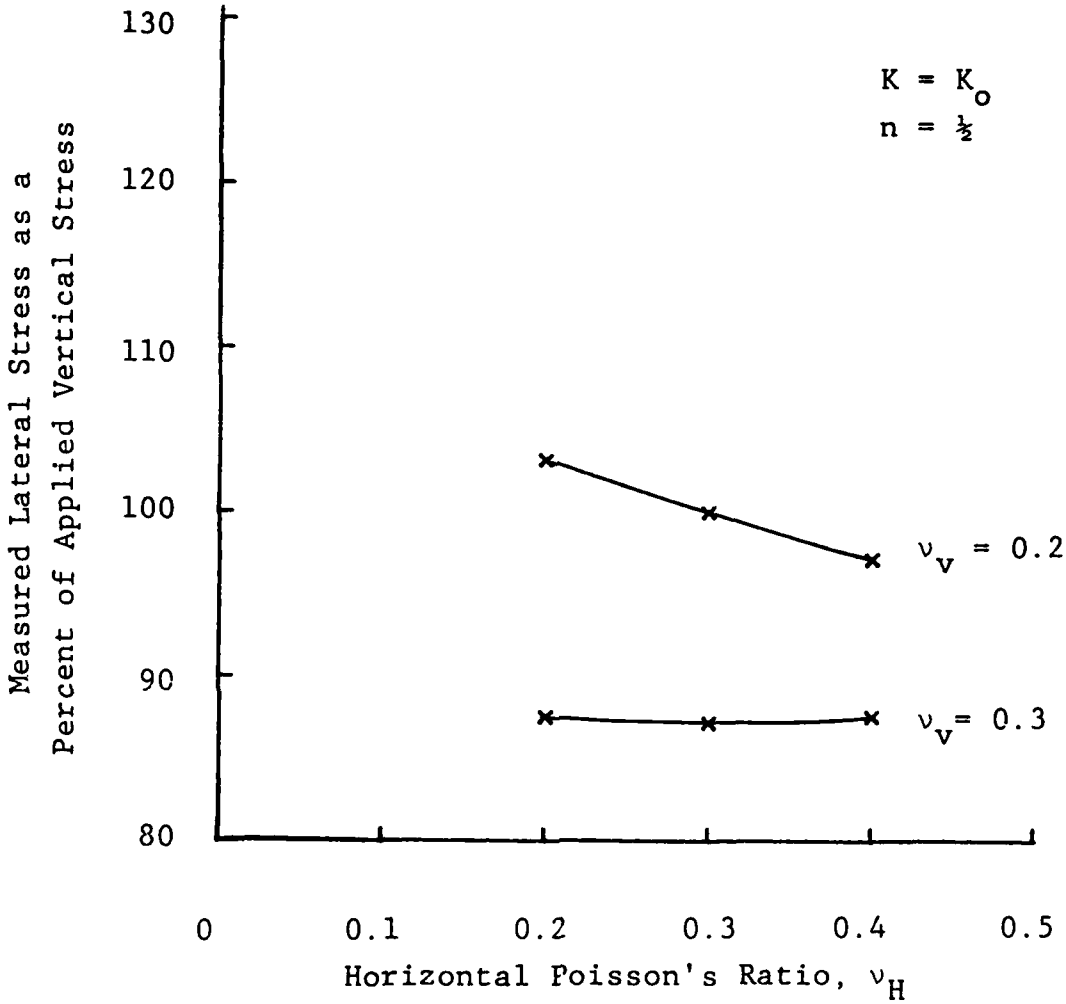

Figure 4.18 Effect of Horizontal Poisson's Ratio on Measured Lateral Stress.

shows the stress cell response normalized by the applied horizontal stress for the at rest condition. There seems to be very little sensitivity to changes in the horizontal Poisson's ratio and this is consistent with the similarities in the response of the stress cell shown in Figures 4.15 and 4.17 where both Poisson's ratios are varied and only the vertical Poisson's ratio is varied respectively. A stress cell measuring lateral stresses is very responsive to changes in the value of Poisson's ratio in the vertical plane and insensitive to changes of Poisson's ratio in the horizontal plane.

The final parameter studied is the response of the stress cell measuring lateral stress to the variation in the applied stress ratio. Figure 4.19 shows for several values of Poisson's ratio and cross-anisotropy the effect of lateral stress ratio on the response of the stress cell measuring lateral stress. The response parallels the free field stress values in all cases. This is quite different from the response of the stress cell measuring vertical stress when the lateral stress ratio was varied as shown in Figure 4.12. For the stress cell measuring lateral stress, the response normalized by the applied vertical stress is directly proportional to the lateral stress ratio for a given value of Poisson's ratio or cross-anisotropy.

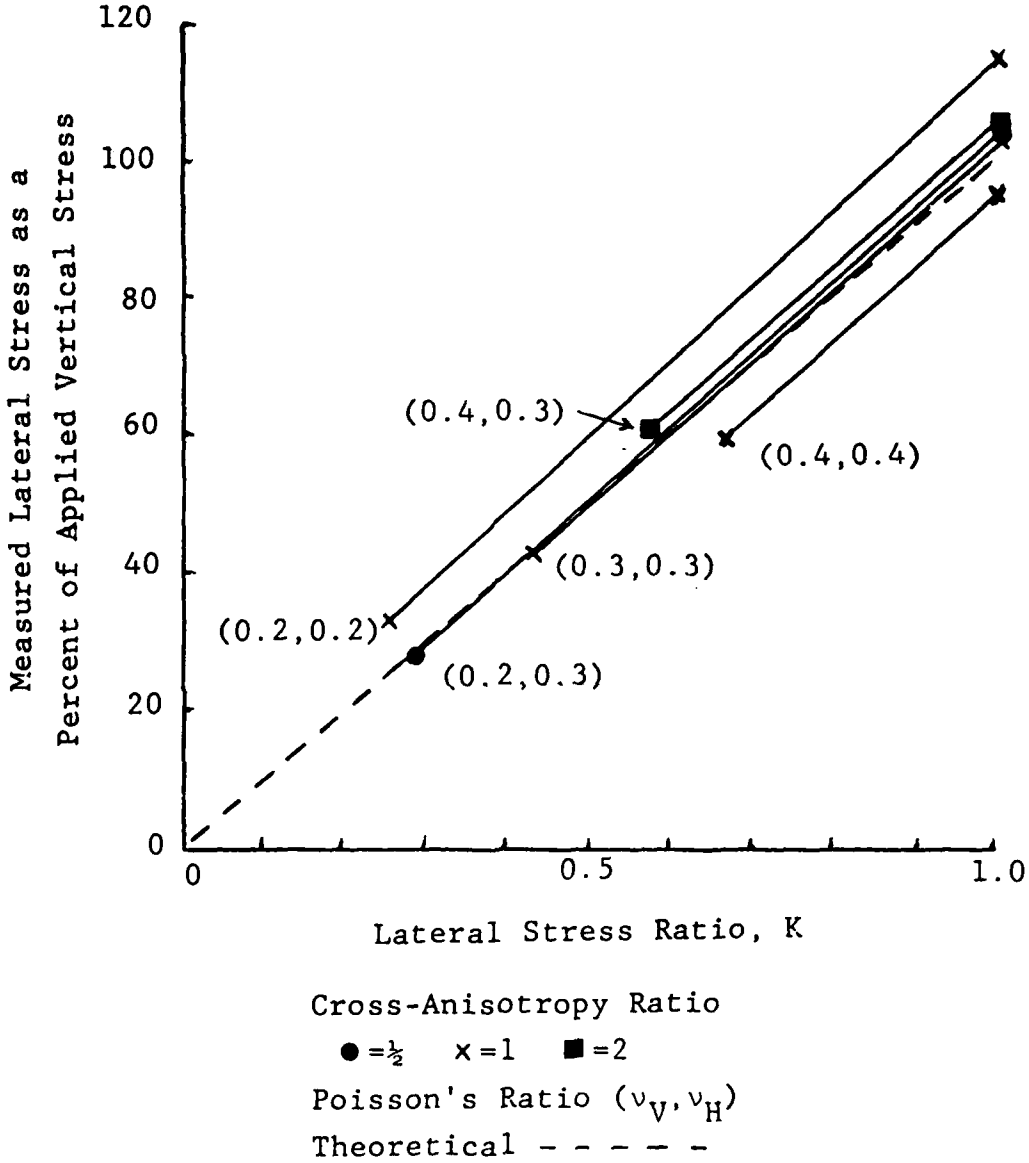

Figure 4.19 Effect of Lateral Stress Ratio on the Measured Lateral Stress.

4.5 CONCLUSIONS

As a result of the finite element analyses performed in this study, the following conclusions can be drawn:

The finite element model results for a rigid ellipsoidal inclusion match the theoretical solution obtained by Askegaard (1963) and discussed in Chapter 3. This step was performed to verify the finite element model and program being used in the analyses.

Results for a rigid disc are nearly the same as for a rigid ellipsoid with the same aspect ratio. This supports the use of the theoretical solution for the ellipsoid to model the behavior of a disc shaped soil stress cell. The differences between a smooth and rough surface between the soil and the stress cell were insignificant. A rough surface with no displacements parallel to the interface was used for all subsequent models.

The response of the Cornell Stress Cell is only slightly affected with changes in the soil modulus for values up to 2000 psi (13.8 MN/m^2). This behavior is consistent with the theoretical response of a cell much stiffer than the soil. The Cornell Stress Cell oriented to measure vertical stress is insensitive to changes in cross-anisotropy. The response is inversely proportional to the value of Poisson's ratio in either the vertical or horizontal planes. Lateral stress rotation, the portion of the lateral stress measured by the stress cell oriented to measure vertical stress, is

inversely proportional to Poisson's ratio. The results from this study are intermediate between the theoretical solution for a rigid ellipsoid (Askegaard, 1963) and the finite element solution of Weiler and Kulhawy (1978).

The results for a stress cell oriented to measure lateral stress parallel the theoretical solution for a rigid ellipsoid with the same orientation. The stress cell response increases with increasing cross-anisotropy for a cell measuring lateral stress. Poisson's ratio in the vertical plane has a pronounced effect on the response of the cell measuring lateral stress. The same cell is largely unaffected by variation in Poisson's ratio in the horizontal plane. The response of the cell measuring lateral stress is directly proportional to the lateral stress ratio.

CHAPTER 5

TESTING EQUIPMENT AND PROCEDURES

In addition to theoretical solutions and finite element modeling of stress cells, an important part of this study was the laboratory calibration and verification of the stress cell performance. The most sophisticated models and elaborate theories are of no use if they cannot be verified by performance. The testing equipment and procedures are described in this chapter with the results shown in the Appendices and discussed in Chapter 7.

The first three sections describe the Cornell Stress Cell used in this study and the equipment and procedures used in calibrating the stress cell in both air and soil. The stress cell, air calibration chamber and soil calibration chamber had all been designed and constructed by Weiler and Kulhawy (1978) and only a few modifications were made as noted in each section.

The fourth section describes the data acquisition system used for air and soil calibration tests. The data acquisition system offered a faster and more precise method of calibrating the stress cells as well as providing the data in digital form for data reduction and plotting by a desktop computer.

Direct shear tests at both constant normal load and constant volume were performed to determine the dilatant

AD-A126 948 LABORATORY DETERMINATION OF HORIZONTAL STRESS IN COHESIONLESS SOIL(U) AIR FORCE INST OF TECH WRIGHT-PATTERSON AFB OH S C BOYCE 1983 2/4

UNCLASSIFIED AFIT/CI/NR-83-4T . F/G 8/13 NL

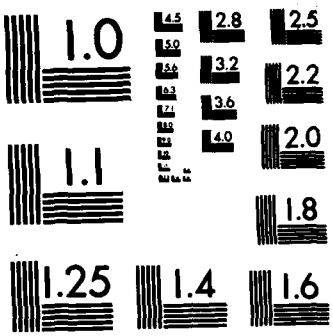

MICROCOPY RESOLUTION TEST CHART
NATIONAL BUREAU OF STANDARDS-1963-A

properties of the filter sand used in the soil calibration tests. These tests are described in section five and help to explain the response of the soil stress cells used in the shaft pullout tests by Stewart and Kulhawy (1981).

5.1 CORNELL STRESS CELL

The soil stress cell used in this study is a deflecting diaphragm strain gaged cell known as the Cornell Stress Cell. The cell was designed by Weiler and Kulhawy (1978) for low stress levels in a laboratory environment. The Cornell Stress Cell was selected for use in this study for two principal reasons:

1. The Cornell Stress Cell was used by Stewart and Kulhawy (1981) in their shaft pullout tests in which major questions arose for the stress cell readings in dense sand. A major objective of this study is to determine the source of these apparent anomalies and provide corrective measures for future applications of the Cornell Stress Cell.
2. The Cornell Stress Cell was designed, constructed and calibrated at Cornell University by Weiler and Kulhawy (1978). That provided a wealth of information on the stress cell including construction details, calibration data and equipment as well as a ready source of stress cells, spare parts and experienced technicians capable of constructing or repairing the instruments.

The Cornell Stess Cell is shown in Figure 5.1 as constructed by Weiler and Kulhawy (1978). The 0.75 inch (19.05 mm) diameter titanium diaphragm was a constant thickness, but the thickness between different cells ranges from 0.012 to 0.030 inches (0.305 to 0.762 mm). The thinner diaphragms provide increased sensitivity but also greater deflection under load than the thicker diaphragms. The optimum conditions would be a very stiff cell with high sensitivity but since both can not be achieved simultaneously, the best compromise for use in filter sand was a 0.020 to 0.025 inch (0.508 to 0.675 mm) diaphragm for the pressure range of 1 to 30 psi (6.89 to 207 kN/m^2).

The silicone and stainless steel outer rings were added to the titanium body by Weiler and Kulhawy (1978) to reduce the cross-sensitivity of the cell. Cross-sensitivity is the response of the strain gage as a result of in-plane stresses on the diaphragm. The combination of stiff and soft rings around the cell greatly reduces the in-plane stress effects on the diaphragm. The rings do not eliminate the problem of lateral stress rotation which is the effect on the stress cell caused by the lateral stresses acting on the material above the diaphragm.

Because the cross-sensitivity of the cell was essentially eliminated by the addition of the outer rings of silicone and stainless steel, a single large strain gage could be applied to the diaphragm. The strain gages used

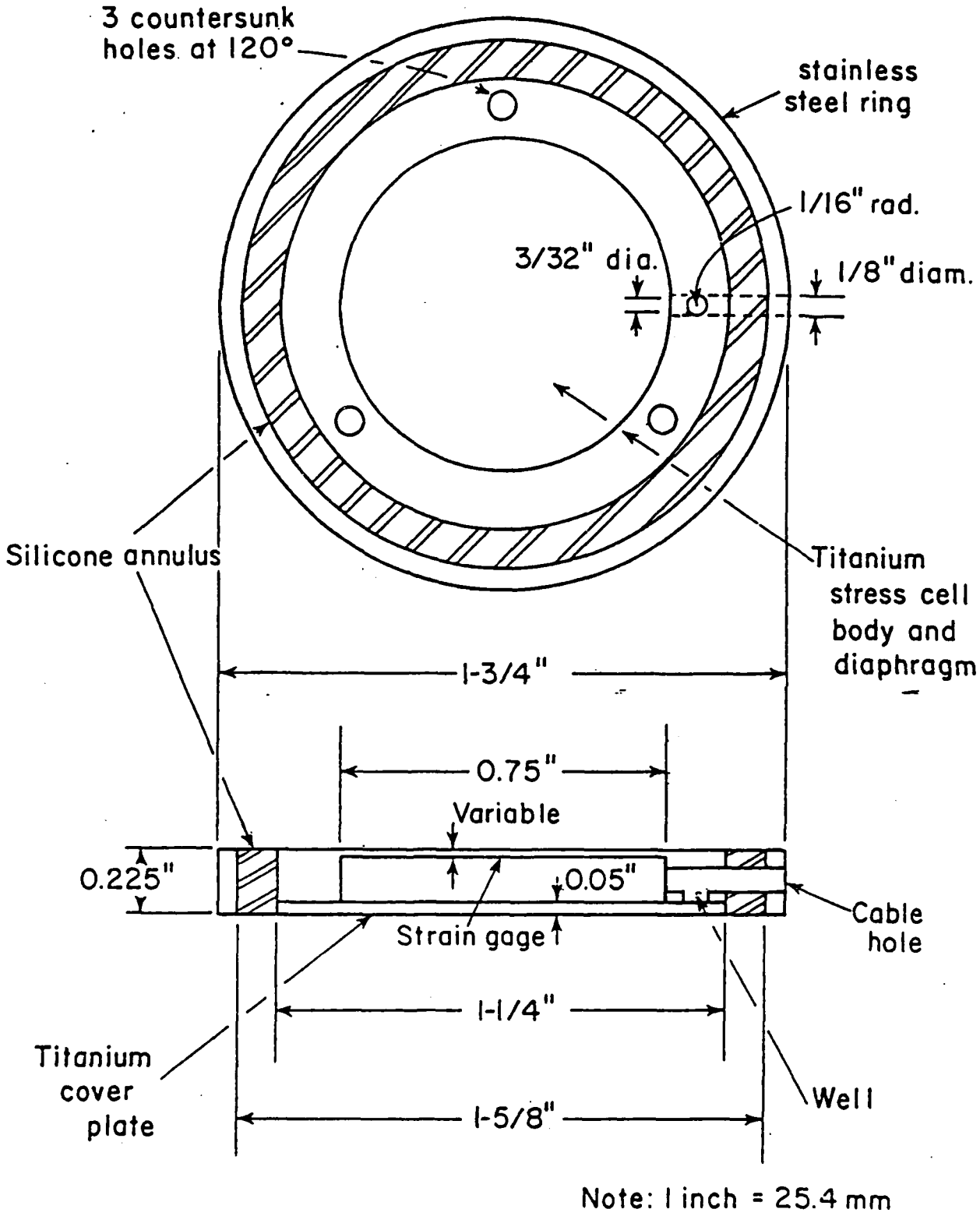

Figure 5.1 Cornell Stress Cell (Weiler and Kulhawy, 1978).

are full bridge, radial and tangential gages specifically designed to optimize the output from a deflecting diaphragm. Similar gages were used as early as 1954 by Redshaw (1954) to provide maximum sensitivity for his soil stress cells.

5.2 AIR CALIBRATION

To convert the output of the strain gage to a stress measurement, it is necessary to calibrate the cell against a known stress. Since the properties of the soil affect the performance of the stress cell, it is important to first calibrate the cell using a fluid. By using a fluid, a uniform pressure can be applied to the diaphragm of the stress cell. The resulting output of the strain gage can be plotted against the known applied pressure to obtain the calibration curve. For ease of calculation and accuracy it is important that the plot of the cell response to the applied pressure be linear and without hysteresis.

The air calibration chamber used in this study was constructed by Weiler and Kulhawy (1978) from a design by Selig (1978) and is shown in Figure 5.2. By sandwiching the stress cell between two butyl rubber diaphragms in the chamber, a uniform uniaxial stress could be applied to the stress cell. By replacing the rubber diaphragms with gaskets, a hydrostatic stress could be applied to the stress cell.

The air supply to the calibration chamber was con-

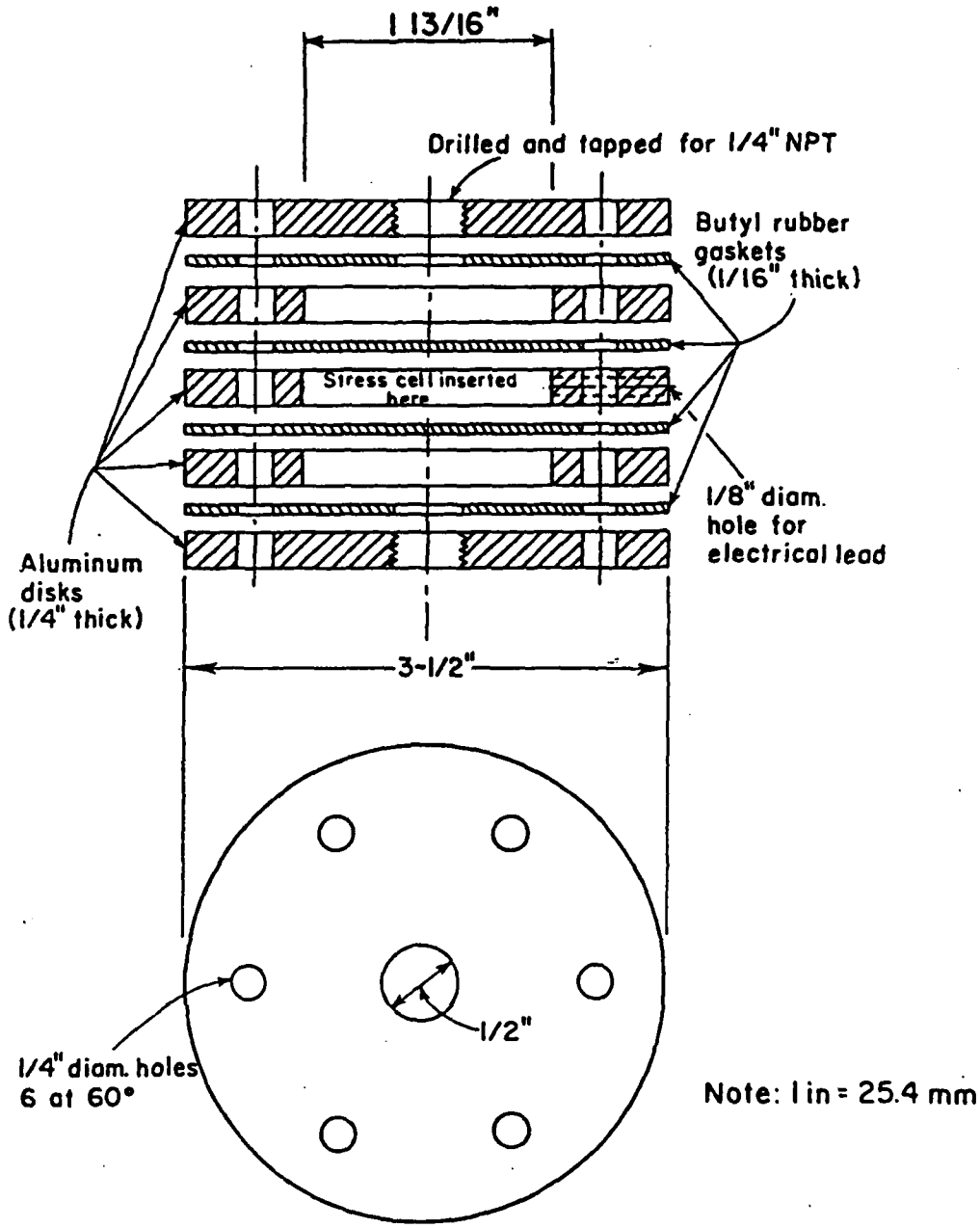

Figure 5.2 Air Calibration Chamber for Soil Stress Cells (Weiler and Kulhawy, 1978).

trolled by a Fairchild-Hiller Model 10 regulator with a range of 0.5 to 30 psi (3.45 to 207 kN/m^2) and an accuracy of 0.01 psi (0.07 kN/m^2). Although the regulator was very accurate the simple dial face was not, and so the air pressure was measured independently on a mercury manometer accurate to 0.2 psi (0.14 kN/m^2) and a pressure transducer. The mercury manometer was read and recorded manually for each pressure applied to the air calibration chamber. The pressure transducer was read and recorded by the data acquisition system described in Section 5.4.

The output of the resistance strain gages was measured by one of two different methods. The first method was to balance manually the electrical output on a Portable Digital Strain Indicator, Budd Company Model P-350 with the output recorded in microstrain. The second method used was the data acquisition system described in Section 5.4 with the output recorded in microvolts per volt of input. To convert the microstrain readings to microvolts per volt, one uses the formula:

$$\frac{\mu V}{V} = \mu\varepsilon \frac{GF}{4} \qquad (5.1)$$

where GF is the gage factor of the strain gage provided by the manufacturer.

The procedure used to calibrate the stress cell was to place the cell in the air calibration chamber with either

the butyl rubber diaphragm or the rubber gaskets, depending on whether uniaxial or hydrostatic stress was desired. Zero readings of the manometer and/or pressure transducer and the stress cell were taken. Air lines with quick-connects then connected the air supply, regulator, air calibration chamber, pressure transducer and manometer. The desired pressure was then applied through the regulator and the cell output and applied pressure recorded. The response of the cell to the applied pressure was not always instantaneous and a time effect was discovered. The time effect is described in detail in Chapter 6 and could be eliminated from the stress cells so that the cell output could be read immediately after applying the pressure. The variation in stress cell output could then be plotted versus the applied pressure to give the air calibration curve. The results are discussed in Chapter 7.

5.3 SOIL CALIBRATION

Calibration of stress cells in the same soil and under the anticipated stress conditions in which they are to be used is essential for accurate measurement of stresses. Because the material properties of the soil such as particle size, modulus, Poisson's ratio and anisotropy can affect the stress cell response, it is necessary to calibrate the stress cells in the same soil in which they are to be used. The magnitude of the applied stress and the ratio of hori-

zontal to vertical stress can also affect the response of a stress cell and must be considered to obtain an accurate indication of the stress cell response.

The soil calibration chamber used in this study was designed and constructed by Weiler and Kulhawy (1978) for calibrating Cornell Stress Cells in filter sand. The soil chamber is shown in Figure 5.3 and consists of an eleven inch (279 mm) inside diameter aluminum pipe which is recessed into stiff aluminum end plates held in place by six threaded rods. A gum rubber sleeve covers the inside of the 16 inch (406 mm) long pipe and goes over the ends of the pipe to act as a gasket between the pipe and the end plates. A separate rubber diaphragm goes over the top of the pipe before placement of the top end plate. Separately regulated and measured vertical and lateral pressures can be applied to the soil through the air supply lines that enter the chamber through the top plate and pipe respectively. Two stress cells can be placed in the soil chamber and the lead wires exit through the base.

With the vertical and lateral stresses being applied separately, triaxial stress conditions can be varied from the condition of zero lateral strain, K_o, through soil failure in triaxial extension. This allows the application of K_o, isotropic or triaxial stress on the soil but not uniaxial stress. The relatively stiff pipe chamber prevents lateral expansion of the soil and so unconfined compression is not possible in this chamber. This is not a serious

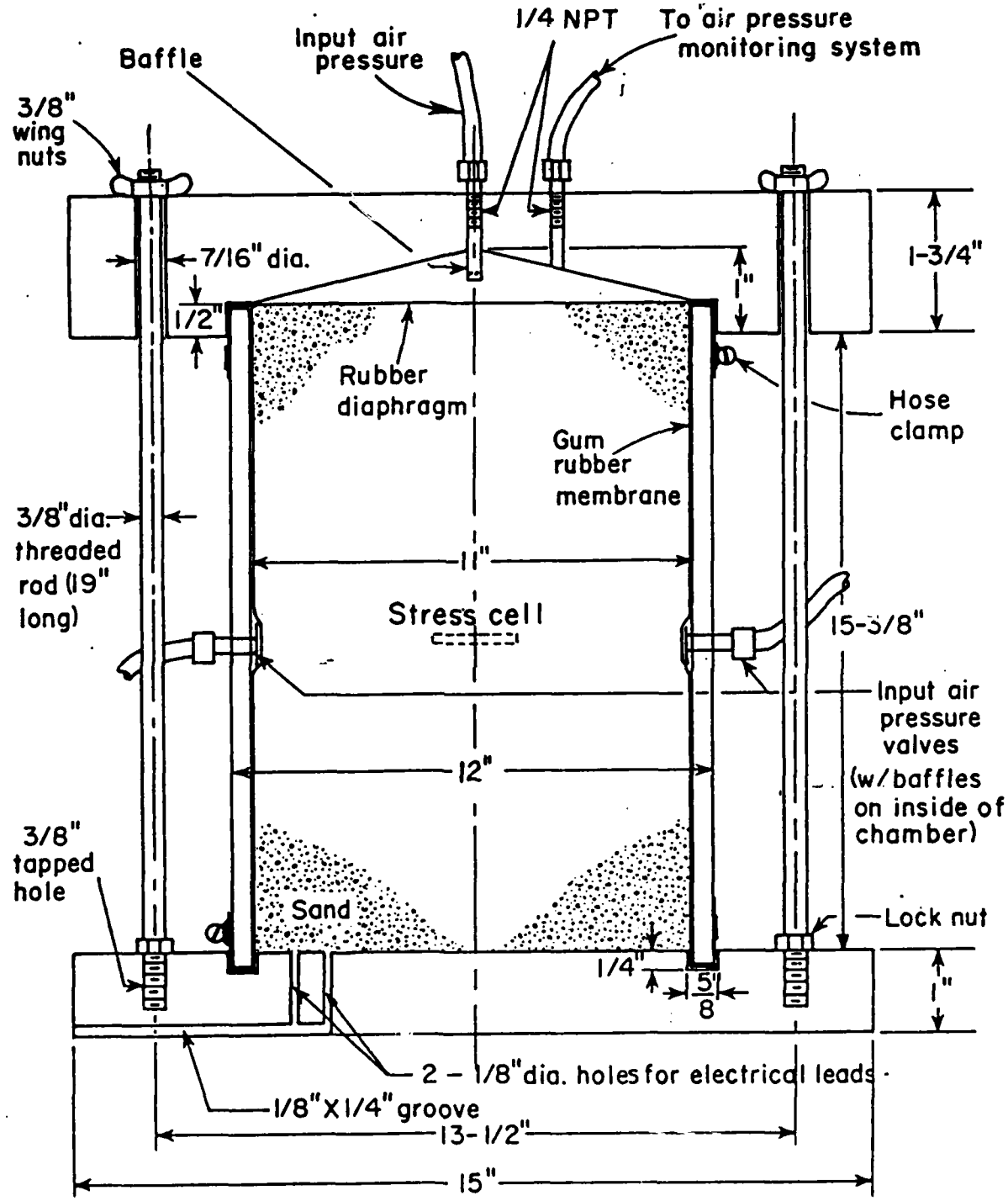

Figure 5.3 Soil Calibration Chamber for Stress Cells (Weiler and Kulhawy, 1978).

drawback, however, since uniaxial stress conditions are rarely found in soil outside of laboratory experiments.

In soil calibration tests, one must assume that the stress being applied to the stress cell is known. Usually the applied stress is assumed equal to the stress on the soil at the stress cell and losses caused by sidewall friction are ignored. For this to be true the friction losses along the sides of the chamber must be reduced as much as possible so the pressure applied to the top of the soil sample is transmitted through the soil and not into the chamber walls. Ingram (1965) measured a thirty percent difference in stress between the 6.5 and 16.5 inch (165 and 419 mm) level of a four foot (1.22 m) diameter soil chamber caused by sidewall friction. One way to reduce the effects of sidewall friction is to make the chamber large so that the effects would not be significant near the center. Osterberg (1940) and McMahon and Yoder (1960) used a soil chamber eight feet (2.44 m) square to calibrate their soil stress cells in an attempt to reduce the friction loss.

Another common method is to allow the soil chamber to compress vertically by using compressible rubber, cork or similar materials between stiff rings to construct the chamber. Kallstenius and Bergau (1956), Bozozok (1970) and Mahmood, Mitchell and Lindblom (1976) all used chambers which were allowed to compress vertically with the soil to reduce friction loss.

Another way to reduce the frictional losses in the soil chamber is to use a low friction material for the chamber. Lazebnik and Smirnov (1964) used polished chrome for their soil chamber to reduce friction. Abbott (1965) studied the transmission loss in soil chambers because of sidewall friction and concluded that the simplest method to reduce friction was a lubricated rubber membrane. This was done in this study by using a second gum rubber membrane along the side of the chamber with silicone grease as a lubricant. The second rubber liner was slightly shorter than the height of the tank so that it could move freely as the soil compressed under load. The silicone is a high viscous grease which allowed displacement between the rubber liners, independently of the magnitude of the lateral stress. For very low stress levels, a dry lubricant such as talc or graphite was used in the early soil tests but was not nearly as convenient as the silicone grease.

One modification of the soil cnamber as constructed by Weiler and Kulhawy (1978) was made for this study. The condition of zero lateral strain, K_o, was important for this study and although that condition could be obtained in the soil calibration chamber simply by assuming the pipe walls were rigid, the magnitude of the lateral stress would be unknown. To measure the lateral stress under the condition of zero lateral strain, a K_o belt was installed in the chamber. The K_o belt is a thin, 0.002 inch (0.051mm),

continuous belt of stainless steel six inches (152 mm) high placed around the soil sample between the two rubber liners. A linear strain gage on the belt was monitored on the manually operated Budd Box and could detect a change in stress of 0.01 psi (68.9 N/m^2). The lateral air pressure could be increased on the soil sample in the calibration chamber as the soil was loaded and the pressure necessary to maintain the strain gage reading constant was the magnitude of the lateral stress for the K_o condition. An added advantage of the K_o belt was that, with the air pressure between the aluminum pipe and outer rubber liner exactly balancing the lateral soil stress, there was no normal stress between the two materials. With no normal stress, the friction between the outer rubber liner and the pipe was eliminated and the only loss due to sidewall friction would be from the slight elongation of the rubber liner near the top of the chamber.

The soil calibration of stress cells required about six hours for set up and testing. The aluminum pipe section was set upon the base plate with the rubber sleeve in place and the K_o belt if desired for that test. A generous portion of silicone grease was applied to the rubber sleeve and the second rubber liner put in place. A small vacuum line was attached to the lateral pressure port to draw the liners up tightly against the pipe section until the soil could be put in place. The cables from the stress cells were threaded

through the holes in the bottom plate along with the K_o belt strain gage cable and the holes sealed with wax to prevent soil loss. Soil placement in the chamber depended on the desired initial density for testing. A funnel with a quarter inch (6.35 mm) wide spout was used to place the sand with zero fall to obtain the highest possible void ratio. Increasing densities were obtained by allowing the sand to rain through the funnel and fall 1, 4 or 8 inches (25.4, 100 or 200 mm). The stress cells were placed at the desired level by simply placing them on the surface and continuing soil placement as before. The initial unit weight of the soil was determined by subtracting the remaining soil from the starting weight of soil and dividing by the volume of the chamber, 0.853 ft^3 (0.0242 m^3). Two other methods of soil placement were used to obtain higher unit weights. Soil was placed in four equal lifts and compacted with a ten pound (44.5 N) drop hammer dropped onto a plywood disc covering the layer. The number of blows per lift depended on the desired final density. The soil was also densified by placing the entire soil calibration chamber on a shaking table and, with a dead weight load applied to the top surface of the soil, the chamber was vibrated to achieve the desired density. Angle iron brackets fastened to the threaded rods were used to hold the pipe section securely to the base during vibration to prevent soil from getting caught between them where the sand grains could puncture the rubber liner.

Once the soil and stress cells were in place the top rubber diaphragm and cover plate were secured with bolts on the threaded rods. The same air pressure regulators, manometer and pressure transducers used in the air calibration were connected to the vertical and lateral pressure ports in the soil calibration chamber using quick-connect hoses. For K_o tests the lateral pressure was adjusted as necessary to maintain a constant output from the strain gage on the K_o belt as the vertical pressure was applied. Readings of the stress cells, usually two cells per test, and applied pressures were taken at increments of pressure both loading and unloading. The data acquisition system described in Section 5.4 greatly simplified the data collection and allowed the test to be performed quite rapidly, usually taking only twenty minutes. For isotropic or hydrostatic stress conditions only one air pressure regulator was used and the hoses were connected so as to provide the same air supply to both the vertical and horizontal ports. Triaxial tests were performed by applying the vertical and lateral pressures separately either neglecting the K_o belt or not even having it in place during the test. Triaxial tests included a constant stress ratio test and triaxial extension with the lateral stress increasing to fail the soil under a constant vertical stress.

5.4 DATA ACQUISITION SYSTEM

A data acquisition system was essential for recording the output of the soil stress cells as it varied with time. Because the initial change in response occurred more rapidly than could be recorded on the manually operated system, the following data acquisition system was used.

The system was a Hewlett-Packard HP-3052A Automatic Data Acquisition System controlled by an HP-9825A desktop computer. Power to the instruments was provided by a zero to nine volt direct current HP-6281A power supply through an interface bank of twenty, five pin Amphinol plugs. Two forty channel HP-3495A scanners allowed as many as eighty instruments to be used at any one time although only five were used at any one time in this study. The electrical output of any channel could be read by an HP-3455A digital voltmeter to an accuracy of one microvolt DC with a maximun frequency of twenty-three readings per second. The entire data acquisition system including the power supplies, interface plugs, scanners and digital voltmeter were all conveniently housed in a wheeled cabinet.

The programmable desktop computer, HP-9825A, controlled the operation of the data acquisition system and permitted channel selection, frequency of readings and recording of data. The raw data of voltage in digital form was typically stored in an array and recorded on tape for each test. Additional programming allowed the raw data to be manipu-

lated and converted into more usable form. An HP-82905A matrix printer was used to obtain a hard copy of the reduced data as each test was performed. The computer was also programmed to allow the test results to be plotted on an HP-7225A plotter.

Once a test was programmed on the computer the data were taken, recorded, reduced and printed and the test results were plotted without any manual interference, which provided speed and precision for the laboratory tests. Because of the tremendous convenience of using the data acquisition system, it was used for most of the air and soil calibration tests. All measurements of stress cell response and applied pressures could be and were taken manually using the Budd Box or mercury manometer, respectively. Manual readings were taken periodically throughout the testing program to ensure the automatic system was giving results consistent with the manual results.

5.5 DIRECT SHEAR AT CONSTANT VOLUME

A key to understanding the performance of soil stress cells in dense granular material is the dilatancy of the soil. One of the most common methods of measuring the volume change characteristics of a sand is to plot the variation in sample height during a direct shear test in which the normal load is held constant. Typical test results are shown in Figures A.5 through A.13 for the filter

sand used in this study.

Another method of determining the dilatancy of the dense granular material would be to measure the increase in normal load necessary to shear the soil at constant volume. This was considered to be similar to the conditions of the dense soil as it was sheared by the pullout of a shaft as performed by Stewart and Kulhawy (1981). The dense sand in zero lateral strain, K_o, conditions could increase in volume only slightly when sheared and therefore the stress would increase as in the constant volume direct shear test.

The volume of the soil in the shear box was held constant during shear by varying the load on the hanger. A lever with the fulcrum on the hanger and the short end secured to the shear frame by an ajustable turnscrew was used to apply load on the soil. The long arm of the lever with a mechanical advantage of five to one was secured to the shear frame by a heavy proving ring to measure the applied normal load. As the proving ring deflected to measure load the turnscrew was adjusted at the other end of the lever to maintain the position of the fulcrum to within 0.001 inch (0.025 mm).

The constant volume direct shear test was performed by first placing the filter sand in a standard square shear box at the desired density. The top cap and hanger were placed on the shear box and zero readings taken on four dial gages, two measuring the horizontal and vertical displacements of

the shear box and two in steel proving rings measuring the horizontal and vertical loads on the shear box. The sand was then sheared at a constant rate of horizontal displacement. As the dense sand sheared and attempted to dilate, the hanger could deflect vertically only as the proving ring on the lever deflected. To prevent any vertical expansion of the sample, the turnscrew on the short arm of the lever was adjusted to compensate for the deflection of the proving ring. With a five to one advantage in the lever, it was quite easy to maintain the hanger and therefore the soil sample at nearly constant volume. Once the sand passed the peak shear stress, the normal load on the hanger had to be reduced to maintain constant volume which again was easily done by adjusting the turnscrew. Results from these constant volume direct shear tests are included in Appendix D and discussed in Chapter 7.

5.6 CONCLUSIONS

The equipment and procedures used in this study have been described in this chapter. These include the Cornell Stress Cell, air and soil calibration of stress cells, the data acquisition system and constant volume direct shear tests on filter sand. The results from these laboratory tests are included in the appendices and summarized in Chapter 7. An attempt was also made to measure the variation in the soil density around a stress cell by freezing

the samples. This was not successful as explained in Appendix F.

CHAPTER 6

TIME EFFECTS OF THE CORNELL STRESS CELL

With the original design and construction of the Cornell Stress Cell (CSC), the thin diaphragm deflection was measured by a special radial and tangential strain gage and it was assumed that the gage would provide nearly instantaneous response to the applied pressure. In their calibration tests, Weiler and Kulhawy (1978) state that "The response of the cell to the air pressure was nearly instantaneous."

However, while performing a rapid calibration of the stress cells in the air calibration chamber, it was discovered that a hysteresis developed in a load-unload cycle. This hysteresis, Figure 6.1, resulted in a positive strain reading after all load had been removed and it was soon discovered that the strain readings increased with time for each load increment and decreased with time for each unload increment. Figure 6.2 shows the variation in output of one cell when holding the pressure at each load increment constant for ten minutes. In an effort to quantify this time effect, numerous time readings on the CSC were conducted and all probable causes of time effects on strain gages were considered. The ensuing investigation resulted in a mathematical procedure for quantifying the time effects, defining the cause, and obtaining a design change to eliminate the problem.

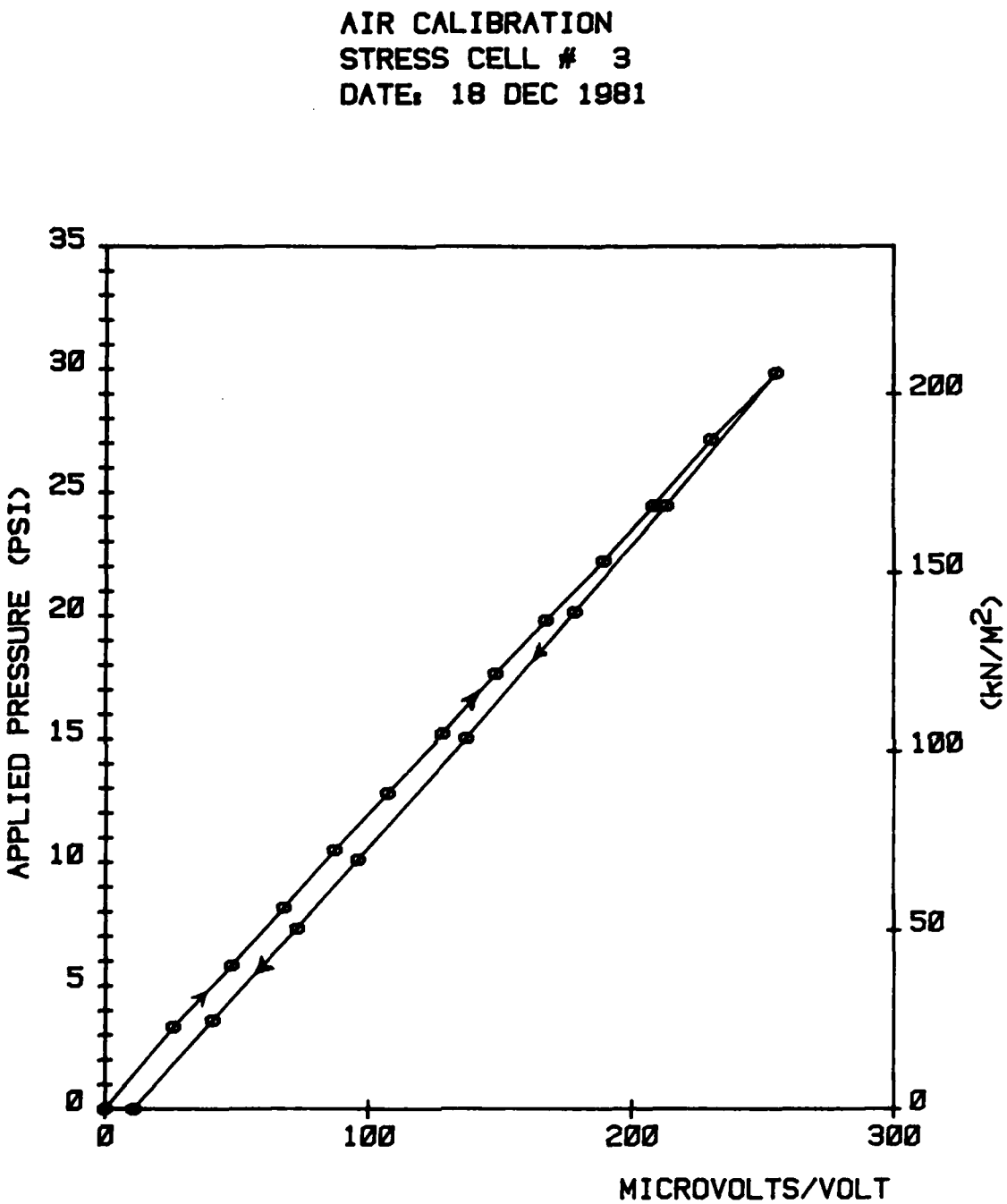

Figure 6.1 Time Effect of Cornell Stress Cell during Air Calibration Test.

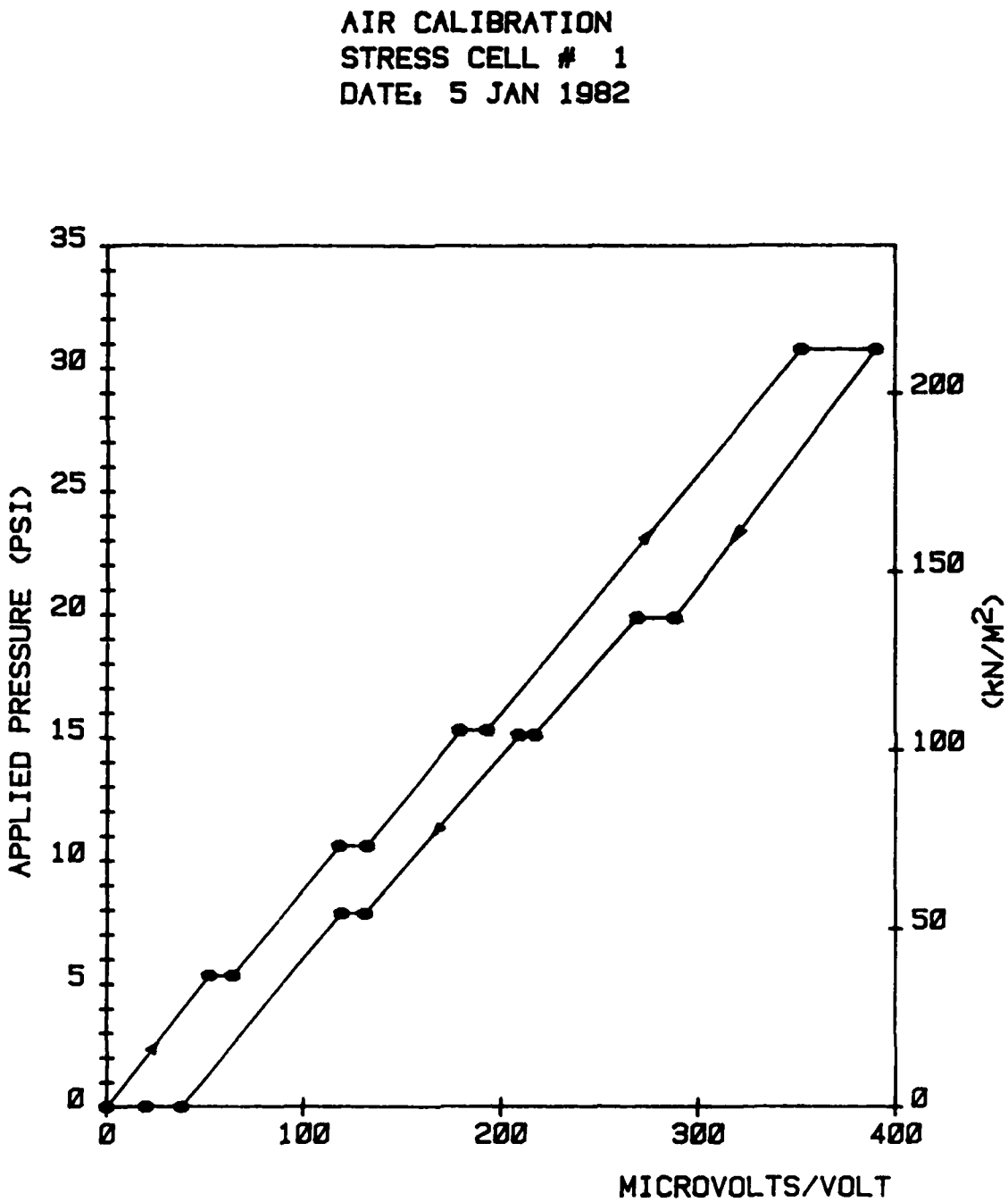

Figure 6.2 Time Effect on Cornell Stress Cell with each Pressure Increment held Constant for Ten Minutes.

6.1 QUANTIFYING THE TIME EFFECT

To define the problem it was necessary to perform extensive tests on the stress cells with time as a variable. Since a major portion of the response occurred within the first few seconds of the applied pressure change it was essential to measure the time response within seconds of varying the load. This was not possible with the manually operated Budd Box, Vishay Model P-350 Portable Strain Indicator. Because of the inability to measure rapid changes in the stress cell response with the manual device, a data acquistion system capable of sampling at a maximum rate of 23 times per second was used for data collection. This system was described in Section 5.4.

The test results showed that the cell response increased at a decreasing rate with each pressure increment and decreased at a decreasing rate with each unload increment, Figure 6.3. The trend seemed quite similar for both loading and unloading cycles, but opposite in sign, and also seemed to vary in proportion to the loading or unloading increment. The results of the time tests were normalized by dividing by the pressure increment and plotted versus log time to obtain a linear variation. This allows the time effect to be expressed as a percent error of the pressure increment per log time. The percent error per log time varied for each cell tested but typical values were two to three percent, with cell number one having an error of

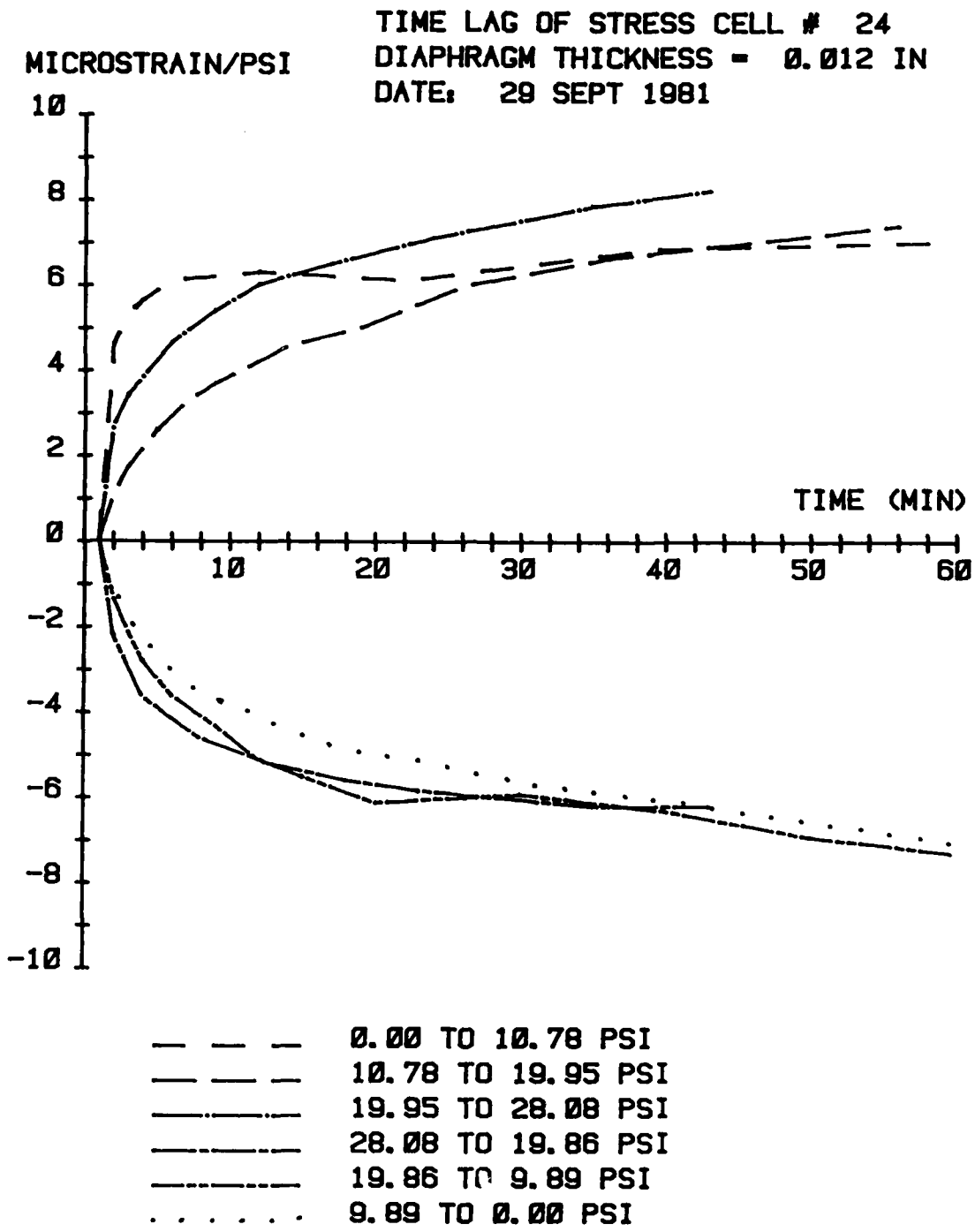

Figure 6.3 Stress Cell Variation with Time, Normalized by the Load Increment.

nearly six percent as shown in Figure 6.4. One minute after applying the pressure increment was arbitrarily chosen as the zero value to standardize the test results, although any time value could have been used with the same results.

Although the time effect could now be taken into account in using the Cornell Stress Cell, the underlying cause had not yet been determined.

6.2 POSSIBLE CAUSES OF TIME EFFECTS IN CSC

Possible causes of time related changes in SR-4 strain gages include: temperature variation, variation in power supply, strain in excess of the gage limits, cement instability and gage creep. Possible causes of time related changes in the stress cell itself include variation in the applied pressure and pressure in excess of the yield stress of the cell diaphragm. Each of these possibilities was considered as a cause for the time effects as measured in the laboratory.

The possible causes from the stress cell itself were considered first, and eliminated as causes for the time effect. The pressure applied to the stress cell was controlled by a Fairchild-Hiller Kendall Model 10 pressure regulator capable of holding a set pressure to within 0.01 psi (0.069 kN/m^2). The pressure was independently measured on a mercury manometer scaled from zero to thirty psi (0 to 207 kN/m2) and read to within one millimeter of mercury

TIME LAG OF STRESS CELL # 1
DIAPHRAGM THICKNESS = 0.020 IN
CALIBRATION CONSTANT = 0.06619 PSI/μV/V
DATE: 5 JAN 1982

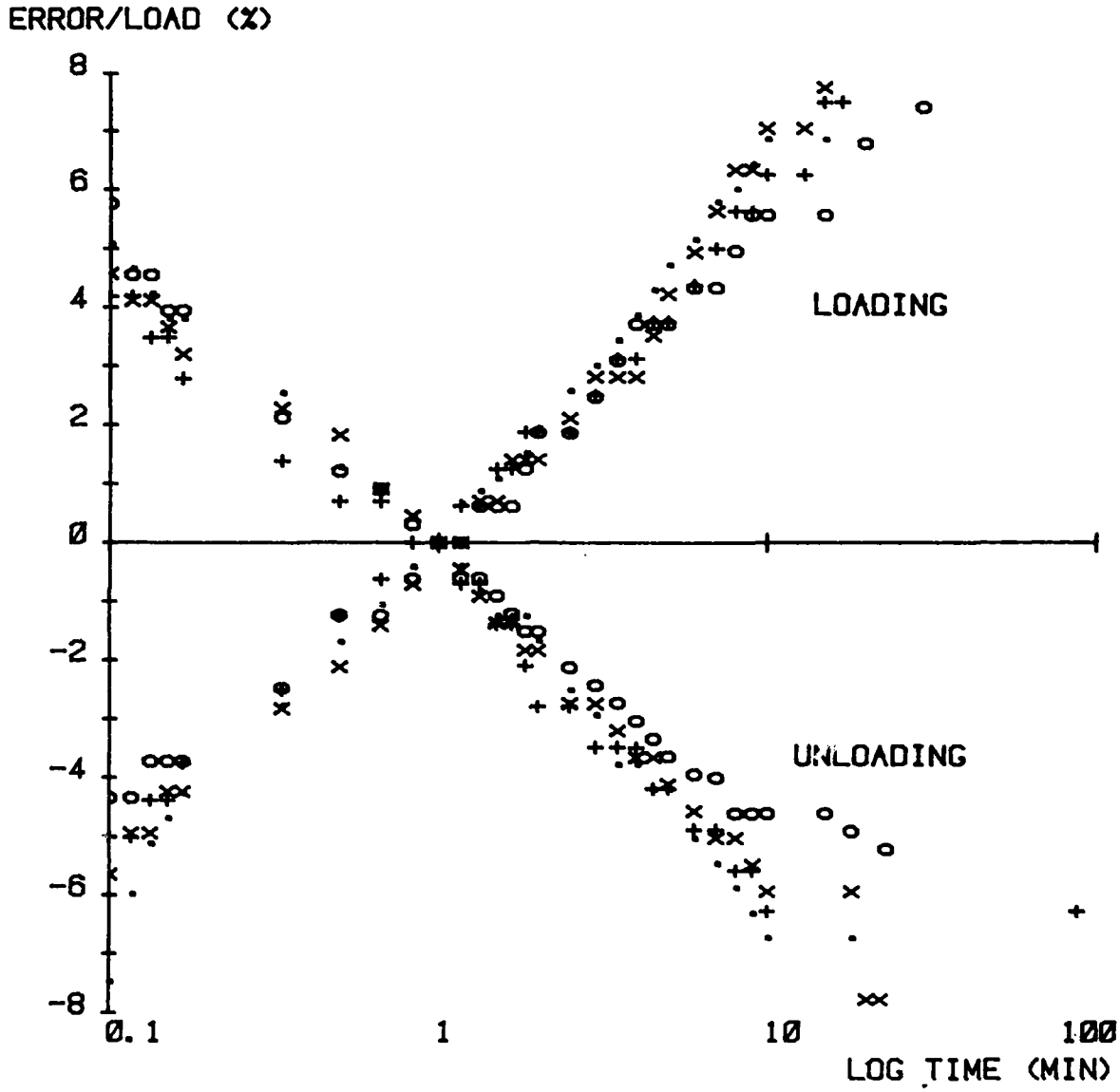

o	0.00 TO 5.33 PSI	o	30.76 TO 19.85 PSI
+	5.33 TO 10.61 PSI	+	19.85 TO 15.10 PSI
×	10.61 TO 15.30 PSI	×	15.10 TO 7.86 PSI
.	15.30 TO 30.76 PSI	.	7.86 TO 0.00 PSI

Figure 6.4 Percent Error per Log Time for Time Effect of the Cornell Stress Cell.

which corresponds to 0.014 psi (0.097 kN/m^2). At no time during testing was there ever a variation in pressure beyond these limits, which are of the same magnitude as the stress cell sensitivity. Therefore variation in pressure can not explain the time effect.

If the pressure applied to the stress cells creates stresses in the diaphragm that approach the yield stress of the material, titanium, then metal creep could occur and cause a time effect. According to Timoshenko (1955), a uniform pressure on a fixed edge circular diaphragm creates a maximum stress at the inside edge of:

$$\sigma_{r_{max}} = \frac{3\ p\ r^2}{4\ t^2} \tag{6.1}$$

in which: p = uniform pressure, r = radius of the diaphragm and t = diaphragm thickness. Even the cell with the thinnest diaphragm of 0.012 inches (0.305 mm) could sustain a pressure of 95.6 psi (659 kN/m^2) before first yield occurs. At stresses below yield and at room temperature, the titanium has negligible creep; it is the ability of titanium to sustain high loads at elevated temperatures that make it useful in the manufacturing of jet engine turbine blades. Therefore the metal creep was eliminated as a possible source of the time effect.

The time related causes of change in SR-4 strain gages were considered as sources of the CSC time effect. A

uniform temperature change can create a change in the strain gage output by inducing a strain proportional to the temperature change. By selective placement of the gages, and matching the coefficients of thermal expansion between the gage and the base metal, a temperature compensating gage may be constructed (Perry and Lissner, 1955). The gages used in the Cornell Stress Cell are of the temperature compensating type: Micro-Measurements EA-05-683JC-120 and Baldwin Lima-Hamilton FAES 4-69-35-S5EL. The coefficient of thermal expansion of titanium is 4.9 parts per million (ppm) per degree Fahrenheit and of the gage is 5.0 ppm/^{o}F. The stress cell should be relatively insensitive to a uniform temperature change. Cells tested in the laboratory showed a variation in the zero value of one microstrain (ppm) per degree Celsius and no change in the slope of the calibration line as shown in Figure 6.5. The calibration tests which displayed the time effect were performed in a temperature controlled room with the cell installed in the aluminum air calibration chamber which would further protect the cell from transient temperature variations such as drafts.

The temperature can also cause change in the strain cell output if a thermal gradient existed across the diaphragm. The diaphragm will deflect because of uneven temperature and the resulting strain will be detected by the gage. There are two possible sources of a thermal gradient in the stress cell. The first is from resistance heating of

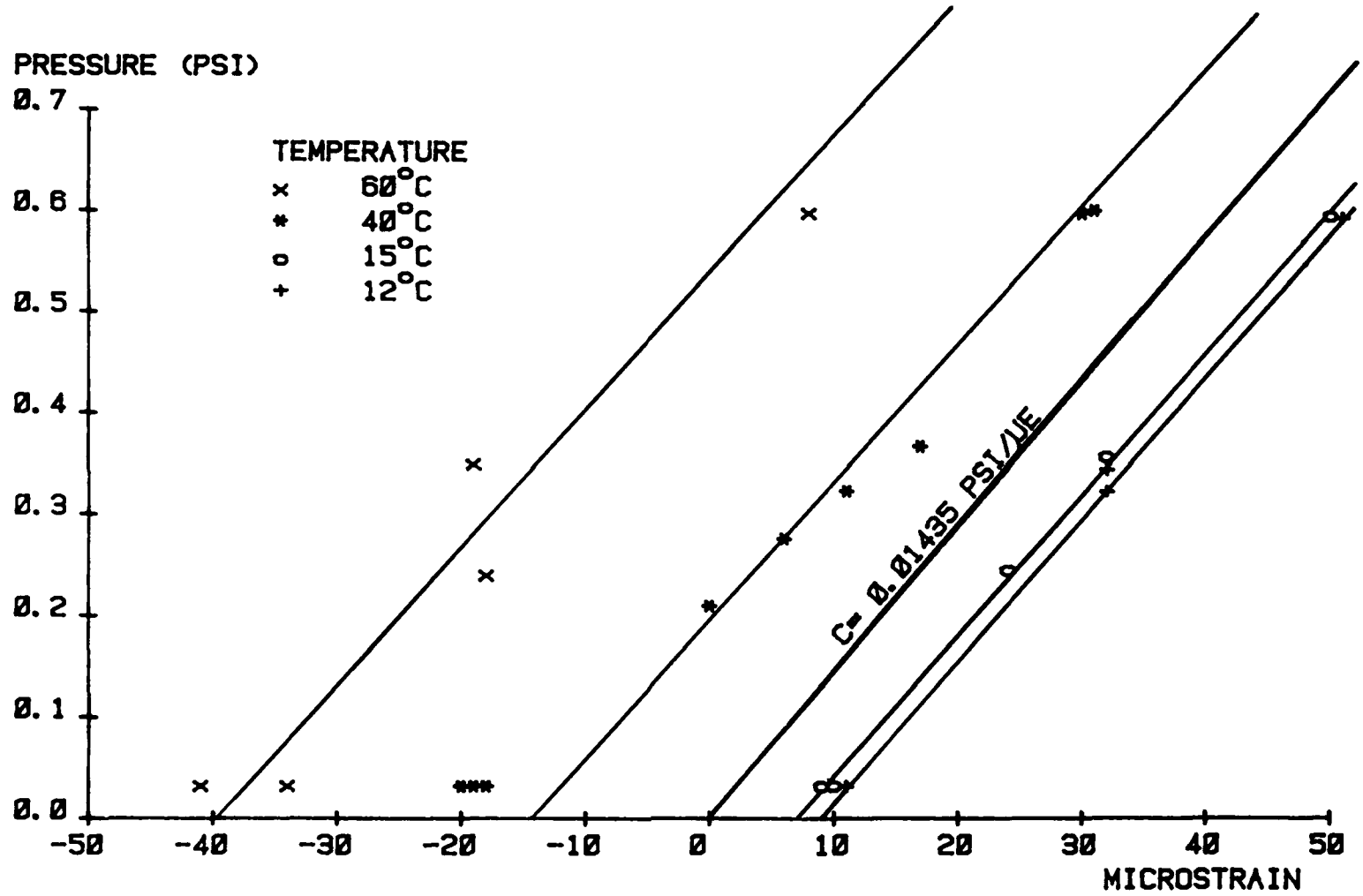

Figure 6.5 Temperature Effects on the Cornell Stress Cell.

the gage caused by current flow through the gage and the second possible source is from rapid pressure variations of the air in the air calibration chamber. The input voltage was nominally two volts for the 120 ohm resistance gage which creates a current of 16 milliamperes, well below the 25 milliamperes recommended by the manufacturer, Micro-Measurements, to prevent resistance heating. The second possible source of temperature variation is because of the rapid compression or expansion of the air in the calibration chamber. When the pressure is increased rapidly the temperature increases and when the pressure decreases rapidly the temperature of the air decreases. However because of the small volume of air required in the air calibration chamber, 2.4 cubic inches (39400 cubic millimeters), and the insulating effect offered by the rubber membranes which cover the cell, this possible temperature gradient is negligible. Even with pressures increased in increments of 0.5 psi (3.45 kN/m^2) several minutes apart, the time effect of the stress cells was still present.

Voltage variation is a common source of time variation in SR-4 strain gages. Since the output voltage of the gage is directly proportional to the input voltage, any change in the input voltage is reflected in the gage output. The voltage can fluctuate because of unsteady generation or change in the temperature as the power source warms up. To eliminate a voltage variation as a cause of the time effect,

the input voltage was recorded and used to normalize the output for each reading of the stress cell. The input voltage was usually within 0.0001 volts of the initial two volt nominal voltage throughout the duration of any test and a single value could have been used with very little loss of accuracy. With such constant power supplied, and use of the actual input voltage at each reading, voltage variation could not be the cause of the time effect.

Adverse time effects can occur if the gage is strained beyond its design limits. The gages used have a strain limit of five percent or 50,000 ppm. The maximum strain of the thinnest gage subjected to thirty psi (207 kN/m^2) of uniform pressure is only 1450 ppm; therefore excessive strain is not the cause of the time effect.

The most common source of time effects in SR-4 strain gages is cement instability or gage creep. This occurs when inelastic shear deformation in the adhesive between the base material and the gage allows the gage to relax with time and thereby gives a strain reading in which the absolute value decreases with time. When the gage is elongated, the shear deformation in the adhesive allows the gage to shorten relative to the base material; when the gage is initially shortened, the gage will elongate relative to the base material. Creep is shown graphically in Figure 6.6b as reported by Matlock and Thompson (1955). The time effect of the Cornell Stress Cell is opposite in sign as shown in

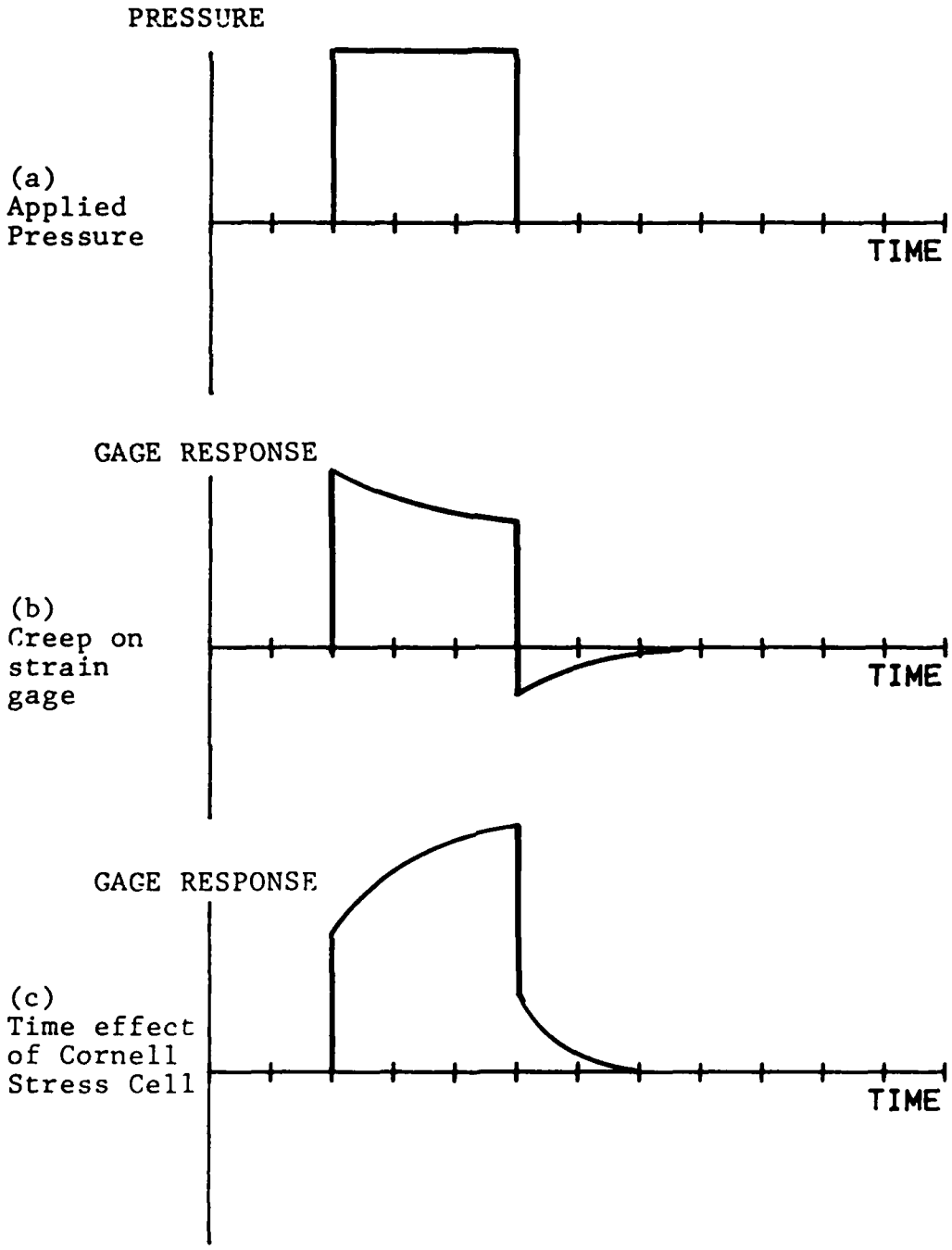

Figure 6.6 Comparison of Gage Creep and the Time Effect of Cornell Stress Cell.

Figure 6.6c, and therefore is not caused by gage creep.

When the possible causes of the time effect on the Cornell Stress Cell because of the titanium cell body and the strain gage had been eliminated, there remained only two other possibilities. First was the friction between the rubber membrane and the titanium diaphragm during deflection of the diaphragm while loading. A frictional force along only one face of a thin plate can cause bending moments which might be measured by the strain gage. If displacement between the rubber and diaphragm was a function of time, then friction could be the source of the time effect. To check this possibility, two different tests were performed. The surface between the cell and the rubber membrane was lubricated using either graphite or talc to reduce any possible frictional effects, and tests were conducted using a dead weight load applied as a point load at the center of the diaphragm. Neither of these testing procedures eliminated or significantly reduced the time effect.

The final possible cause of the time effect was not related to the cell, the strain gage or the testing equipment but was the coating of polyurethene, Micro-Measurements M-Coat A, applied to waterproof and protect the strain gage. If the M-Coat A were to contribute a measurable portion of the strength of the diaphragm, then as the diaphragm was deflected the M-Coat A would carry part of the load. Since the coating is plastic it can not sustain a significant load

and as it releases the load, the diaphragm would carry an increasing portion of the total load applied.

6.3 CAUSE OF TIME EFFECT IN CSC

Gage reinforcement because of the load transfer between the plastic waterproofing and the metal diaphragm matches the behavior of the time effect in the Cornell Stress Cell shown in Figure 6.6c. To verify that this was the cause of the time effect, several of the stress cells with measured time effects were treated with Toluene or Acetone solvents to remove the plastic waterproofing layer and were recalibrated. A typical recalibration is shown in Figure 6.7 for a cell which previously had a time effect of two percent error per log time. The linear calibration results were without any hysteresis and tests with the load held constant for ten minutes at each increment of load were without measurable time effects.

During removal of the waterproofing on some of the cells it was discovered that the strain gage lead wires were encased in the polyurethene coating and securely fastened to the diaphragm. The lead wires could act as reinforcement for the coating and aggravate the time effect of the cell. In all the stress cells which displayed a time effect of two percent error per log time or greater, at least one of the four lead wires was bonded to the diaphragm by the waterproof coating of M-Coat A.

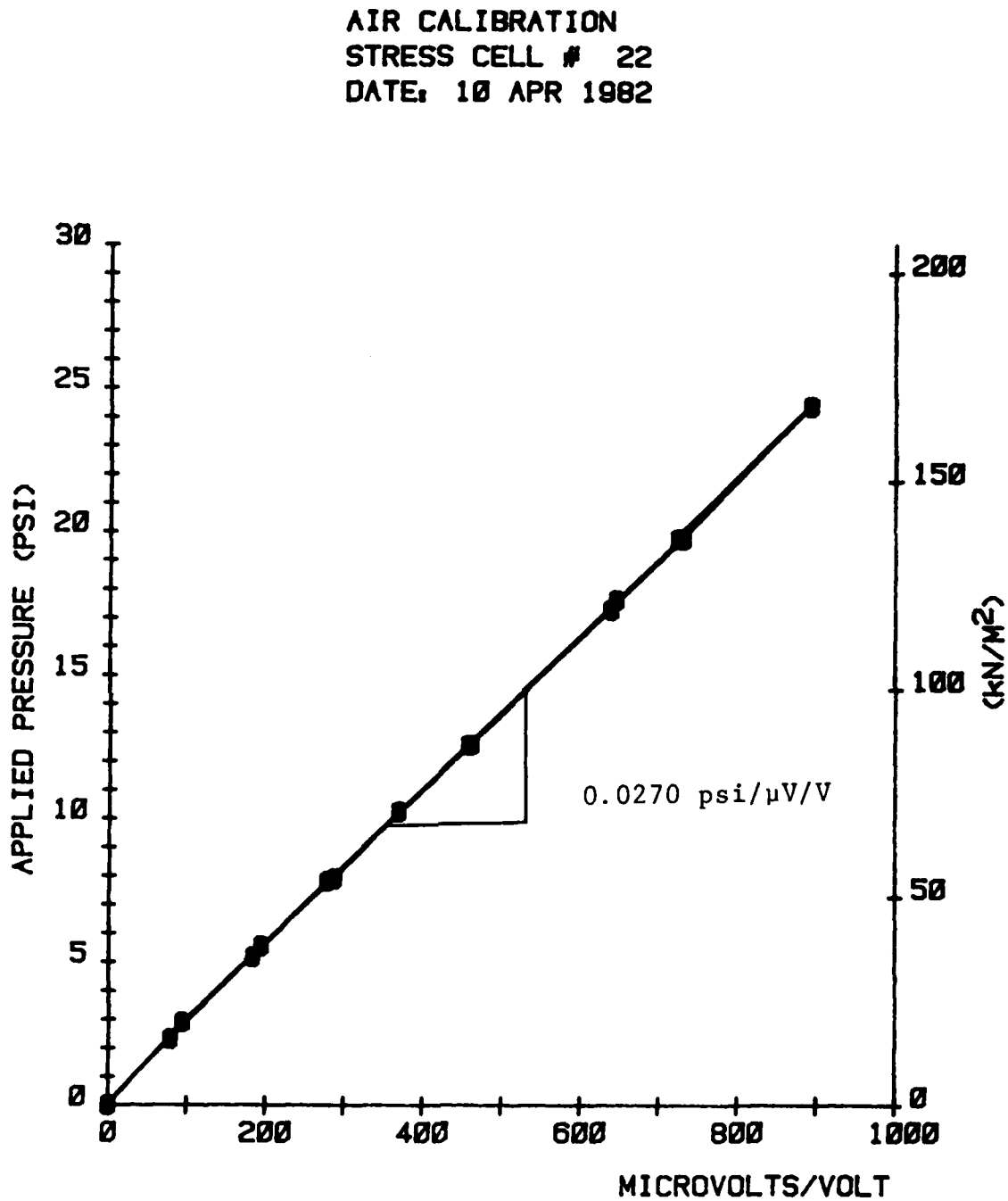

Figure 6.7 Air Calibration for Cornell Stress Cell with Waterproofing Removed.

The cause of the time effect on the Cornell Stress Cell is gage reinforcement because of load transfer from the waterproof coating to the diaphragm. When the waterproof coating bonded the lead wires to the diaphragm, the time effect was exaggerated to values as large as six percent error per log time.

The gage reinforcement of the thin diaphragm stress cells is only rarely mentioned in the stress cell literature. In a 1955 Bulletin by the Waterways Experiment Station discussing stress cell design, Woodman (1955) states, "The waterproofing material must not be so stiff as to cause undue resistance to movement of the diaphragm". This correctly describes the problem of gage reinforcement in the CSC but there is no specific recommendation for design, no indication of the relative magnitude or the effect of waterproofing on the time effects. Dorsey (1980) mentions gage reinforcement of thin diaphragms and states, "This effect (gage reinforcement) can become so serious that it is not possible to correct it by changes in strain gage design".

6.4 SOLUTION TO ELIMINATE TIME EFFECTS

To eliminate the time effects on the Cornell Stress Cell, the waterproof coating of M-Coat A must be removed by using Toluene or Acetone solvent. A new protective coating of M-Coat A may be applied in a single thin coat with care taken to keep the lead wires from bonding to the diaphragm.

A soft flexible waterproof coating such as Micro-Measurements M-Coat C made of silicon rubber would provide protection without creating gage reinforcement and would be considered superior to M-Coat A for this application. The waterproofing on existing cells which display no time effects should not be removed since the cells perform satisfactorily and damage to the gage is possible during removal of the waterproofing.

CHAPTER 7

LABORATORY TEST RESULTS

Theory and computer models are useful tools for the engineer but the only real proof is in successful performance. In Chapter 3 the theoretical treatment of soil stress cells was discussed and in Chapter 4 the finite element modeling of the stress cells was explained. This chapter is a discussion and summary of the results from the laboratory tests performed for this study.

Section one describes the results of the air calibration of Cornell Stress Cells after the time effects from gage reinforcement had been eliminated. The second section describes the results from the measurement of the lateral stress ratio, K_o, for conditions of zero lateral strain using the K_{oz} belt on the eleven inch (280 mm) diameter sample. The third section summarizes the results from the calibration of Cornell Stress Cells in filter sand under K_o, isotropic and triaxial stress conditions. The final section of this chapter discusses the results of constant volume direct shear tests on filter sand and their significance to the understanding of the shaft pullout test results of Stewart and Kulhawy (1981).

7.1 AIR CALIBRATION OF CORNELL STRESS CELLS

Soil stress cells must be calibrated against a known uniform stress to convert the cell output to a stress reading. The most common method for accomplishing this calibration is with an air pressure chamber, although fluid pressure chambers are also used. The calibration of the Cornell Stress Cell was performed with an air calibration chamber as described in Section 5.2. The desired results from the air calibration are a linear calibration line without hysteresis.

Chapter 6 describes the investigation into the time effect of the Cornell Stress Cell which was caused by gage reinforcement from the polyurethane waterproof coating. When using very thin diaphragms, the plastic waterproof coating could carry a measurable portion of the applied load. Being plastic however, the coating could not sustain the load and it was slowly transferred to the diaphragm resulting in increased output with time. The time effect caused a hysteresis which had to be eliminated before proper air calibrations could be performed and this was done by removing the waterproof coating.

Once the time effect problem was eliminated, the air calibration of the Cornell Stress Cells resulted in linear calibrations. A typical plot of cell output in microvolts per volt versus the applied air pressure is shown in Figure

7.1. The calibration is linear and without hysteresis throughout the pressure range of 30 psi (207 kN/m^2). The calibration plot is the same for both uniaxial applied stress and hydrostatic stress conditions. This dual calibration was performed to verify the lack of cross-sensitivity in the Cornell Stress Cells to a uniform lateral stress. The air pressure acting against the edge of the cell had no noticeable effect on the calibration. This does not mean that the cell is insensitive to concentrated lateral loads as was demonstrated by Weiler and Kulhawy (1978). The outer rings of stainless steel and silicone are used to reduce the effects of concentrated lateral loads and eliminate the problem of cross-sensitivity.

Table 7.1 summarizes the calibration constants for the Cornell Stress Cells used during this investigation. Most of the cells were calibrated during the investigation of the time effect and were not used in any soil calibration tests. The variation in cell output between cells of the same nominal thickness is probably caused by the use of two different strain gages in the cells, Micro-Measurements EA-05-683JC-120 and Baldwin Lima-Hamilton FAES 4-69-35-S5EL, with resistances of 120 and 350 ohms respectively. Some variation is also expected in the diaphragm thickness because of the milling tolerance of 0.001 inch (0.025 mm) which would result in a variation in the calibration constants.

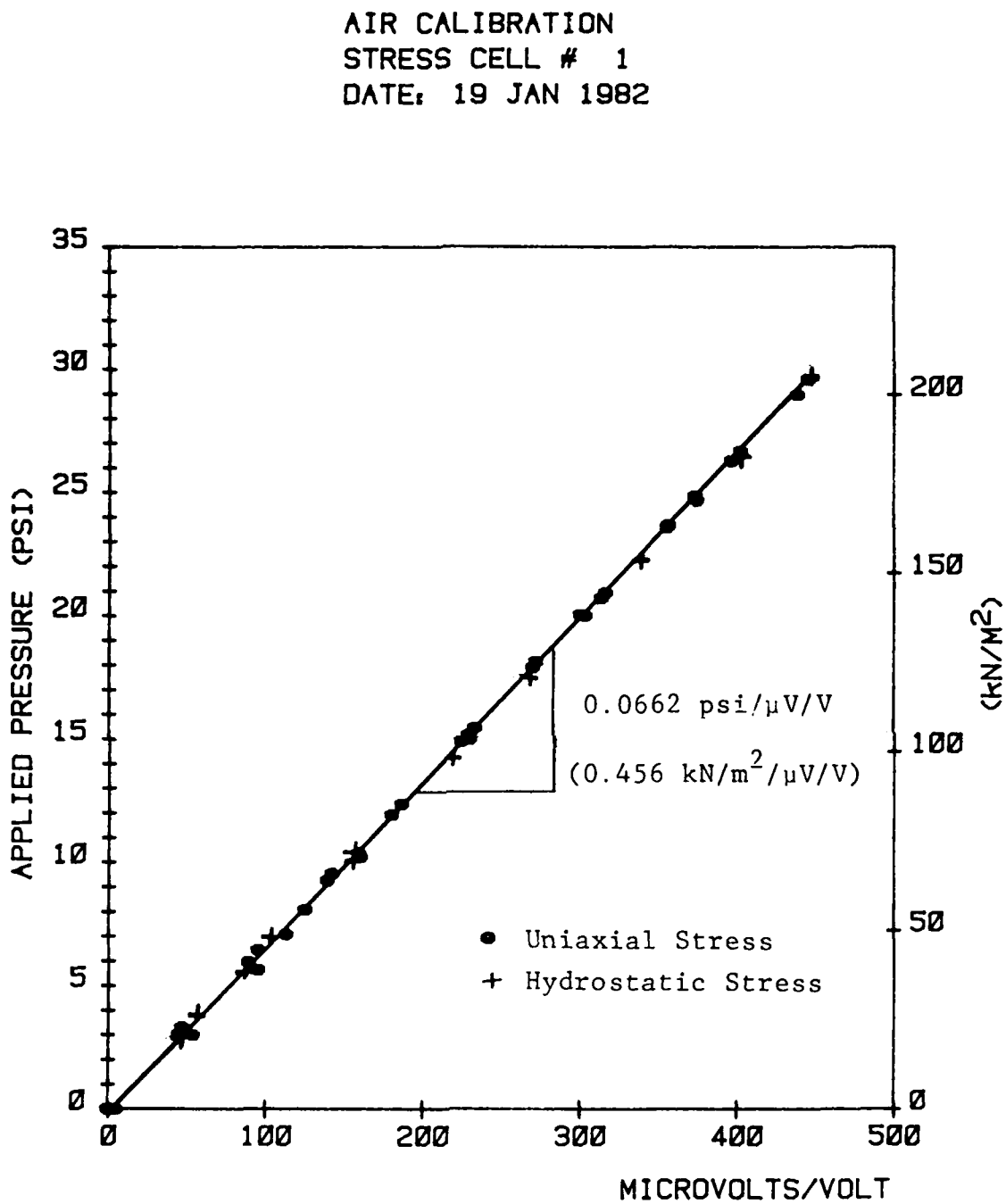

Figure 7.1 Air Calibration of Cornell Stress Cell #1.

Cell #	Diaphragm Thickness (inches)	Calibration Constants (psi/μV/V)
A	0.025	0.1783
1	0.020	0.0662
3	0.025	0.1323
9	0.025	0.1087
10	0.025	0.0653
11	0.020	0.0715
12	0.025	0.0959
13	0.025	0.0667
15	0.030	0.1407
17	0.020	0.0588
18	0.015	0.0287
19	0.015	0.0257
20	0 015	0.0257
21	0.015	0.0277
22	0.015	0.0270
23	0.012	0.0171
24	0.012	0.0101

Note: 1 inch = 25.4 mm
1 psi = 6.89 kN/m^2

Table 7.1 Calibration Constants for Cornell Stress Cells.

All the air calibration tests performed after the time effects had been eliminated were linear and without hysteresis as shown in Figures 6.7 and 7.1. The calibration process proved to be fast, easy and repeatable and is recommended for future air calibrations.

7.2 K_o CONDITIONS IN FILTER SAND

The condition of zero lateral strain upon vertical loading in the soil is known as at rest conditions. The ratio of lateral to vertical stress under these conditions of zero lateral strain is K_o, the coefficient of horizontal soil stress at rest. The K_o conditions are found in soils deposited in a sedimentary environment where the soil is deposited over a wide lateral extent which leads to uniaxial vertical strain. The soil subject to load from a wide footing is also under uniaxial strain. The ratio of lateral to vertical soil stress may range from the active case, K_A, to the passive case, K_P, which are the limiting values at failure. The K_o condition is a special case where there is no lateral deformation and represents an intermediate value between the limiting values at failure. Although the lateral stress ratio is very sensitive to lateral deformations, the K_o condition more nearly approximates many earth conditions than would uniaxial stress or hydrostatic stress conditions often performed in the laboratory. The K_o

condition was of particular interest in this study and was used for many theoretical solutions and in finite element modeling and soil calibration tests.

The coefficient of horizontal soil stress at rest was determined in this study by measuring the air pressure necessary to maintain zero strain in the K_o belt as described in Section 5.3. The results from seventeen separate K_o tests are included in Appendix C. The K_o values for the initial loading cycle are summarized in Figure 7.2. The theoretical values for K_o as a function of the friction angle are also plotted for comparison. Jáky (1944) determined the variation of K_o with friction angle to be:

$$K_o = (1 + (2/3)\sin\emptyset)(1 - \sin\emptyset)/(1 + \sin\emptyset) \qquad (7.1)$$

which is often abbreviated to:

$$K_o = 1 - \sin\emptyset \qquad (7.2)$$

Hendron (1963) solved the problem of K_o for elastic spheres and found it to vary with friction angle to give:

$$K_o = \frac{1}{2}\,\frac{1 + \sqrt{6}/8 - 3\sqrt{6}/8\,\sin\emptyset}{1 - \sqrt{6}/8 + 3\sqrt{6}/8\,\sin\emptyset} \qquad (7.3)$$

Many researchers have found that Jáky's solution fits data for most angular sands and Hendron's solution is a better

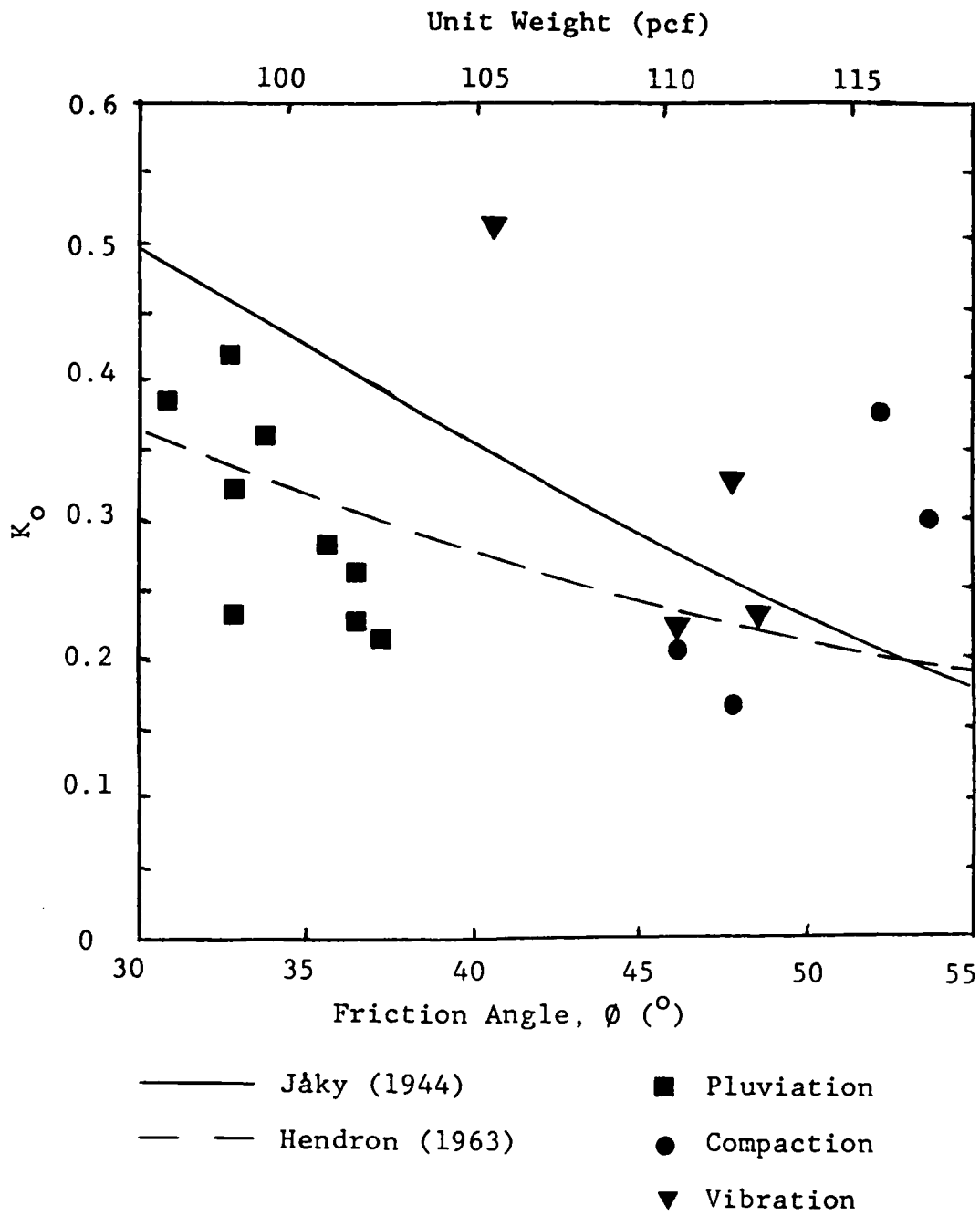

Figure 7.2 K_o Values for Filter Sand.

fit for rounded sand particles.

Although each individual test in Appendix C seems to give good results, when plotted together there is considerable scatter compared to the theoretical solutions. Some of this scatter could be from the wide range of friction angles measured for filter sand as shown in Figure A.4. With a variation of several degrees in the friction angle, each point on Figure 7.2 could be moved left or right and only a general trend of decreasing K_o values with increasing friction angle can be obtained from this data.

The K_o values plotted in Figure 7.2 for the two compacted samples with the highest unit weights may be too high. The values shown are for the first cycle of loading which was only 10 psi (68.9 kN/m^2) of applied vertical stress. If the applied stress is less than the maximum past stress, the K_o value would be for an overconsolidated sample which is known to be larger than the K_o value for a normally consolidated sample. For both of these highly compacted samples, the K_o values decrease for subsequent loadings at higher applied vertical stresses. With the K_o values for these two dense samples reduced from 0.38 and 0.30 to 0.30 and 0.27, respectively, all the dense samples seem to fit the solutions proposed by Jåky and Hendron quite well. The medium dense sample prepared by light vibration with a K_o value of 0.51 has the largest deviation from the theoretical solutions. All the pluviated samples have lower K_o values

than those proposed by Jáky (1944) and in one case as much as 50 percent lower. This could perhaps be caused by the soil structure formed during the pluviation to create the low unit weights. The looseness of the structure could give an incomplete lateral stress transfer resulting in lower K_o values. Except for the heavily compacted samples already mentioned, there is no consistent trend in the K_o values for subsequent cycles of loading, although the changes are all small.

These K_o tests are larger and looser than any other K_o tests found in the literature which are usually performed in special oedometers or standard triaxial testing apparatus. The effects of both sample size and sample preparation could result in the differences seen between the tests performed in this study and those from the literature.

Schmidt (1966,1967) determined that the change in the lateral stress ratio for at rest conditions during unloading could be expressed as:

$$K_o = K_{o_{N.C.}} OCR^{\alpha} \qquad (7.4)$$

where $K_{o_{N.C.}}$ was the lateral stress ratio at rest for primary loading and OCR was the Over Consolidation Ratio. The alpha, α, value was the slope of the log K_o versus log OCR and Schmidt determined a range of alpha for sands to be from 0.3 to 0.5. Sherif and Ishibashi (1981) suggested

alpha to be nearly constant at 0.7 for the sands they tested. Mayne and Kulhawy (1982), using data from 67 sands and 32 clays, determined alpha to be equal to sinØ with a correlation coefficient of about 0.7. The results for alpha values from the filter sand used in this study are shown in Figure 7.3 as they varied with unit weight. The general trend is for alpha to increase with increasing unit weight as was reported by Al-Hussaini and Townsend (1975) and Mayne and Kulhawy (1982). However Alpan (1967) reported that the alpha values in sand decreased from 0.5 to 0.4 with increasing friction angle or density. With such contrasting values and trends for alpha reported in the literature it is not surprising to find such wide scatter as shown in Figure 7.3. As with the K_o values, the test results for each test appear very good but when plotted together display considerable scatter. The loose filter sand has alpha values near 0.3 and the dense filter sand has alpha values near 0.7 but there is too much scatter in the data to draw any firm correlations. Again the question of the influence of structure between loose pluviated samples and dense compacted samples must be raised. The loose pluviated samples show much less increase in lateral stress for unloading than do the dense samples, perhaps because of the loose structure in the soil which inhibits full lateral stress transfer.

The K_o belt seemed to work well in determining the coefficient of horizontal soil stress at rest for each test

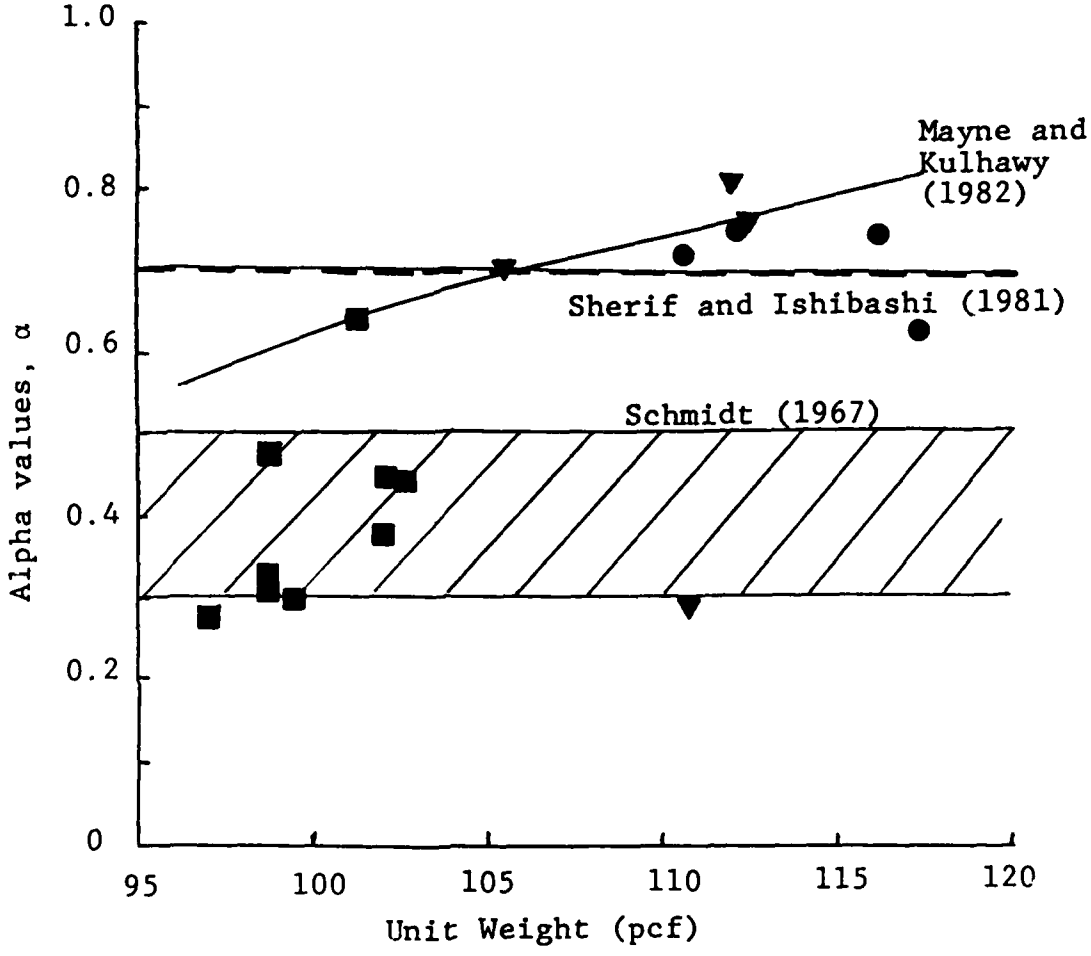

$$K_o = K_{o_{N.C.}} OCR^{\alpha}$$

Figure 7.3 Alpha Values for Filter Sand.

in the filter sand. Only general trends could be obtained from the data because of considerable scatter between tests. The K_o values decrease and the alpha values increase with increasing unit weight of the filter sand.

7.3 SOIL CALIBRATION OF CORNELL STRESS CELLS

For proper interpretation of soil stress cell results it is essential to have calibrated the cells in the same soil and under the same loading conditions as expected in the application. The only soil used in this study is filter sand described in Appendix A. The applied stress conditions included K_o, isotropic and triaxial stress on loose, medium dense and dense sand. The soil calibration chamber and procedures are described in Section 5.3.

The results from all the soil calibration tests are shown in Appendix B. Each plot shows the stress cell response in psi (1 psi = 6.89 kN/m^2) versus the applied stress in psi. An ideal calibration would be a straight line with a slope of 1.0 for both loading and unloading. This would happen only if the stress-strain properties of the cell exactly matched the properties of the soil. Since the stress-strain properties of the soil vary with stress level, that requires the properties of the ideal stress cell to also vary with stress level. This ideal stress cell has never been constructed and the study of stress cell theory has led to the conclusion that a cell which is very stiff

relative to the soil will produce a nearly constant error over a wide range of conditions. A constant error in the stress measurements can easily be corrected in the interpretation of test results by applying a registration value, R. The registration is the slope of the stress cell response versus the applied stress as shown for the loading cycle beneath each figure in Appendix B as determined by a least squares linear regression program. Registration values greater than 1.0 occur when the stress cell responds with a measured stress greater than the applied stress, which is known as overregistration. When the stress cell responds with a value lower than the free field stress, it is called underregistration. Upon unloading the soil, the stress cell response lags behind the applied stress and results in a hysteresis loop. The hysteresis is determined by dividing the maximum deviation from the straight line, with a slope equal to the registration, by the maximum applied stress and then is expressed as a percent. Most of the figures in Appendix B show the stress cell response for several loading cycles and the behavior on unloading appears repeatable.

Figures B.1 through B.21 show the soil calibration of the Cornell Stress Cell in K_o conditions of zero lateral strain and the results for the first cycle of loading are summarized in Table 7.2. The registration value, the range of registration values and its standard deviation for the

Filter Sand	Vertical Stress: Registration Value	Vertical Stress: Registration σ	Vertical Stress: Hysteresis (Percent) Loading	Vertical Stress: Hysteresis (Percent) Unloading	Horizontal Stress: Registration Value	Horizontal Stress: Registration σ	Horizontal Stress: Hysteresis (Percent) Loading	Horizontal Stress: Hysteresis (Percent) Unloading
Loose (5)	1.17 (0.82-1.41)	0.25	0.0	12.4	1.17 (1.04-1.24)	0.09	0.0	6.5
Medium (2)	0.97 (0.91-1.03)	0.08	5.0	27.0	1.38 (1.14-1.62)	0.34	2.5	-6.0
Dense (7)	0.90 (0.48-1.32)	0.32	4.7	16.4	1.23 (1.01-1.68)	0.24	-2.5	5.8

(Number of Tests)
(Range of Registration Values)
σ = standard deviation

(+ = overregistration)
(- = underregistration)

Table 7.2 Results of K_o Soil Calibration Tests.

tests, as well as the hysteresis (in percent) for both loading and unloading cycles are included. The loose tests were all prepared by pluviation of the sand through air with a height of fall of four inches (100 mm) or less. The medium dense tests were prepared by pluviation of the sand through air for an eight inch (200 mm) drop or by mild vibration of the aluminum tank. The dense tests were prepared by vigorous vibration or compaction in lifts using a drop hammer.

The registration values for horizontal stress measurements in K_o conditions are higher than for vertical stress measurements in the same tests. The standard deviation for the registration values is smaller for lateral stress than vertical stress in both loose and dense sand but is larger for lateral stress in medium dense sand. It is not possible to sort out how much of this deviation is from placement effects and how much is from the soil-cell interaction. Tests on the effect of placement of soil stress cells by Hadala (1967) showed a twenty percent deviation in the registration caused by the inherent difference in placement.

The hysteresis is an indication of nonlinearity and is relatively small in loading for both vertical and lateral stress measurements. Upon unloading the hysteresis is several times larger for the cells measuring vertical stress than for the horizontal stress measurements. Weiler and Kulhawy (1978) attributed the large hysteresis on unloading

to lateral stress rotation from the large lateral stresses which remain in a soil when unloaded in K_o conditions. Figures B.1 through B.3 depict K_o soil calibration tests using Cornell Stress Cells with diaphragms only 0.015 inches (0.38 mm) thick. The results are nonlinear for loading with such thin diaphragms and cells with 0.025 inch (0.64 mm) thick diaphragms were used for all subsequent soil calibration tests. These early test results are not included in the compilation of data in Table 7.2.

For subsequent cycles of loading in the K_o condition, the registration value decreased for all but one lateral stress measurement and for all ten vertical stress measurements which had an initial registration greater than 0.90. For the four vertical stress measurements with an initial registration less than 0.83 the registration value increased with subsequent loading cycles. This change in registration could be from the reduction of placement effects with cyclic loading as noted by Hadala (1967). The hysteresis in subsequent loading cycles decreases algebraically for loading and increases for unloading in the vertical stress measurements. Lateral stress measurements in K_o conditions have a nearly constant hysteresis for subsequent loading cycles and for unloading the hysteresis increases only slightly.

Calibration of Cornell Stress Cells in filter sand under hydrostatic or isotropic stress conditions are shown in Figures B.22 through B.33 and the results for the first

cycle of loading are summarized in Table 7.3. The registration values for lateral stress measurements for all densities of sand are lower than the registration values for vertical stress. The standard deviation of the lateral stress measurements is also smaller for both loose and dense sand indicating less variable measurements for lateral stress. The hysteresis for loading is generally small but the hysteresis for unloading is large for both vertical and lateral stress measurements. This large hysteresis on unloading in all densities of sand was not expected and cannot be explained by using lateral stress rotation as in the K_o conditions.

Considering both the K_o and isotropic soil calibrations, the only small hysteresis on unloading occurs for the lateral stress measurement in K_o conditions. The hysteresis may be a function of strain compatibility rather than from only lateral stress rotation. Whenever there is strain in the soil sample normal to the cell face, a hysteresis averaging nearly twenty percent is present upon unloading. Only for the special case of lateral stress measurement with zero lateral strain is the hysteresis below twenty percent and averages about five percent for all soil densities.

For subsequent loading cycles with increasing hydrostatic stress levels, the registration values generally decrease for both vertical and horizontal stress measurements. The hysteresis for the loading portion of each cycle

Filter Sand	Vertical Stress: Registration Value	Vertical Stress: Registration σ	Vertical Stress: Hysteresis (Percent) Loading	Vertical Stress: Hysteresis (Percent) Unloading	Horizontal Stress: Registration Value	Horizontal Stress: Registration σ	Horizontal Stress: Hysteresis (Percent) Loading	Horizontal Stress: Hysteresis (Percent) Unloading
Loose (4)	1.34 (1.08-1.87)	0.36	-3.0	18.3	1.03 (0.91-1.15)	0.10	1.0	21.5
Medium (1)	1.23		1.0	12.0	0.95		7.0	16.0
Dense (6)	1.04 (0.70-1.22)	0.22	-4.5	21.0	0.68 (0.50-0.94)	0.18	-1.5	25.0

(Number of Tests)
(Range of Registration Values)
σ = standard deviation

(+ = overregistration)
(- = underregistration)

Table 7.3 Results of Isotropic Soil Calibration Tests.

decreased algebraically and for the unloading portion of each cycle increased.

All soil calibration tests which were neither K_o nor isotropic are labeled triaxial and are shown in Figures B.34 through B.51. For each triaxial soil calibration test, a stress path (Lambe and Whitman, 1969) is included to show the loading sequence on the sample. Most triaxial tests were loaded isotropically and then the lateral stress held constant while the vertical stress was varied. It was possible in this way to fail the sample in triaxial extension. The results for the first cycle of loading for all the triaxial soil calibration tests are summarized in Table 7.4. No triaxial tests on medium dense filter sand were performed in this study. The registration values are closer to 1.0 for lateral stress measurements than for the vertical stress measurements. The standard deviation for the loose filter sand is only three percent for both vertical and horizontal stress measurements and over twenty percent for the dense filter sand. The loading hysteresis is again small but there is very large hysteresis upon unloading for vertical stress measurements in dense sand. This is caused by the failure of the soil in triaxial extension. As the soil approaches failure, the soil near the stress cell fails first from stresses concentrated there and transfers its stress to adjacent nonyielding portions. This results in a large increase in measured vertical stress at failure as can

Filter Sand	Vertical Stress: Registration Value	Vertical Stress: Registration σ	Vertical Stress: Hysteresis (Percent) Loading	Vertical Stress: Hysteresis (Percent) Unloading	Horizontal Stress: Registration Value	Horizontal Stress: Registration σ	Horizontal Stress: Hysteresis (Percent) Loading	Horizontal Stress: Hysteresis (Percent) Unloading
Loose (3)	1.14 (1.11-1.17)	0.03	-2.0	24.0	0.98 (0.96-1.01)	0.03	2.7	19.3
Dense (6)	0.86 (0.47-1.10)	0.23	-3.0	46.8	0.89 (0.69-1.28)	0.22	5.0	2.8

(Number of Tests)
(Range of Registration Values)
σ = standard deviation

(+ = overregistration)
(- = underregistration)

Table 7.4 Results of Triaxial Soil Calibration Tests.

be seen in Figure B.35 which is a typical triaxial test result. The stress cell measuring lateral stress in dense sand does not seem to be adversely affected by the soil failure and has an unloading hysteresis of less than three percent.

7.4 DIRECT SHEAR AT CONSTANT VOLUME

The tendency of a granular material to change volume during shear was discovered by Reynolds (1885) although he attached no practical significance to his discovery. The contribution of dilatancy to the frictional strength of a soil was best explained by Rowe (1962) who broke the frictional strength into three components: sliding friction, rearragement of particles effect and the dilatancy effect. The purpose of this investigation was not to separate the frictional strength into its components but to determine the effect of shear at constant volume on the resulting normal stress. It was supposed that the high pullout resistance of the shaft in dense sand (Stewart and Kulhawy, 1981) could be caused by an increased normal stress from the dilatancy of the soil.

Fifteen direct shear tests at constant volume were performed for this study as described in Section 5.5. The individual test results are reported in Appendix D and summarized here.

Shear tests performed at constant volume in dense sand

require additional confining stress to prevent the positive volume change associated with dilatancy. The additional stress required to prevent dilatancy has two other effects on the soil behavior as reported by Lee and Seed (1967). The additional confining stress reduces the brittle characteristics of the stress-strain curve and increases the strain to failure for the soil. A comparison of the results for a constant volume direct shear test with the results for a direct shear test at constant normal stress clearly shows these effects. Figure A.8 is a direct shear test performed on a dense sample of filter sand, void ratio of 0.50, with a peak friction angle of fifty two degrees, a residual friction angle of forty degrees and a shear displacement at failure of 1.2 mm. A nearly identical sample of filter sand, void ratio of 0.49, sheared at constant volume is shown in Figure D.7. The peak friction angle for the test at constant volume is fourty two degrees, the residual friction angle is thirty eight degrees and the shear displacement at failure is 6.0 mm.

As the sample of dense filter sand was sheared in the direct shear test, it attempted to expand or dilate and an additional load was applied to prevent its expansion. The applied normal load was adjusted to keep the sample at constant volume and increased as the sample was sheared until failure occurred. The peak normal load at failure divided by the corrected area of the sample is called the

critical normal stress and represents the normal stress generated to shear the sample at constant volume. Figure 7.4 shows the variation in the critical normal stress with the void ratio of the sample. The critical normal stress is seen to be very dependent on the void ratio, particularly at high densities. This behavior was reported by Seed and Lee (1967) who found that the critical stress depended only on the void ratio of the soil and was independent of the initial applied stress. Three tests performed on filter sand, void ratio of 0.52, with initial normal stresses of 2.42, 10.34 and 15.61 psi (16.9, 71.3 and 107.6 kN/m^2) all had a critical normal stress of 91 psi (627 kN/m^2) as shown in Figure 7.4. Seed and Lee (1967) report that the critical normal stress in direct shear may be five to thirty percent higher than the critical confining pressure in triaxial tests performed at constant volume.

For a dense sample of filter sand to fail in direct shear at constant volume the normal stress on the sample must be increased to the critical normal stress. If the sample of dense sand was sheared at constant volume the normal stress on the failure surface would increase up to the critical normal stress. This increased normal stress is generated by the soil attempting to dilate against the confinement of the direct shear box. Similar behavior could be expected in the pullout tests of shafts in dense sand. As the shaft is pulled from the soil, a failure surface

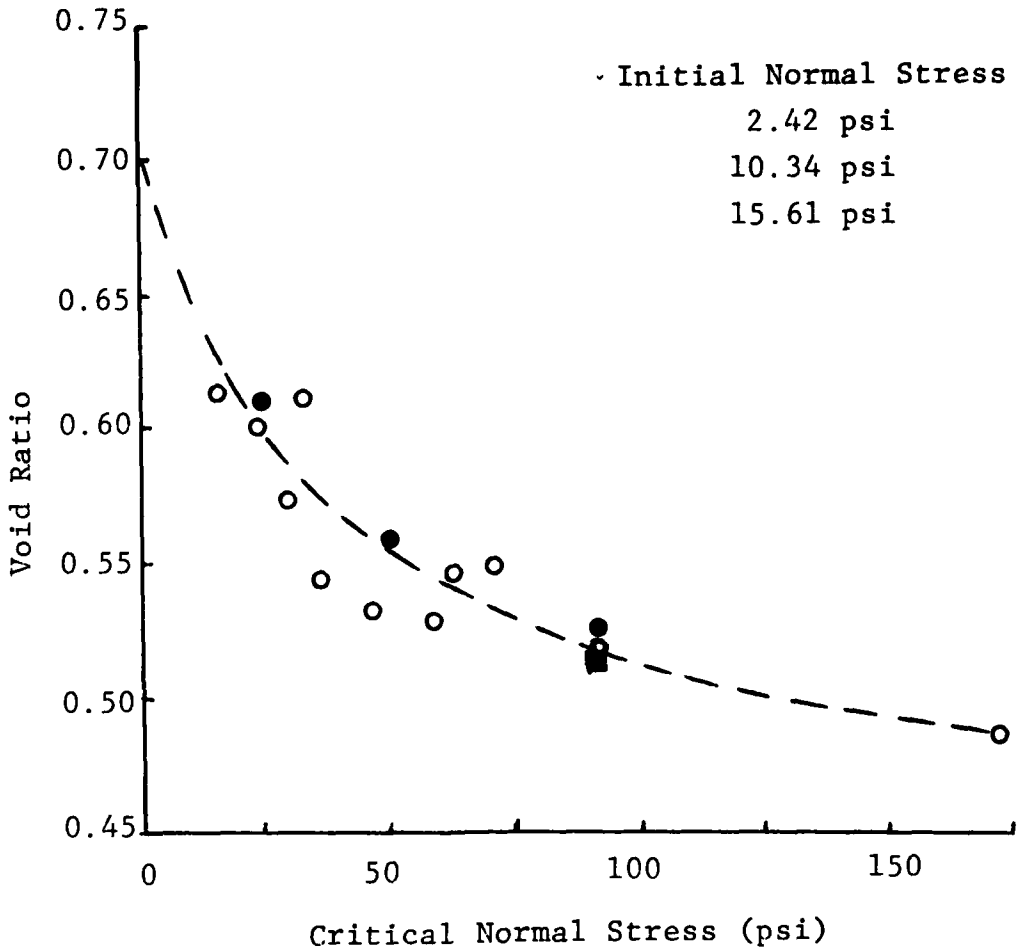

Note: 1 psi = 6.89 kN/m^2

Figure 7.4 Critical Normal Stress for Constant Volume Direct Shear Tests.

develops in the soil along the rough shaft. As the dense soil is sheared it attempts to expand against the confinement of the dense sand around the shaft. Certainly some expansion takes place around the shaft but only as the lateral stress increases from the shearing dilatancy.

The increased normal stress on a shaft caused by the dilatancy of the soil being sheared is very similar to the behavior of rock socketed shafts. As the shaft is loaded, the shear between the shaft and the rock creates dilation which increases the lateral stress on the shaft. This behavior has been documented by Williams (1980) who also performed laboratory tests for direct shear at constant normal stiffness by applying the normal load on the sample with a heavy spring so that the normal stress varied with dilation.

The increased lateral stress on the shaft caused by dilation of the dense sand explains the high pullout resistance of the shafts and the performance of the soil stress cells installed to measure the lateral stresses. Stewart and Kulhawy (1981) correctly assumed that the pullout resistance of the shafts was directly proportional to the normal stress on the shaft. However it was incorrectly assumed that the lateral stress was a constant throughout the pullout test. Stewart and Kulhawy back-calculated the lateral stress on the shaft that existed at failure and assumed that the same stress must have existed in the soil

prior to testing. This is incorrect for dense sands prepared by vibration where the shear in the soil during testing causes dilation and an increase in the lateral stress. The lateral stress generated from the shaft pullout would not be as large as the critical normal stress in the direct shear tests because some volume change is likely to occur, but could increase an order of magnitude or more over the initial lateral stress. The significance of this increased stress during shear had not generally been recognized as noted from this quote from Lambe and Whitman (1969), "The case of shear at constant volume is of little importance when dealing with dry sand."

Stewart and Kulhawy (1981) justified the large in situ lateral stresses as being from preloading of the soil during soil placement. The placement technique for dense sand was to compact in six inch (150 mm) lifts using a vibratory compactor. Even though the sand was compacted, it was not heavily preloaded as would be required for compaction of a clay soil. The vibrator used applied only 10 psi (68.9 kN/m^2) surcharge to the soil as it densified the lift. Ingold (1980) has written an excellent article on the lateral stresses created during the compaction of fill in lifts and has shown how a nearly constant lateral stress with depth is created. The results from Ingold's work and the lateral stresses discussed by Stewart and Kulhawy (1981) in their section on scale effects match extremely well.

Using the insight gained from the constant volume direct shear tests on dense filter sand, the results for Stewart and Kulhawy's shaft pullout tests in dense sand were reevaluated. At first there seemed to be no consistency from the stress cell output during the tests but a sign error was discovered in the reported results. The stress cell readings were switched from the manually operated Budd boxes after the fill and construction phases of the test to the data acquisition system, described in Section 5.4, for the loading phase of the test. An increasing stress on the soil stress cell that results in a positive increase on the Budd box will give a decreasing output on the data acquisition system. Although the conversion between the Budd box output in microstrain and the data acquisition system output in microvolts per volt was handled correctly, the sign of the output was not reversed for all data in the loading phase of the tests reported by Stewart and Kulhawy (1981).

The corrected shaft pullout test results for the soil stress cells in dense filter sand are included in Appendix E. The corrected results for the loose and medium dense filter sand are not included because of the relatively small variation in the stress cell output during the loading phase of the test. The corrected stress cell results show a spike in the radial stress measurements for those stress cells nearest the shaft both for the casing pull during the construction phase and at failure in the loading phase. Both

the tangential and vertical stress cells show a decrease in the measured stress whenever the radial stress increases. This behavior is now understood to be caused by the increased lateral stress from dilation of the dense sand. The vertical stress decreases because the shear against the shaft is reducing the vertical stress near the shaft. The tangential stress decreases because of the slight expansion of the soil around the shaft caused by the increased radial stress from dilation. The stress cells installed at a distance of 15 to 20 inches (381 to 508 mm) display no effects during either the construction phase or the loading phase of the test which indicates the small zone of influence around the shaft for the dilation effects.

It was shown in Section 7.3 that the stress cells measuring vertical stress did not respond correctly near failure in triaxial extension. To check that a stress cell measuring stress normal to a failure plane would respond correctly, a stress cell was placed in the direct shear box before running a constant volume direct shear test. The cell consistently overregistered and at peak shear stress the registration value was 1.09. Upon unloading there was a positive hysteresis of twenty percent. Therefore the cell responded well and its behavior was similar to that described in Section 7.3 for K_o soil calibration. The shear failure surface less than one inch (25.4 mm) from the cell face had no apparent adverse effects on the cell response.

The conclusion to be drawn from these constant volume direct shear test results is that the stress cells used in the shaft pullout tests by Stewart and Kulhawy (1981) were performing correctly, but the interpretation of their performance was not well understood. The large differences between the measured lateral stress prior to testing and the stress determined from the load on the shaft at failure are caused by the dilatancy of the dense filter sand. As the shaft is loaded, the soil along its perimeter is sheared and, as it attempts to expand, the lateral stresses are increased. The failure load on the shaft is to be determined from the lateral stress caused by dilation and not from the in situ lateral stress for soil deposits prepared by vibration. The lateral stress from dilation of the soil around the shaft would be a function of the initial void ratio of the soil and its stiffness. The denser and stiffer the soil, the larger would be the lateral stress generated during shear. The laboratory tests represent an upper bound because the shaft test is not constant volume and the stiffness of the soil in situ would be related to the lateral stress prior to testing. For soil deposits prepared by preloading, in which high lateral stresses can develop, the dilatancy effect will still be present. However it may not dominate as in dense sands prepared by vibration which do not develop high lateral stresses in situ.

CHAPTER 8

GUIDELINES FOR MEASURING LATERAL STRESS WITH STRESS CELLS

Both general and specific conclusions can be drawn from this investigation on the use of soil stress cells for measuring lateral stress. The investigation included a survey of previous lateral stress measurements with stress cells and a three pronged approach to analyze the stress cell behavior. The three approaches were: a theoretical analysis of a stress cell-like inclusion in an infinite, elastic, isotropic material, a finite element analysis of stress cells and laboratory calibration under varying stress conditions and soil densities.

The literature review has shown that stress cells in soft clay perform well regardless of the orientation of the cell. In sands the performance of stress cells had been erratic except for stress measurements against retaining structures. The best performance in any soil is obtained when several measurements are averaged together to help eliminate the random scatter from placement effects. There is little confidence in the stress measured from a single stress cell and repetitive measurements are essential.

The theoretical solution was obtained for the stress on a rigid oblate spheroid in an infinite, elastic, homogeneous and isotropic material, oriented as if the stress cell it was representing was measuring lateral stress. The stress

was found to vary with Poisson's ratio, lateral stress ratio and the aspect ratio of the spheroid. Under conditions of zero lateral strain, K_o, the measured stress is insensitive to the aspect ratio of the inclusion. This means that the design of a stress cell measuring lateral stress under K_o conditions does not depend on the aspect ratio of the cell.

The theoretical solution also showed that there is no error in the measured stress when Poisson's ratio of the material is 0.5. This explains why the use of stress cells in soft clays has given such good results. The difference between the free field stress and the measured stress increases with decreasing Poisson's ratio. For unloading conditions in sands the tangent Poisson's ratio may become very small and give a large error as a result. This could explain the large hysteresis seen in the soil calibration tests in isotropic stress conditions for both vertical and lateral stress measurements. As the Poisson's ratio of the soil decreases upon unloading, the error in the stress measured by the stress cell increases, thereby creating the twenty percent hysteresis seen in the laboratory test. In addition to the hysteresis seen in unloading from the low values of tangent Poisson's ratio, there would be lateral stress rotation effects for the K_o conditions.

The effect of cross-anisotropic soil properties on stress cell performance was investigated using the finite element method. Stress cells oriented to measure vertical

stress were nearly unaffected by changes in the cross-anisotropy ratio from 0.5 to 2.0. The response of a stress cell measuring lateral stress increases as the cross-anisotropy ratio increases. This change is small however compared to the effect of Poisson's ratio on the response of a stress cell measuring lateral stress. If the cross-anisotropy ratio increases from 0.5 for loose sands to 1.0 for dense sands (Ladd, et al., 1977) the lateral stress cell response would increase about five percent of the applied vertical stress. This was not observed in the soil calibration tests. So although the cross-anisotropy ratio does affect the response of a stress cell measuring lateral stress, the effect is small compared to that for Poisson's ratio or placement effects.

The effects of placement on the response of stress cells can be reduced by careful and simple placement procedures. Using identical methods in both the soil calibration tests and in the applications will ensure minimum errors. The placement of stress cells oriented to measure lateral stress is more difficult than for stress cells placed to measure vertical stress. This increased difficulty could account for some of the variation in the stress cell response. The random placement errors can be reduced by averaging the results from several stress cells measuring the same stress field.

The lateral stress ratio, K, was found to have a large

influence on the response of a stress cell measuring vertical stress. For the stress cell measuring lateral stress, the response is directly proportional to the lateral stress ratio. As the lateral stress increases so does the response of the stress cell measuring lateral stress and no correction is needed for the ratio of lateral to vertical stress.

Poisson's ratio of the soil has the largest effect of any parameter on the response of stress cells measuring lateral stress. Poisson's ratio for the vertical plane has a much greater influence on the response than the Poisson's ratio in the horizontal plane. Interpreting the results of soil stress cells would be quite easy if the Poisson's ratio of the soil was known. But the value of Poisson's ratio varies with stress level and strain conditions so that it is rarely known with any degree of certainty.

The soil calibration of the stress cells in the laboratory has shown that stress cells measuring lateral stresses perform as well or better than cells measuring vertical stress in the same test. Although the registration value and the hysteresis on unloading between cells oriented differently may be different, there is no evidence that stress cells measuring lateral stresses do not perform satisfactorily. The difference in performance is justification for proper soil calibration in the same soil and under the same stress conditions expected in an application prior to the interpretation of the results.

Stress cells measuring vertical stress were found to grossly overregister when the soil failed in triaxial extension. No erratic performance was observed for stress cells measuring lateral stresses in the same triaxial extension tests. Stress cells measuring stress normal to the failure plane in direct shear also performed satisfactorily during shear failure. Therefore, if a stress cell is to be used in a situation in which the soil might approach the failure stress, then prior soil calibration is required to ensure adequate performance.

A cell that is designed for vertical stress measurements is quite adequate for lateral stress measurements and no design modifications are suggested. The performance of the stress cell will change with the orientation of the cell and soil calibration tests at various orientations are essential for proper interpretation of the results.

In conclusion, the recommendations for the design, calibration and use of stress cells to measure lateral stresses in soil are:

1. A stress cell designed for measuring vertical stresses is completely satisfactory for measuring lateral stresses, and no special design considerations are necessary.

2. The theoretical solution for a rigid ellipsoidal inclusion in an infinite, elastic, homogeneous and isotropic material is a good representation of the

behavior of a disc-like soil stress cell and may be used to predict stress cell performance.

3. The registration values and performance of stress cells will vary with the cell orientation and soil calibration of the stress cells must include cells at the same orientation intended in the application. There is no evidence that lateral stress measurements can not be as accurate as vertical stress measurements.

4. Soil calibration of stress cells is essential for proper interpretation of stress cell results. Any attempt to use stress cells without prior soil calibration is destined for failure.

5. Placement effects can be reduced by using simple placement techniques and redundant stress cells. The confidence of the stress cell results should increase with the number of stress cells used in the testing program. The results of a single stress cell reading should not be used as the sole indication of soil stress.

6. Under some soil failure conditions, the stress cells continue to perform satisfactorily. Only proper soil calibration tests can confirm whether the cells will continue to perform near soil failure conditions.

CHAPTER 9

SUMMARY AND CONCLUSIONS

The theoretical solution for a rigid elipsoid is a good representation for a disc-like stress cell. The solution can be expressed to model a stress cell measuring either vertical or horizontal stress.

The equipment and procedures used for calibrating stress cells in air and soil were quite satisfactory and are recommended for future testing and calibration. The K_o belt in the large triaxial soil calibration chamber allowed the determination of the lateral stress ratio for conditions of zero lateral strain and at the same time helped to reduce sidewall friction between the sample and the chamber.

The time effect of the Cornell Stress Cell was caused by the reinforcement of the thin diaphragm from the plastic waterproofing which had been applied to the cells. The time effect from this reinforcement was aggravated by the lead wires which were secured to the diaphragm by too generous an application of the waterproofing. The time effect was eliminated by removing the polyurethane coating and replacing it with a single thin coat of silicone waterproofing.

The lateral stress ratio for conditions of zero lateral strain was measured using a K_o belt on an eleven inch (279 mm) diameter sample. The K_o value was found to decrease with increasing density or friction angle. At low densities

where the samples were prepared by pluviation through small heights, the K_o values were consistently lower than the theoretical solutions. This could be from the loose structure of the sand which inhibits lateral stress transfer during loading. The retention of the lateral stress during unloading was found to be larger for dense samples than for the loose pluviated ones. The alpha values for dense samples were near 0.7 while the loose samples had alpha values near 0.3. Again the question of sample preparation and soil structure must be raised to explain these differences.

The stress cell results for lateral stress measurements from the shaft pullout tests in dense sand performed by Stewart and Kulhawy (1981) are consistent with the increased lateral stress created during shear. As the shaft is loaded to failure, the dense sand along the failure surface attempts to dilate. Since the soil is confined laterally by the presence of more dense, stiff soil, the dilation is restricted and large lateral stresses may be generated. The stress cells nearest the shaft indicated this large increase in lateral stress during shear for both the casing pull and the shaft pullout tests. The pullout load on the shaft is then a function of the peak lateral stress from dilation effects and not from the in situ lateral stress prior to testing, at least for soil deposits prepared by vibration. The peak lateral stress is a function of the initial void

ratio and the stiffness of the soil, which in turn are dependent on the initial lateral stress. The implication here is that vibratory densification of sands does not create very high lateral stresses in situ, as previously thought.

Lateral stresses in cohesionless soil can be measured using soil stress cells. The behavior of the stress cell in soil is affected by the orientation of the cell and proper soil calibration tests are essential. The soil calibration of the stress cells must use the same soil, the same stress conditions and the same cell orientation to obtain correct results.

REFERENCES

Abbott, P. A., "Effects of Boundary Friction on Transmission of Static Stress Through Sand in Cylindrical Tanks," Technical Report AFWL-TR-64-108, Air Force Weapons Laboratory, Kirtland AFB, New Mexico, 1965, 41 p.

Abbott, P. A., Simmons, K. B., Reiff, C. M. and Mitchell, S., "Recent Soil Stress Gage Research," Proceedings, International Symposium on Wave Propagation and Dynamic Properties of Earth Materials, University of New Mexico, August 1967, pp. 221-238.

Agarwal, S. L. and Venkatesan, S., "An Instrument to Measure Skin Friction and Normal Earth Pressure on Deep Foundations," Instruments and Apparatus for Soil and Rock Mechanics, Special Technical Publication No. 392, ASTM, 1965, pp. 152-169.

Al-Hussaini, M. M. and Townsend, F. C., "Investigation of K_o Testing in Cohesionless Soil," Technical Report No. S-75-16, U. S. Army Engineer Waterways Experiment Station, Vicksburg, Mississippi, December 1975, 70 p.

Alpan, I., "The Empirical Evaluation of the Coefficient K_o and K_{oR}," Soils and Foundations, Japanese Society of Soil Mechanics and Foundation Engineering, Vol. VII, No. 1, January 1967, pp. 31-40.

Askegaard, V., "Measurement of Pressure in Solids by Means of Pressure Cells," Bulletin No. 17, Structural Research Laboratory, Technical University of Denmark, Copenhagen, 1963, 31 p.

Audibert, J. M. E. and Tavenas, F. A., Discussion of "Evaluation of Stress Cell Performance," by R. J. Krizek, M. H. Farzin, A. E. Z. Wissa and R. T. Martin, Journal of the Geotechnical Engineering Division, ASCE, Vol. 101, No. GT7, July 1975, pp. 705-707.

Baker, T. H. W., "Transportation, Preparation and Storage of Frozen Soil Samples for Laboratory Testing," Soil Specimen Preparation for Laboratory Testing, Special Technical Publication No. 599, ASTM, 1976, pp. 88-112.

Barden, L., "Stresses and Displacements in a Cross-Anisotropic Soil," Geotechnique, Vol. 13, No. 3, September 1963, pp. 198-210.

Bates, R. C., "SMRL Soil Stress Cell," Proceedings, 7th Engineering Geology and Soils Engineering Symposium, University of Idaho, Moscow, Idaho, April 1969, pp. 9-32.

Bauer, G. E., "Instrumentation of a 50-ft (15.2 m) Deep Braced Excavation," Performance Monitoring for Geotechnical Construction, Special Technical Publication No. 584, ASTM, 1974, pp. 32-57.

Bernhard, R. K., "Biaxial Stress Fields in Noncohesive Soils Subjected to Vibratory Loads," Symposium on Soil Dynamics, Special Technical Publication No. 305, ASTM, 1961, pp. 3-14.

Boussinesq, J., "Application of Potentials to the Study of the Equilibrium and the Movement of Elastic Soils," Paris, 1885, as referenced by Lambe, T. W. and Whitman, R. V., Soil Mechanics, John Wiley and Sons, Inc., 1969.

Bozozuk, M., "Field Instrumentation of Soil," Proceedings, Conference on the Design and Installation of Pile Foundations and Cellular Structures, Lehigh University, Bethlehem, Pennsylvania, April 1970, pp. 145-157.

Brown, S. F., "State of the Art Report on Field Instrumentation for Pavement Experiments," Transportation Research Record No. 640, Transportation Research Board, 1977, pp. 13-28.

Brown, S. F. and Pell P. S., "Subgrade Stress and Deformation Under Dynamic Load," Journal of the Soil Mechanics and Foundations Division, ASCE, Vol. 93, No. SMI, January 1967, pp. 17-46.

Buck, G. F., "An Interim Report on the Cell Action Studies Connected With Research on Pressure Measurements in Sand," Proceedings, Midland Soil Mechanics and Foundation Society, Vol. 4, 1961, pp. 95-105.

Carder, D. R., "Finite Element Analyses of the Performance of Rigid Plate Soil Pressure Cells," Ground Engineering, Vol. 9, No. 8, November 1976, pp. 40-41, 46.

Carder, D. R., Pocock, R. G. and Murray, R. T., "Experimental Retaining Wall Facility -- Lateral Stress Measurements with Sand Backfill," Laboratory Report No. 766, Transport and Road Research Laboratory, Crowthorne, Berkshire, England, 1977, 14 p.

Carlson, R. W., "Performance Tests on Stress Meters," International Water Power and Dam Construction, Vol. 30, No. 4, April 1978, pp. 39-44.

Collins, R., Lee, K. J., Lilly, G. P. and Westmann, R. A., "Mechanics of Pressure Cells," Experimental Mechanics, Vol. 12, No. 11, November 1972, pp. 514-519.

Coutinho, A., "Theory of an Experimental Method for Determining Stresses Not Requiring Accurate Knowledge of the Modulus of Elasticity," Publications, International Association for Bridge and Structural Engineering, Vol. 9, 1949, pp. 83-103.

D'Appolonia, D. J., Whitman, R. V. and D'Appolonia, E., "Sand Compaction with Vibratory Rollers," Journal of the Soil Mechanics and Foundations Division, ASCE, Vol. 95, No. SM1, January 1969, pp. 263-284.

Dolezalová, M., "Geostatic Stress State in Cross-Anisotropic Soil Deposits," Proceedings, 4th Danube-European Conference on Soil Mechanics and Foundation Engineering, Bled, Yugoslavia, June 1974, pp. 155-160.

Dorsey, J., "Errors in Strain Gage Transducers," IMEKO TC3 Conference on Weighing Technology, International Measurement Confederation, Krakow, Poland, September 1980, pp. 17-22.

Durelli, A. J. and Riley, W. F., "Performance of Embedded Pressure Gages Under Static and Dynamic Loadings," Symposium on Soil Dynamics, Special Technical Publication No. 305, ASTM, 1961, pp. 20-37.

Edwards, R. H., "Stress Concentrations Around Spherical Inclusions and Cavities," Journal of Applied Mechanics, Vol. 18, No. 1, March 1951, pp. 19-30.

Eschelby, J. D., "The Determination of the Elastic Field of an Ellipsoidal Inclusion and Related Problems," Proceedings of the Royal Society of London, Series A, Vol. 241, No. 1226, August 20, 1957, pp. 376-396.

Forsyth, R. A. and Jackura, K., "Recent Developments in Earthwork Instrumentation," Proceedings, ASCE Specialty Conference on Subsurface Exploration for Underground Excavation and Heavy Construction, New England College, Henniker, New Hampshire, August 1974, pp. 254-268.

Fossberg, P. E., "Load-Deformation Characteristics of Three Layer Pavement Containing Cement-Stabilized Base," Ph.D. Thesis, University of California at Berkeley, 1970, 349 p.

Foster, C. R. and Fergus, S. M., "Stress Distribution in a Homogeneous Soil," Research Report No. 12-F, Highway Research Board, Washington DC, January 1951, 34 p.

Goldbeck, A. T., "The Measurement of Earth Pressure on Retianing Walls," Proceedings, Highway Research Board, Vol. 18, Part II, 1938, pp. 66-80.

Goodier, J. N., "Concentration of Stress Around Spherical and Cylindrical Inclusions and Flaws," Transactions, ASME, APM-55-7, 1933, pp. 39-44.

Hadala, P. F., "The Effect of Placement Method on the Response of Soil Stress Gages," Proceedings, International Symposium on Wave Propagation and Dynamic Properties of Earth Materials, University of New Mexico, August 1967, pp. 255-263.

Hast, N., "Measuring Stresses and Deformations in Solid Materials," Handlingar, Ingenoir Ventskagns Akademiem, No. 178, Stockholm, Sweden, 1943, 23 p.

Hendron, A. J. Jr., "The Behavior of Sand in One-dimensional Compression," Ph.D. Thesis, University of Illinois, Urbana, 1963, 300 p.

Hummel, F. H. and Finnan, E. J., "Distribution of Pressure on Surfaces Supporting a Mass of Granular Material," Proceedings, Institution of Civil Engineers, Vol. 212, 1921, pp. 369-392.

Hvorslev, M. J., "The Changeable Interaction Between Soils and Pressure Cells; Tests and Reviews at the Waterways Experiment Station," Technical Report No. S-76-7, U. S. Army Engineer Waterways Experiment Station, Vicksburg, Mississippi, June 1976, 275 p.

Ingold, T., "Lateral Earth Pressures," Civil Engineering, Vol. 75, No. 883, February 1980, pp. 45-47, 49,50, 52, 54, 56, 28.

Ingram, J. K., "The Development of a Free-Field Soil Stress Gage for Static and Dynamic Measurements," Instruments and Apparatus for Soil and Rock Mechanics, Special Technical Publication No. 392, ASTM, 1965, pp. 20-36.

Jåky, J., "The Coefficient of Earth Pressure at Rest," Journal, Society of Hungarian Architects and Engineers, Budapest, Hungary, October 1944, pp. 355-358.

Johannessen, I. J., "Test Section and Installation of Test Equipment, Oslo Subway," Proceedings, Brussels Conference on Earth Pressure Problems, Vol. II, 1958, pp. 99-107.

Jones, C. J. F., "Field Measurements of Earth Pressures Against Motorway Retaining Walls and Bridge Abutments," Symposium on Field Instrumentation in Geotechnical Engineering, London, 1973, pp. 207-219.

Kallstenius, T. and Bergau, W., "Investigations of Soil Presssure Measuring by Means of Cells," Proceedings, Royal Swedish Geotechnical Institute, No. 12, Stockholm, 1956, 50 p.

Kasch, U. R., Coyle, H. M., Bartoskewitz, R. E. and Sarver, W. G., "Lateral Load Test of a Drilled Shaft in Clay," Research Report No. 211-1, Texas Transportation Institute, Texas A&M University, 1977, 96 p.

Kennard, M. F., Penman, A. D. M. and Vaughan, P. R., "Stress and Strain Measurements in the Clay Core at Balderhead Dam," Transactions, 9th International Congress on Large Dams, Vol. 3, Istanbul, Turkey, 1967, pp. 129-151.

Kenney, T. C., "Field Measurements of In Situ Stresses in Quick Clays," Proceedings, Geotechnical Conference, Vol. I, Oslo, Norway, 1967, pp. 49-55.

Kjaernsli, B., "Test Results: Oslo Subway," Proceedings, Brussels Conference on Earth Pressure Problems, Vol. II, 1958, pp. 108-117.

Kohnke, P. C., "ANSYS Theoretical Manual," Swanson Analysis System, Inc., Houston, Pennsylvania, November 1977.

Krivoritov, A. P., "State of Stress of a Sand Mass under a Plate Lying at a Shallow Depth," Soil Mechanics and Foundation Engineering, Vol. 8, No. 1, January-February 1969, pp. 20-24.

Krizek, R. J., Farzin, M. H., Wissa, A. E. Z. and Martin, R. T., "Evaluation of Stress Cell Performance," Journal of the Geotechnical Engineering Division, ASCE, Vol. 100, No. GT12, December 1974, pp. 1275-1295.

Kruse, G. H., "Measurement of Embankment Stresses on a Hundred-Foot-High Retaining Wall," Instruments and Apparatus for Soil and Rock Mechanics, Special Technical Publication No. 392, ASTM, 1965, pp. 131-142.

Ladd, C. C., Foott, R., Ishihara, K., Schlosser, F. and Poulos, H. G., "Stress-Deformation and Strength Characteristics," Proceedings, 9th International Conference on Soil Mechanics and Foundation Engineering, Vol. II, Tokyo, 1977, pp. 421-494.

Lambe, T. W., Soil Testing for Engineers, John Wiley and Sons, Inc., New York, 1951, 165 p.

Lambe, T. W. and Whitman, R. V., Soil Mechanics, John Wiley and Sons, Inc., New York, 1969, 553 p.

Lazebnik, G. E. and Smirnov, A. A., "Measurement of Stresses under a Rigid Foundation Block in the Field," Soil Mechanics and Foundation Engineering, No. 2, March-April 1964, pp. 71-78.

Lee, K. L. and Seed, H. B., "Drained Strength Characteristics of Sands," Journal of the Soil Mechanics and Foundations Division, ASCE, Vol. 93, No. SM6, November 1967, pp. 117-141.

Liu, J.-Y., "Direct Shear Tests on Filter Sand," unpublished data, Cornell University, Ithaca, New York, December 1978.

Loh, Y.C., "Internal Stress Gauges for Cementitious Materials," Proceedings, Society for Experimental Stress Analysis, Vol. XI, No. 2, 1954, pp. 13-28.

Love, A. E. H., A Treatise on the Mathematical Theory of Elasticity, 2 Volumes, Cambridge University Press, 1892, 643 p.

Mackey, R. D., "A Three Dimensional Pressure Cell," Civil Engineering and Public Works Review, Vol. 61, No. 755, December 1966, pp. 1487-1488.

Mahmood, A., Mitchell, J. K. and Lindblom, U., "Effect of Sample Preparation Method on Grain Arrangement and Compressibility in Sand," Soil Specimen Preperation for Laboratory Testing, Special Technical Publication No. 599, ASTM, 1976, pp. 169-192.

Mann, R. J., "Lateral Earth Pressure," Cornell Civil Engineer, Vol. 21, 1913, pp. 387-398.

Marcuson, W. F., III and Franklin, A. G., "State of the art of undisturbed Sampling of Cohesionless Soils," Miscellaneous Paper No. GL-79-16, U. S. Army Engineer Waterways Experiment Station, Vicksburg, Mississippi, 1979, 26 p.

Massarsch, K. R., Holtz, R. D., Holm, B, G. and Fredriksson, A., "Measurement of Horizontal In-Situ Stresses," Proceedings, ASCE Specialty Conference on In-Situ Measurement of Soil Properties, Vol. 1, Raleigh, North Carolina, June 1975, pp. 266-286.

Matlock, H. and Thompson, S. A., "Creep in Bonded Electric Strain Gages," Proceedings, Society for Experimental Stress Analysis, Vol. XII, No. 2, 1955, pp. 181-188.

Mayne, P. W. and Kulhawy, F. H., "A Review of the Relationship Between K_o and OCR," Journal of the Geotechnical Engineering Division, ASCE, Vol. 108, No. GT6, June 1982, pp. 851-872.

McMahon, T. F. and Yoder, E. J., "Design of a Pressure-Sensitive Cell and Model Studies of Pressures in a Flexible Pavement Subgrade," Proceedings, Highway Research Board, Vol. 39, 1960, pp. 650-682.

McNary, J. V., "Earth Pressure Against Abutment Walls Measured with Soil Pressure Cells," Public Roads, Vol. 6, No. 5, July 1925, pp. 102-106.

McNulty, J. W., "An Experimental Investigation of Arching in Sand," Technical Report No. 1-674, U. S. Army Engineer Waterways Experiment Station, Vicksburg, Mississippi, 1965, 171 p.

Mead, B. E., "Measurement of Earth Pressures on a Sheet Pile Breastwork," Proceedings, 4th Australia-New Zealand Conference on Soil Mechanics and Foundation Engineering, 1963, pp.34-36.

Mitchell, J. K., Guzikowski, F. J. and Villet, W. C. B., "Fabric Analysis of Undisturbed Sands from Niigata, Japan," Technical Report No. S-78-11, U. S. Army Engineer Waterways Experiment Station, Vicksburg, Mississippi, September 1978, 104 p.

Monfore, G. E., "An Analysis of the Stress Distribution In and Near Stress Gauges Embedded in Elastic Solids," Laboratory Report No. SP-26, Structural Research Section, Research and Geology Division, Branch of Design and Construction, U. S Bureau of Reclamation, Denver, Colorado, 26 June 1950, 42 p.

Morgan, J. R. and Gerrard, C. M., "Anisotropy and Non-Linearity in Sand Properties," Proceedings, 8th International Conference on Soil Mechanics and Foundation Engineering, Vol. 1, Moscow, 1973, pp. 287-292.

Nelson, P., "Petrographic Analysis of Filter Sand," unpublished data, Cornell University, Ithaca, New York, September 1980.

Øien, K., "An Earth Pressure Cell for Use on Sheet Piles: Oslo Subway," Proceedings, Brussels Conference on Earth Pressure Problems, Vol. II, 1958, pp. 118-126.

Osterberg, J. O., "A Study of Methods of Measuring Soil Pressure and Their Relation to Soil Properties," Ph.D. Thesis, Cornell University, 1940, 95 p.

Peattie, K. R. and Sparrow, R. W., "The Fundamental Action of Earth Pressure Cells," Journal of the Mechanics and Physics of Solids, Vol. 2, No. 3, April 1954, pp.141-155.

Penman, A. D. M. and Mitchell, P. B., "Initial Behavior of Scammonden Dam," Proceedings, 10th International Congress on Large Dams, Vol. 1, Montreal, 1970, pp. 723-747.

Perry, C. C. and Lissner, H. R., The Strain Gage Primer, McGraw Hill, New York, 1955, 281 p.

Pickering, D. J., "Anisotropic Elastic Parameters for Soil," Geotechnique, Vol. 20, No. 3, 1970, pp. 271-276.

Redshaw, S. C., "A Sensitive Miniature Pressure Cell," Journal of Scientific Instruments, Vol. 31, No. 12, December 1954, pp. 467-469.

Reynolds, O., "On the Dilatancy of Media Composed of Rigid Particles in Contact," Philosophical Magazine and Journal of Science, Series 5, Vol. 20, No. 127, December 1885, pp. 469-481.

Rowe, P. W., "The Stress Dilatancy Relations for Static Equilibrium of an Assembly of Particles in Contact," Proceedings of the Royal Society of London, Series A, Vol. 269, No. 1339, 9 October 1962, pp. 500-527.

Rowe, P. W. and Biggs, A., "Measurements on Model Strutted Sheet Pile Excavations," Proceedings, 5th International Conference on Soil Mechanics and Foundation Engineering, Vol. II, London, 1961, pp. 473-478.

Rowe, P. W. and Peaker, K. R., "Passive Earth Pressure Measurements," Geotechnique, Vol. 15, No. 1, 1965, pp. 57-78.

Schmidt, B., Discussion of "Earth Pressures at Rest Related to Stress History," by Brooker, E. W. and Ireland, H. O., Canadian Geotechnical Journal, Vol. 3, No. 4, November 1966, pp. 239-242.

Schmidt, B., "Lateral Stress in Uniaxial Strain," Bulletin No. 23, Danish Geotechnical Institute, Copenhagen, 1967, pp. 5-12.

Scott, J. D. and Kilgor, J., "Experience with Some Vibrating Wire Instruments," Canadian Geotechnical Journal, Vol. 4, No. 1, February 1967, pp. 100-123.

Scott, J. D., Wilson, N. E. and Bauer, G. E. "Analysis and Performance of a Braced Cut in Sand with Large Deformations," Canadian Geotechnical Journal, Vol. 9, No. 4, April 1972, pp. 384-406.

Seaquist, W. H., "Accuracy of Goldbeck Cell in Laboratory Tests," Engineering News Record, 7 June 1934, pp. 730-734.

Seed, H. B. and Lee, K. L., "Undrained Strength Characteristics of Cohesionless Soils," Journal of the Soil Mechanics and Foundations Division, ASCE, Vol. 93, No. SM6, November 1967, pp. 333-360.

Selig, E. T., Personal communication, February 1978.

Shelson, W., "Soil-Pressure Gage," Ontario-Hydro Research News, Vol. 10, No. 3, July-September 1958, pp.24-25.

Sherif, M. A. and Ishibashi, I., "Overconsolidation Effects on K_o Values," Proceedings, 10th International Conference on Soil Mechanics and Foundation Engineering, Vol. I, 1981, pp.785-788.

Sowers, G. F., Robb, A. D., Mullis, C. H. and Glenn, A. J., "The Residual Lateral Pressures Produced by Compacting Soils," Proceedings, 4th International Conference on Soil Mechanics and Foundation Engineering, Vol. II, London, 1957, pp. 243-247.

Sparrow, R. W. and Tory, A. C., "Behavior of a Soil Mass Under Dynamic Loading," Journal of the Soil Mechanics and Foundations Division, ASCE, Vol. 92, No. SM3, May 1966, pp. 59-83.

Stewart, J. P. and Kulhawy, F. H., "Experimental Investigation of the Uplift Capacity of Drilled Shaft Foundations in Cohesionless Soil," Contract Report B-49(6), to Niagara Mohawk Power Corporation by Cornell University, May 1981, 397 p.

Tavenas, F. A., Blanchette, G., Leroueill, S., Roy, M., and LaRochelle, P., "Difficulties in the In-Situ Determination of K_o in Soft Sensitive Clays," Proceedings, ASCE Specialty Conference on In-Situ Measurement of Soil Properties, Vol. 1, Raleigh, North Carolina, June 1975, pp. 450-476.

Taylor, D. W., "Review of Pressure Distribution Theories and Earth Cell Investigations," Contract Report W22-053-Eng-185, U. S. Army Engineer Waterways Experiment Station, Chapter 2, Vicksburg, Mississippi, November 1945, pp. 211-236.

Taylor, D. W., "Review of Pressure Distribution Theories, Earth Pressure Cell Investigations and Pressure Distribution Data," Contract Report W22-053-Eng-185, U. S. Army Engineer Waterways Experiment Station, Vicksburg, Mississippi, April 1947, pp. 179-332.

Terzaghi, K., "Stress Distribution in Dry Sand and in Saturated Sand Above a Yielding Trap Door," Proceedings, 1st International Conference on Soil Mechanics and Foundation Engineering, Vol. I, Cambridge, Massachusetts, 1936, pp. 307-311.

Terzaghi, K., Theoretical Soil Mechanics, John Wiley and Sons, Inc., New York, 1943, 510 p.

Terzaghi, K. and Peck, R. B., Soil Mechanics in Engineering Practice, 2nd Edition, John Wiley and Sons, Inc., New York, 1967, 729 p.

Thomas, H. S. H. and Ward, W. H., "The Design, Construction and Performance of a Vibrating-Wire Earth Pressure Cell," Geotechnique, Vol. 19, No. 1, March 1969, pp. 39-51.

Timoshenko, S., Strength of Materials, Part II, "Advanced Theory and Problems," 3rd Edition, D. Von Nostrand Co. Inc., New York, 1955, 510 p.

Turnbull, W. J., Maxwell, A. A. and Ahlvin, R. G., "Stresses and Deflections in Homogeneous Soil Masses," Proceedings, 5th International Conference on Soil Mechanics and Foundation Engineering, Vol. 2, Paris, 1961, pp. 337-345.

Trautmann, C., Personal communication, November 1982.

Trollope, D. H. and Lee, I. K., "The Measurement of Soil Pressures," Proceedings, 5th International Conference on Soil Mechanics and Foundation Engineering, Vol. 2, Paris, 1961, pp. 493-499.

Walberg, F. C., "Freezing and Cyclic Triaxial Behavior of Sands," Journal of the Geotechnical Engineering Division, ASCE, Vol. 104, No. GT5, May 1978, pp. 667-671.

Weiler, W. A., Jr. and Kulhawy, F. H., "Behavior of Stress Cells in Soil," Contract Report B-49(4), to Niagara Mohawk Power Corporation by Cornell University, October 1978, 290 p.

Weiler, W. A., Jr. and Kulhawy, F. H., "Factors Affecting Stress Cell Measurements in Soil," Journal of the Geotechnical Engineering Division, ASCE, Vol. 108, No. GT12, December 1982.

Woodman, E. H., "Pressure Cells for Field Use," Bulletin No. 40, U. S. Army Engineer Waterways Experiment Station, Vicksburg, Mississippi, January 1955, 33 p.

Williams, A. F., "Principles of Side Resistance Development in Rock Socketed Piles," Proceedings, 3rd Australia-New Zealand Conference on Geomechanics, Vol. 1, Wellington, 1980, pp. 87-94.

Wolf, K., "Distribution of Stress in a Half-plane and a Half-space of Anisotropic Material," Zeit. Angew. Math. u. Mech., Vol. 15, 1935, pp. 249-254, as referenced by Barden, L., "Stresses and Displacements in a Cross-Anisotropic Soil," Geotechnique, Vol. 13, No. 3, September 1963, pp. 198-210.

Uff, J. F., "In Situ Measurements of Earth Pressure For a Quay Wall at Seaforth, Liverpool," Proceedings, Conference on In Situ Investigations of Soils and Rocks, London, 1969, pp. 229-239.

Yoshini, Y., Hatanaka, M. and Hiroshi, O., "Undisturbed Sampling of Saturated Sands by Freezing," Soils and Foundations, Japanese Society of Soil Mechanics and Foundation Engineering, Vol. 18, No. 3, September 1978, pp. 59-73.

APPENDIX A

PHYSICAL PROPERTIES OF FILTER SAND

The cohesionless material used for all soil tests in this study is a processed uniform sand commercially available for use in swimming pool filters, hence the name filter sand. The oven dried sand was purchased in eight pound bags from W. F. Saunders & Son, Box 308, Nedrow, New York. This is the same material used by Weiler and Kulhawy (1978) and by Stewart and Kulhawy (1981) whose test results for the filter sand are summarized here.

The grain size distribution is shown in Figure A.1 for five different analyses by four different technicians. The differences in grain size are attributed to the segregation of particles that occurs when the sand is poured into a conical pile. Because the coarse fraction rolls further, it is concentrated along the perimeter of the pile. Figure A.2 shows the grain size distribution for the filter sand used for fifteen different soil calibration tests between 15 September 1981 and 26 March 1982. The degradation of the particle size because of handling and repeated loading is insignificant and the grain size may be considered to be constant throughout the testing period.

The minimum unit weight is 98.8 pcf (15.5 kN/m^3) and the maximum dry unit weight is 116.7 pcf (18.3 kN/m^3) as performed by Stewart in accordance with ASTM D-2049-69. The

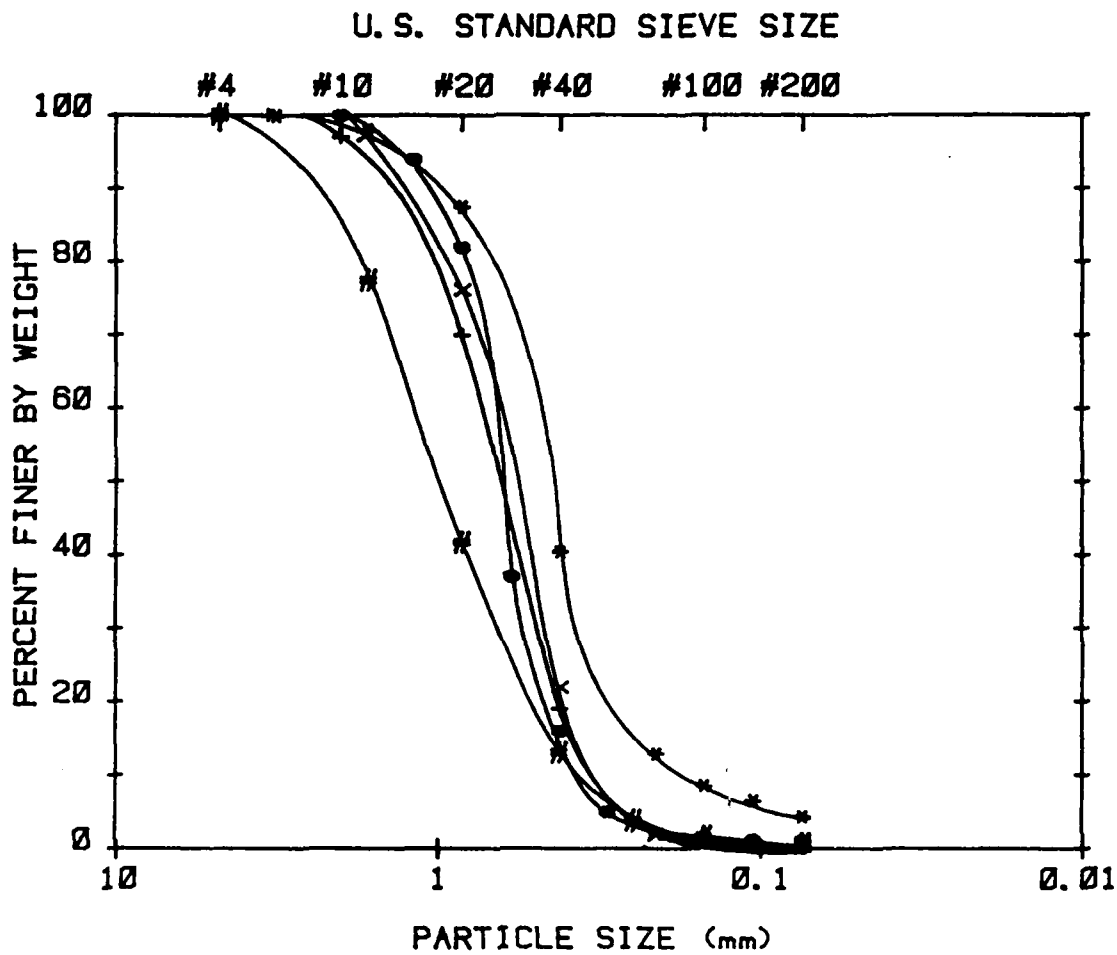

o W.F. SAUNDERS & SON
+ WEILER & KULHAWY 1978
× STEWART & KULHAWY 1981
* FINE FRACTION, This Study
# COARSE FRACTION, This Study

Figure A.1 Grain Size Distribution of Filter Sand.

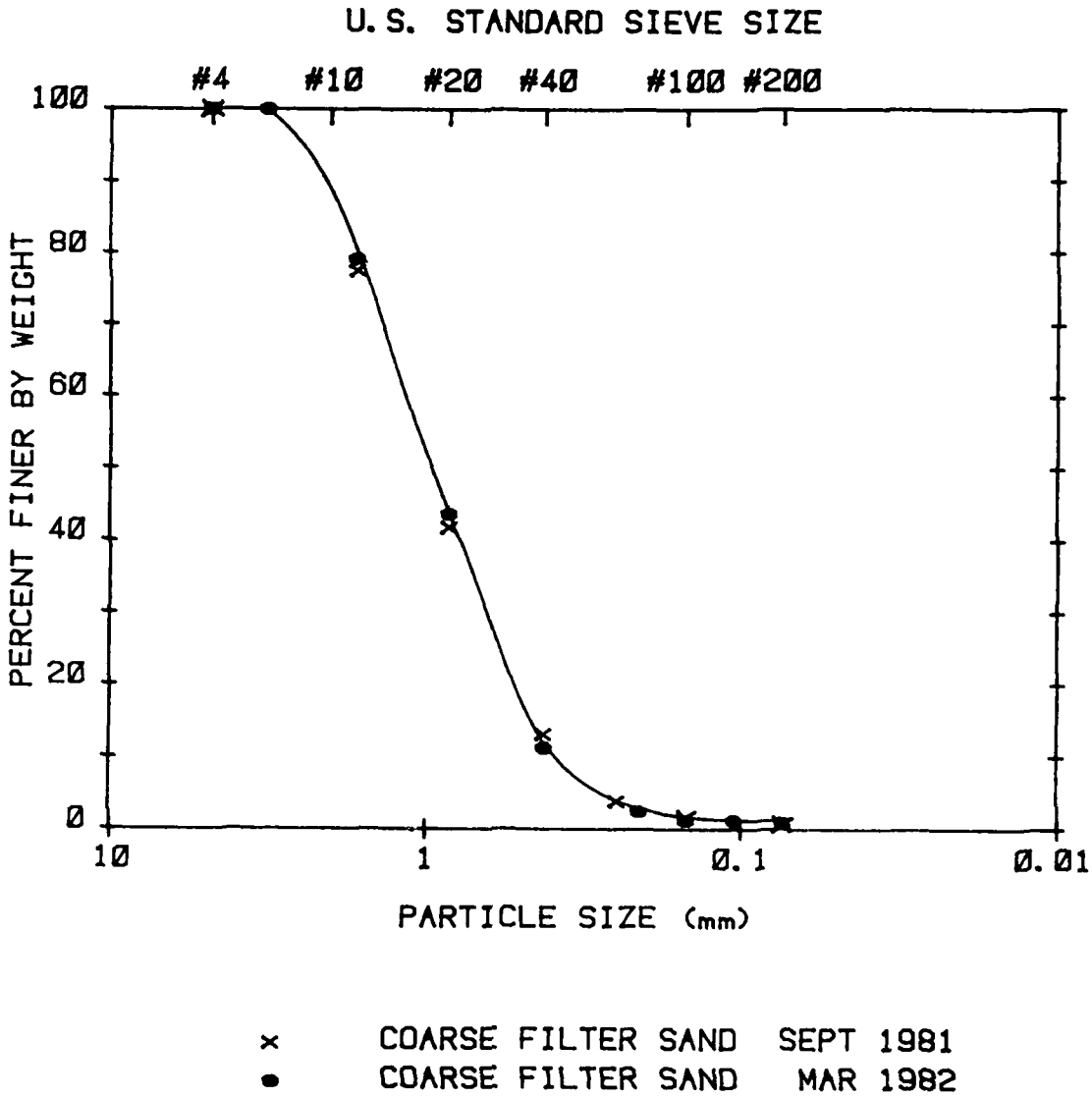

Figure A.2 Grain Size Distribution Showing Lack of Degradation From Handling.

specific gravity of solids is 2.74. A petrographic analysis as performed by Nelson (1980) in accordance with ASTM C-295-65 is shown in Table A.1.

The compaction curve for filter sand using the Standard Proctor compaction test is shown in Figure A.3. The optimum water content appears to be ten percent, where the peak occurs in the dry unit weight. However, a higher unit weight is possible for the air dried sand. All compaction done in this study was done on air dried sand.

The shear tests on filter sand are summarized in Figure A.4. The variation in friction angle with unit weight is thought to be caused by the variation in the coarse fraction (Stewart and Kulhawy, 1981). The direct shear tests by Trautmann (1982) were done with a hard maple frame replacing the heavy brass frame for the upper part of the shear box to reduce the effective normal stress. Figures A.5 through A.13 are the results of the direct shear tests done for this study and are summarized in Table A.2. The normal load was held constant and the normal stress was calculated using the corrected area which explains the linear increase in the normal stress with shear displacement. The tests were performed for two different height samples compacted for variation in the initial void ratio as shown on each figure.

	Count	% of Total
Single Crystal Grains		
Calcite	1	0.4
Quartz	55	20.1
Feldspar	6	2.2
Polycrystalline Grains		
Lithic Fragments		
Quartzite	34	12.4
Limestone	105	38.3
Dolostone	5	1.8
Siltstone/Fine Sandstone	56	20.4
Igneous	4	1.5
Shale	4	1.5
Fecal Pellets	3	1.1
Opaque Mineral	2	0.7
Trace Mineral	2	0.7
	Σ 274	Σ 100 %

Table A.1 Petrographic Analysis of Filter Sand (Nelson, 1980).

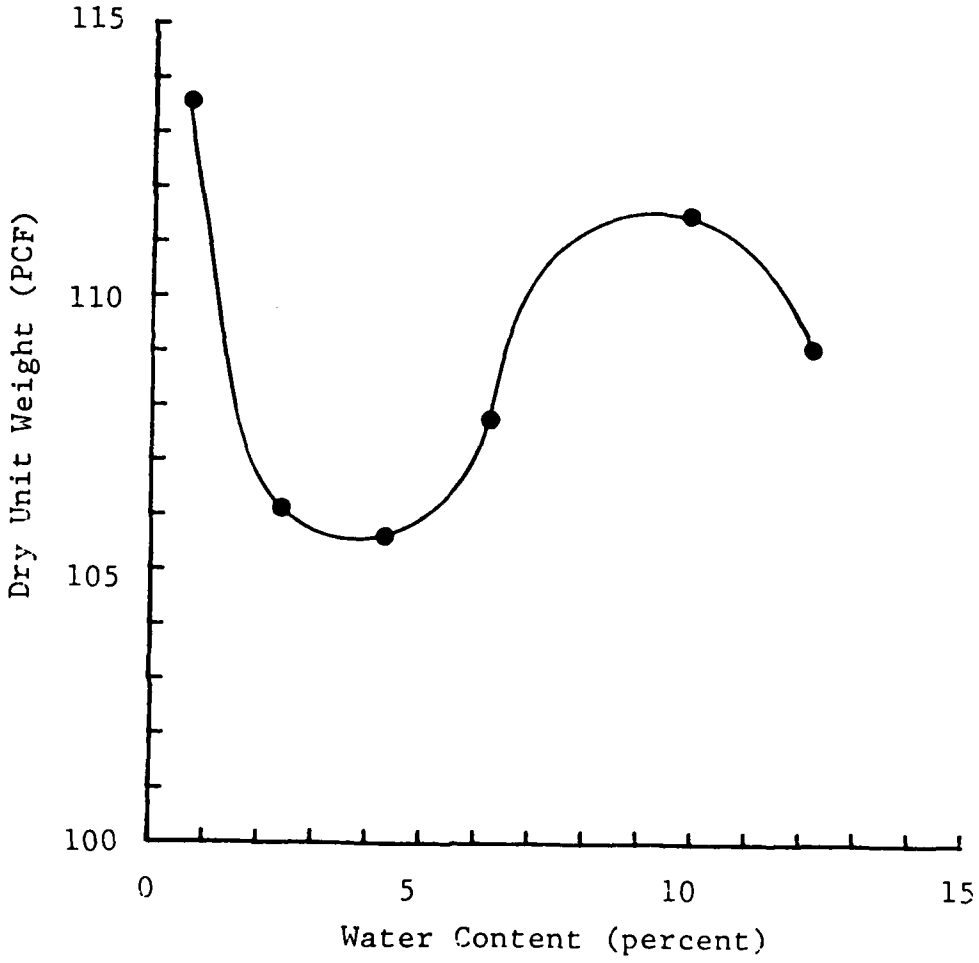

Note: 1 pcf = 16.02 kg/m^3

Figure A.3 Standard Proctor Compaction Curve for Filter Sand.

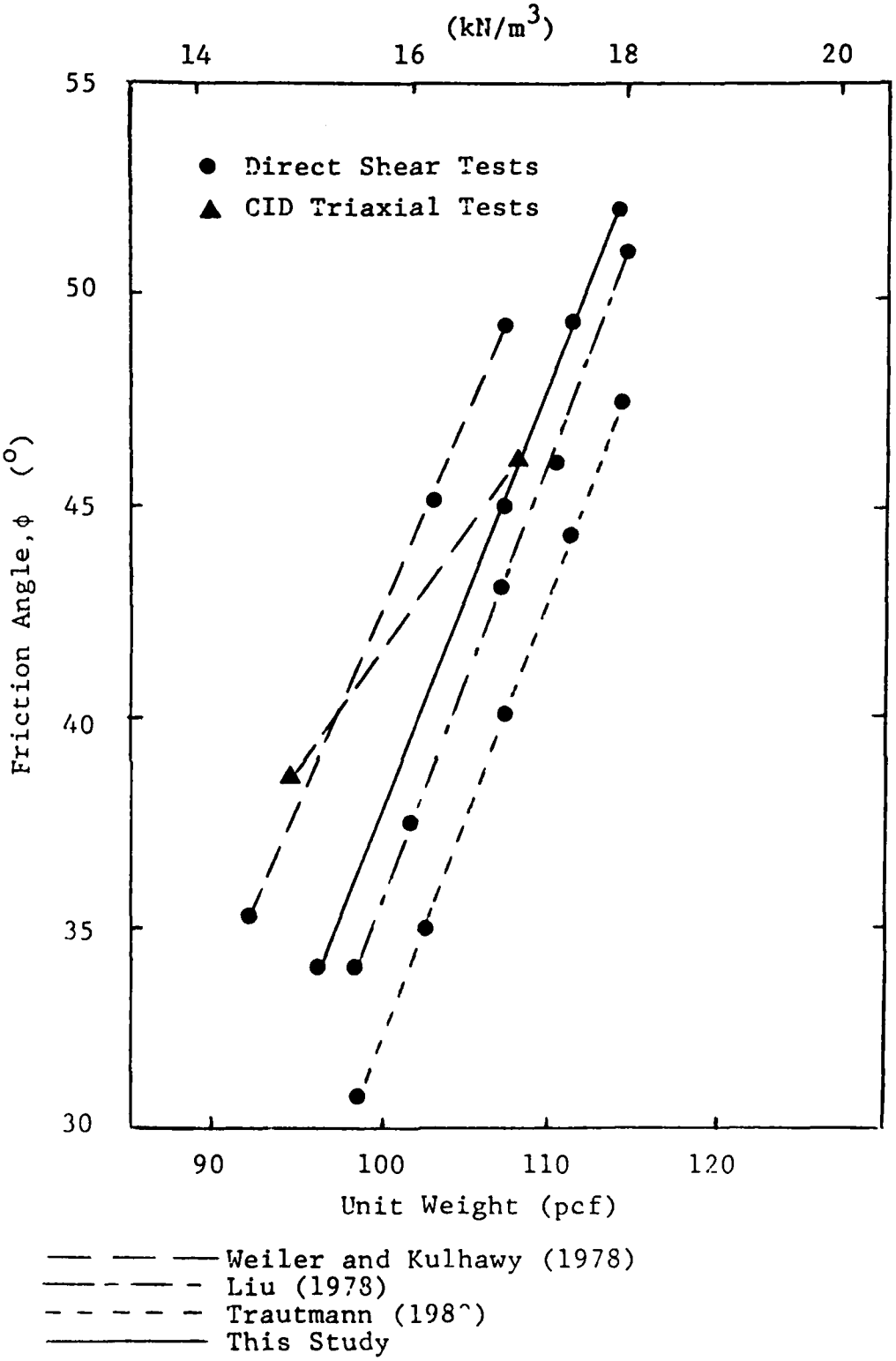

Figure A.4 Friction Angle Variation with Unit Weight.

Figure No.	Initial Void Ratio	Initial Height (mm)	Initial Normal Stress (psi)	Peak Friction ϕ_{max}	Peak Friction Disp. (mm)	Residual Friction ϕ_{CV}	Residual Friction Disp. (mm)	Maximum Height Change (mm)
A.5	0.77	50.75	2.65	34.0	4.6	34.0	4.6	-0.13
A.6	0.60	"	"	45.0	1.2	39.9	4.2	+0.47
A.7	0.54	"	"	49.3	1.1	39.9	4.2	+0.59
A.8	0.50	"	"	52.0	1.2	40.7	5.0	+0.71
A.9	0.73	33.02	2.42	44.8	4.0	43.3	9.0	+0.09
A.10	0.73	29.21	"	44.8	4.0	44.1	5.5	-0.07
A.11	0.66	"	"	46.2	2.5	44.8	6.0	+0.13
A.12	0.62	33.02	"	47.3	2.0	43.3	8.0	+0.32
A.13	0.49	"	"	58.1	1.1	45.4	7.0	+0.72

Table A.2 Summary of Direct Shear Tests on Filter Sand.

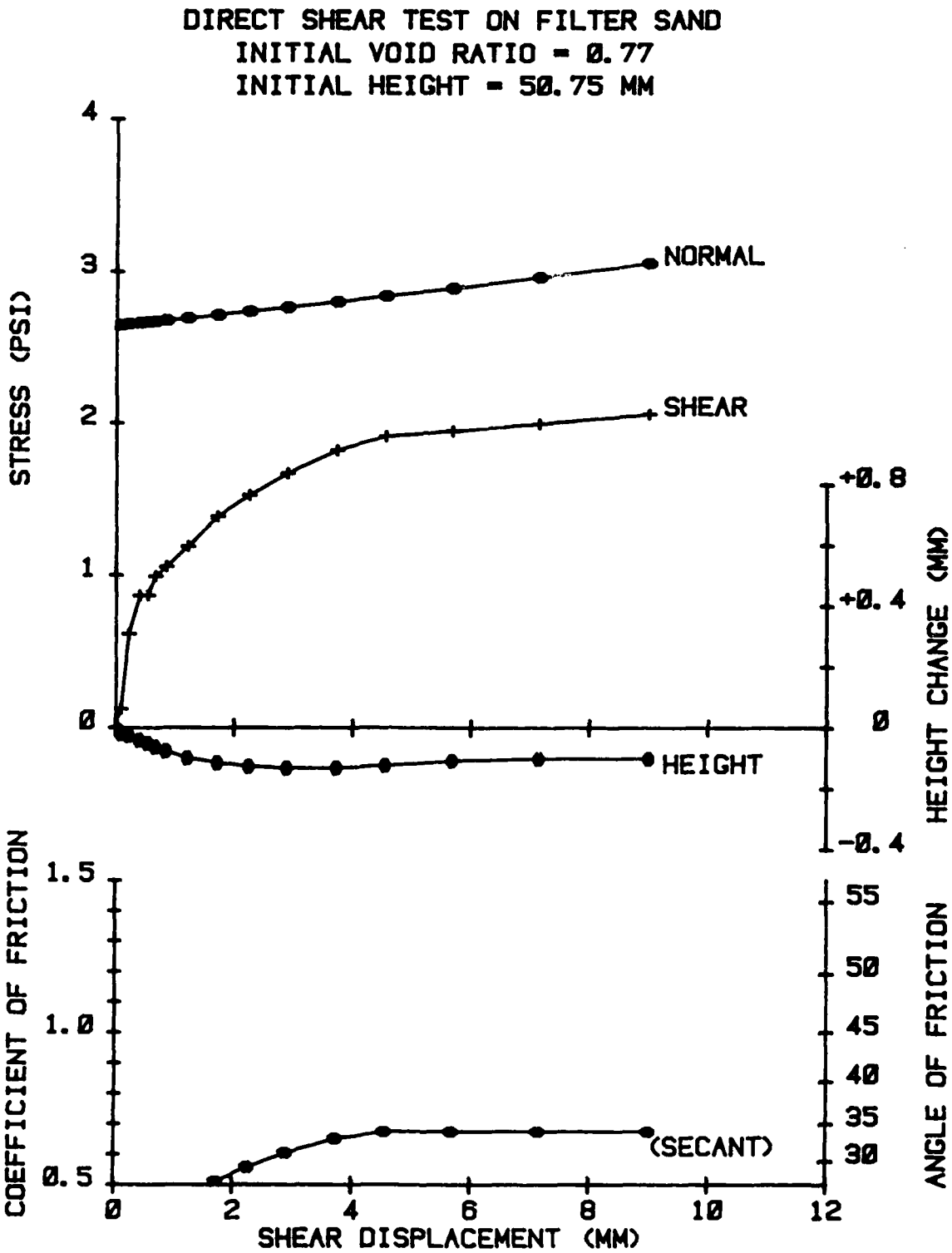

Figure A.5 Direct Shear Test on Filter Sand

AD-A126 948 LABORATORY DETERMINATION OF HORIZONTAL STRESS IN COHESIONLESS SOIL(U) AIR FORCE INST OF TECH WRIGHT-PATTERSON AFB OH S C BOYCE 1983 3/4

UNCLASSIFIED AFIT/CI/NR-83-4T F/G 8/13 NL

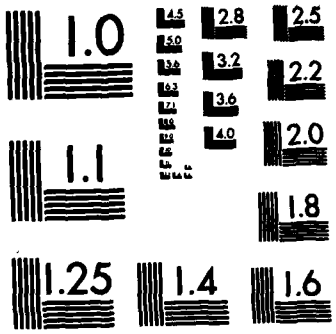

MICROCOPY RESOLUTION TEST CHART
NATIONAL BUREAU OF STANDARDS-1963-A

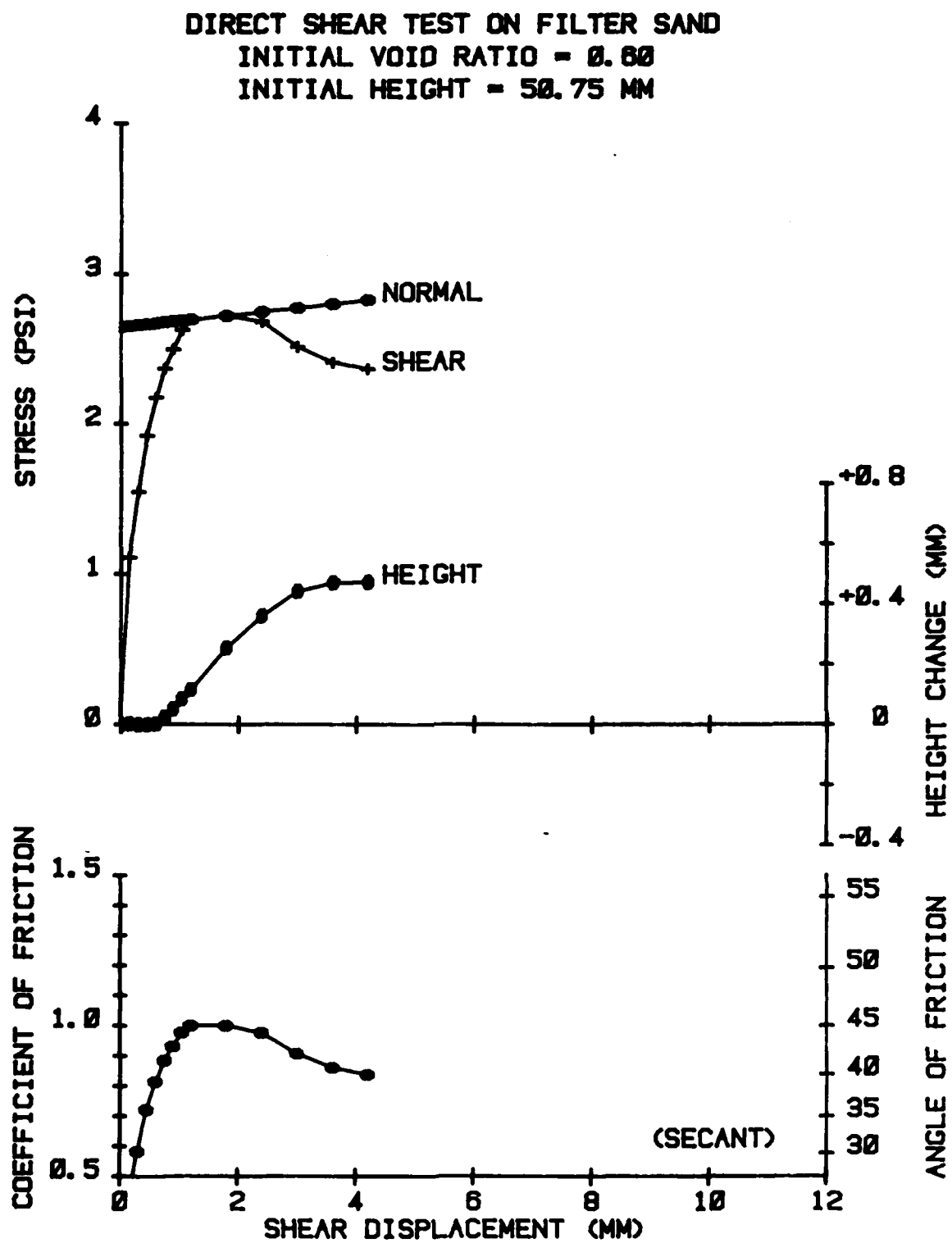

Figure A.6 Direct Shear Test on Filter Sand.

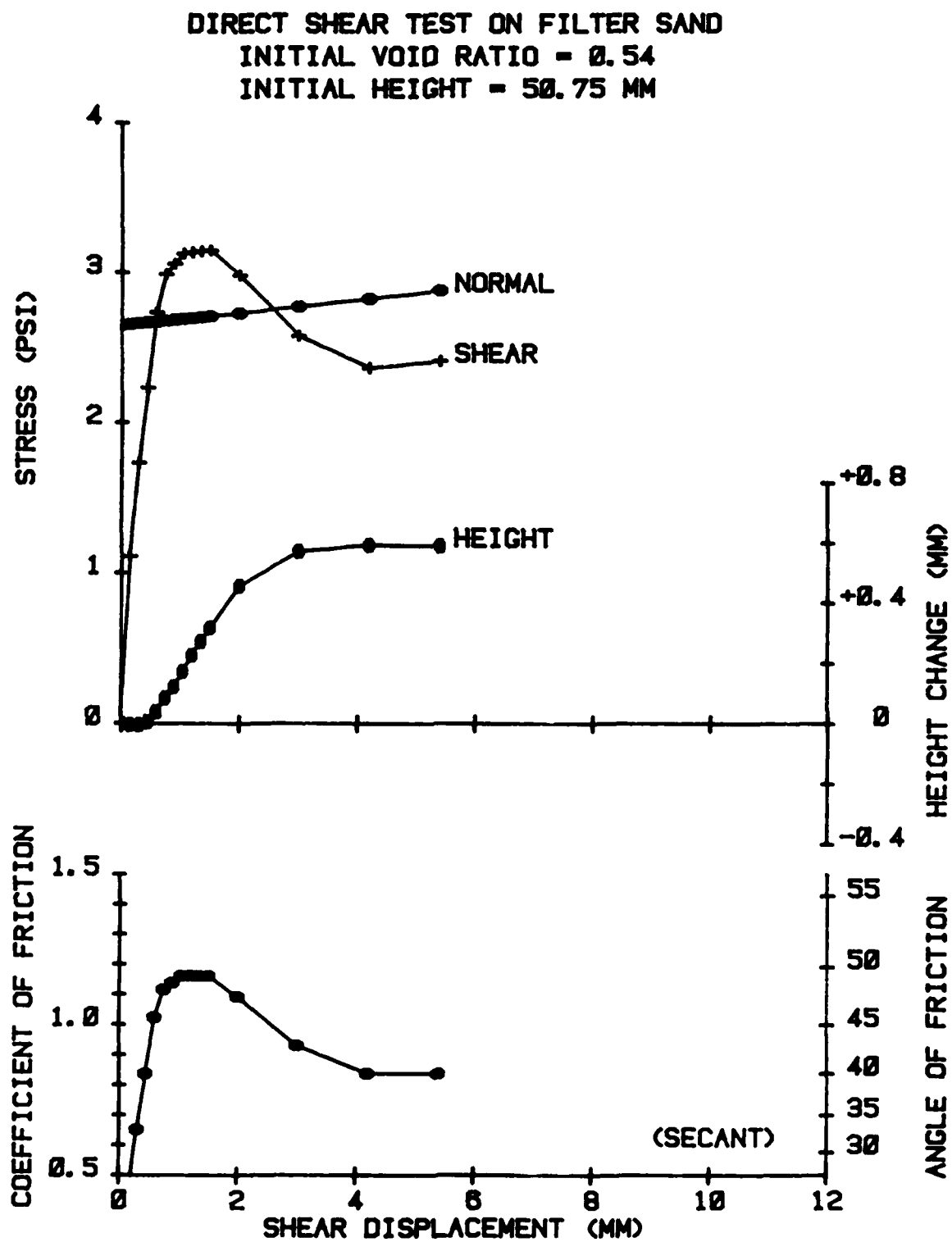

Figure A.7 Direct Shear Test on Filter Sand.

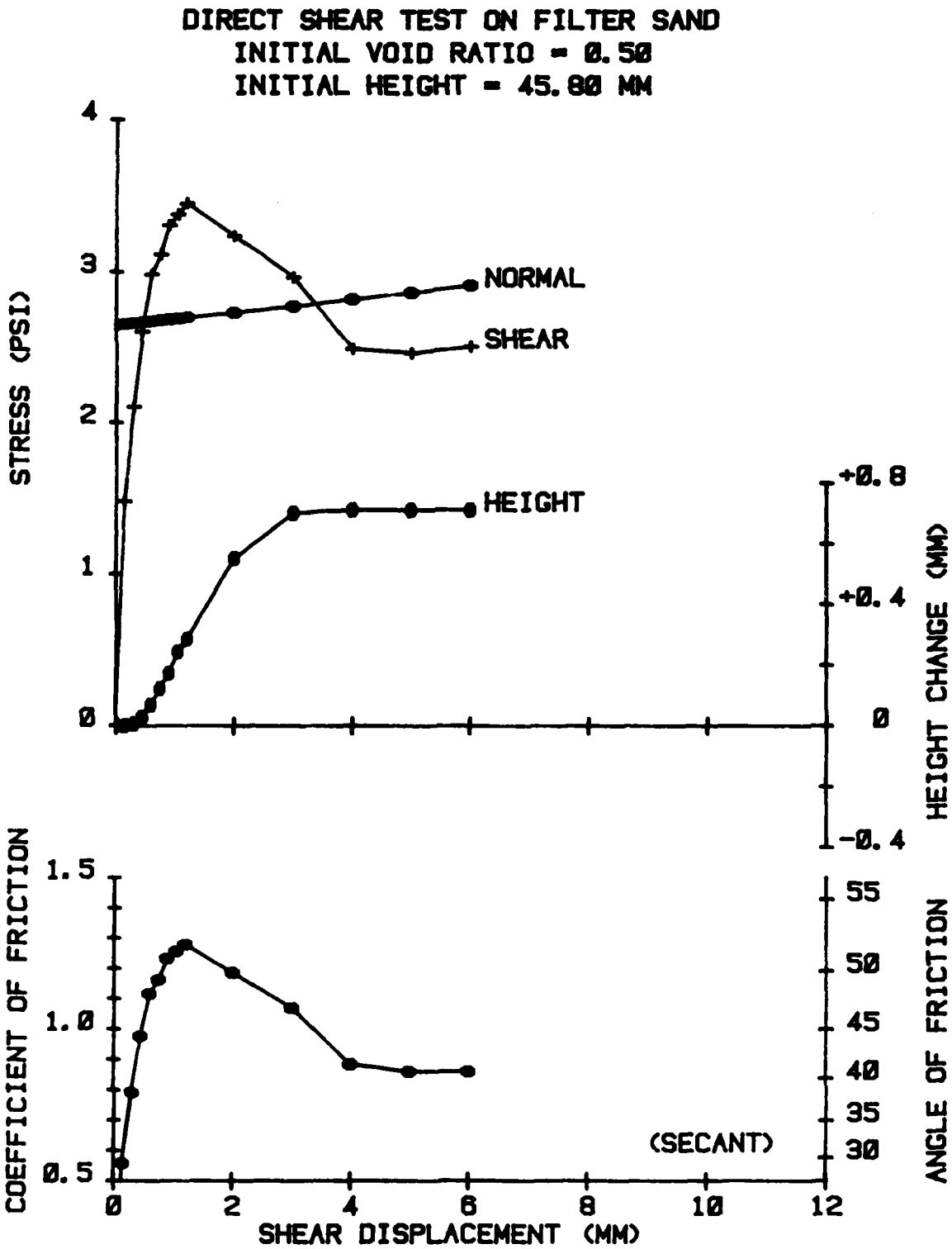

Figure A.8 Direct Shear Test on Filter Sand.

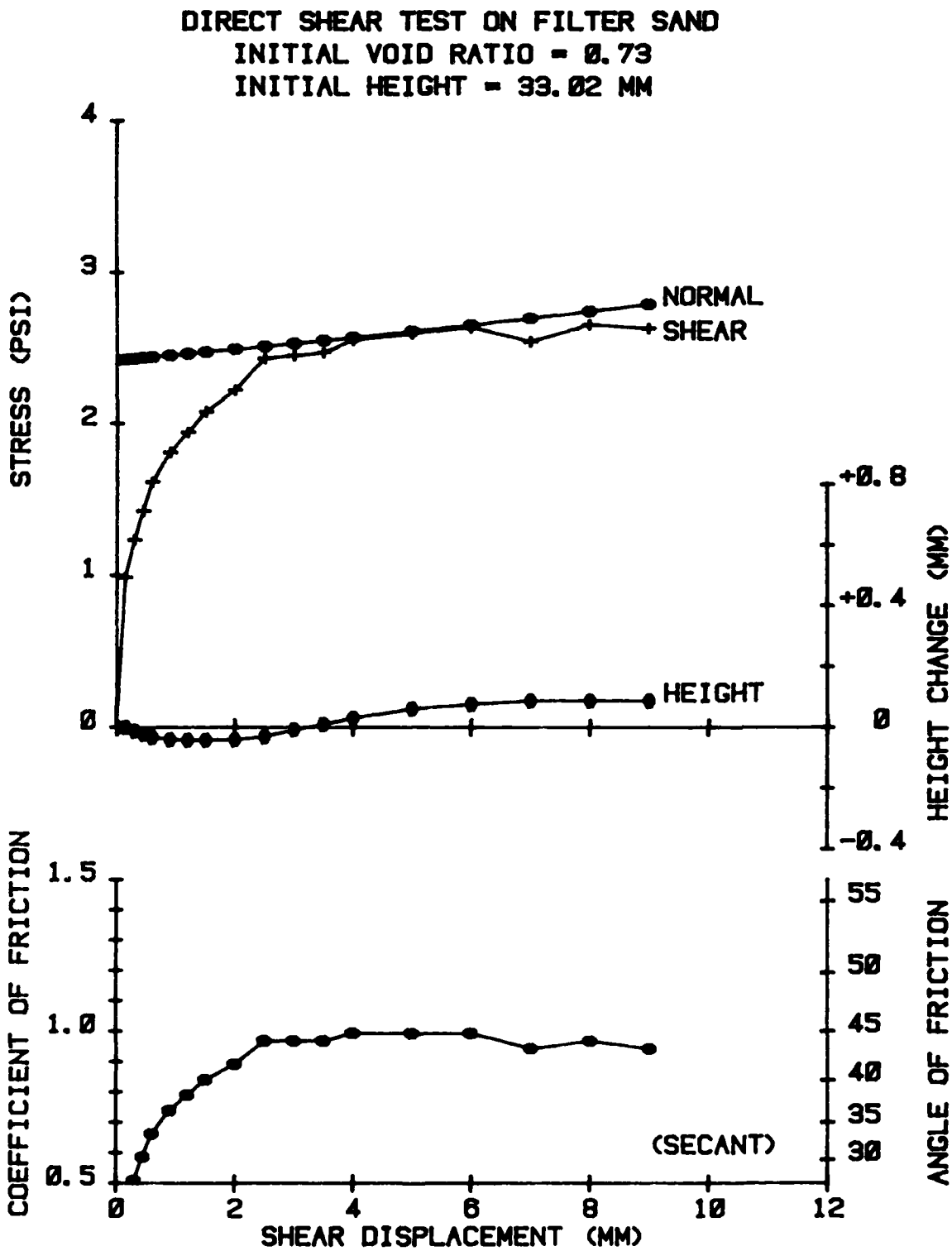

Figure A.9 Direct Shear Test on Filter Sand.

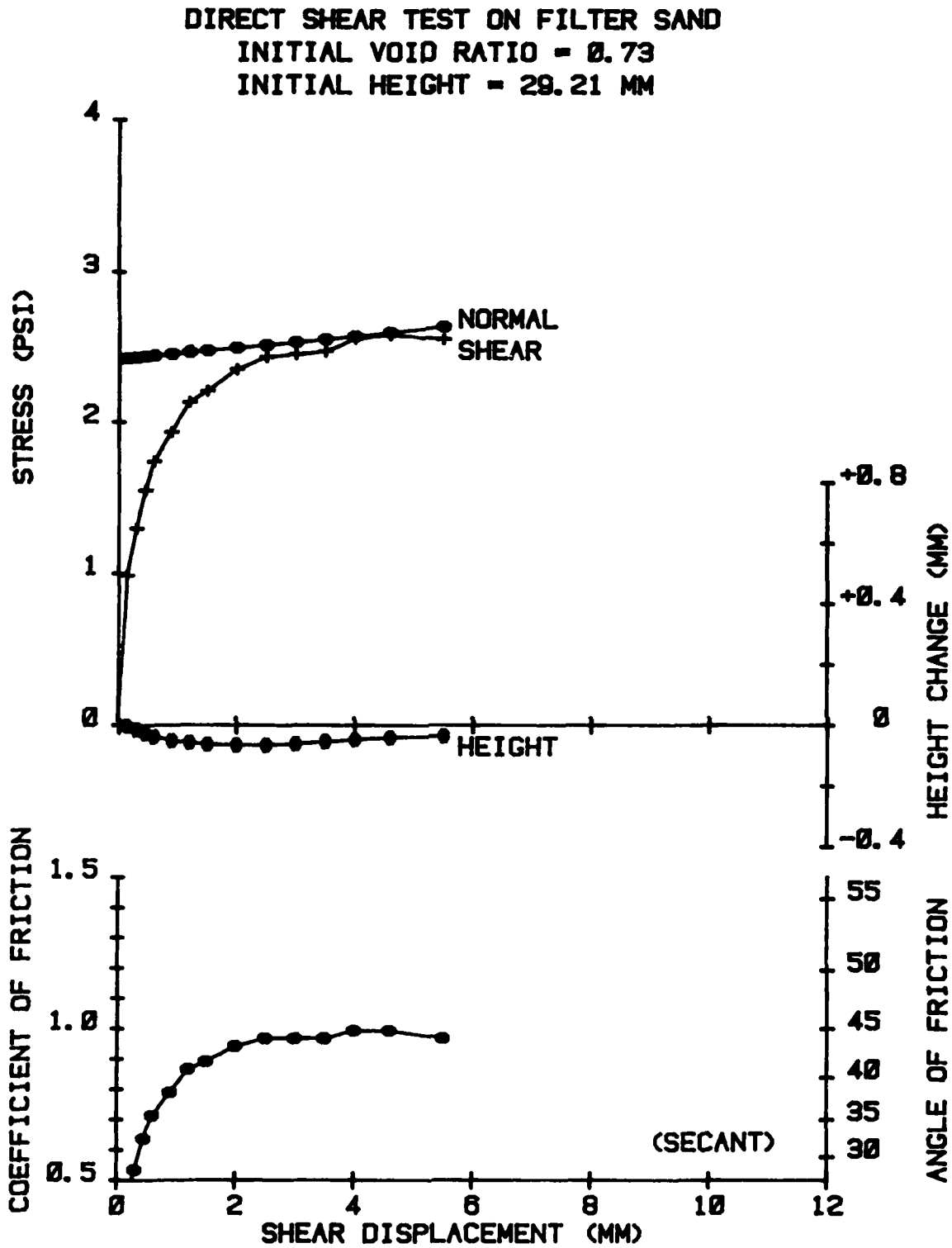

Figure A.10 Direct Shear Test on Filter Sand.

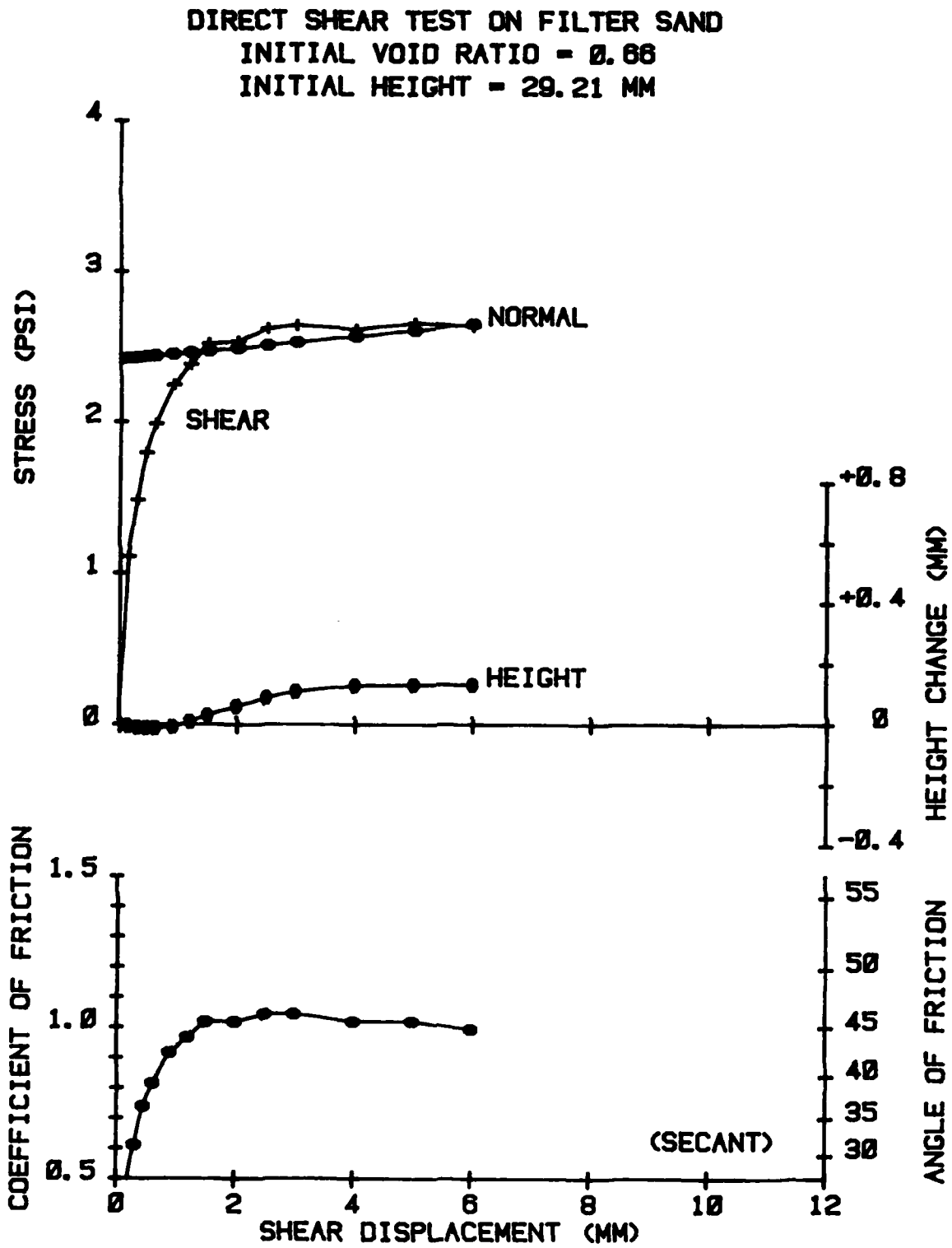

Figure A.11 Direct Shear Test on Filter Sand.

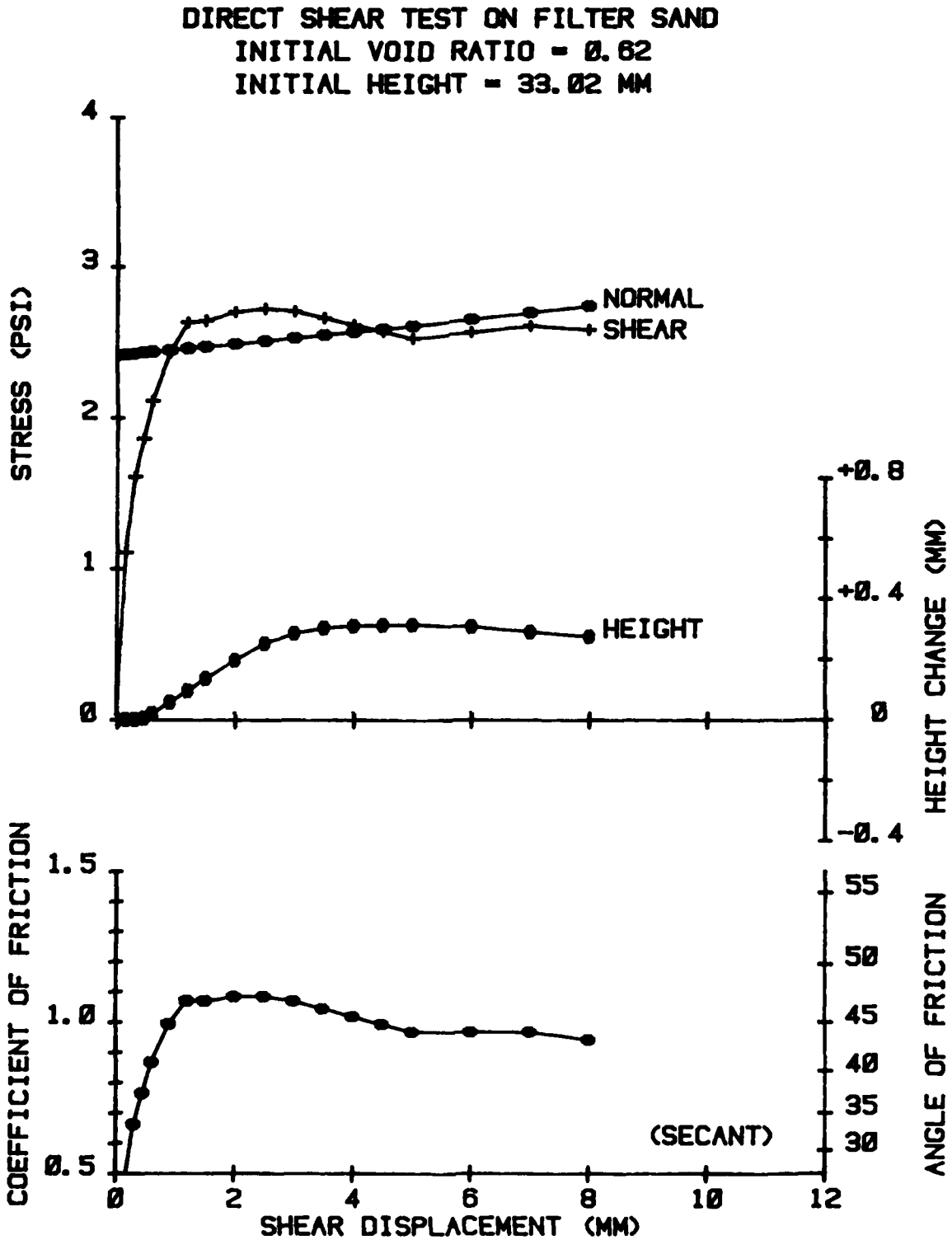

Figure A.12 Direct Shear Test on Filter Sand.

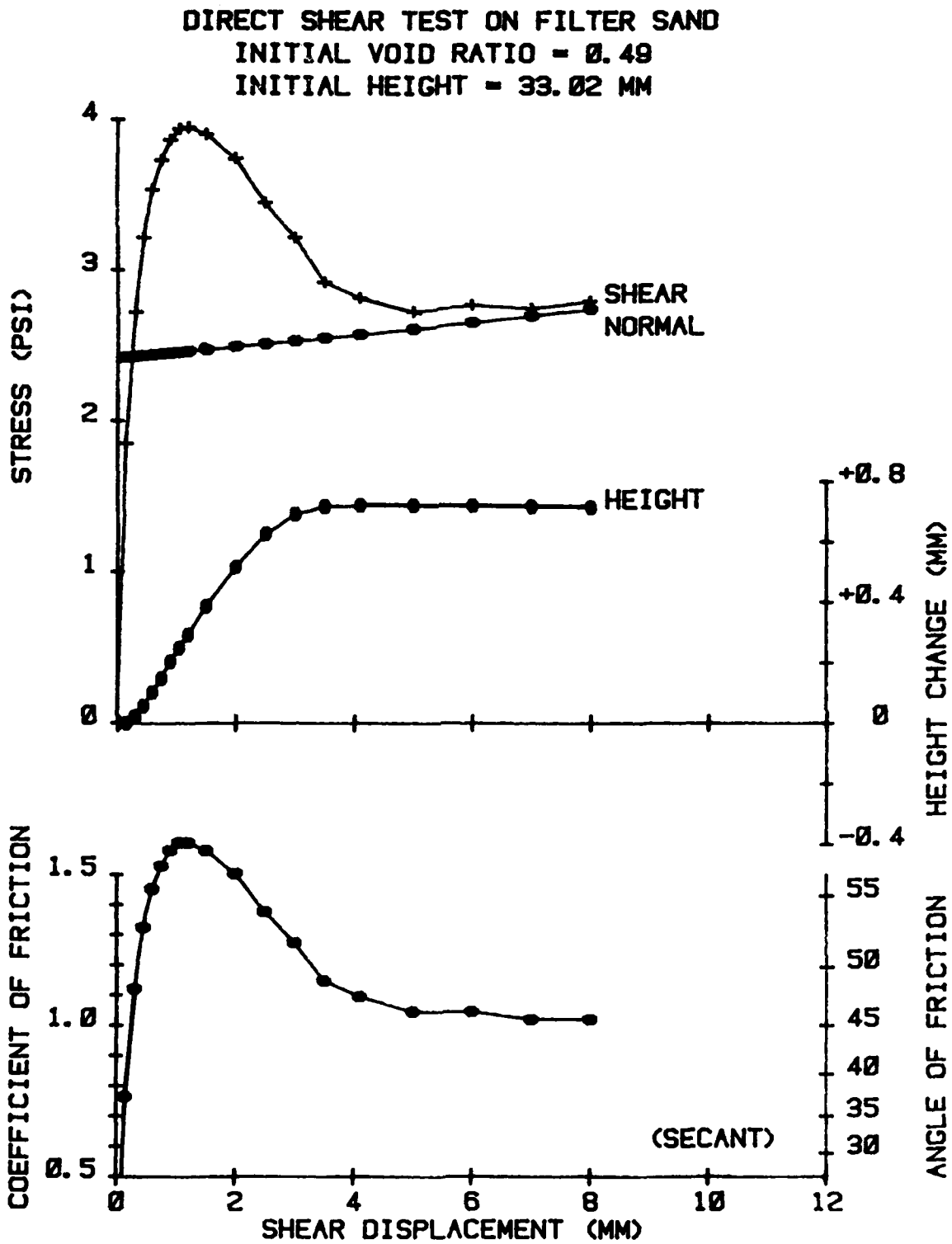

Figure A.13 Direct Shear Test on Filter Sand.

APPENDIX B

SOIL CALIBRATION OF CORNELL STRESS CELLS

The calibration of stress cells in the same soil and under the same stress conditions expected for their application is essential to obtain accurate measurements. The results from all the soil calibrations performed for this study are included here. Figures B.1 through B.3 are K_o soil calibrations using thin, 0.015 inch (0.38 mm), diaphragm cells. Figures B.4 through B.21 are K_o soil calibrations using the thicker, 0.025 inch (0.64 mm), diaphragm cells which were used for all remaining soil calibrations. Figures B.22 through B.33 are soil calibrations for isotropic stress conditions. Figures B.34 through B.51 are for triaxial soil calibrations including the stress path applied for each test.

The soil calibrations generally include the results from a cell measuring vertical stress and a second cell in the same test measuring the lateral stress. The results are plotted with the measured stress versus the applied stress for both cells through several cycles of loading for most tests. The overburden or weight of soil above the stress cell was included with the applied vertical stress for accuracy. The slope of the loading portion of the calibration line was determined from a least squares linear regression program using all the loading data points for each

cycle. The registration is listed for each cycle of loading as the registration value, R, below each plot. In nearly every test the measured stress during the unloading phase was higher than during the loading phase. This is referred to as a positive hysteresis in the load-unload cycle. The results from these calibration tests are summarized in Tables B.1 through B.3 and discussed in Section 7.3.

Figure No.	Initial Void Ratio	Cycle No.	Maximum Vertical Stress (psi)	Vertical Stress R	Vertical Stress Hysteresis Load	Vertical Stress Hysteresis Unload	Horizontal Stress R	Horizontal Stress Hysteresis Load	Horizontal Stress Hysteresis Unload
B.1	0.743(P)	1	10	0.83	3	32	Not Measured		
		2	20	0.70	-4	38			
		3	30	0.61	-9	43			
		10	30	0.58	-10	45			
	0.531(C)	1	15	0.58	-11	39			
		2	15	0.50	-15	35			
		10	15	0.46	-18	32			
B.2	0.735(P)	1	12	0.72	-2	22	0.93	4	10
		2	12	0.69	3	22	0.99	-3	10
B.3	0.690(P)	1	30	0.68	-3	28	0.96	4	13
		2	30	0.64	-7	36	0.81	-2	7
B.4	0.678(P)	1	10	1.41	-2	17			
		2	20	1.31	-3	22	1.40	-2	4
		3	30	1.23	-4	26	1.34	-4	6
		10	30	1.19	-7	23	1.36	2	8
B.5	0.735(P)	1	10	0.82	1	13	1.23	-3	4
		2	20	0.85	-1	16	1.26	2	6
		3	30	0.86	-2	19	1.21	1	9
B.6	0.735(P)	4	70	0.91	-1	29	1.15	-6	13
B.7	0.678(S)	5	15	1.19	-3	18	1.68	-3	5
		6	30	1.03	-6	21	1.47	-3	8

Table B.1 Summary of K_o Soil Calibration Tests.

Figure No.	Initial Void Ratio	Cycle No.	Maximum Vertical Stress (psi)	Vertical Stress R	Vertical Stress Hysteresis Load	Vertical Stress Hysteresis Unload	Horizontal Stress R	Horizontal Stress Hysteresis Load	Horizontal Stress Hysteresis Unload
B.8	0.548(C)	1	10	0.92	1	19	1.68	-5	-4
		2	20	0.85	-2	24	1.90	4	6
		3	30	0.80	-5	28	1.87	-2	4
B.9		4	10	0.99	-9	13	1.59	-3	2
B.10	0.668(P)	1	10	1.03	2	19	1.62	-4	-7
B.11		2	10	0.91	-5	18	1.56	2	-9
B.10		3	30	0.86	-3	24	1.45	-1	-4
		4	10	0.82	-6	29	1.43	2	2
B.12	0.530(V)	1	10	0.72	6	13	1.12	-1	4
		2	20	0.74	2	17	1.06	-3	7
		3	30	0.72	-2	22	0.97	-4	7
B.13	0.736(P)	1	10	1.41	-2	20	1.04	2	5
		2	20	1.22	-5	27	1.05	-2	4
		3	30	1.09	-8	31	1.08	1	5
B.14	0.624(V)	1	10	0.91	8	35	1.14	-1	-5
		2	20	0.84	-1	28	1.04	1	4
		3	30	0.71	-4	32	0.97	-2	6
B.15	0.548(V)	1	10	0.58	15	18	1.01	-2	12
		2	20	0.82	6	22	0.95	1	12
		3	30	0.82	-4	24	0.92	-3	14

Table B.1 Cont. Summary of K_o Soil Calibration Tests.

Figure No.	Initial Void Ratio	Cycle No.	Maximum Vertical Stress (psi)	Vertical Stress R	Vertical Stress Hysteresis Load	Vertical Stress Hysteresis Unload	Horizontal Stress R	Horizontal Stress Hysteresis Load	Horizontal Stress Hysteresis Unload
B.16	0.772(P)	1	10	1.10	3	-5	1.17	-1	13
		2	30	0.97	-3	11	1.16	1	19
B.17	0.765(P)	1	10	1.10	0	17	1.24	2	4
		2	20	1.10	-4	24	1.18	-4	5
		3	30	1.05	-6	27	1.13	-5	5
B.18	0.524(V)	1	10	0.48	8	11	1.19	-2	8
		2	20	0.59	5	17	1.08	-1	9
		3	30	0.62	2	19	1.00	-2	8
B.19	0.474(C)	1	10	1.32	3	20	1.09	-2	8
		2	20	1.17	-2	24	0.81	-2	8
		3	30	1.03	-5	26	0.76	-3	10
B.20		4	30	1.15	-11	25			
B.20	0.459(C)	1	10	1.25	1	17			
		2	10	1.17	-3	16	Not Measured		
		10	10	1.13	-5	15			
		25	10	1.10	-6	14			
B.21	0.459(C)	1	10	1.00	-1	17	1.27	-3	7
		2	20	0.90	-2	22	1.06	-8	7
		3	30	0.82	-4	24	0.93	-8	8

P = Pluviation C = Compaction (+ = overregistration)
V = Vibration (- = underregistration)

Table B.1 Cont. Summary of K_o Soil Calibration Tests.

Figure No.	Initial Void Ratio	Cycle No.	Maximum Stress (psi)	Vertical Stress R	Vertical Stress Hysteresis Load	Vertical Stress Hysteresis Unload	Horizontal Stress R	Horizontal Stress Hysteresis Load	Horizontal Stress Hysteresis Unload
B.22	0.724(P)	1	10	1.87	-3	15	0.99	5	19
		2	20	1.66	-3	19	0.96	-1	24
		3	30	1.47	-5	23	0.89	-4	30
B.23	0.695(P)	1	10	1.23	1	12	0.95	-7	16
		2	20	1.23	0	17	0.96	-4	27
		3	30	1.16	-2	19	0.85	-7	30
B.24	0.552(V)	1	10	1.20	-3	15	0.94	-5	23
		2	20	1.04	-6	19	0.78	-9	28
		3	30	0.93	-8	22	0.69	-12	31
B.25	0.539(V)	1	10	0.70	-3	24	0.83	1	9
		2	20	0.56	-9	28	0.78	-3	12
		3	30	0.47	-14	33	0.75	-4	15
B.26	0.705(P)	1	20	1.26	-3	14	0.91	-1	23
		2	30	1.18	-4	15	0.86	-2	27
B.27	0.548(V)	1	20	1.06	-6	22	0.69	-3	27
B.28	0.712(P)	1	30	1.15	-3	13	1.06	1	28
B.29	0.720(P)	1	30	1.08	-3	31	1.15	-1	16
B.30	0.524(V)	1	30	0.85	-3	24	0.54	1	33
B.31	0.474(C)	1	30	1.20	-8	26	0.50	-2	37

Table B.2 Summary of Isotropic Soil Calibration Tests.

Figure No.	Initial Void Ratio	Cycle No.	Maximum Stress (psi)	Vertical Stress R	Vertical Stress Hysteresis Load	Vertical Stress Hysteresis Unload	Horizontal Stress R	Horizontal Stress Hysteresis Load	Horizontal Stress Hysteresis Unload
B.32	0.459(C)	1	10	1.22	-4	15	0.55	-1	21
		10	10	1.16	-8	13	0.56	-11	17
		25	10	1.14	-8	13	0.58	-12	17
B.33		26	30	0.95	-9	21	0.49	5	34

P = Pluviation
V = Vibration
C = Compaction

(+ = overregistration)
(- = underregistration)

Table B.2 Cont. Summary of Isotropic Soil Calibration Tests.

Figure No.	Initial Void Ratio	Cycle No.	Maximum Vertical Stress (psi)	Vertical Stress R	Vertical Stress Hysteresis Load	Vertical Stress Hysteresis Unload	Horizontal Stress R	Horizontal Stress Hysteresis Load	Horizontal Stress Hysteresis Unload
B.35	0.552(V)	1	15	1.18	8	29	0.89	-10	6
B.37	0.539(V)	1	30	0.47	-14	33	0.75	-4	15
B.39	0.767(P)	1	10	1.13	3	-7	1.01	5	8
		2	20	1.14	2	5	0.97	1	13
B.41	0.705(P)	1	30	1.11	-7	28	0.96	6	20
B.43	0.548(V)	1	15	0.99	7	69	0.75	6	-5
B.45	0.712(P)	1	30	1.17	-2	51	0.97	-3	30
B.47	0.524(V)	1	15	0.86	-5	52	0.99	7	15
		2	30	0.76	5	51	0.76	-10	18
B.49	0.459(C)	1	30	0.86	-9	26	0.69	17	18
		2	30	0.71	2	41	0.48	8	8
B.51	0.459(C)	1	30	0.82	-5	22	1.28	20	-32

P = Pluviation
V = Vibration
C = Compaction

(+ = overregistration)
(- = underregistration)

Table B.3 Summary of Triaxial Soil Calibration Tests.

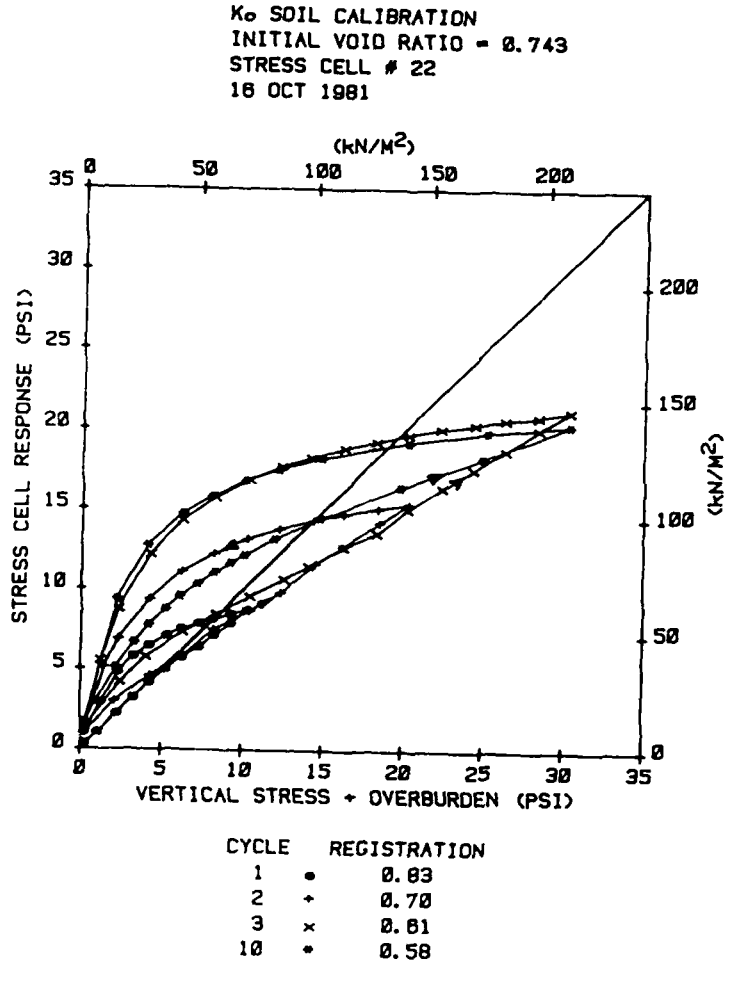

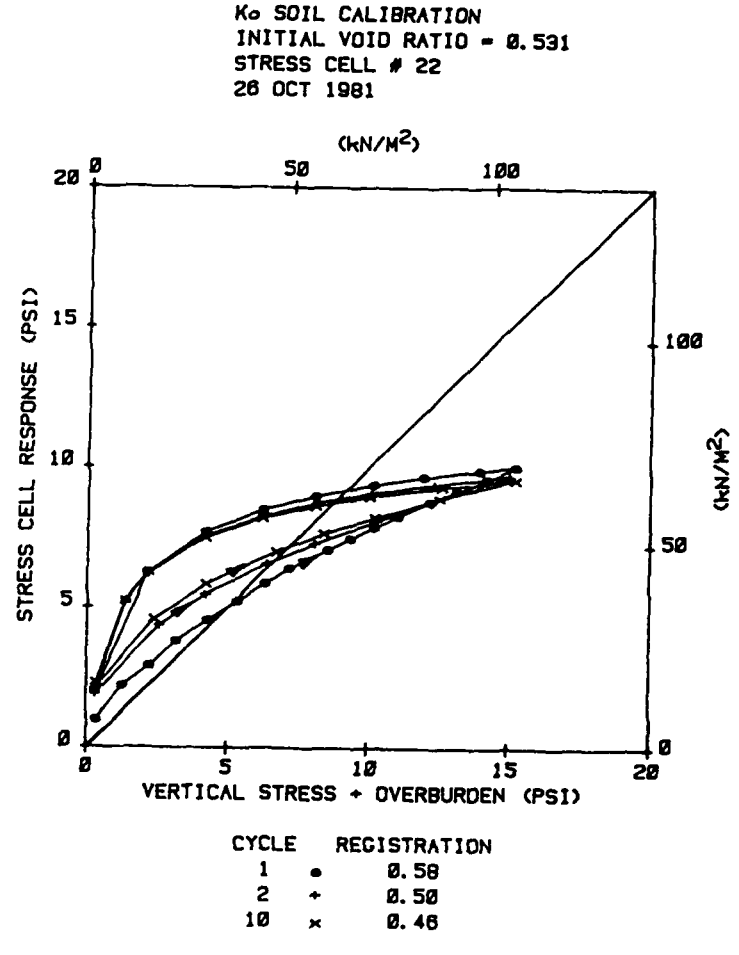

Figure B.1 K_o Soil Calibration.

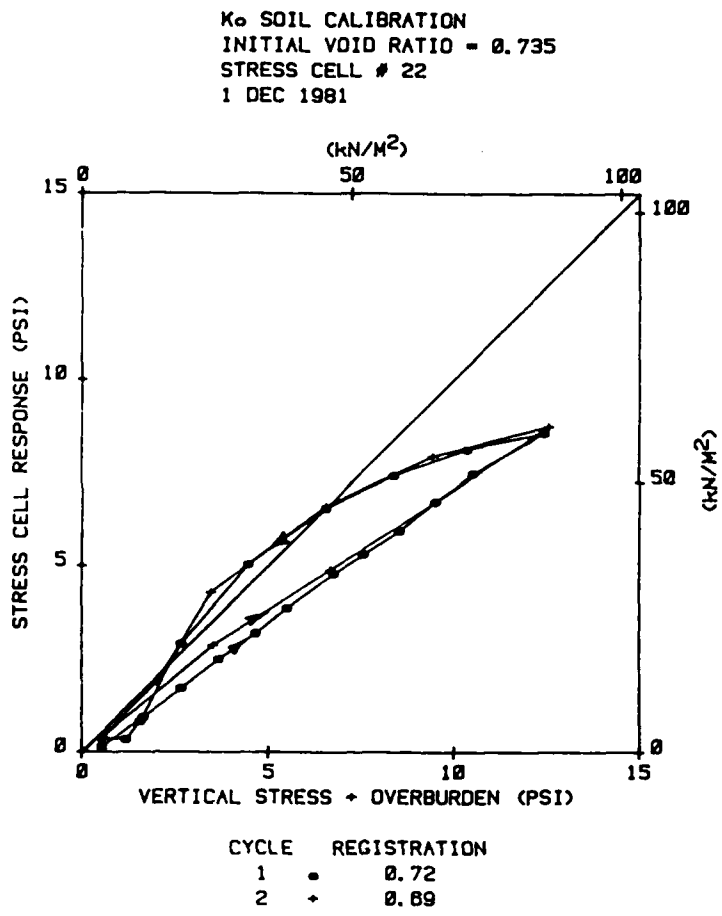

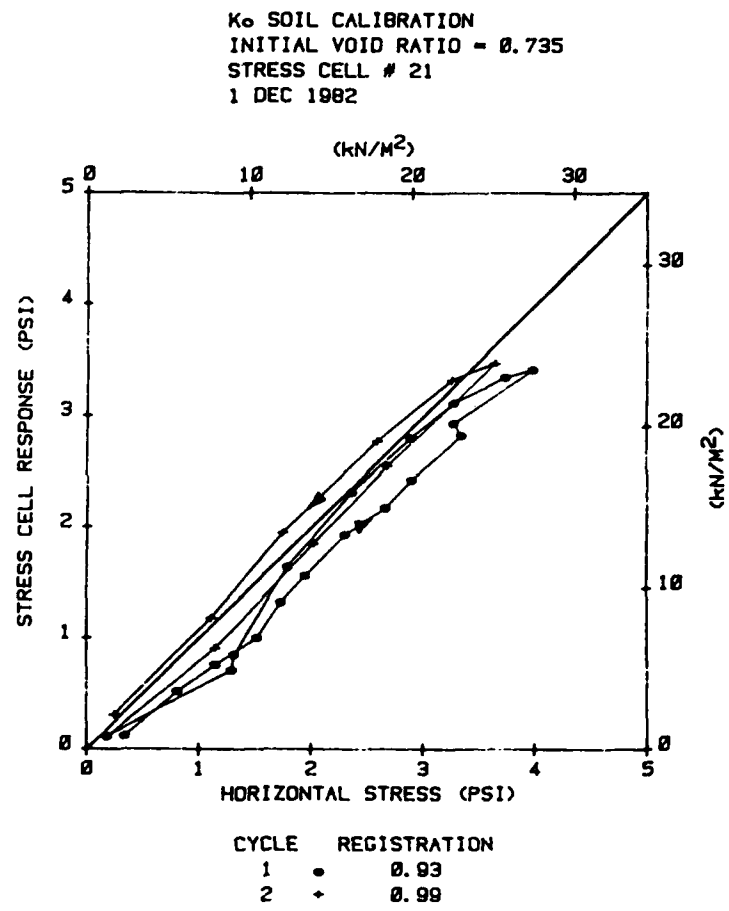

Figure B.2 K_o Soil Calibration.

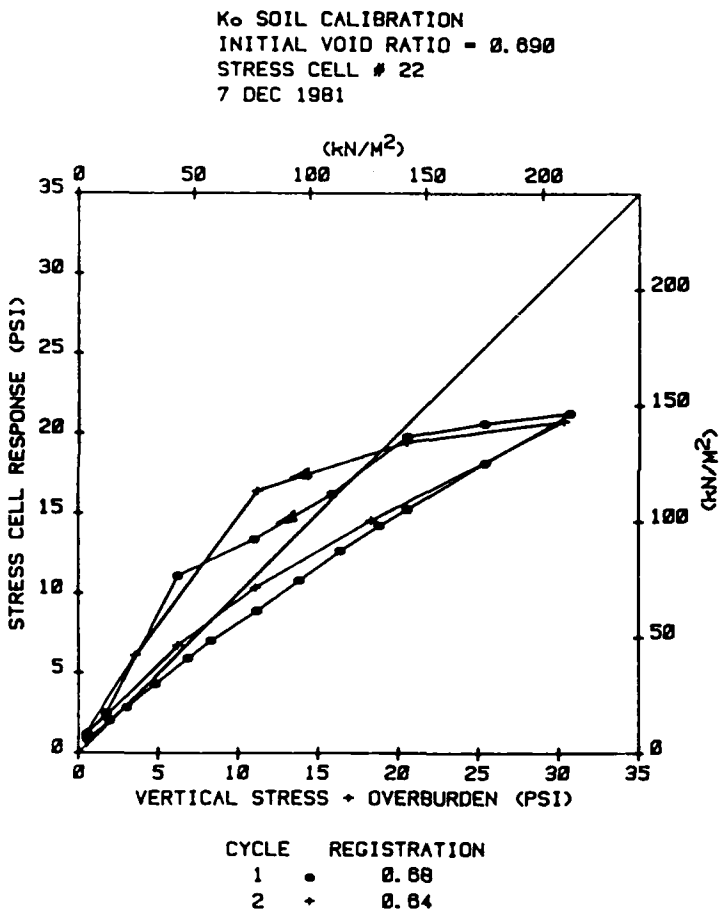

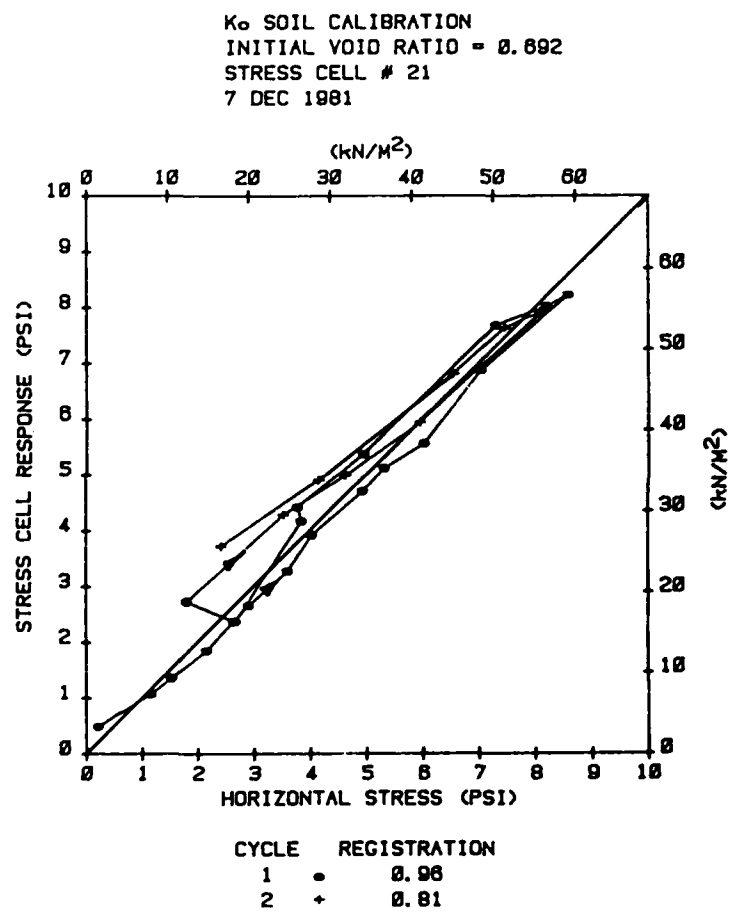

Figure B.3 K_o Soil Calibration.

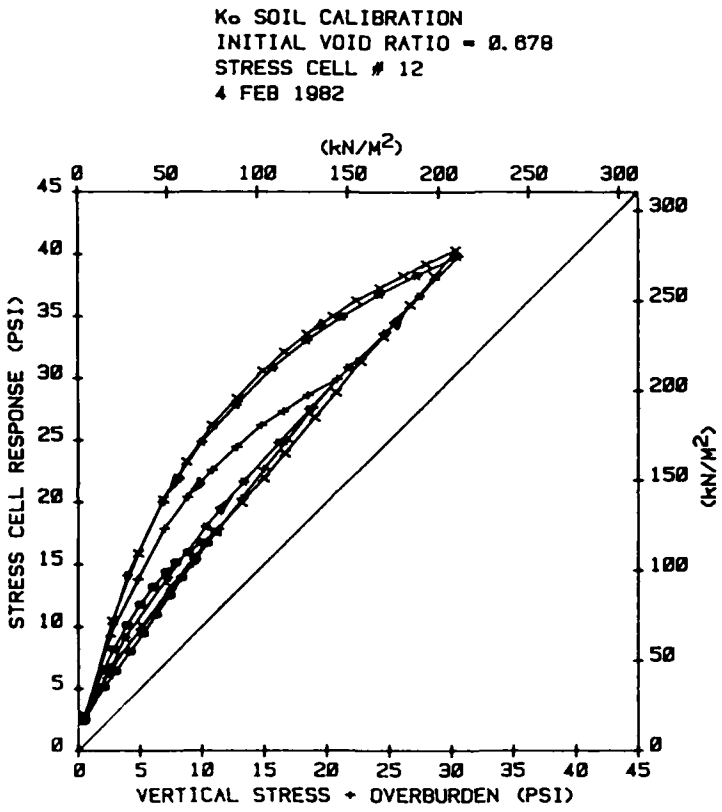

CYCLE		REGISTRATION
1	•	1.41
2	+	1.31
3	×	1.23
10	*	1.19

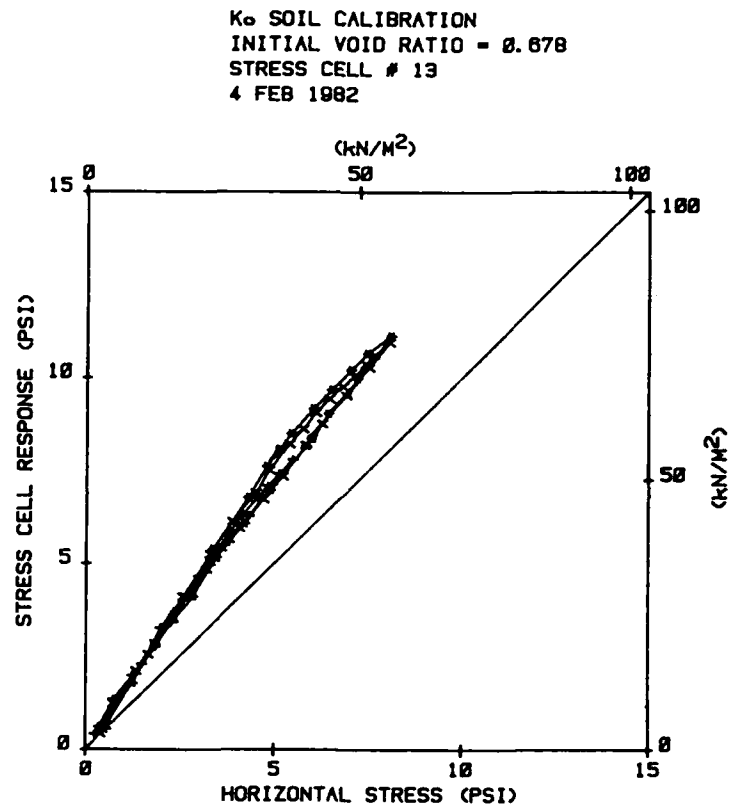

CYCLE		REGISTRATION
2	+	1.40
3	×	1.34
10	*	1.36

Figure B.4 K_o Soil Calibration.

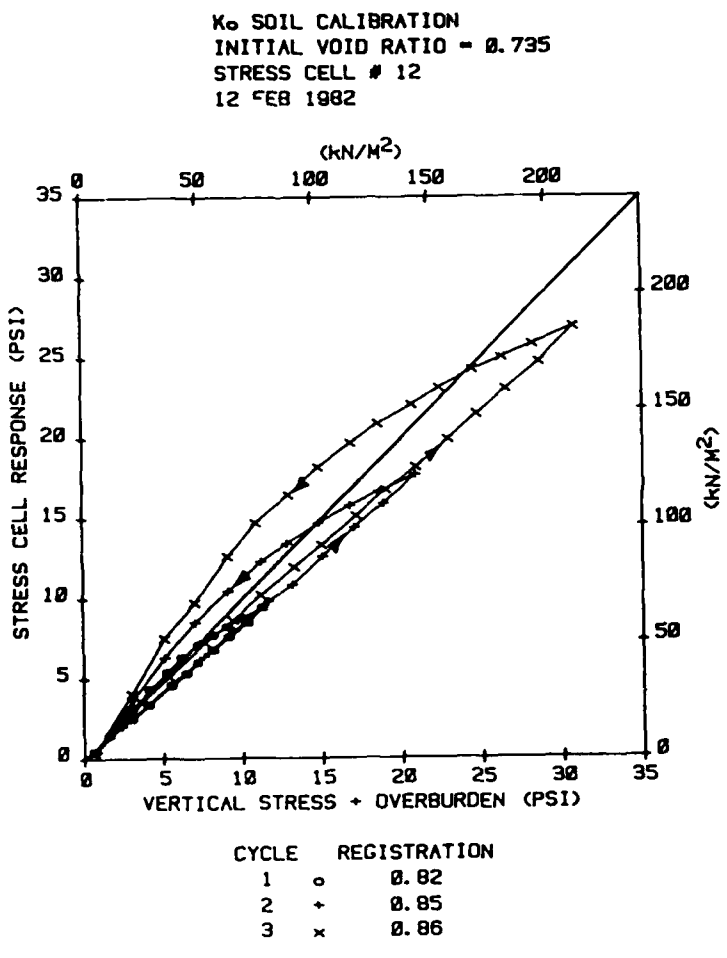

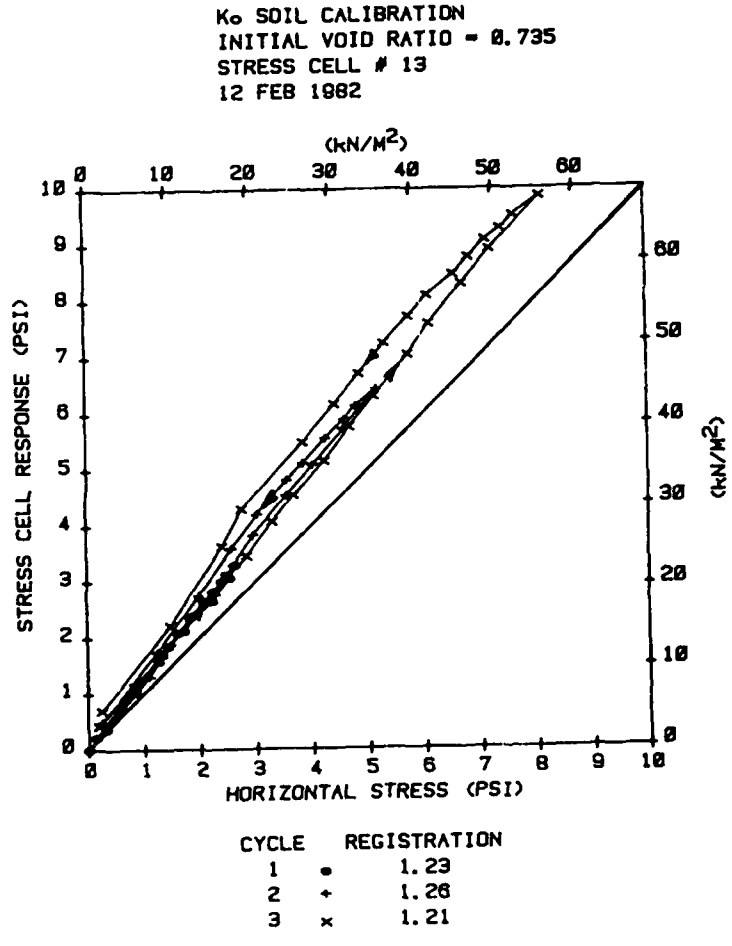

Figure B.5 K_o Soil Calibration.

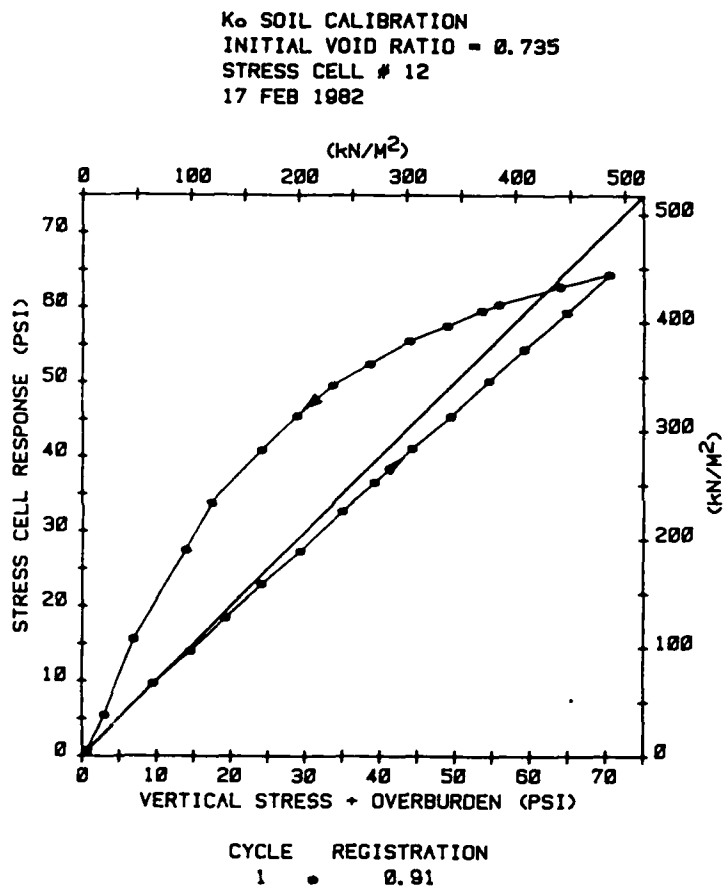

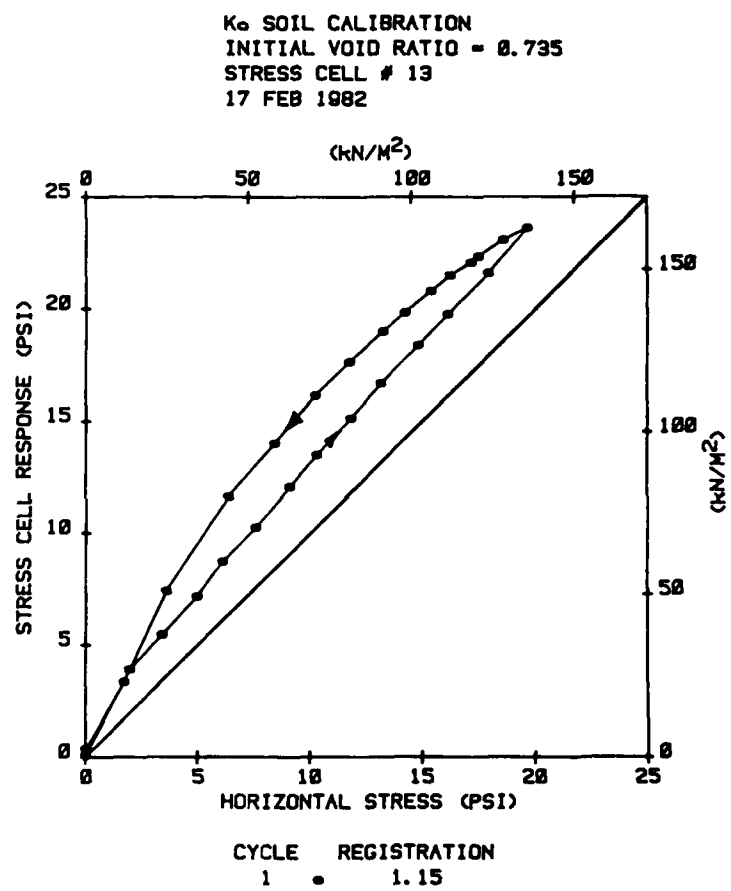

Figure B.6 K_o Soil Calibration.

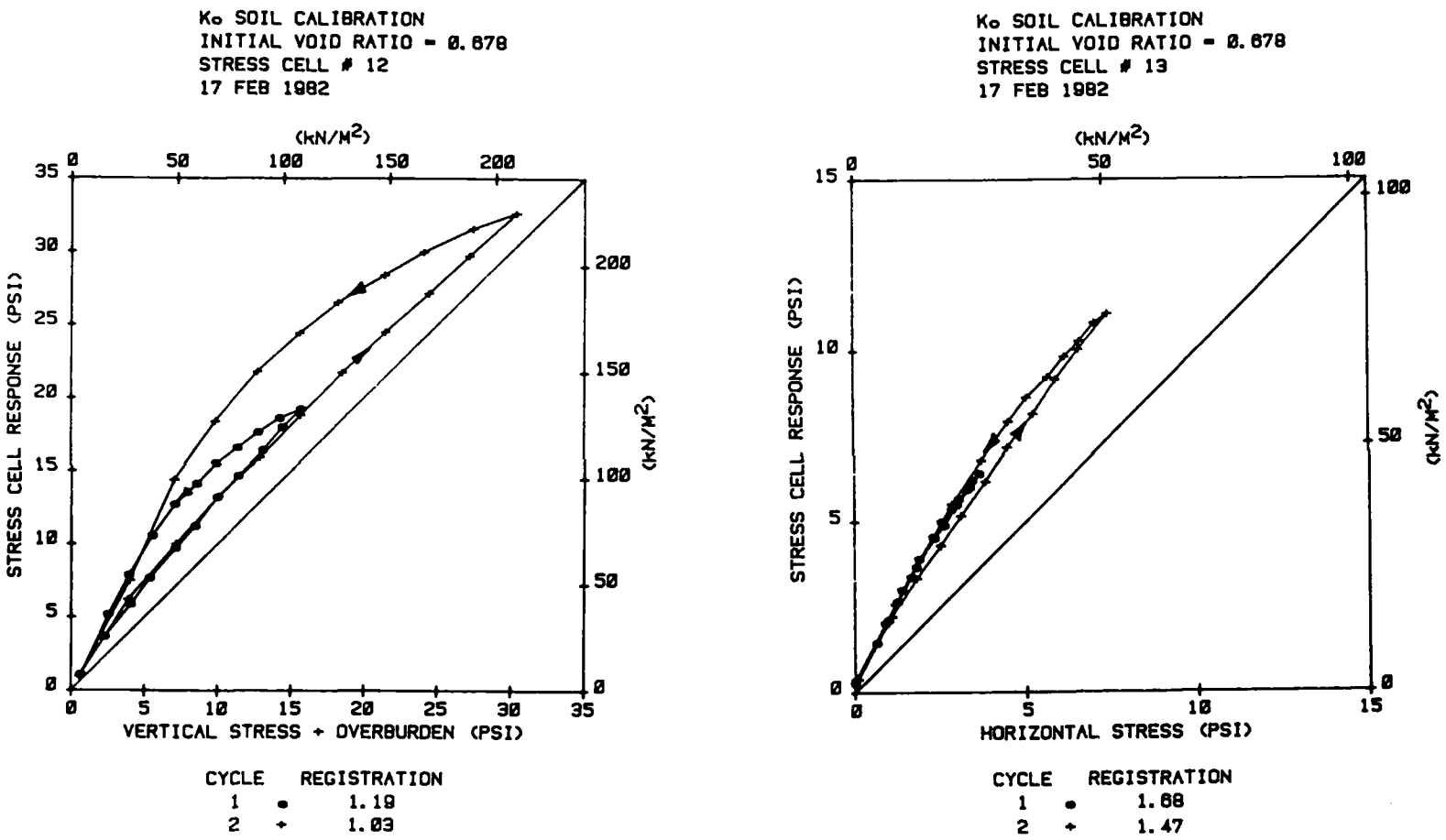

Figure B.7 K_o Soil Calibration.

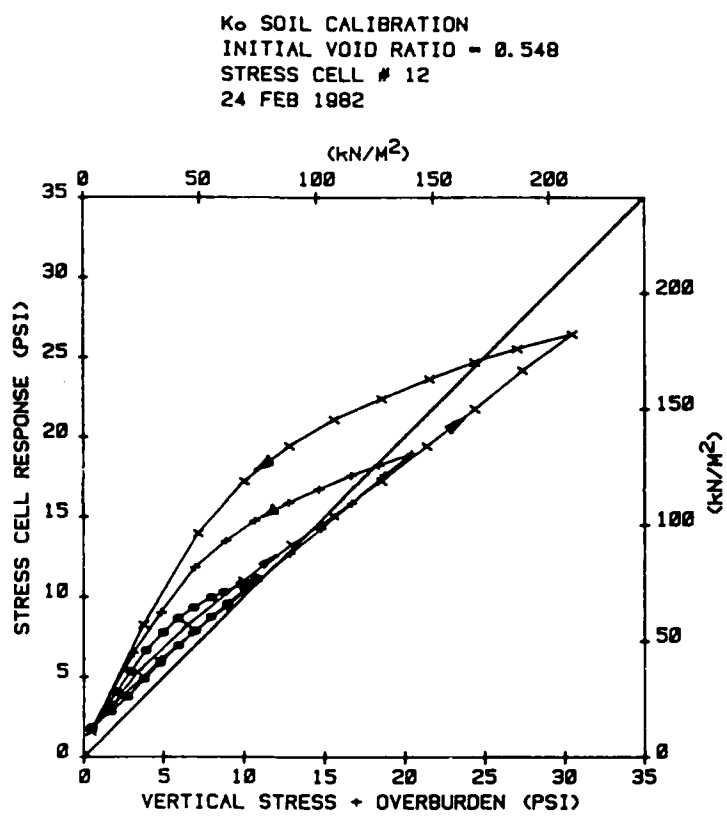

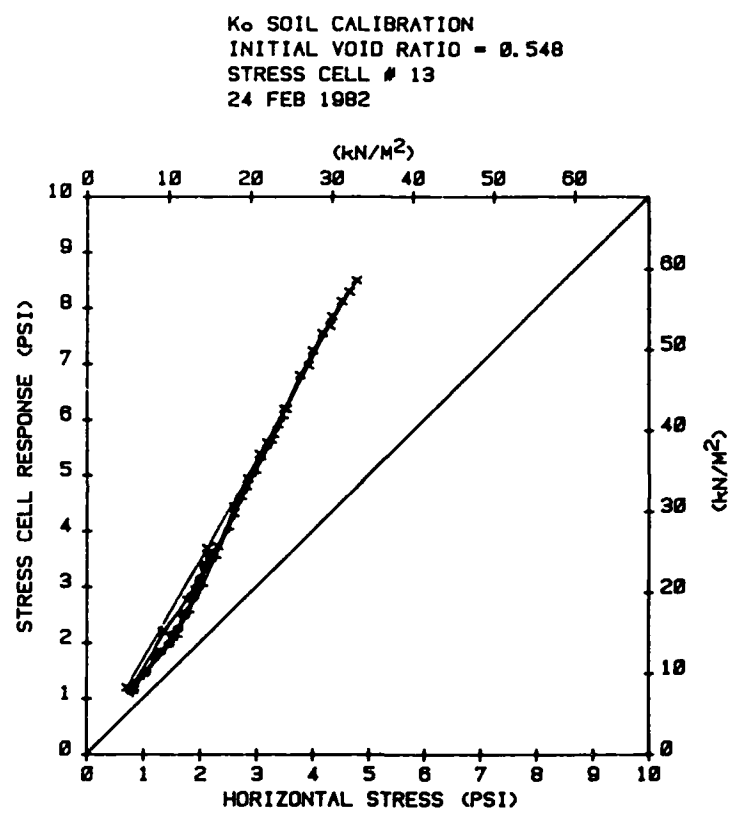

Figure B.8 K_o Soil Calibration.

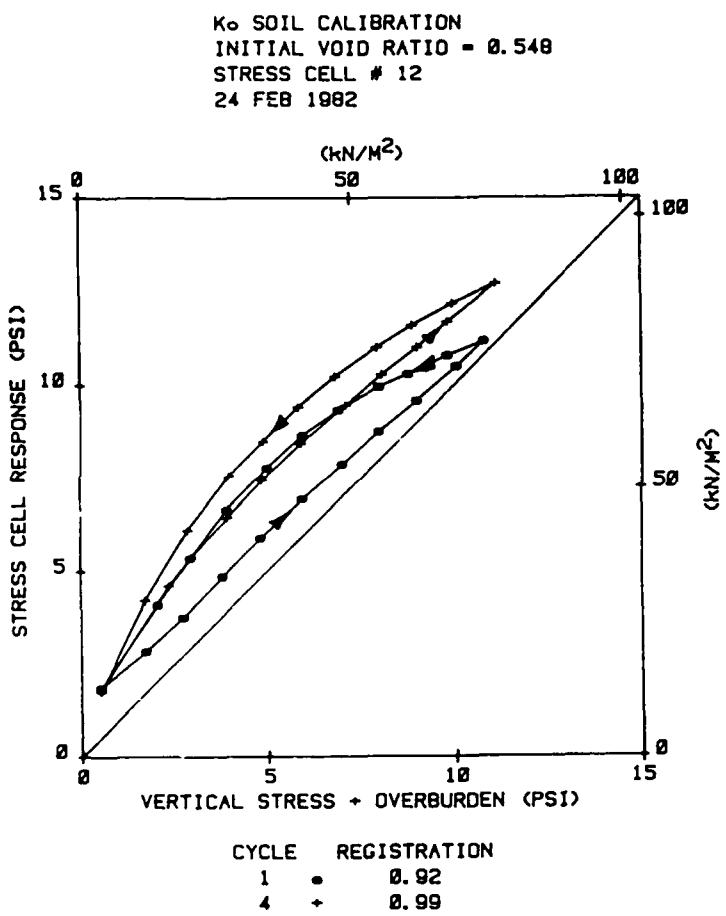

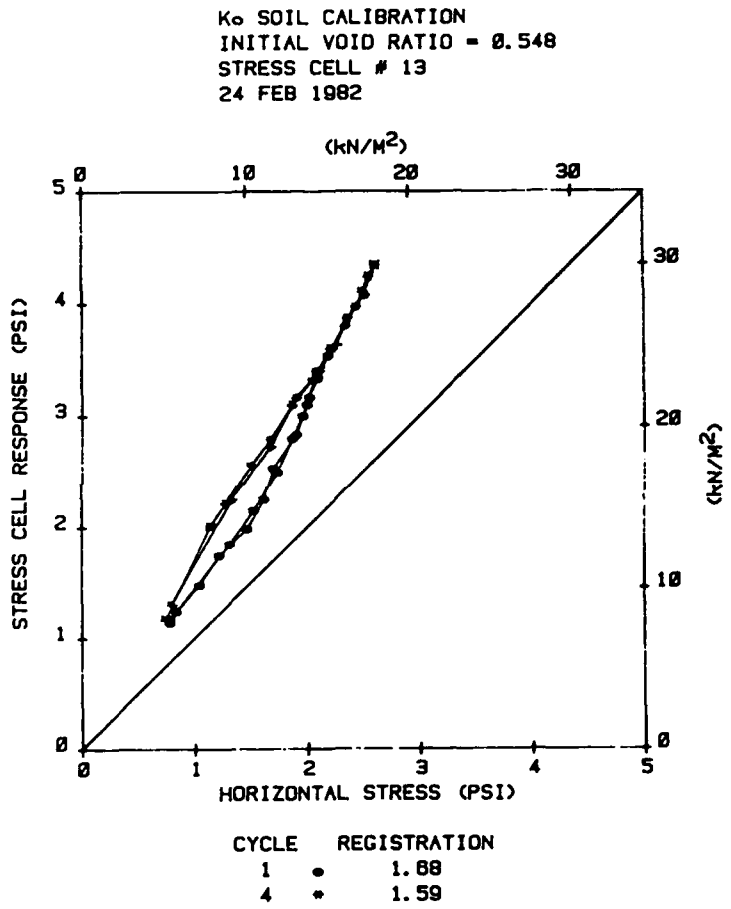

Figure B.9 K_o Soil Calibration.

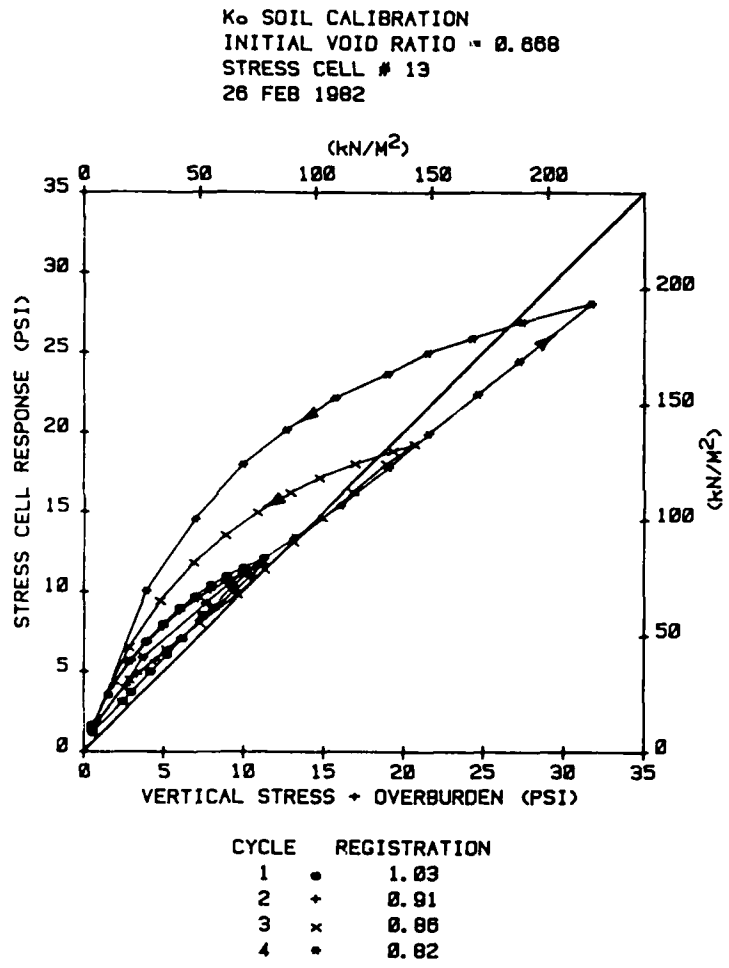

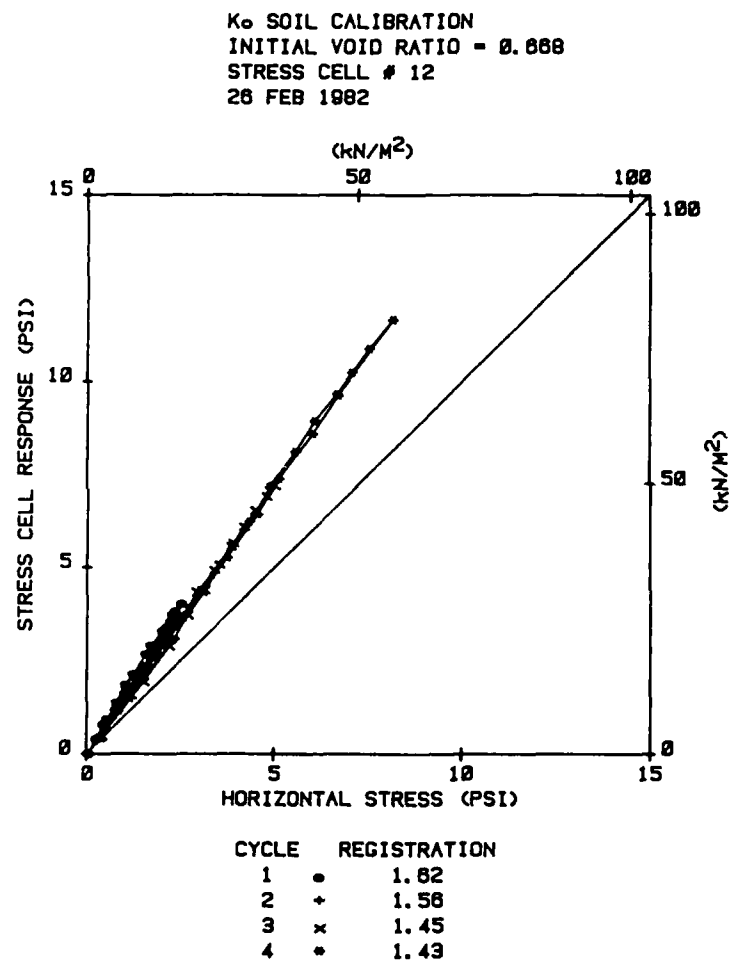

Figure B.10 K_o Soil Calibration.

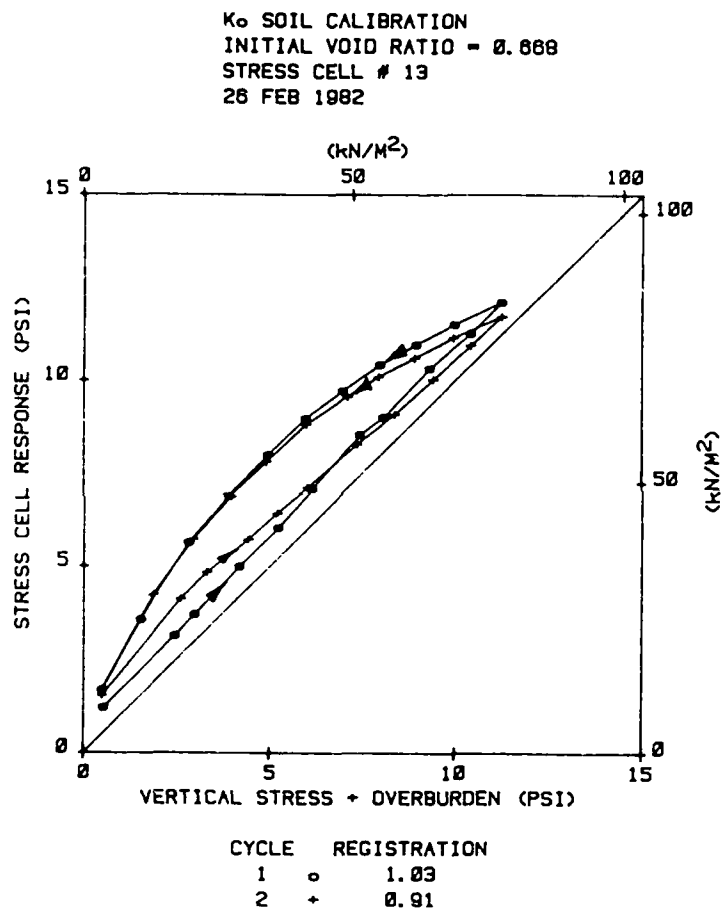

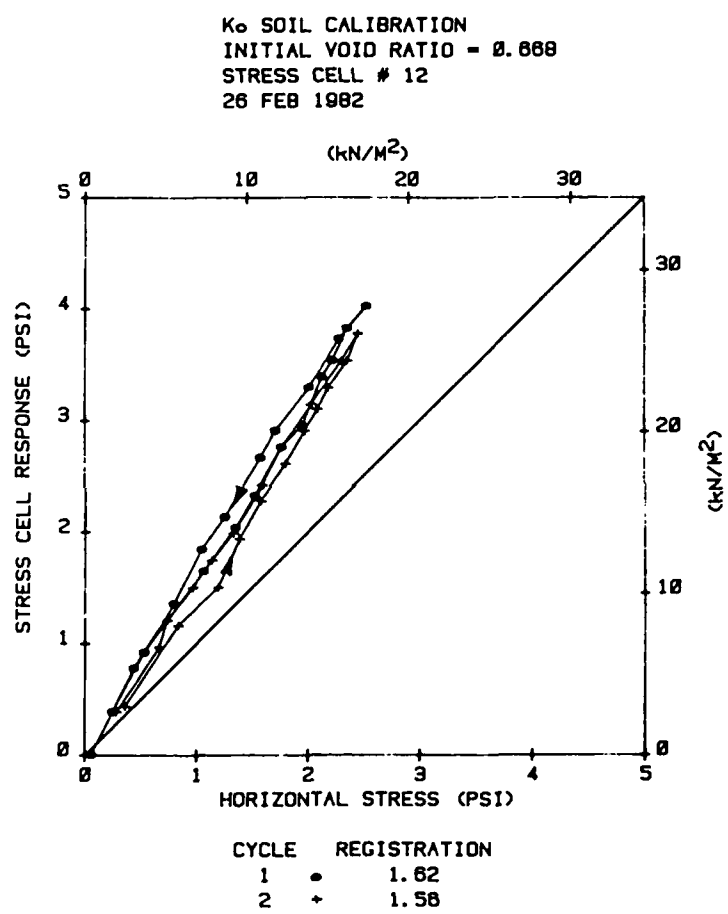

Figure B.11 K_o Soil Calibration.

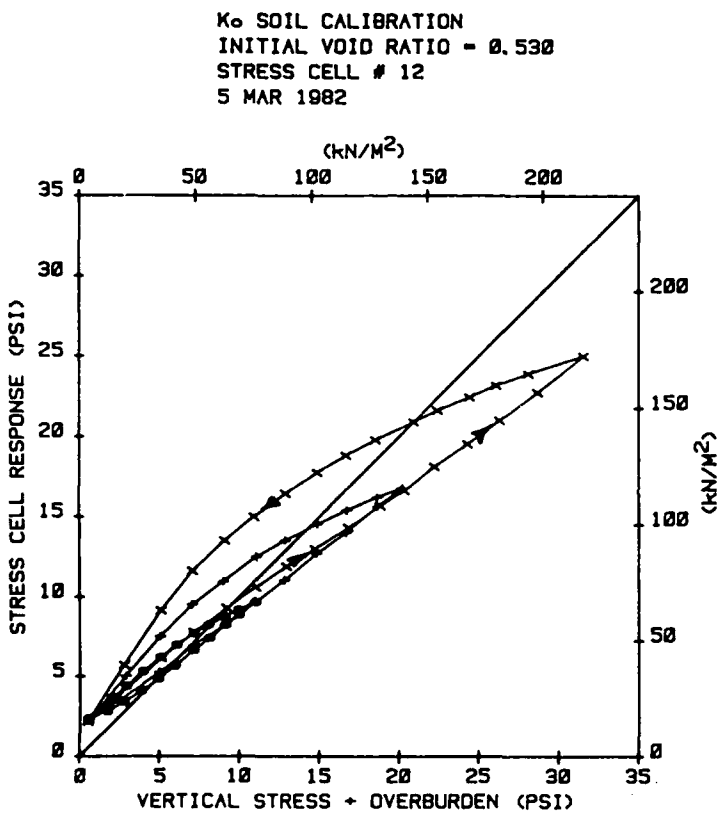

CYCLE		REGISTRATION
1	o	0.72
2	+	0.74
3	x	0.72

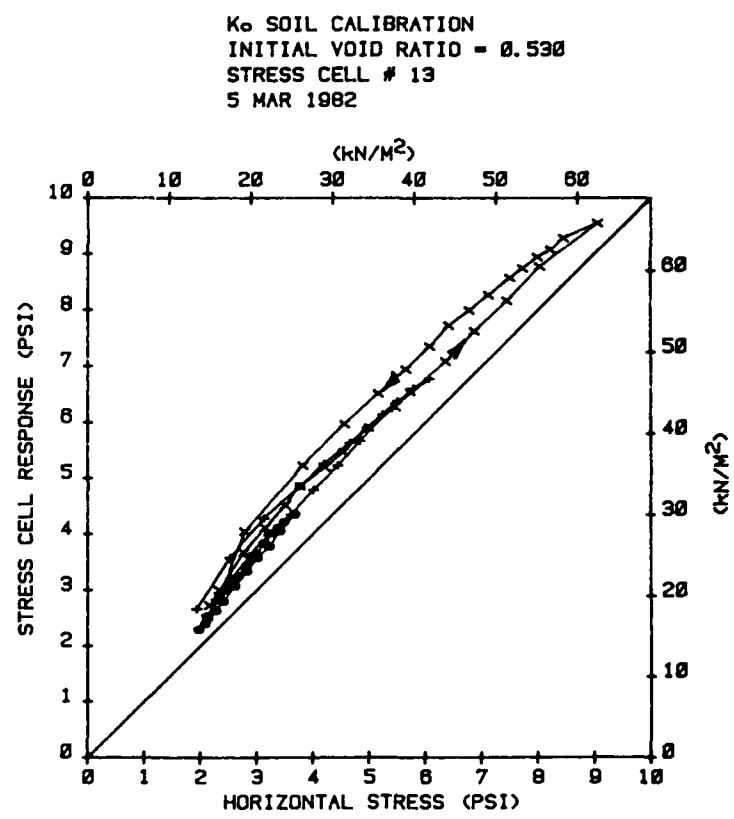

CYCLE		REGISTRATION
1	•	1.22
2	+	1.06
3	x	0.97

Figure B.12 K_o Soil Calibration.

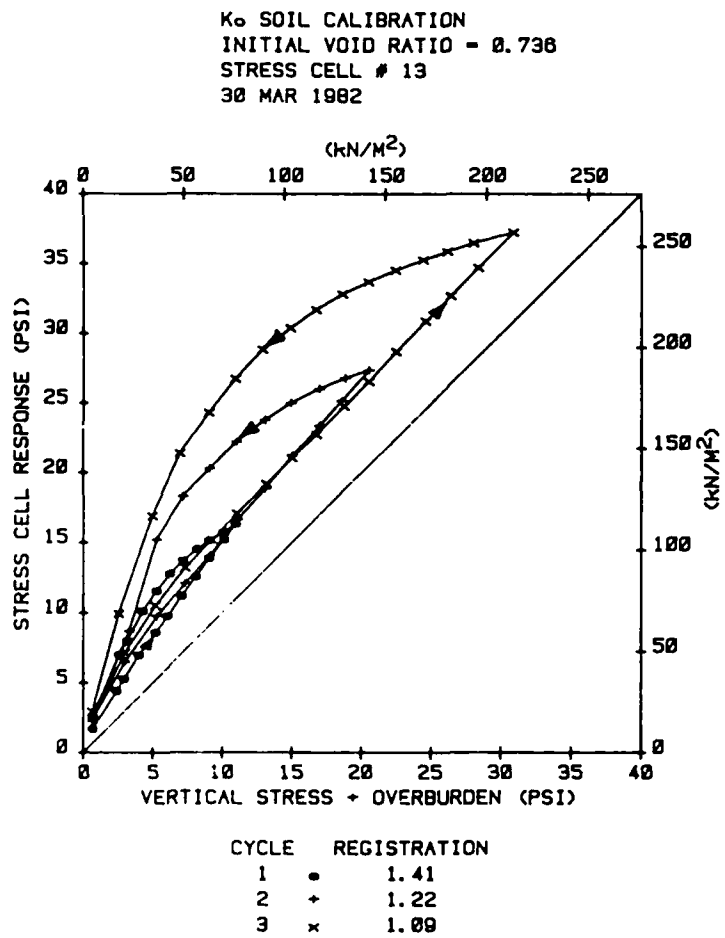

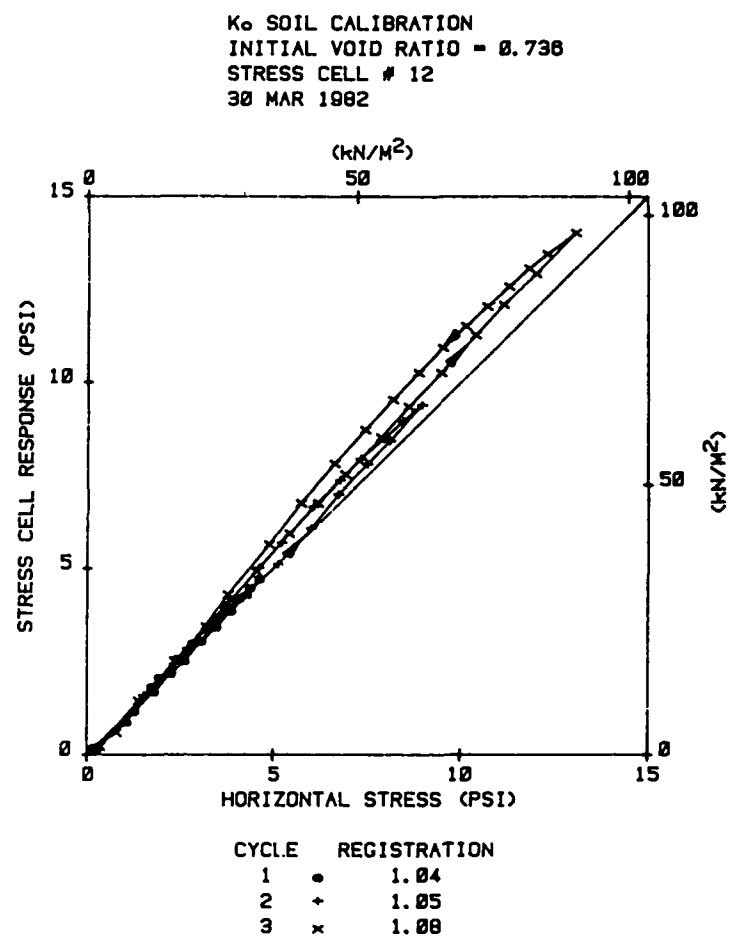

Figure B.13 K_o Soil Calibration.

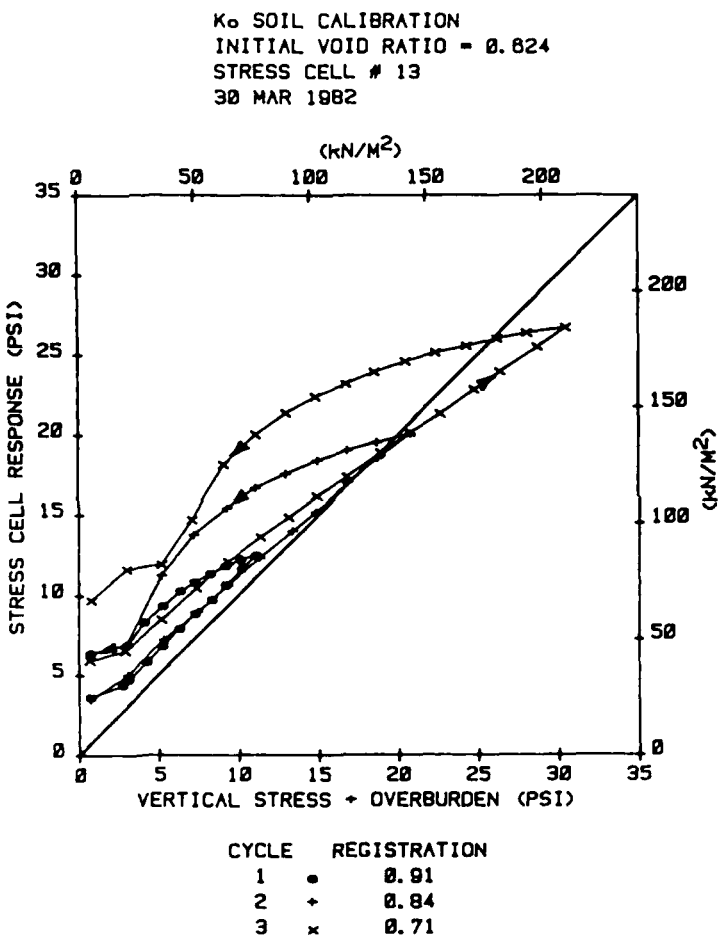

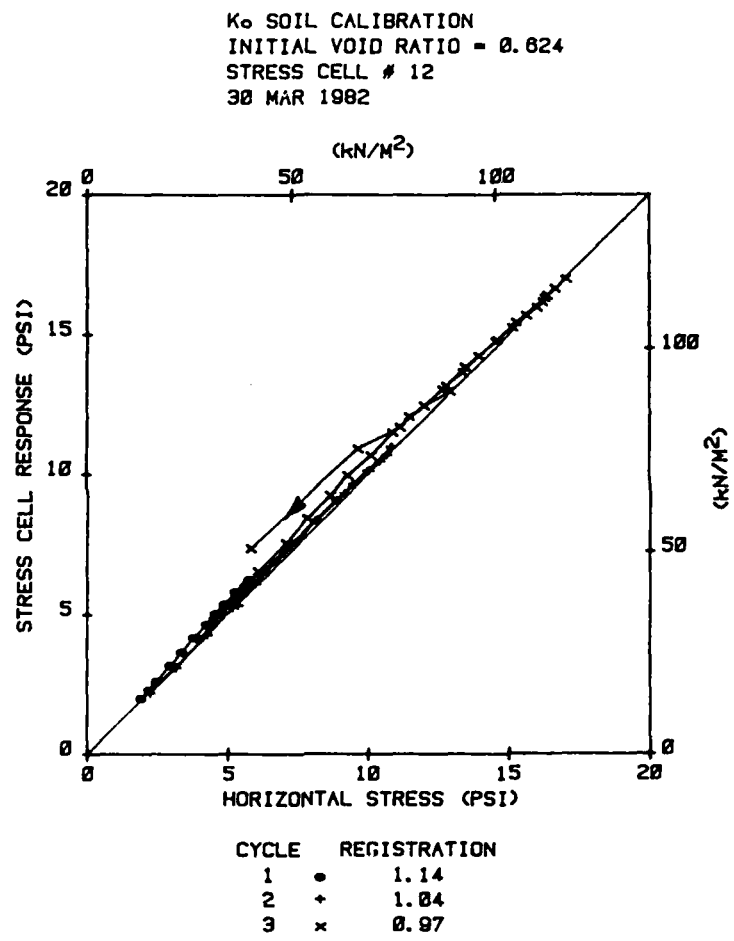

Figure B.14 K_o Soil Calibration.

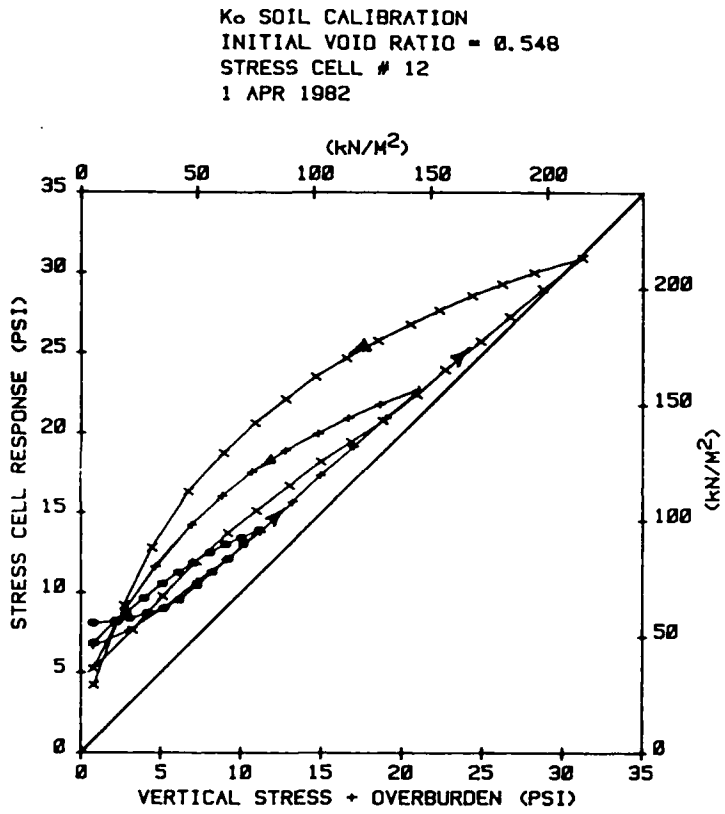

CYCLE		REGISTRATION
1	•	0.58
2	+	0.82
3	×	0.82

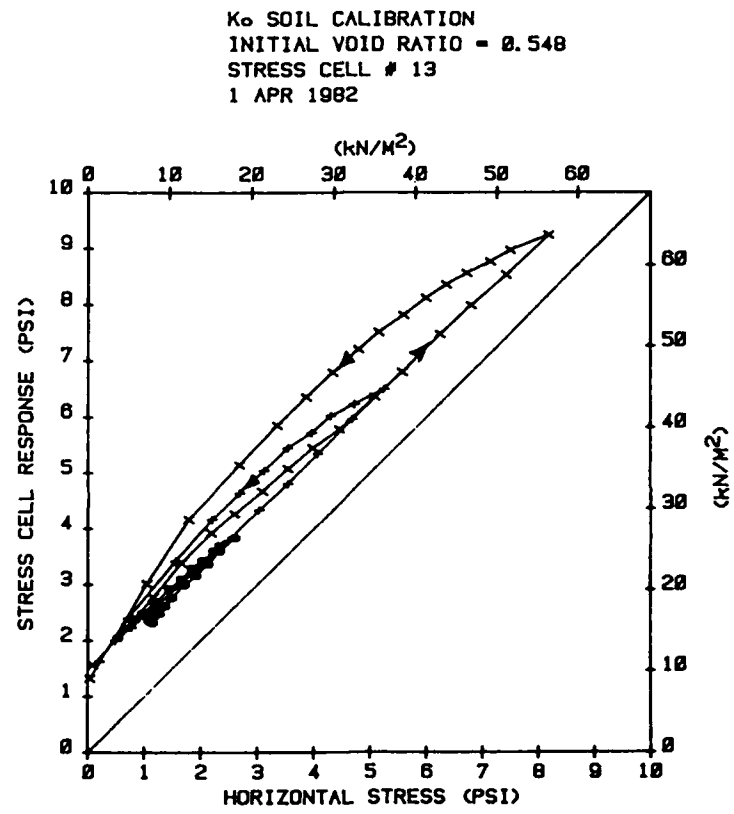

CYCLE		REGISTRATION
1	•	1.01
2	+	0.95
3	×	0.92

Figure B.15 K_o Soil Calibration.

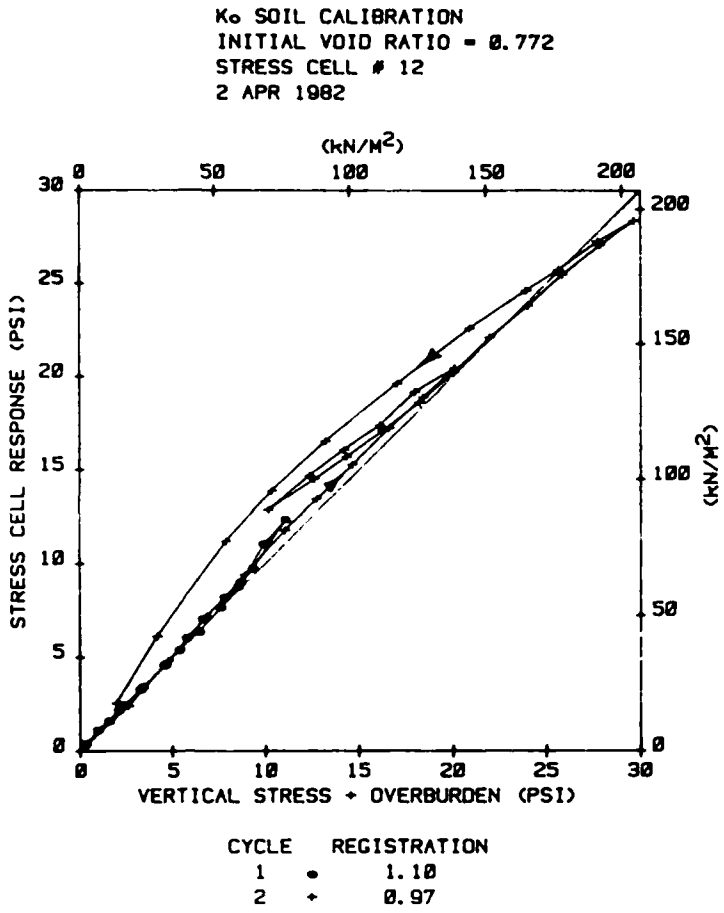

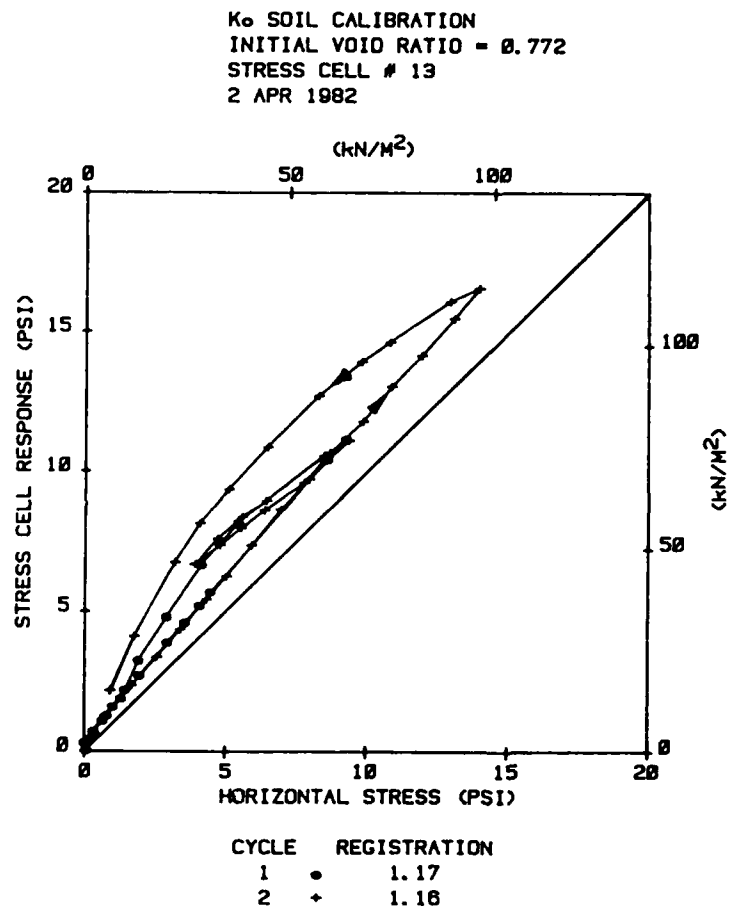

Figure B.16 K_o Soil Calibration.

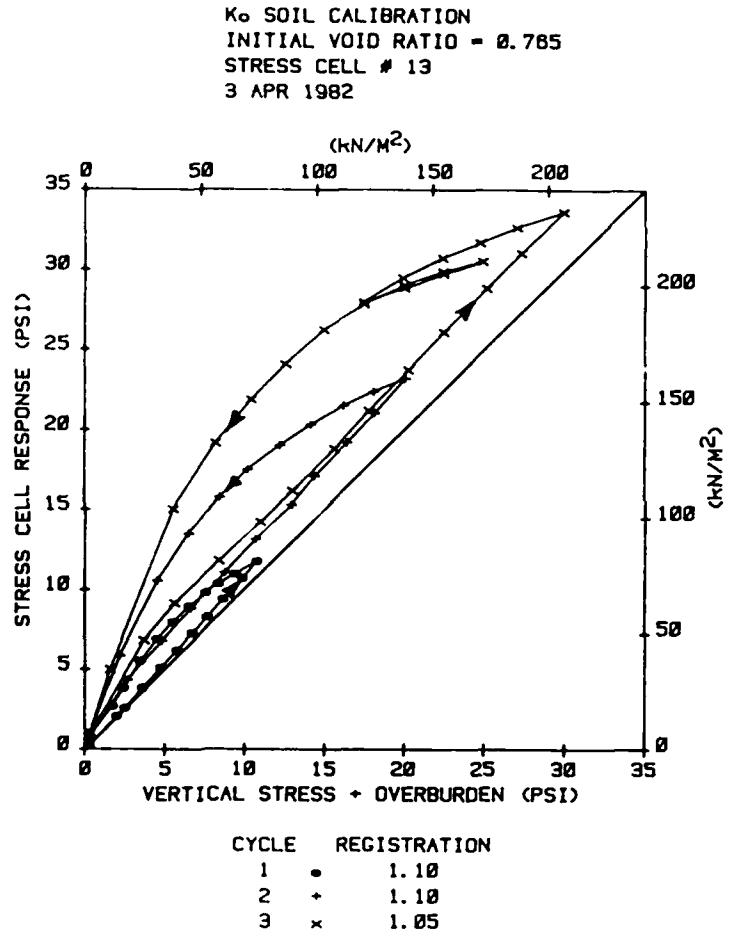

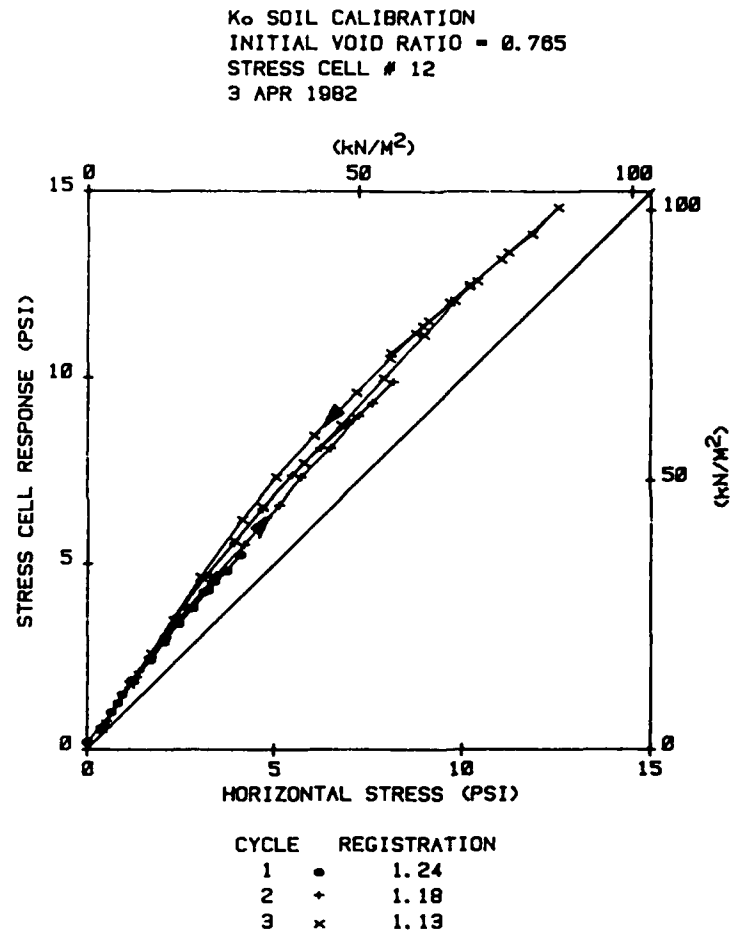

Figure B.17 K_o Soil Calibration.

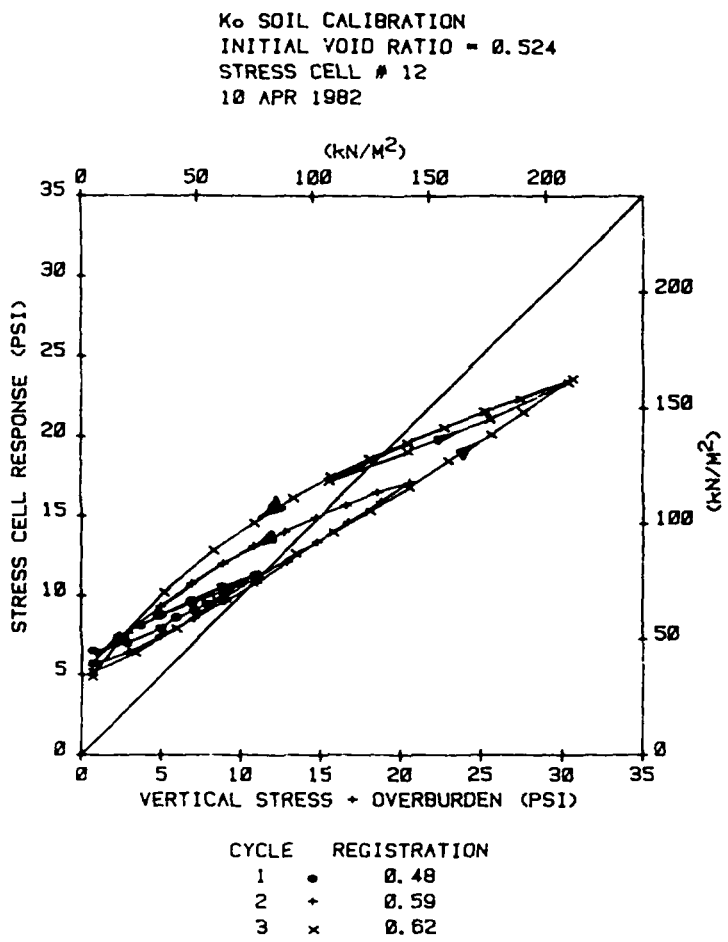

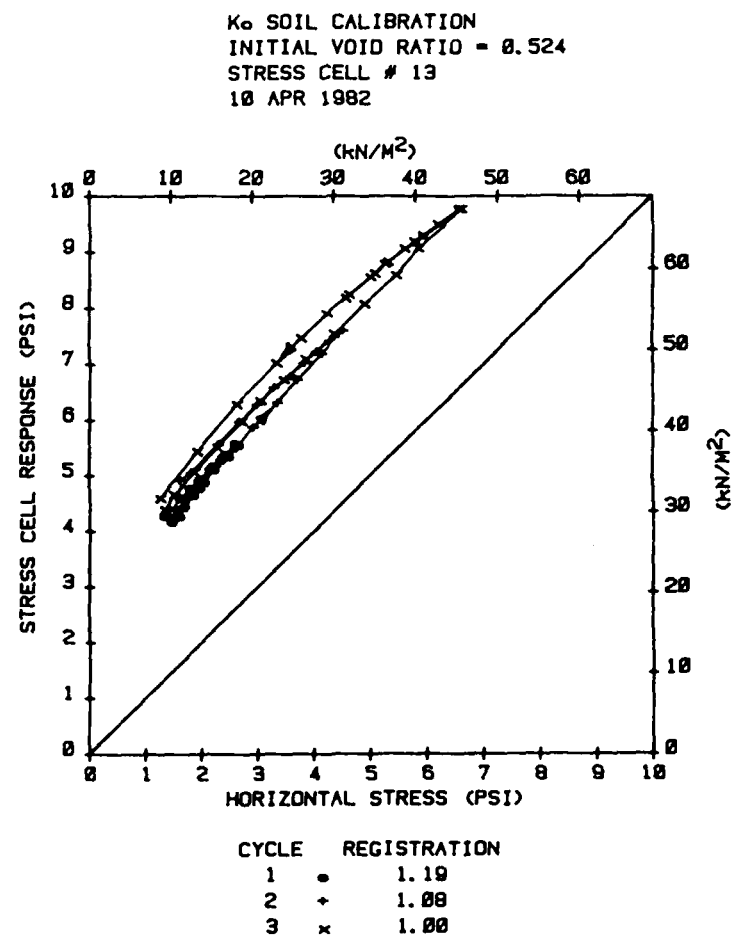

Figure B.18 K_o Soil Calibration.

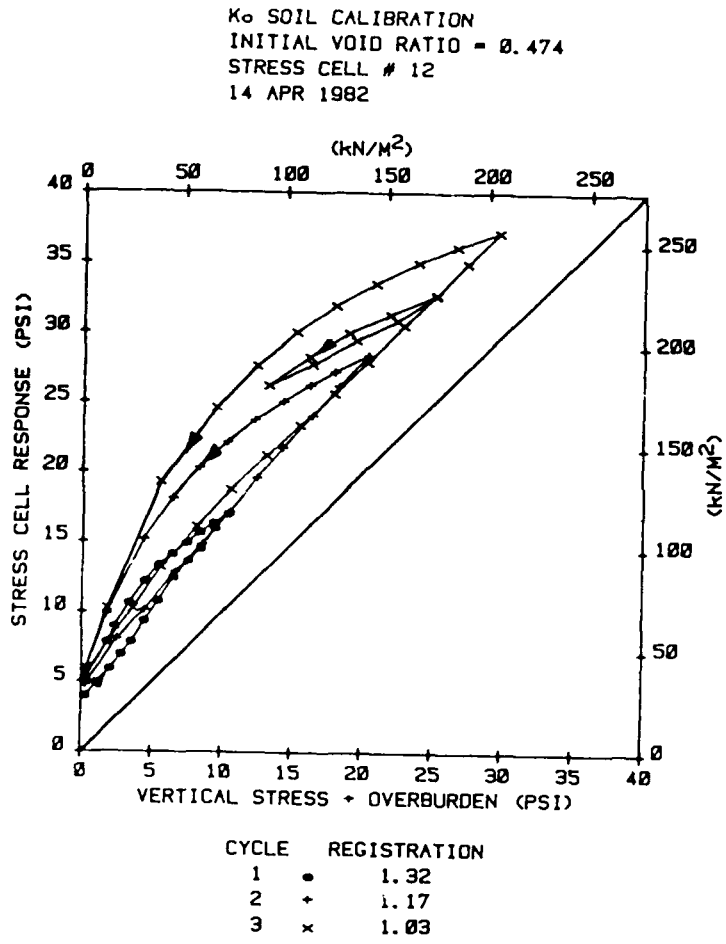

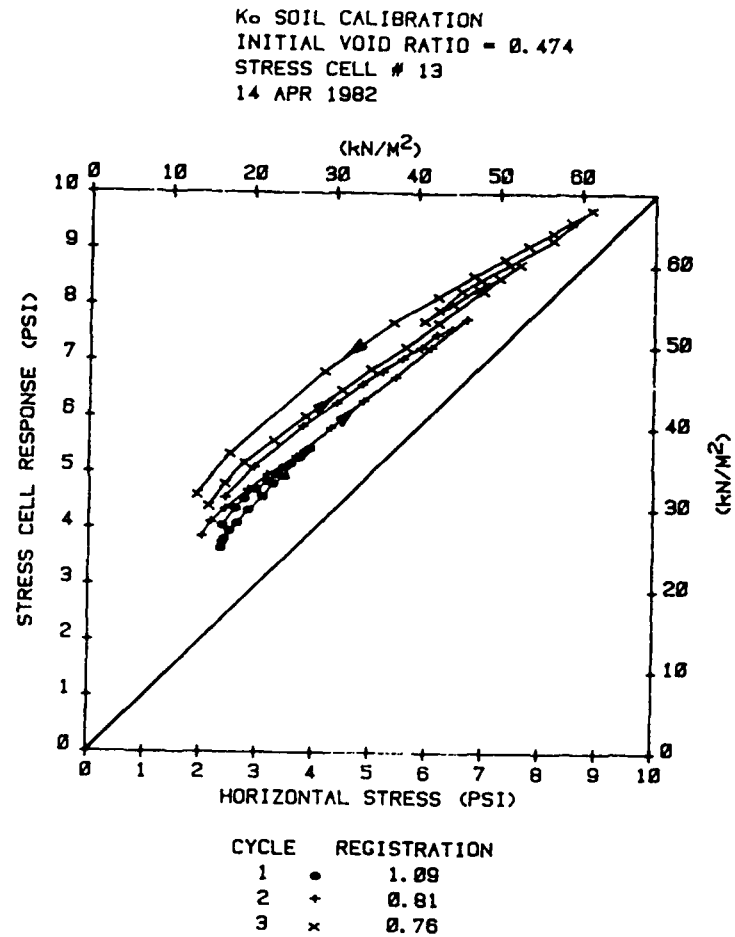

Figure B.19 K_o Soil Calibration.

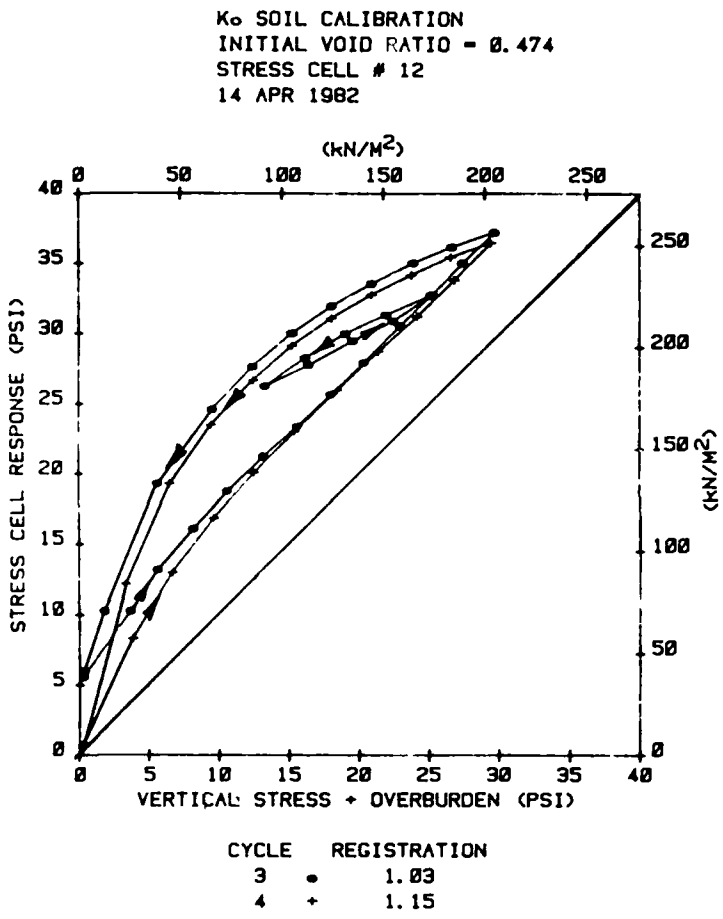

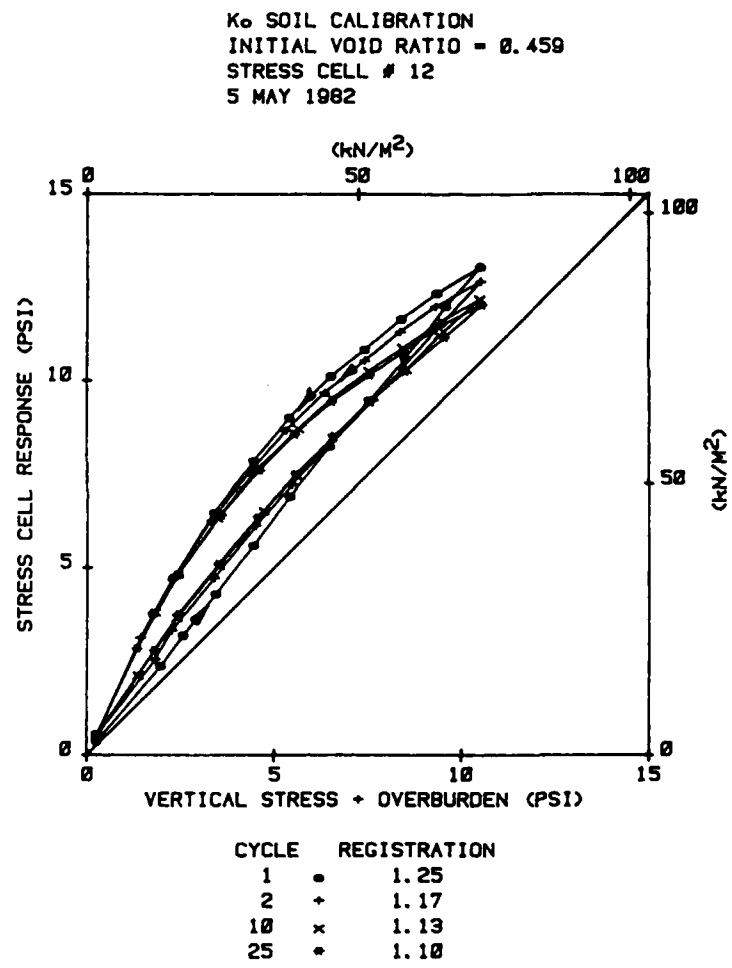

Figure B.20 K_o Soil Calibration.

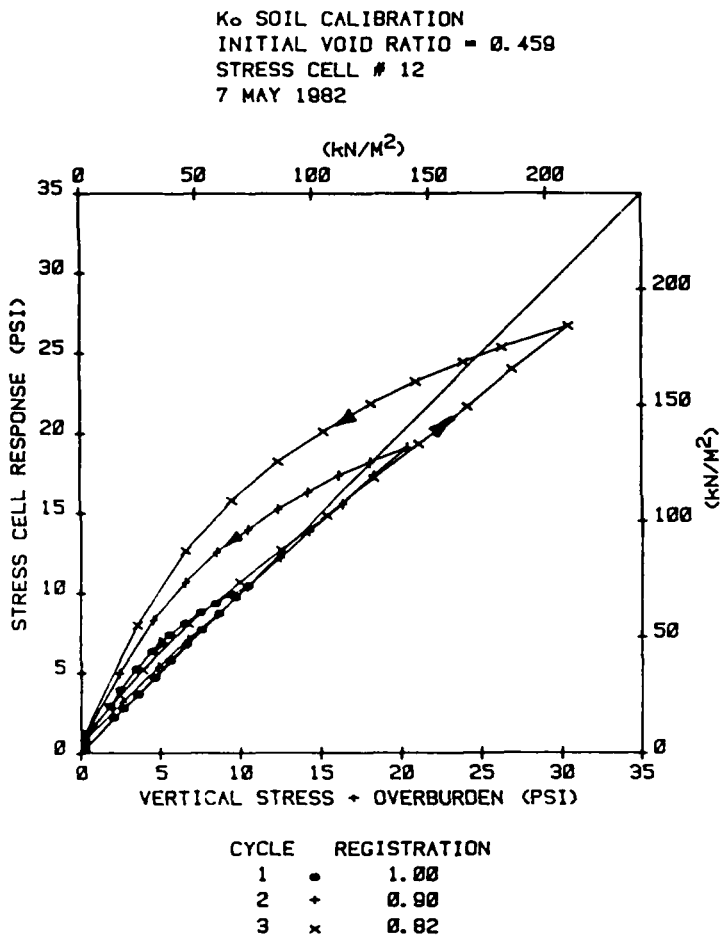

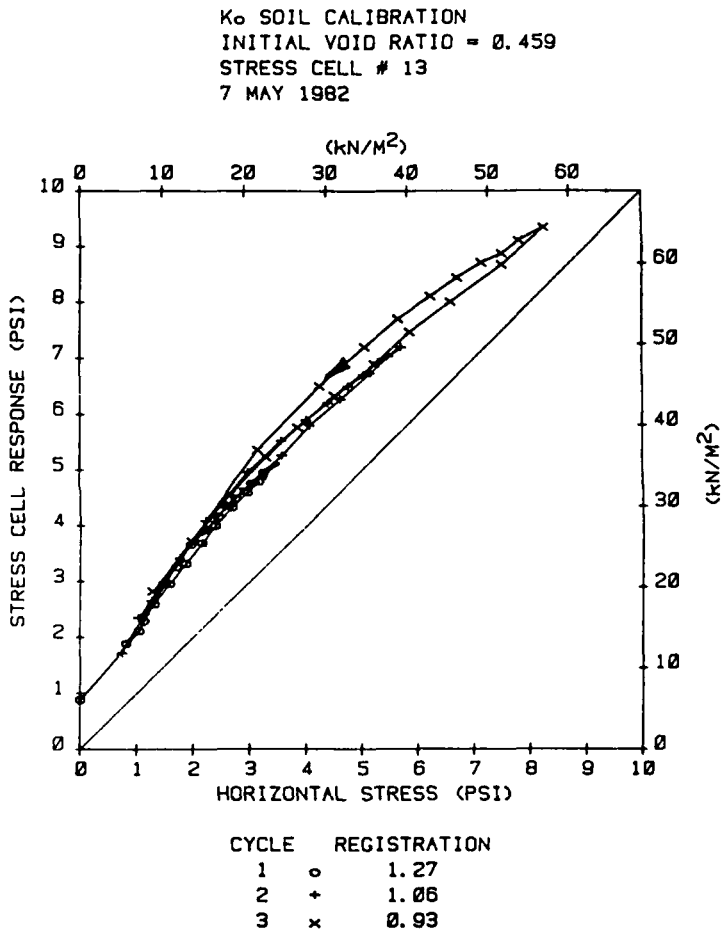

Figure B.21 K_o Soil Calibration.

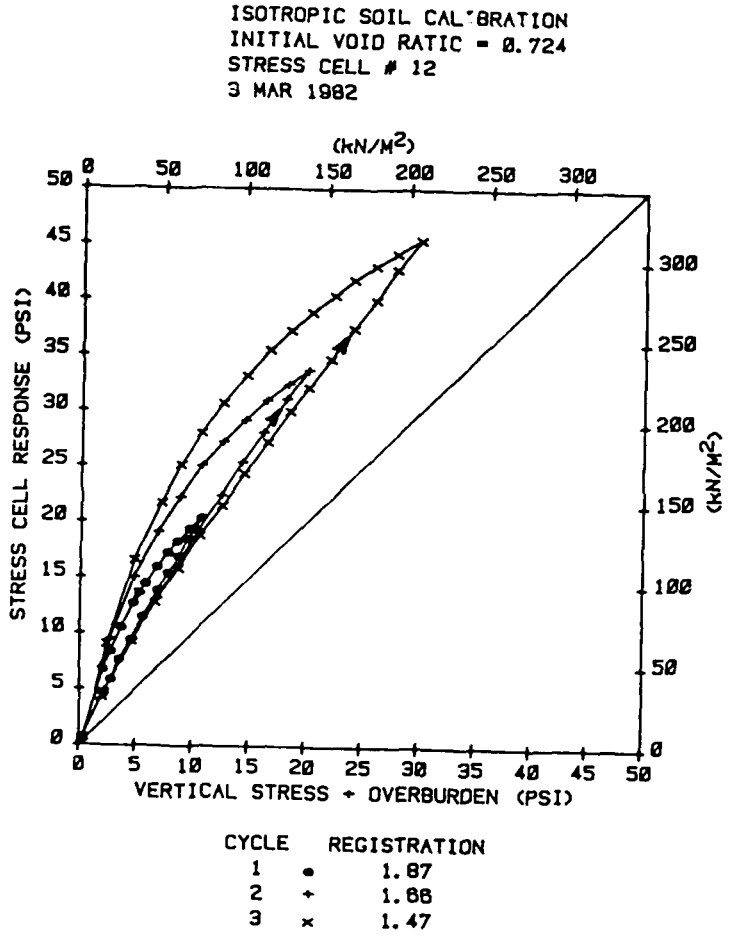

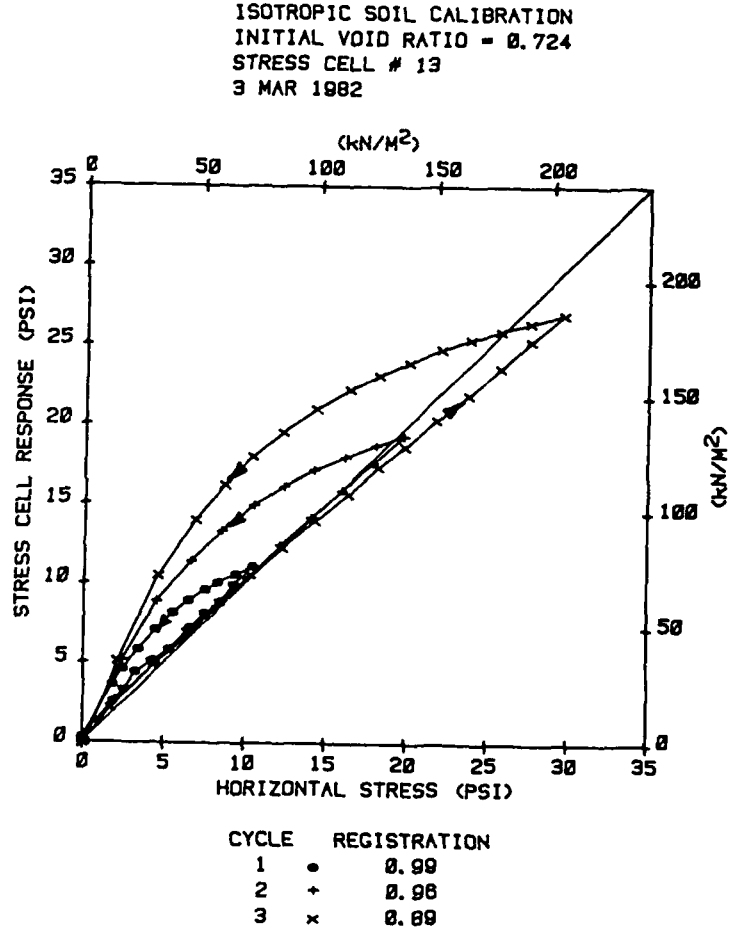

Figure B.22 Isotropic Soil Calibration.

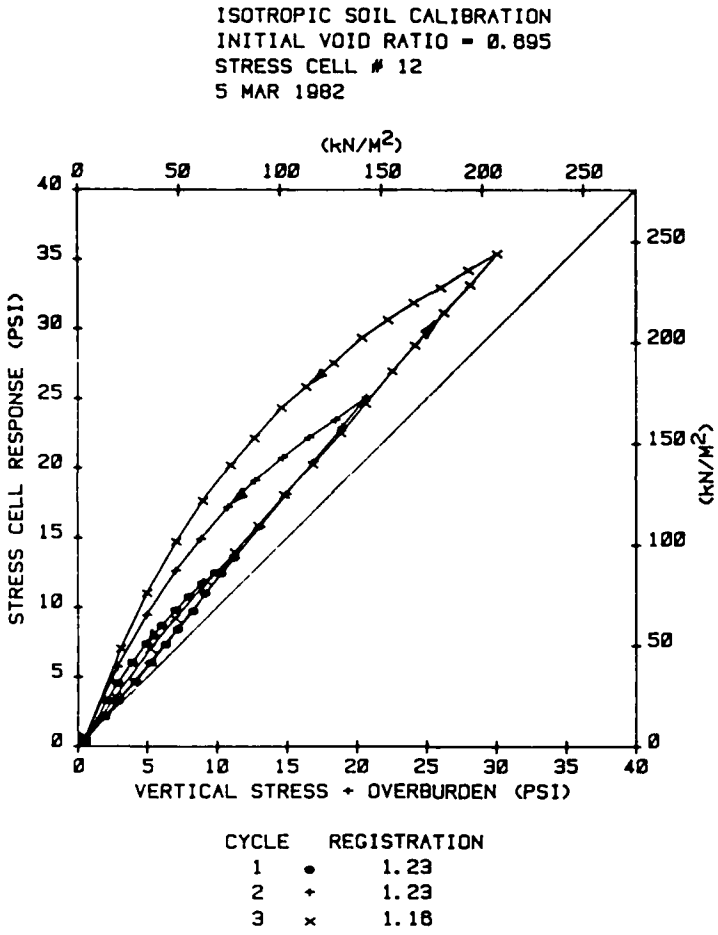

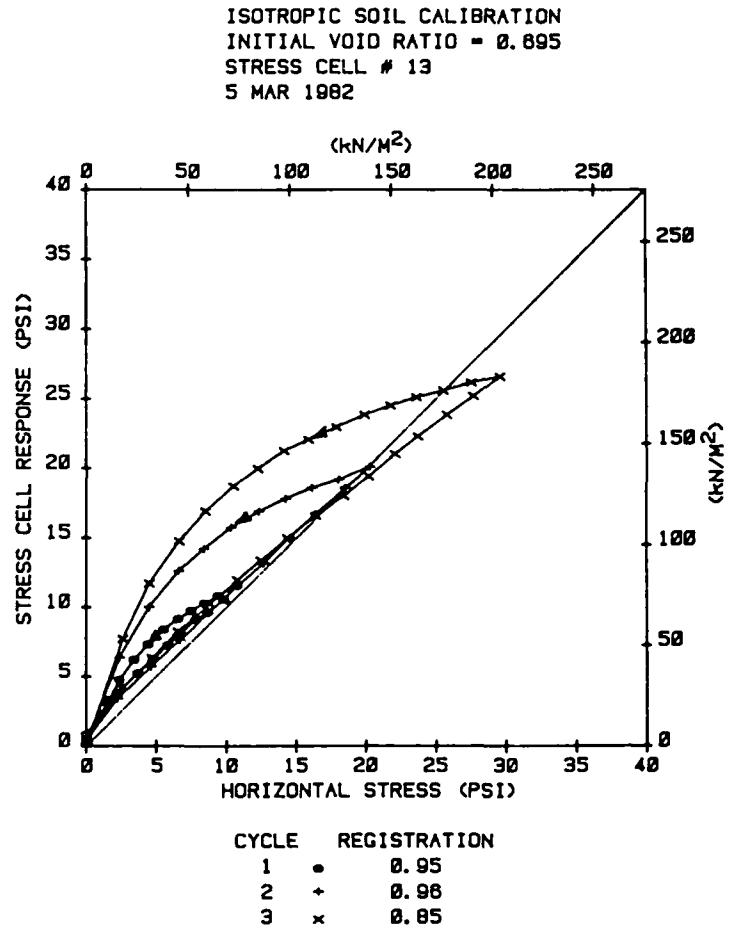

Figure B.23 Isotropic Soil Calibration.

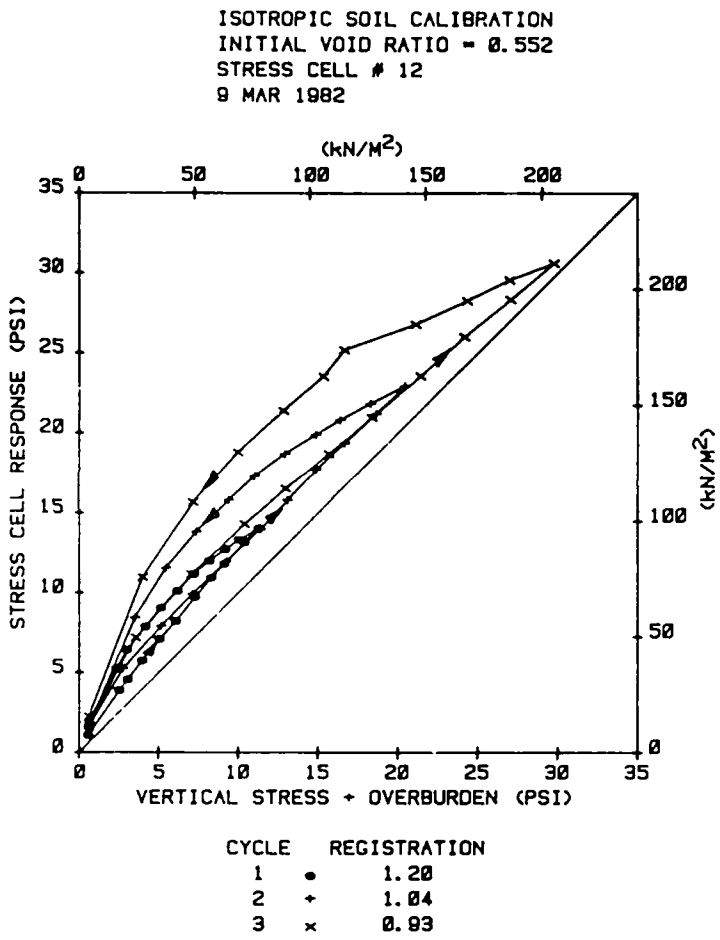

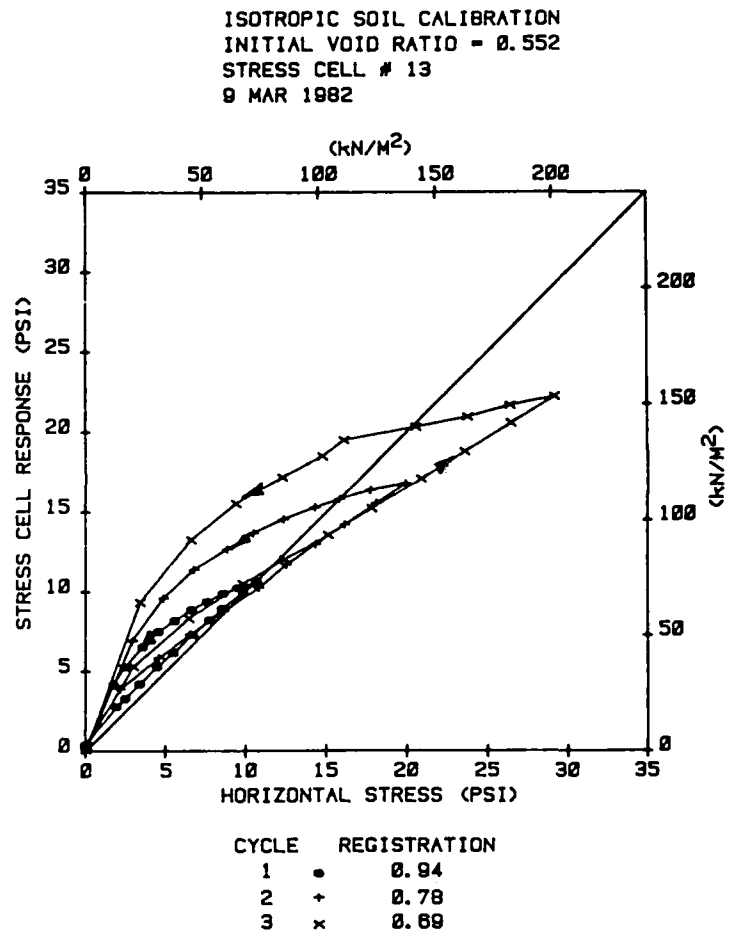

Figure B.24 Isotropic Soil Calibration.

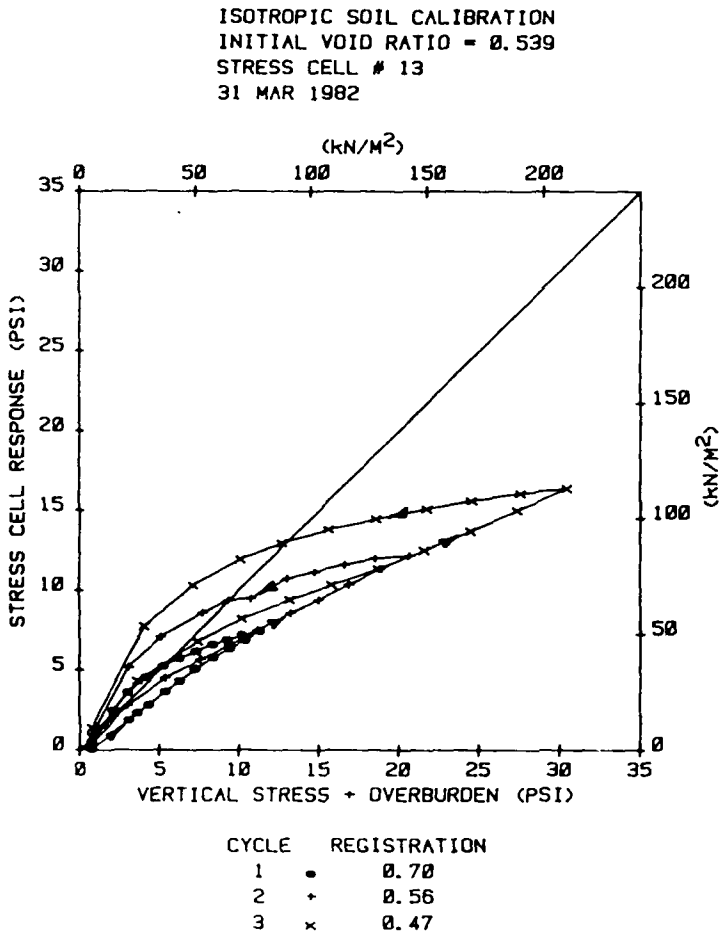

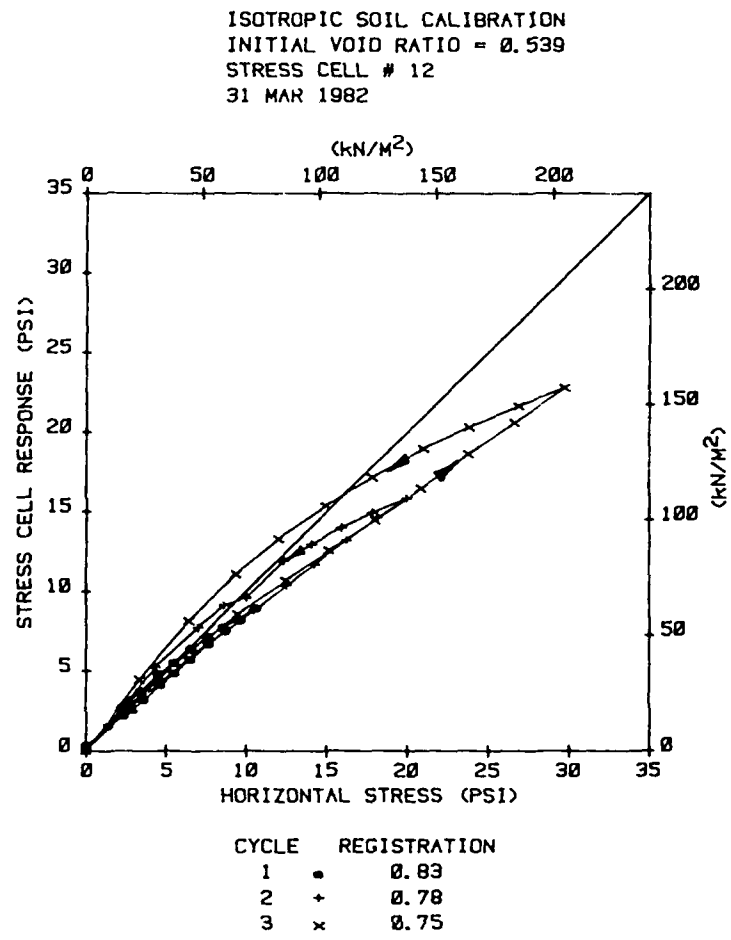

Figure B.25 Isotropic Soil Calibration.

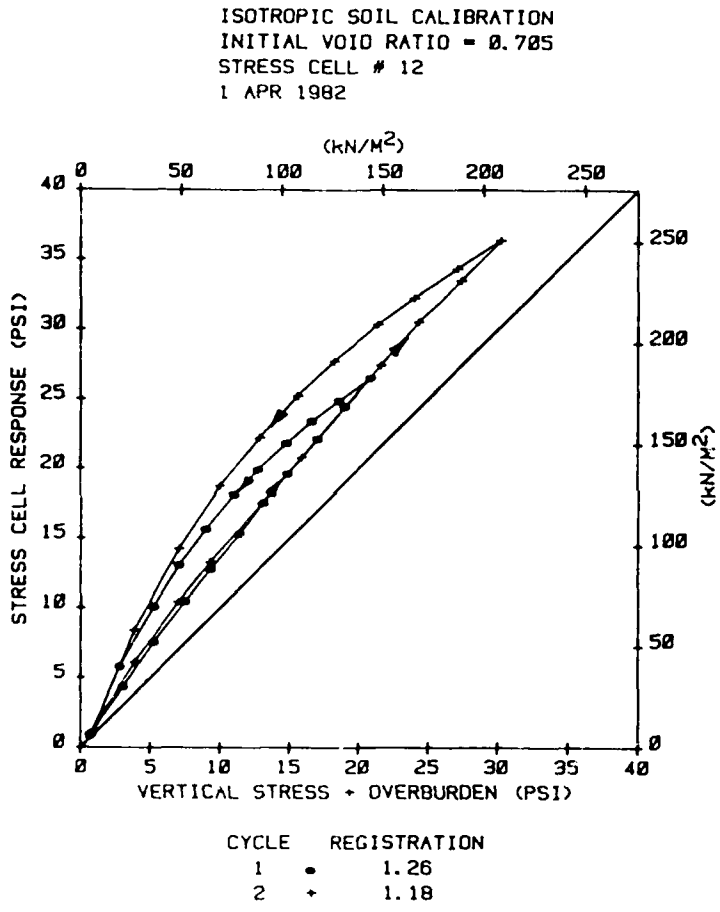

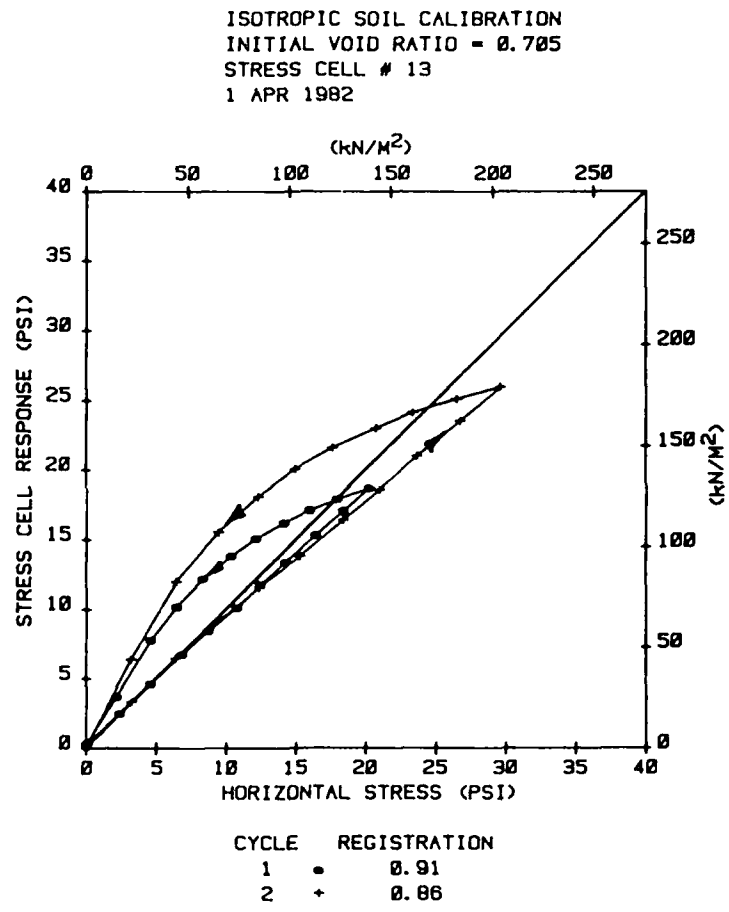

Figure B.26 Isotropic Soil Calibration.

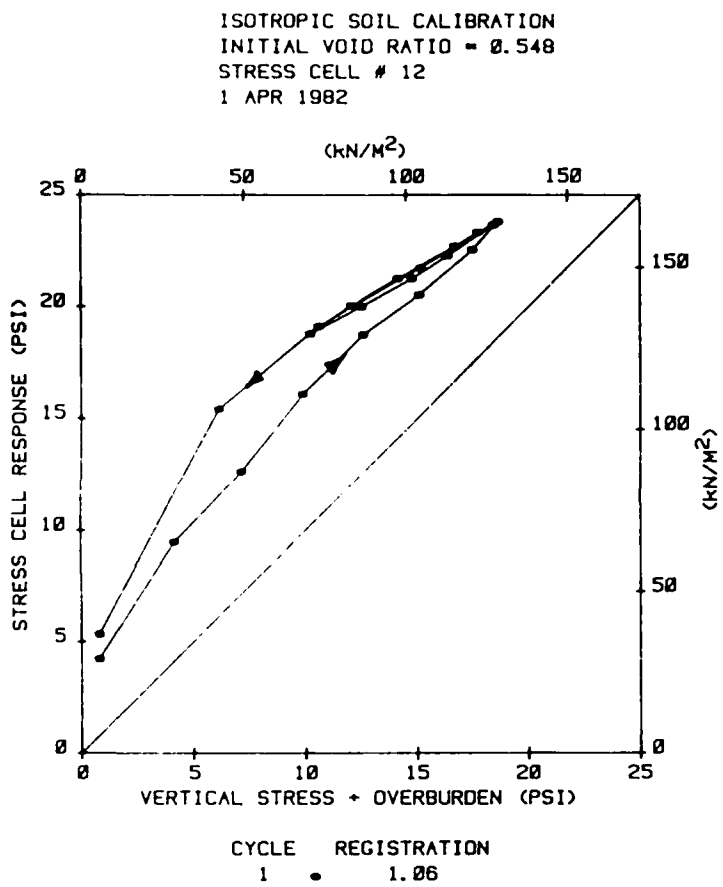

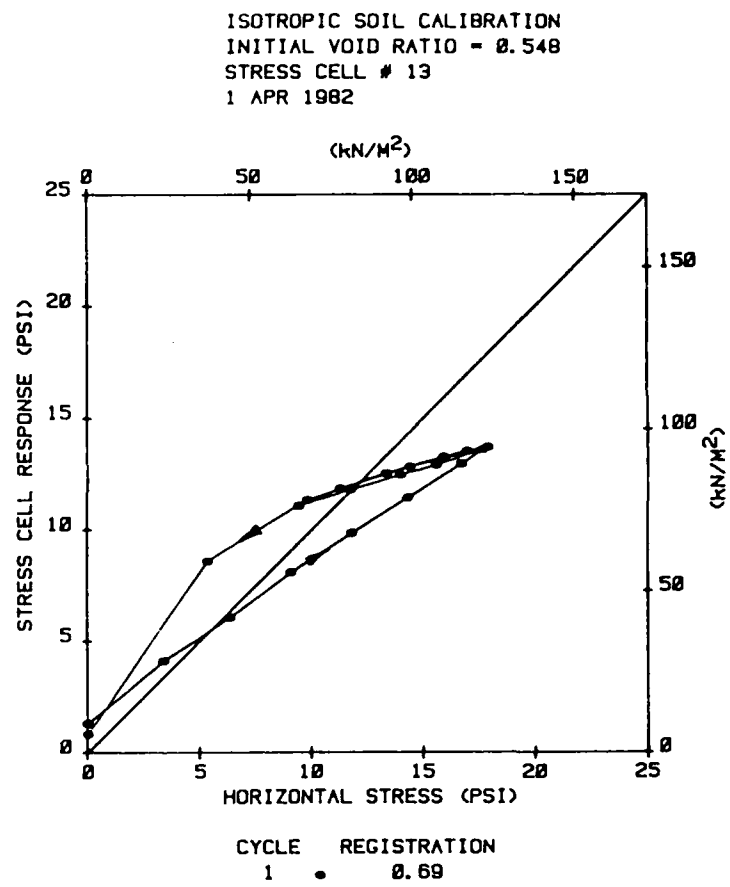

Figure B.27 Isotropic Soil Calibration.

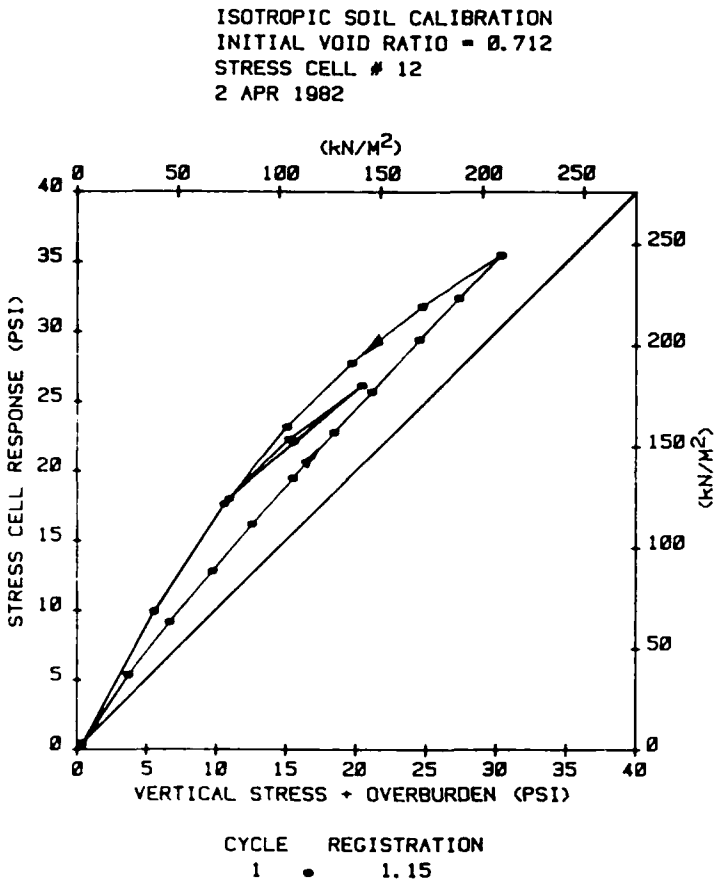

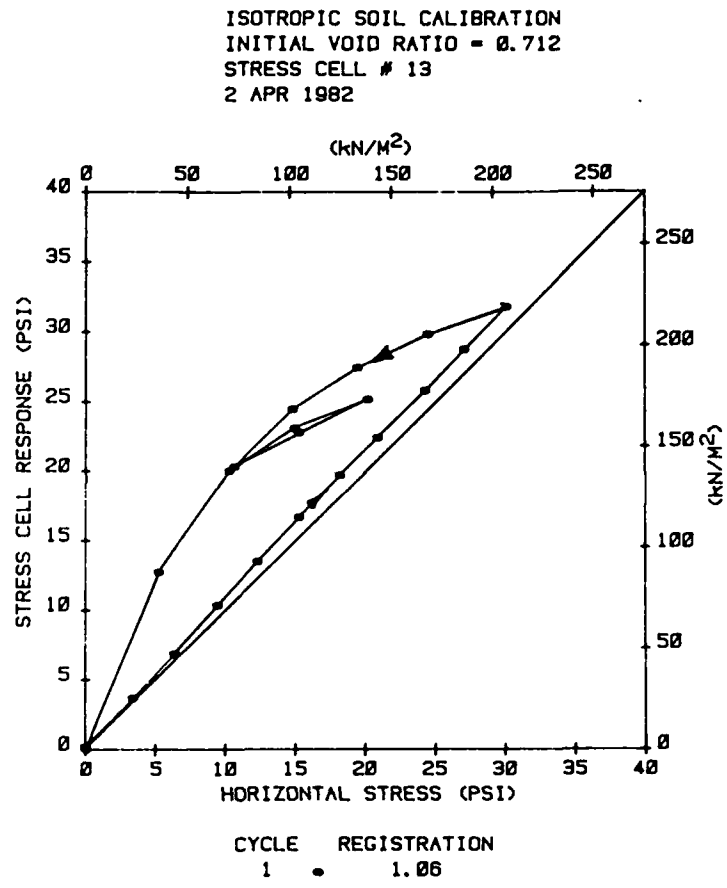

Figure B.28 Isotropic Soil Calibration.

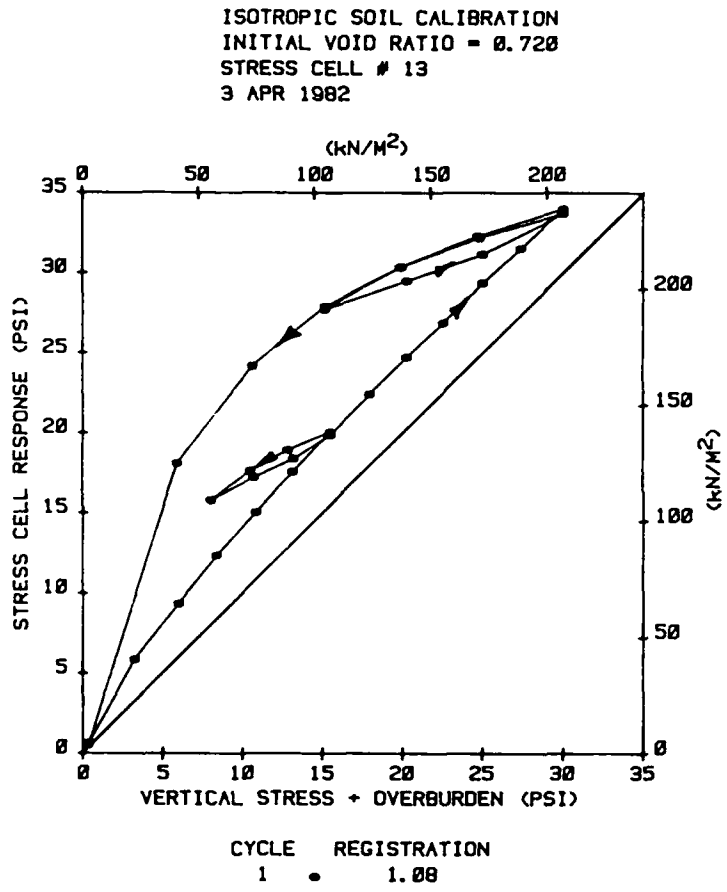

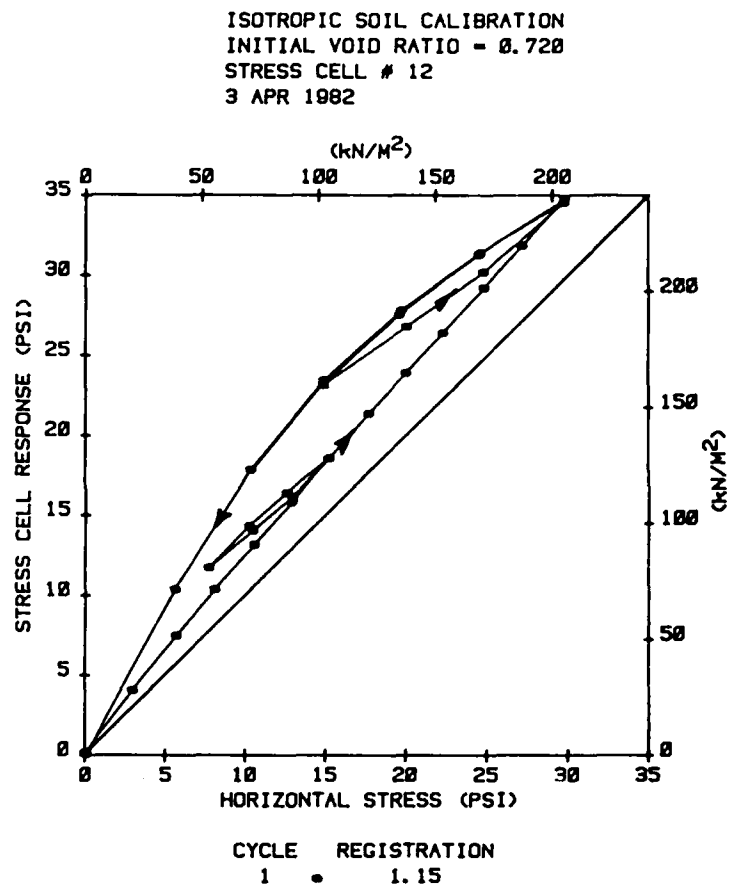

Figure B.29 Isotropic Soil Calibration.

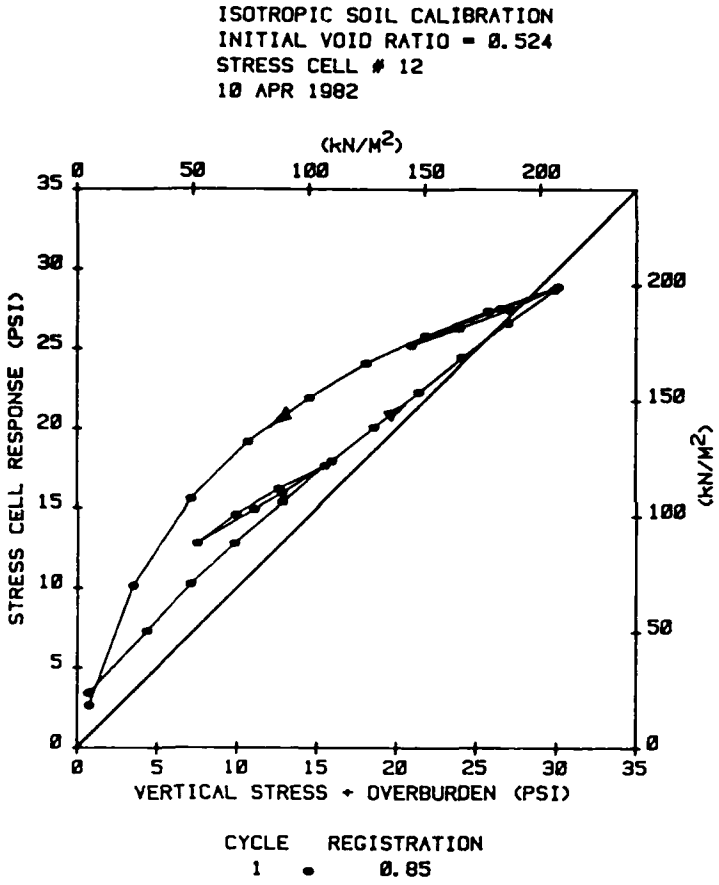

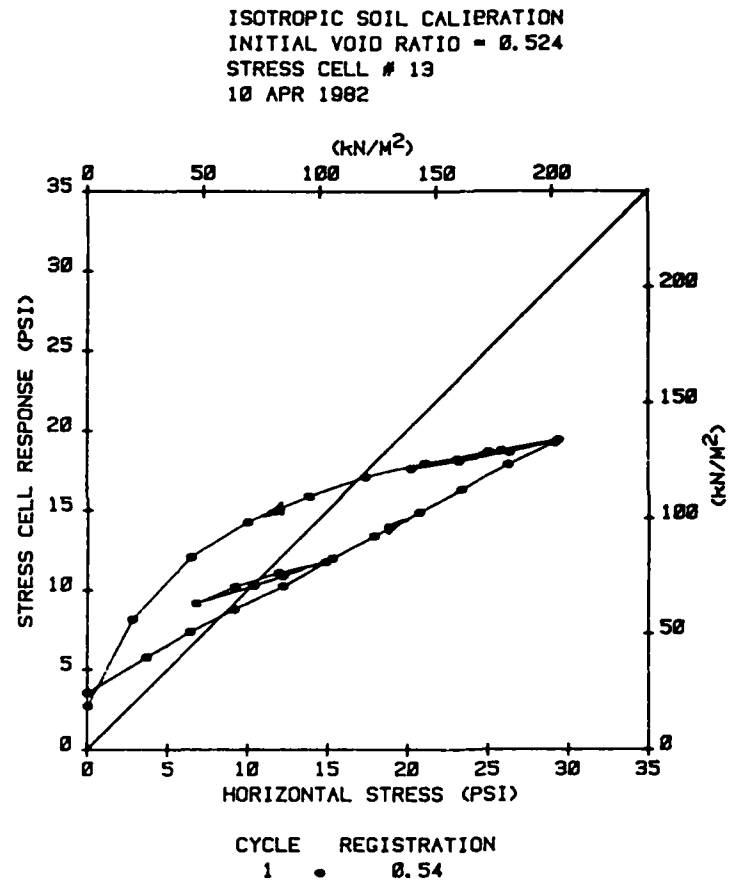

Figure B.30 Isotropic Soil Calibration.

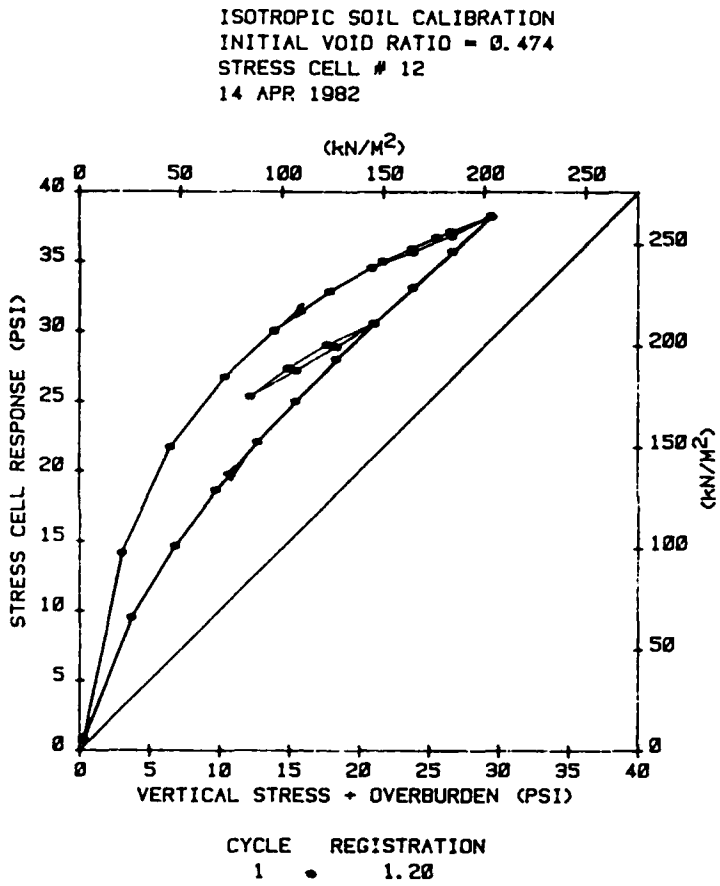

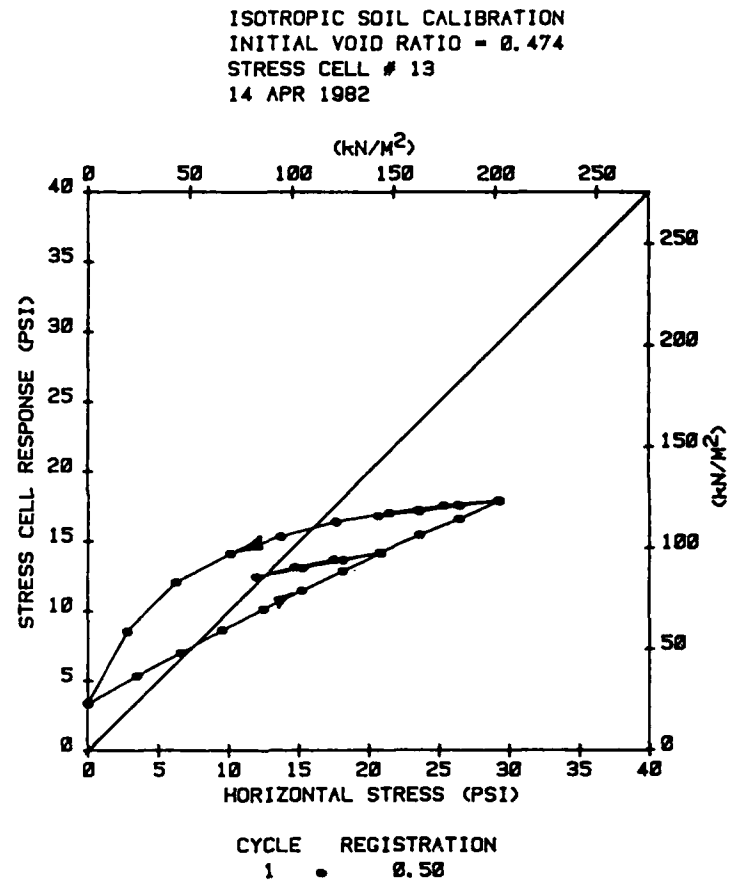

Figure B.31 Isotropic Soil Calibration.

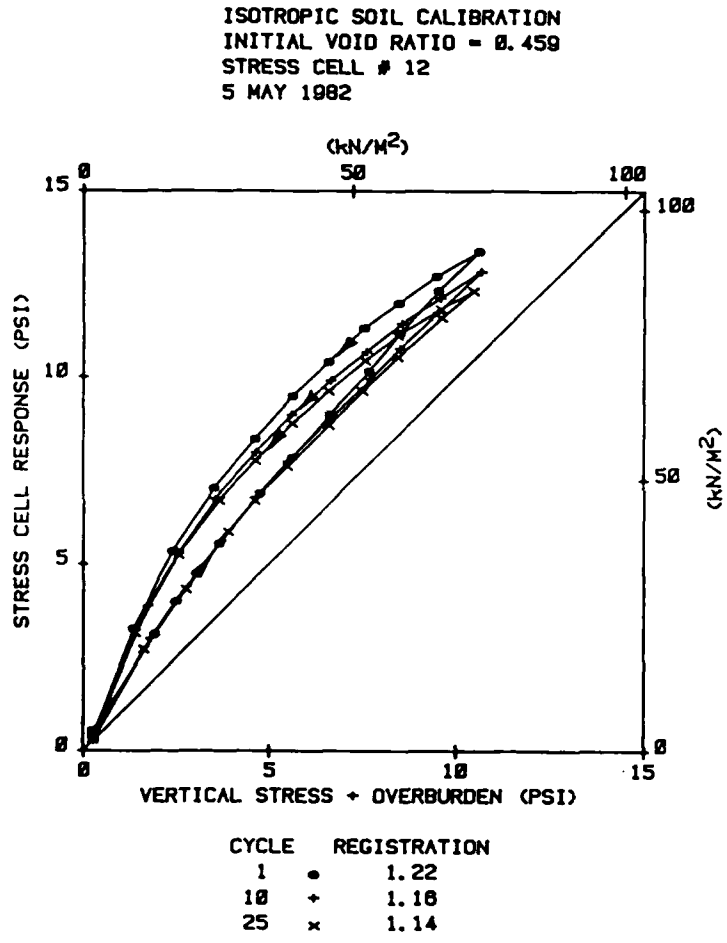

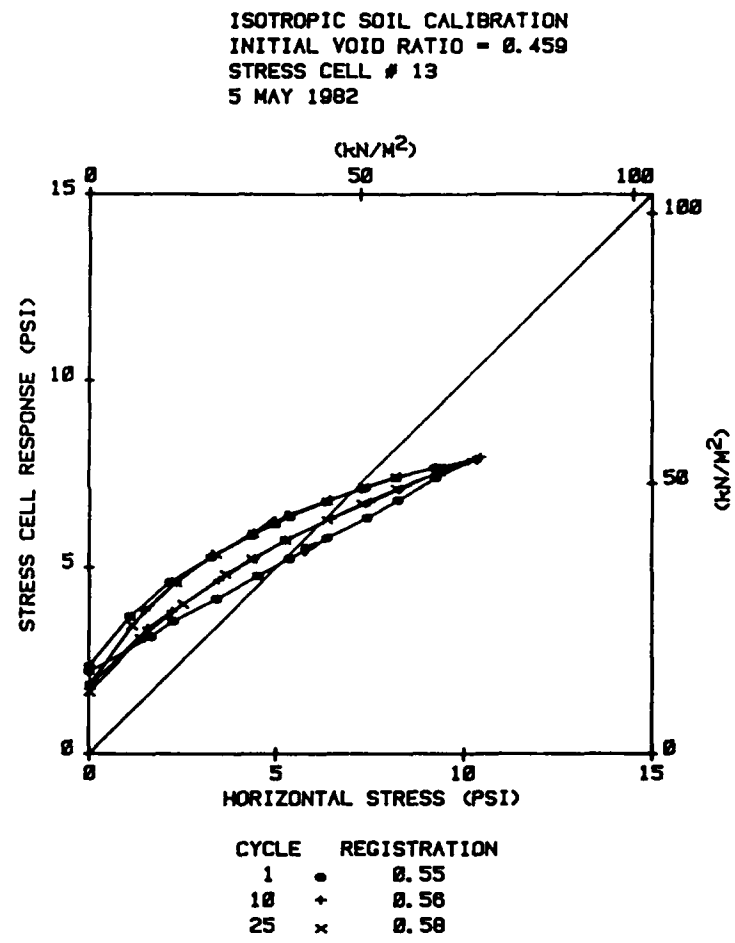

Figure B.32 Isotropic Soil Calibration.

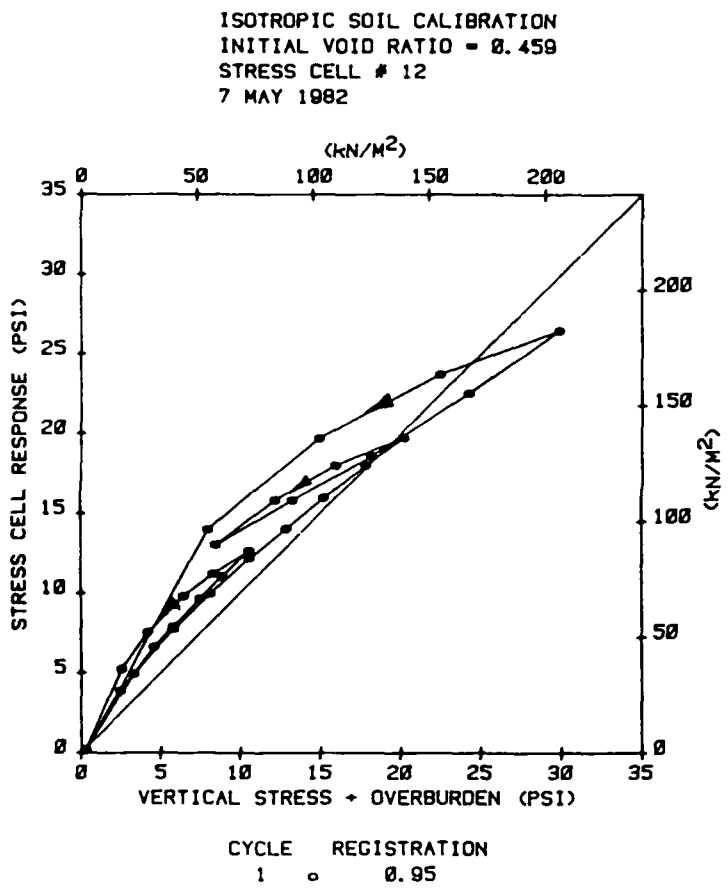

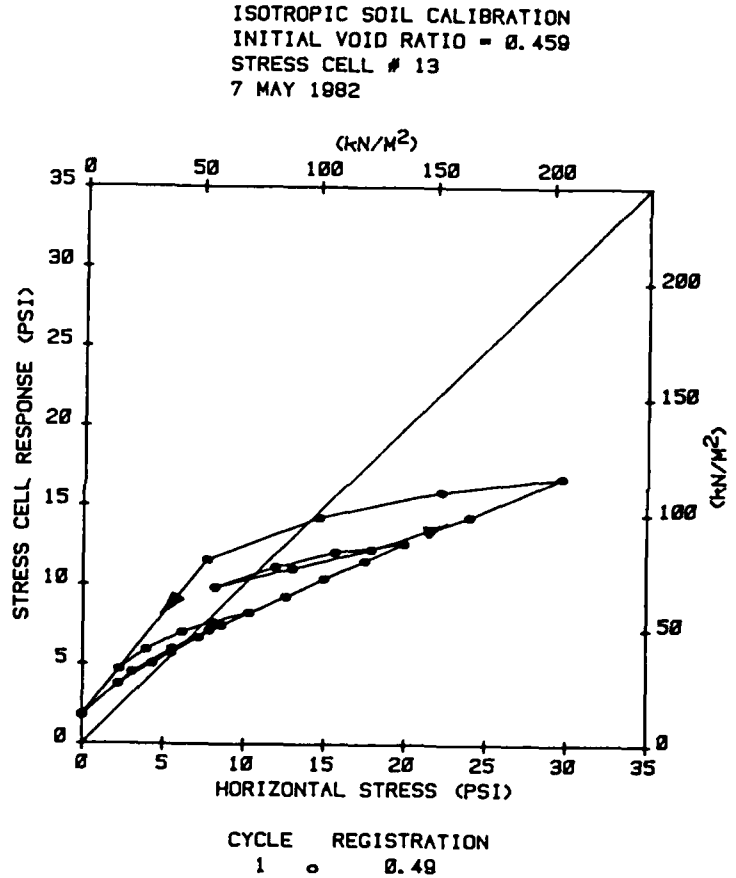

Figure B.33 Isotropic Soil Calibration.

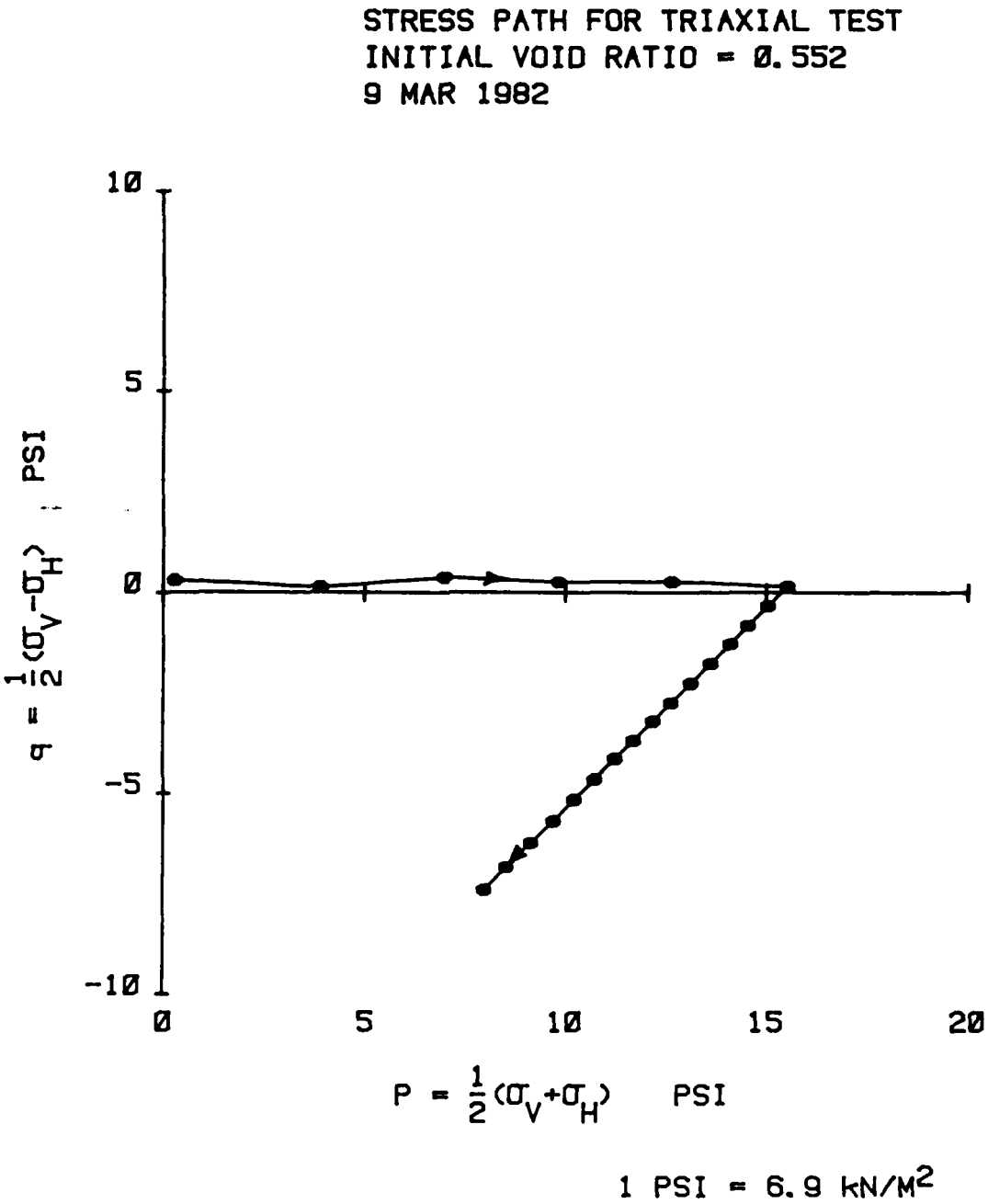

Figure B.34 Triaxial Stress Path.

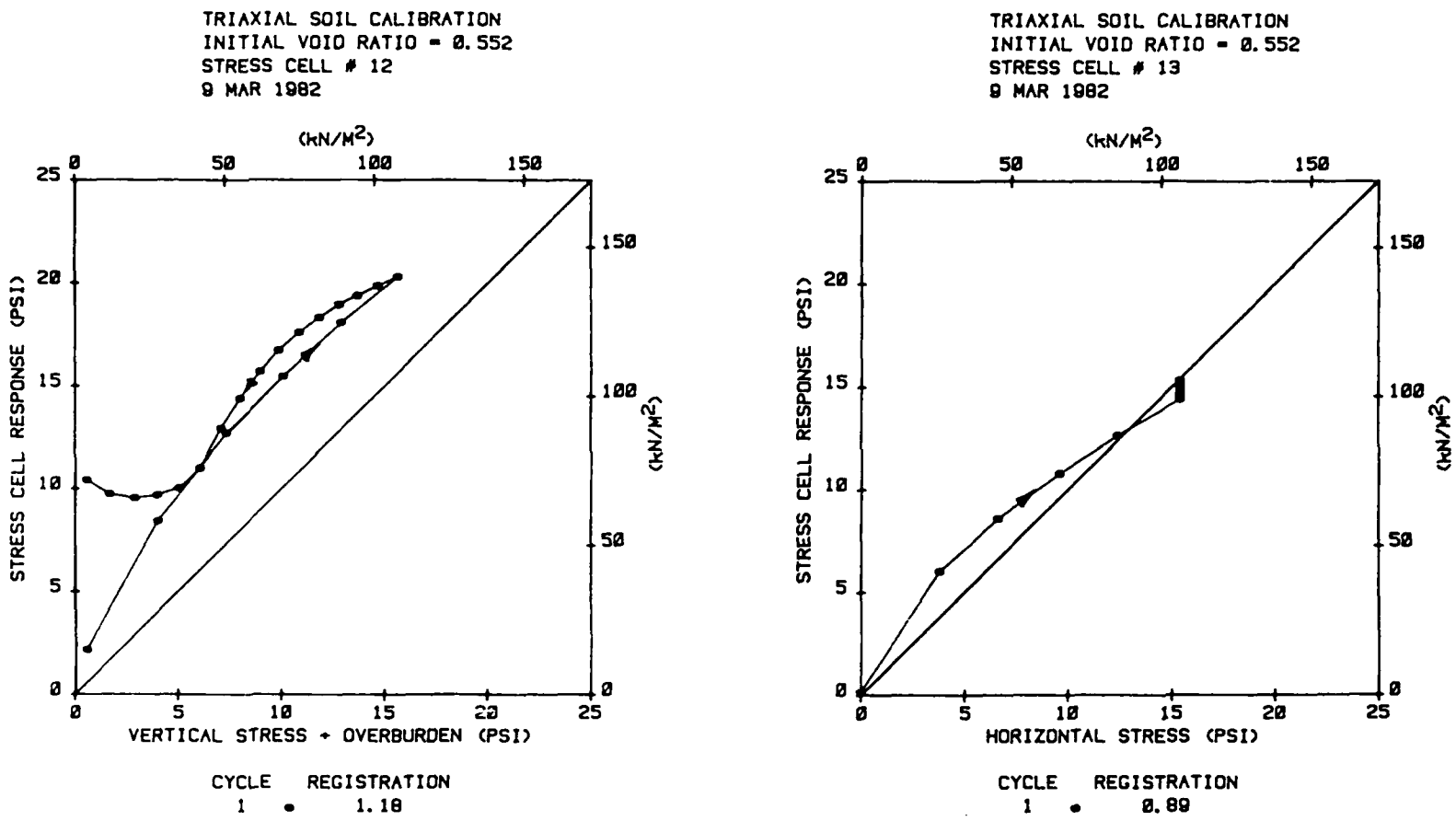

Figure B.35 Triaxial Soil Calibration.

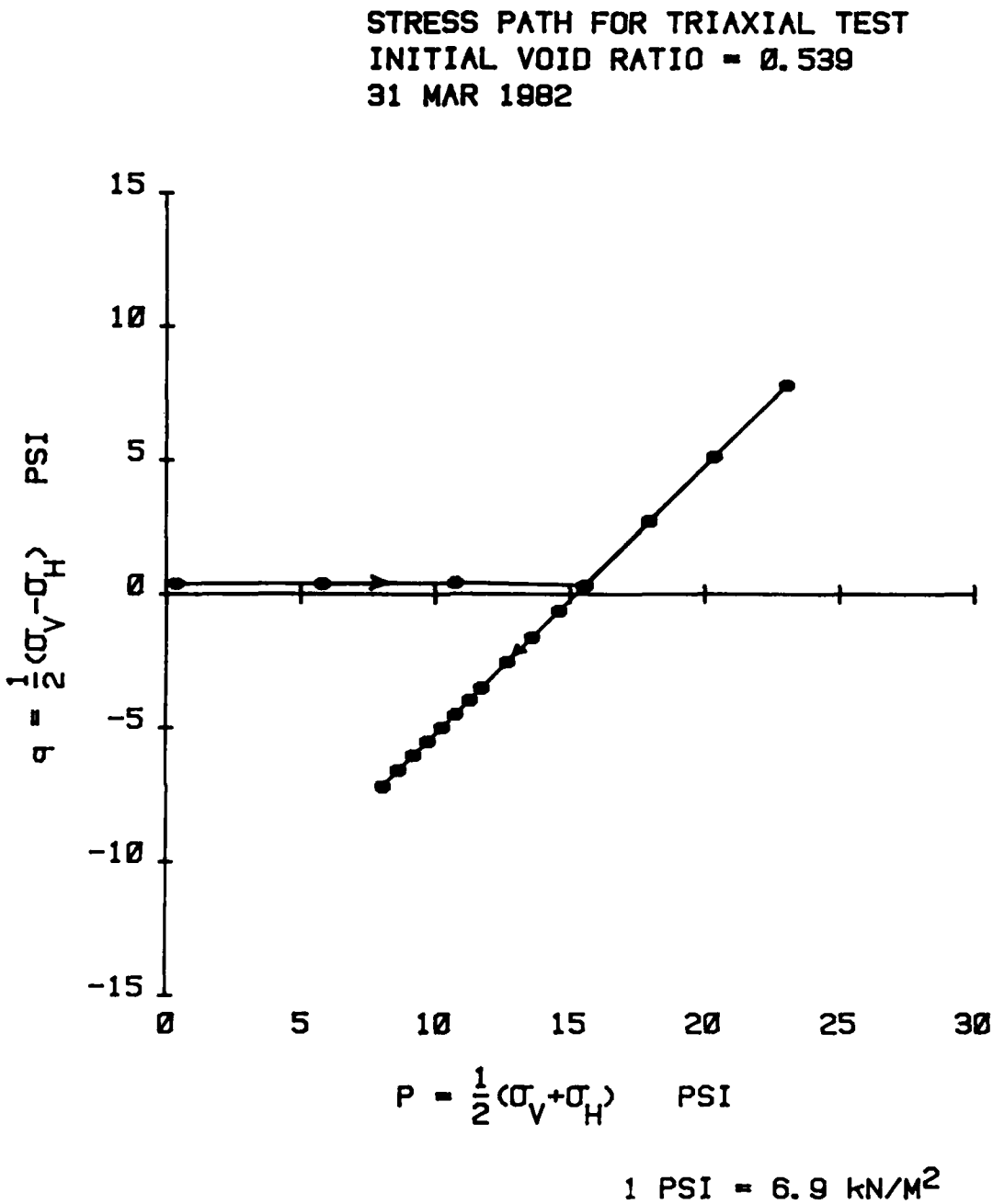

Figure B.36 Triaxial Stress Path.

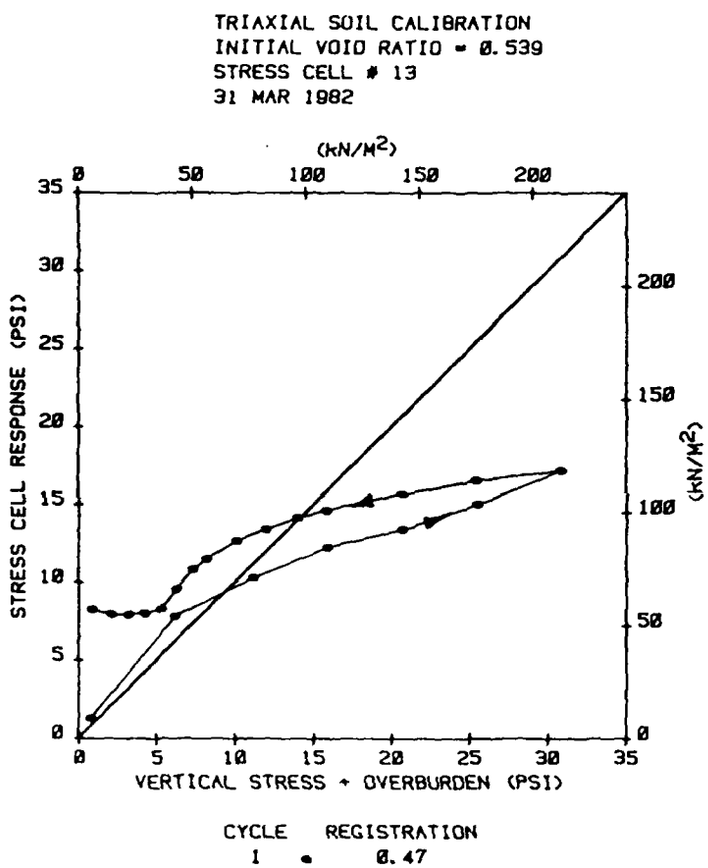

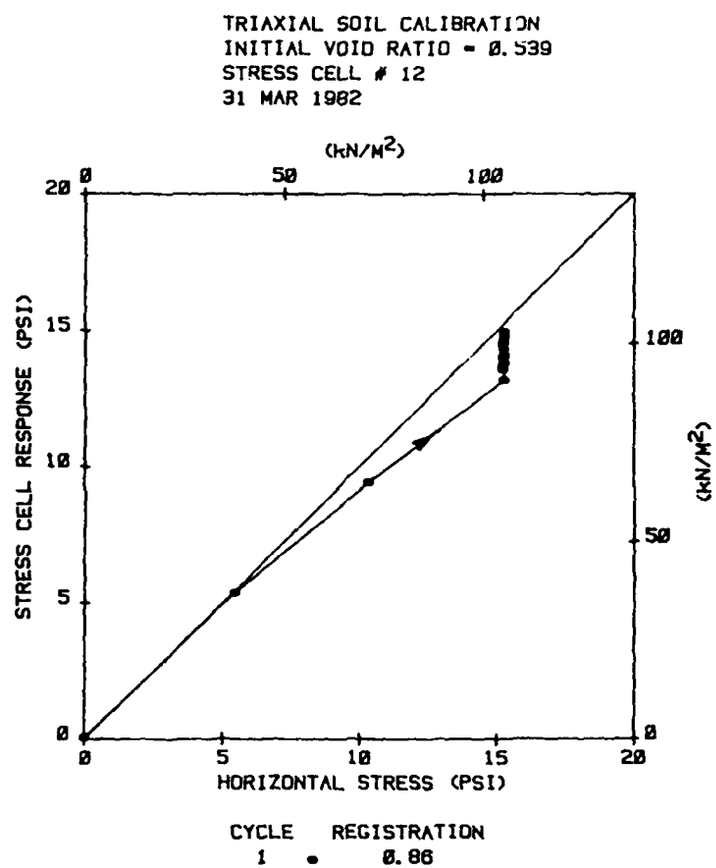

Figure B.37 Triaxial Soil Calibration.

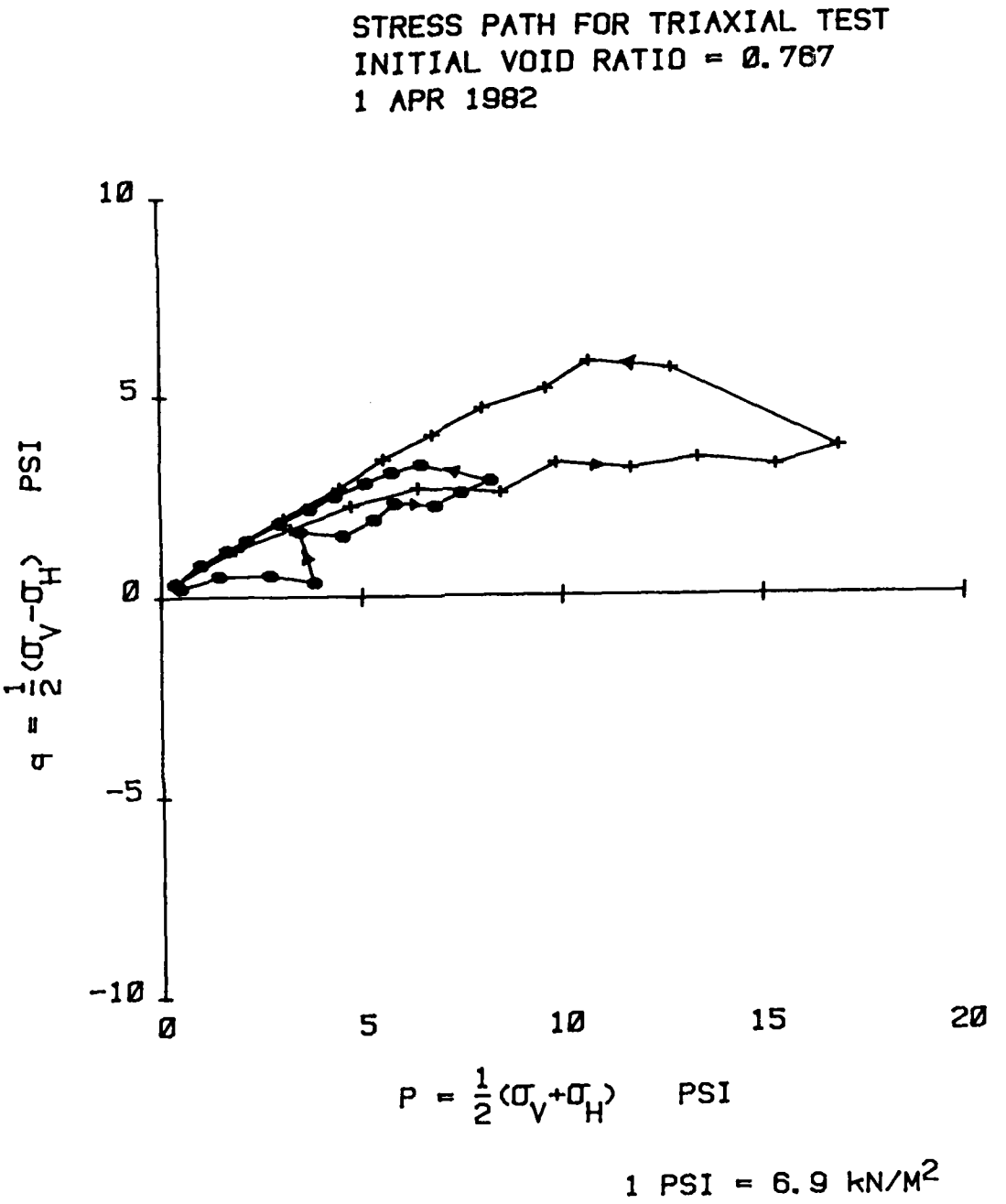

Figure B.38 Triaxial Stress Path.

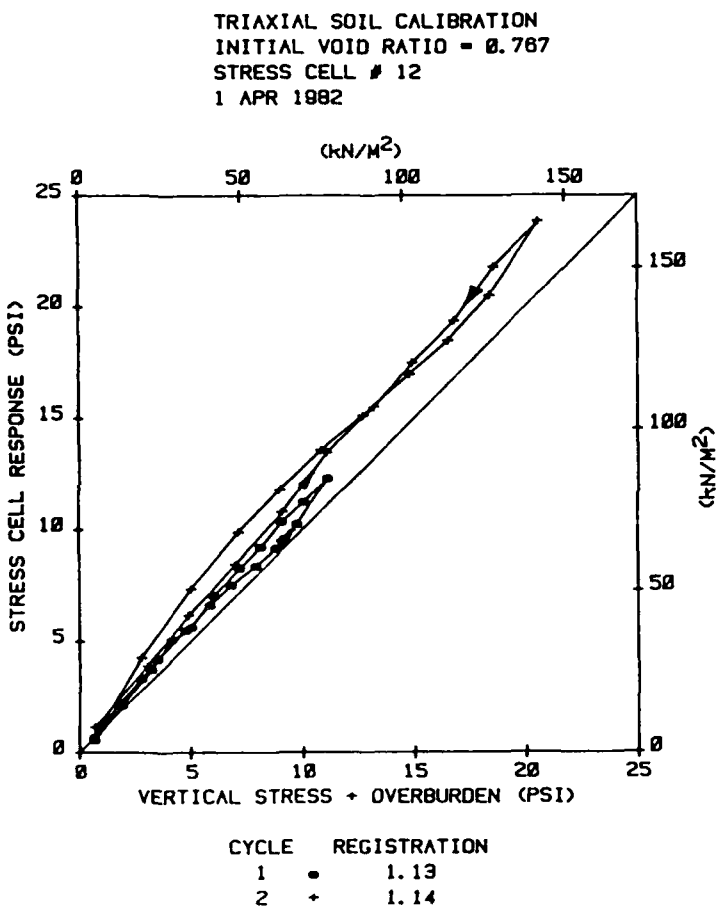

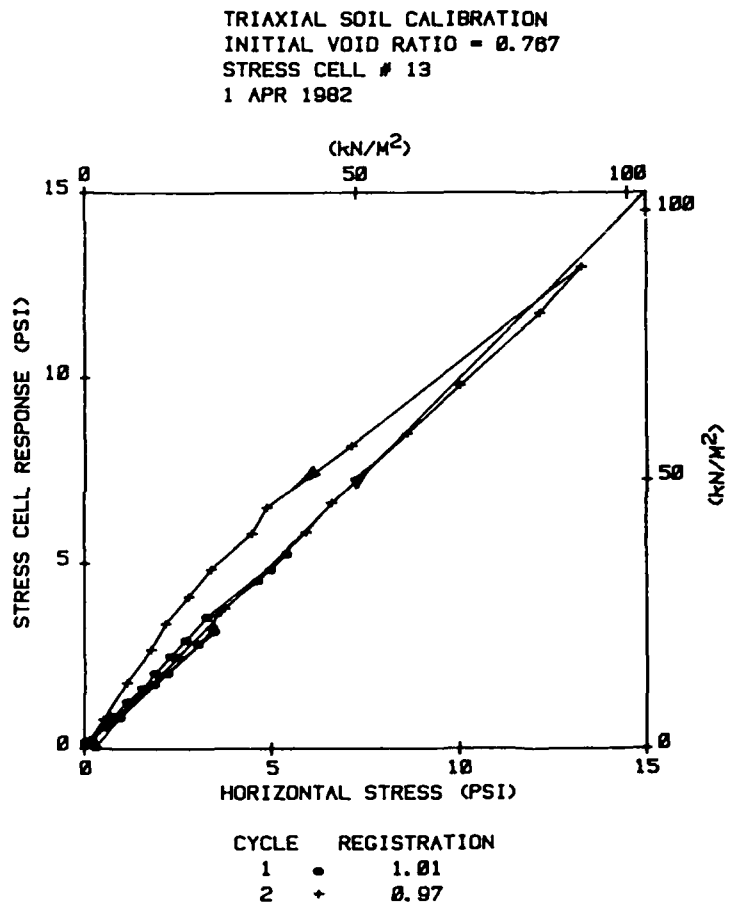

Figure B.39 Triaxial Soil Calibration.

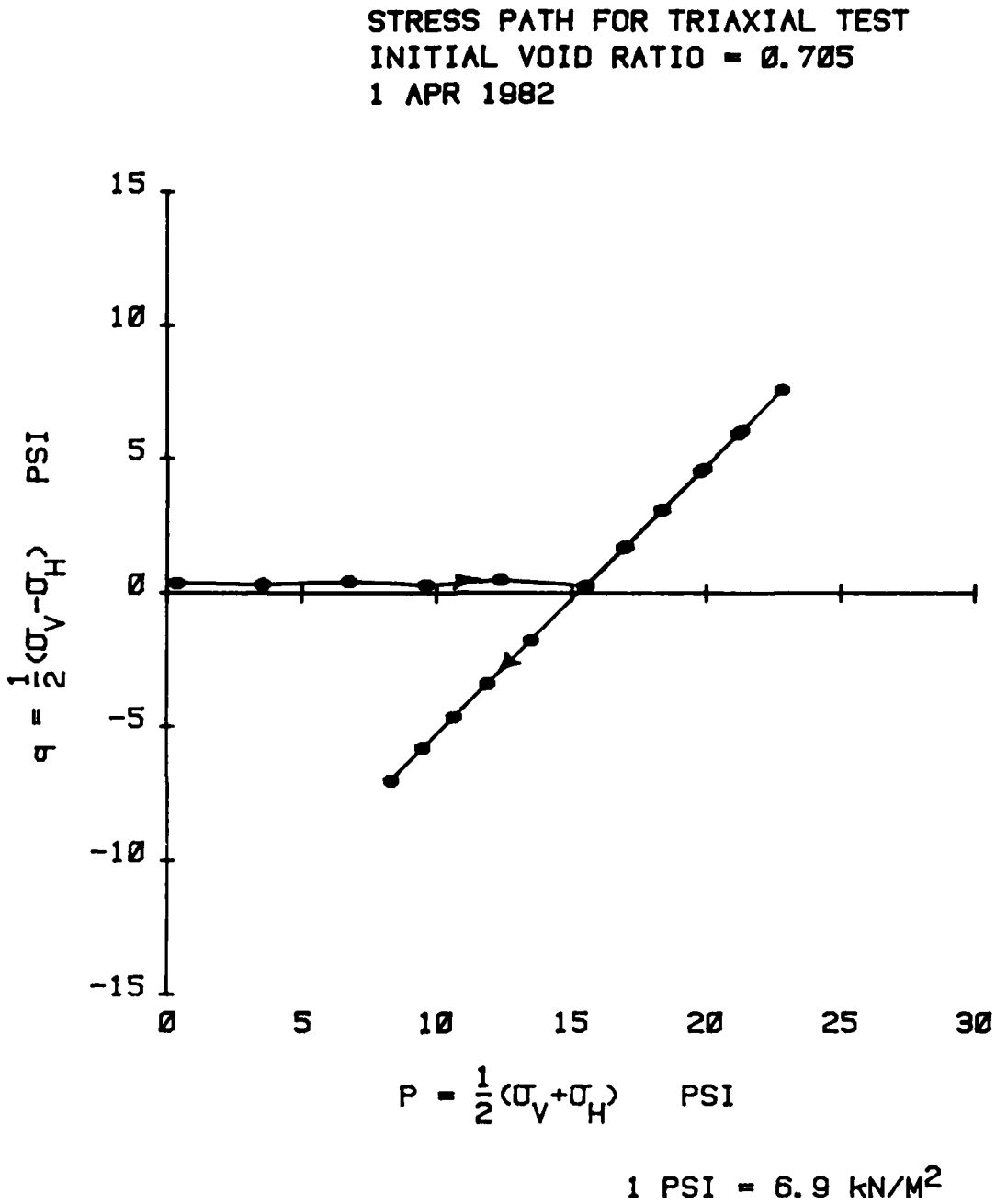

Figure B.40 Triaxial Stress Path.

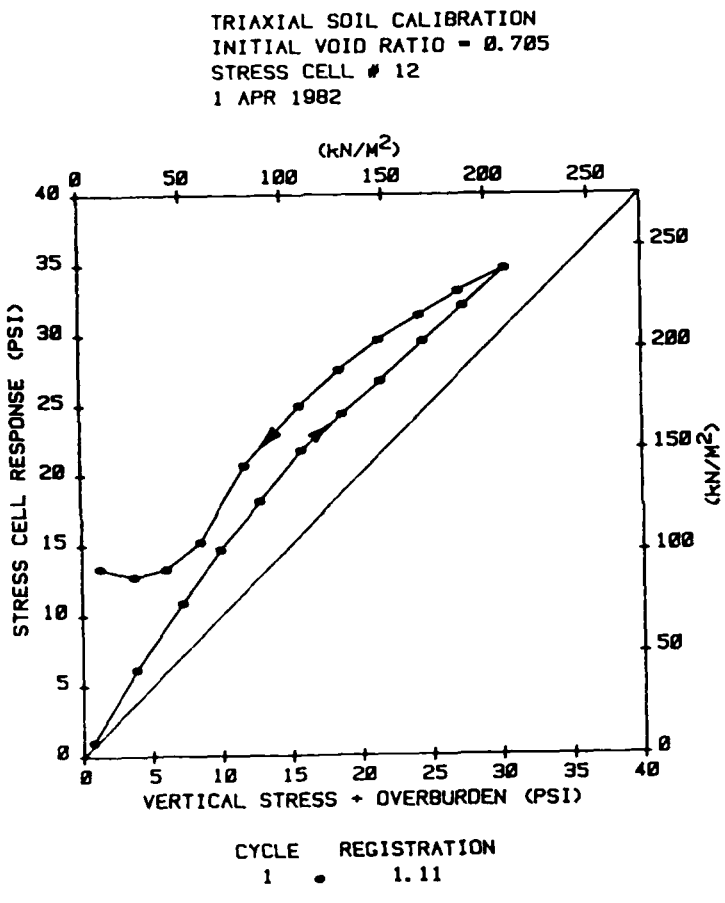

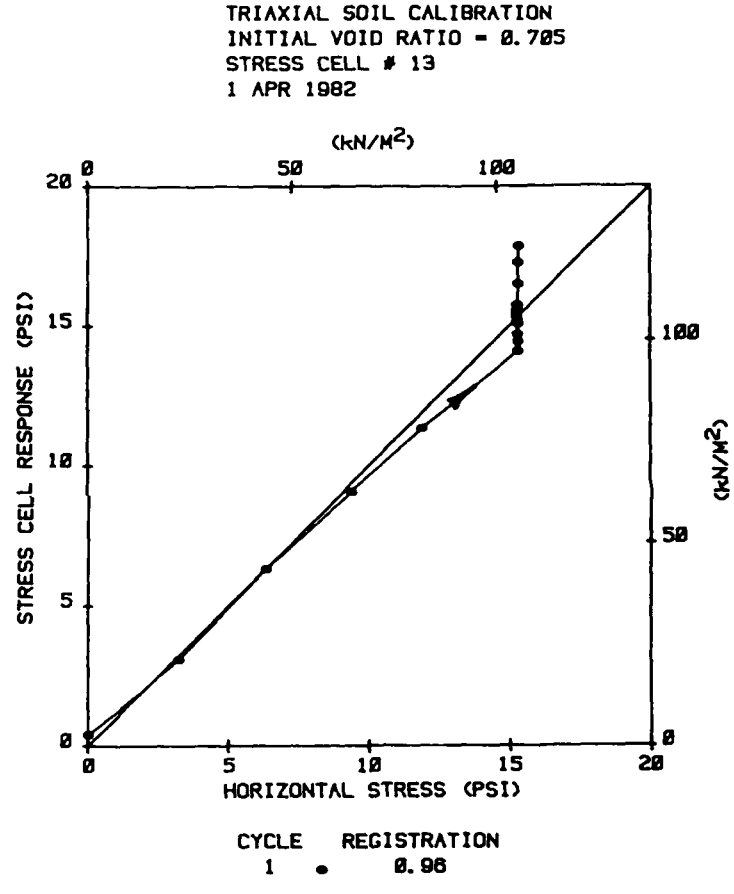

Figure B.41 Triaxial Soil Calibration.

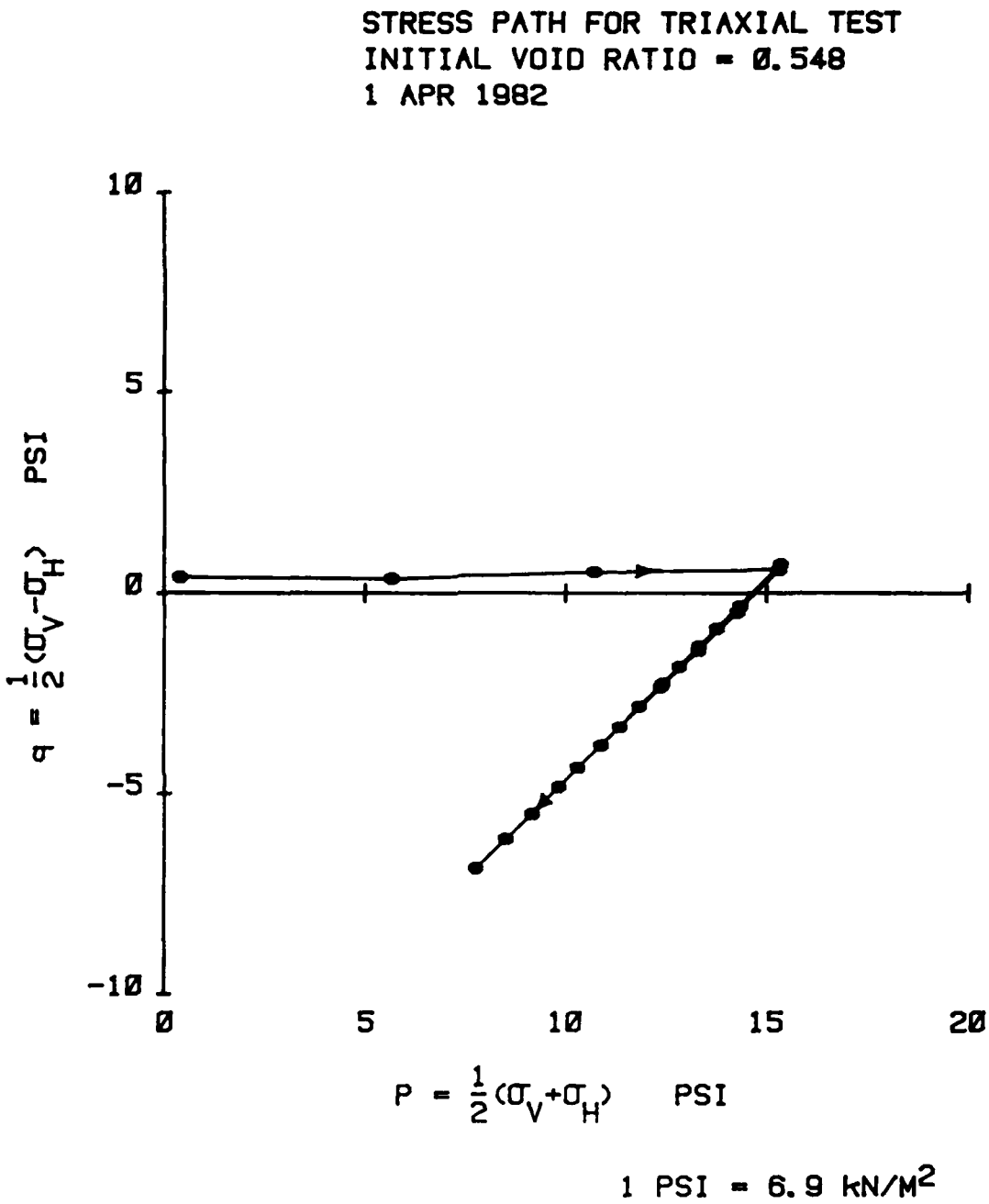

Figure B.42 Triaxial Stress Path.

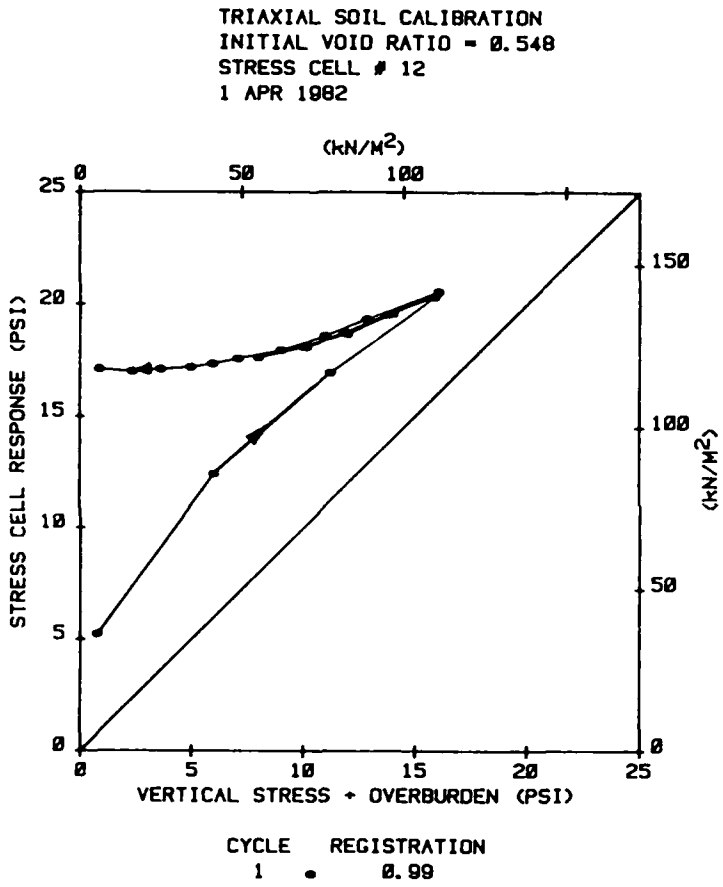

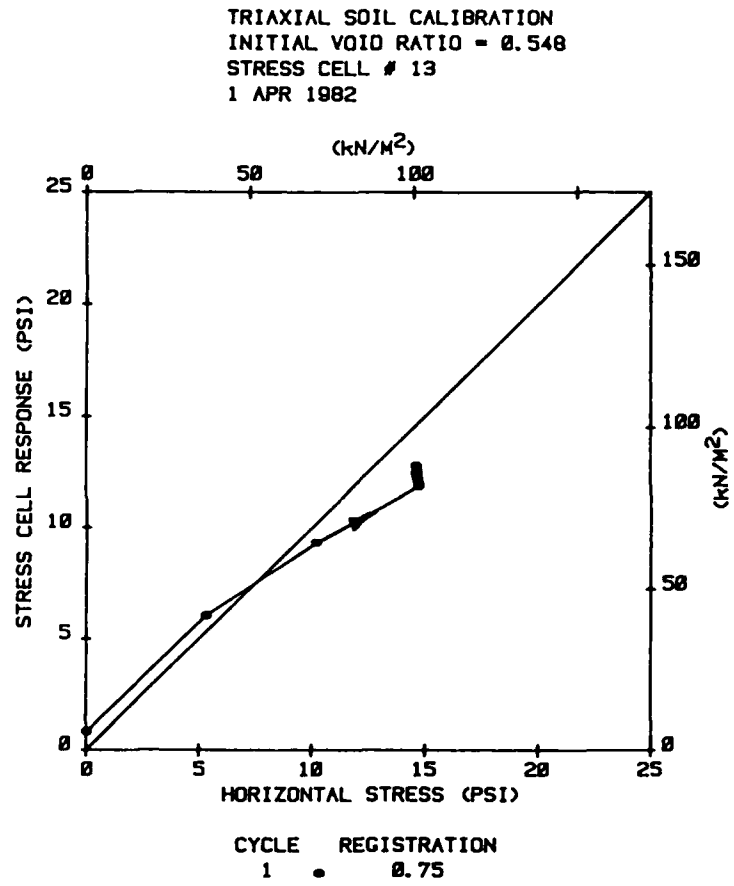

Figure B.43 Triaxial Soil Calibration.

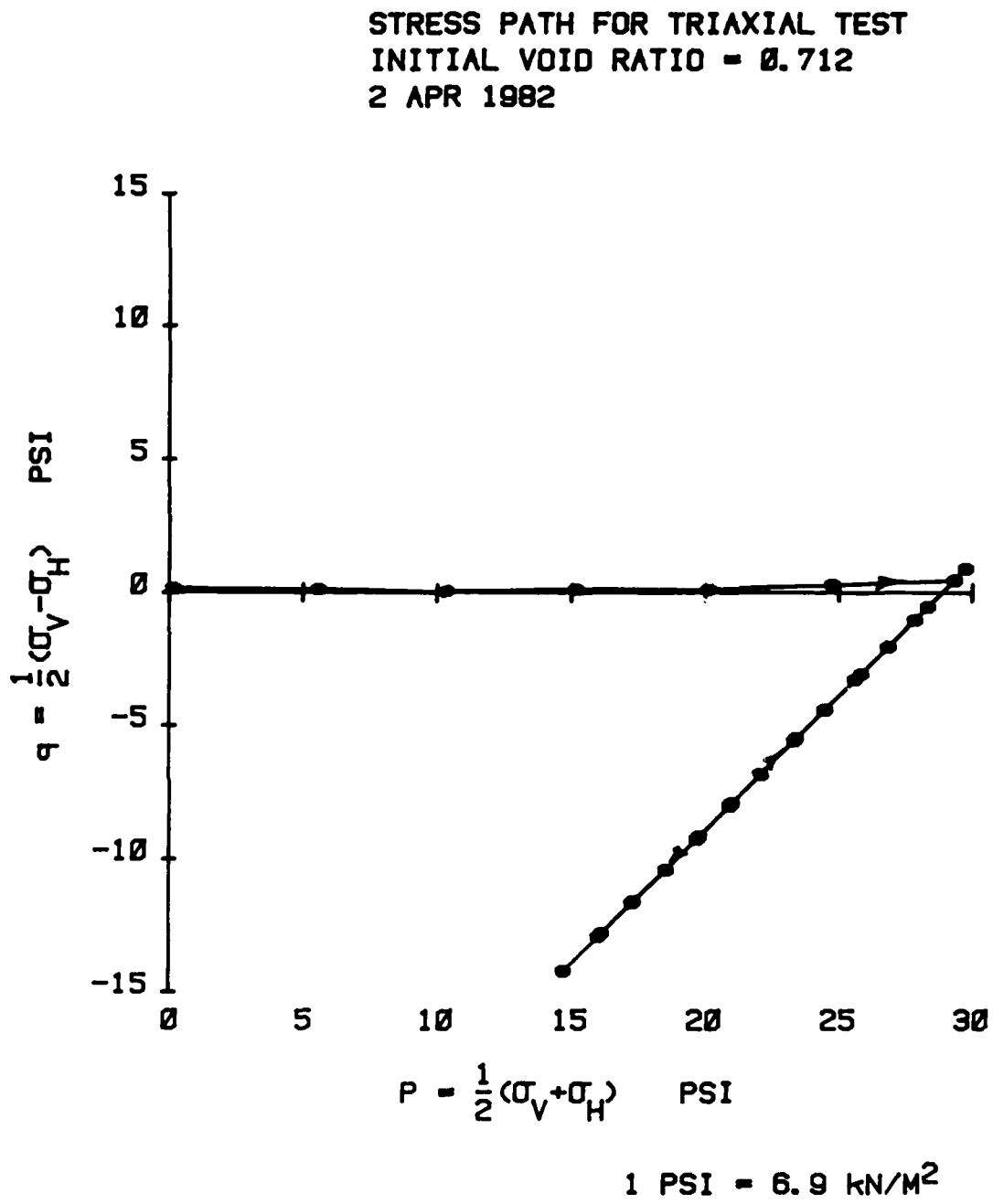

Figure B.44 Triaxial Stress Path.

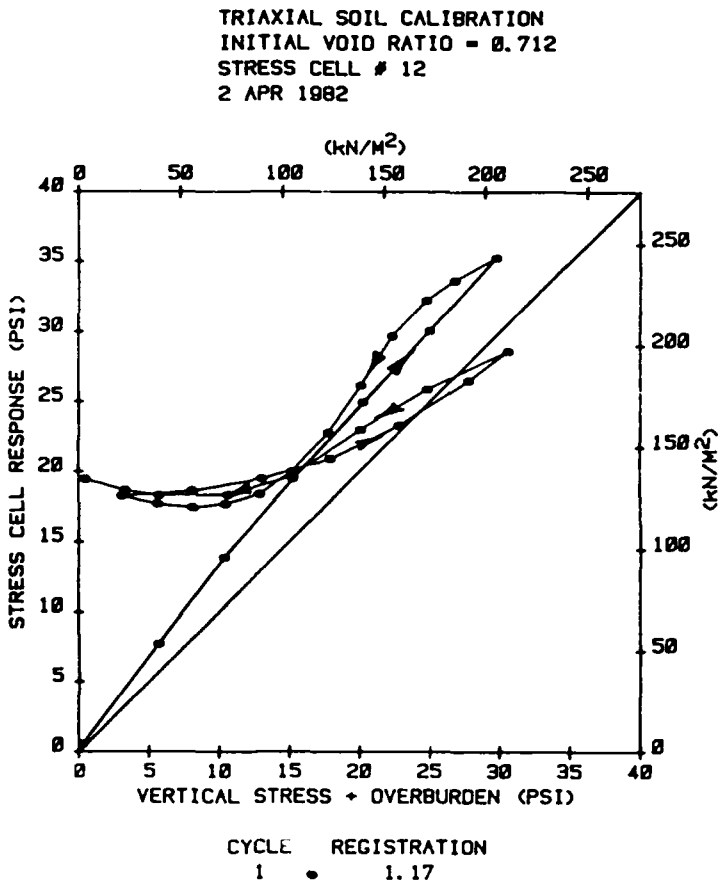

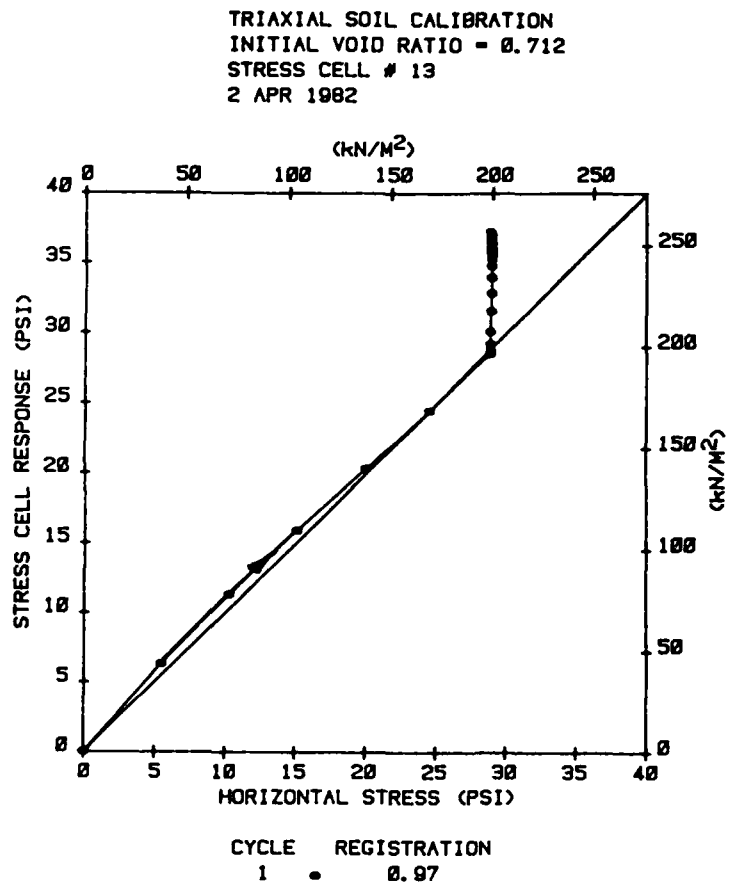

Figure B.45 Triaxial Soil Calibration.

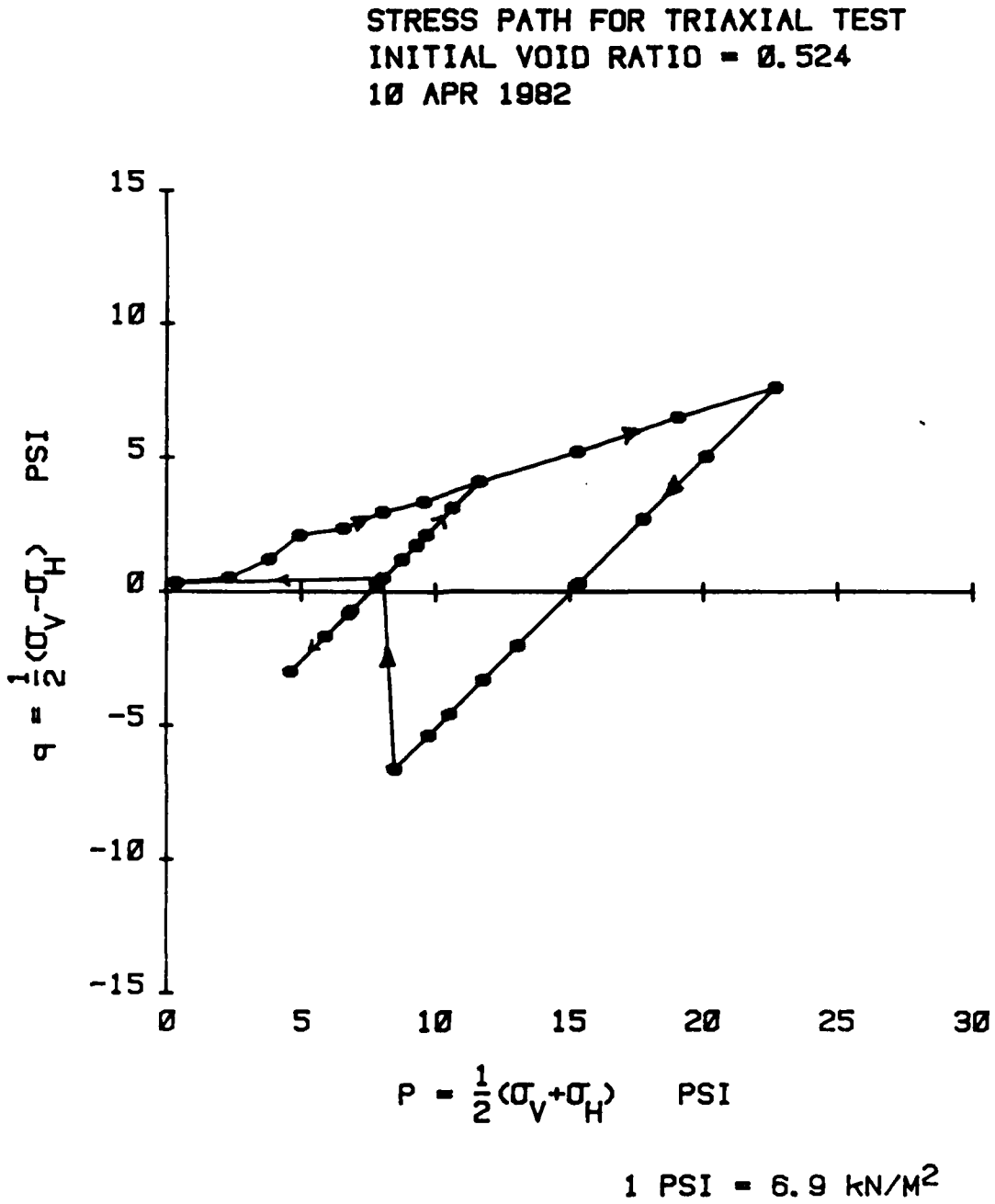

Figure B.46 Triaxial Stress Path.

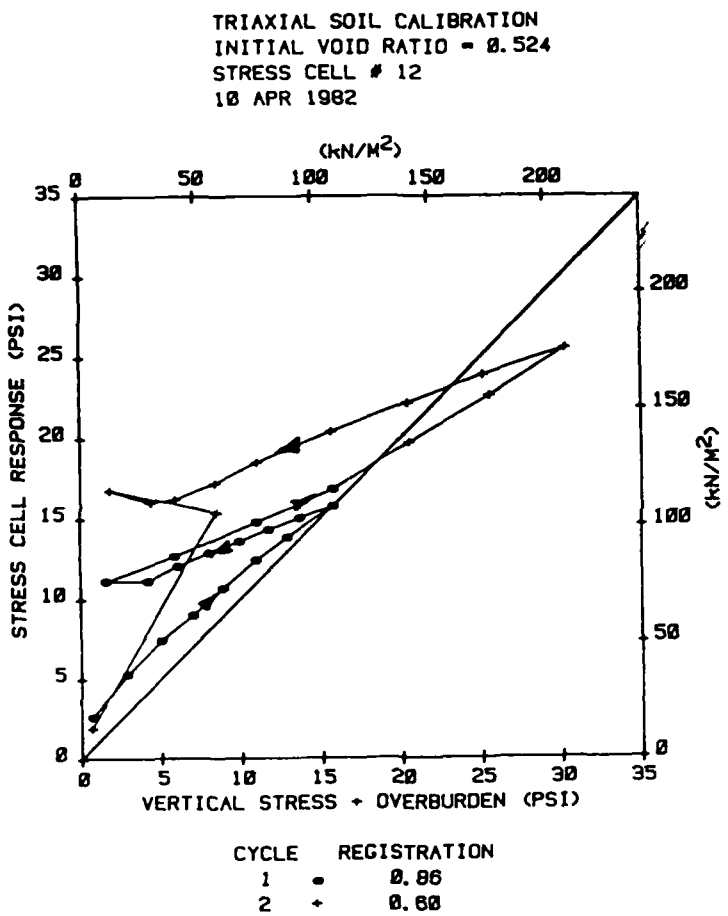

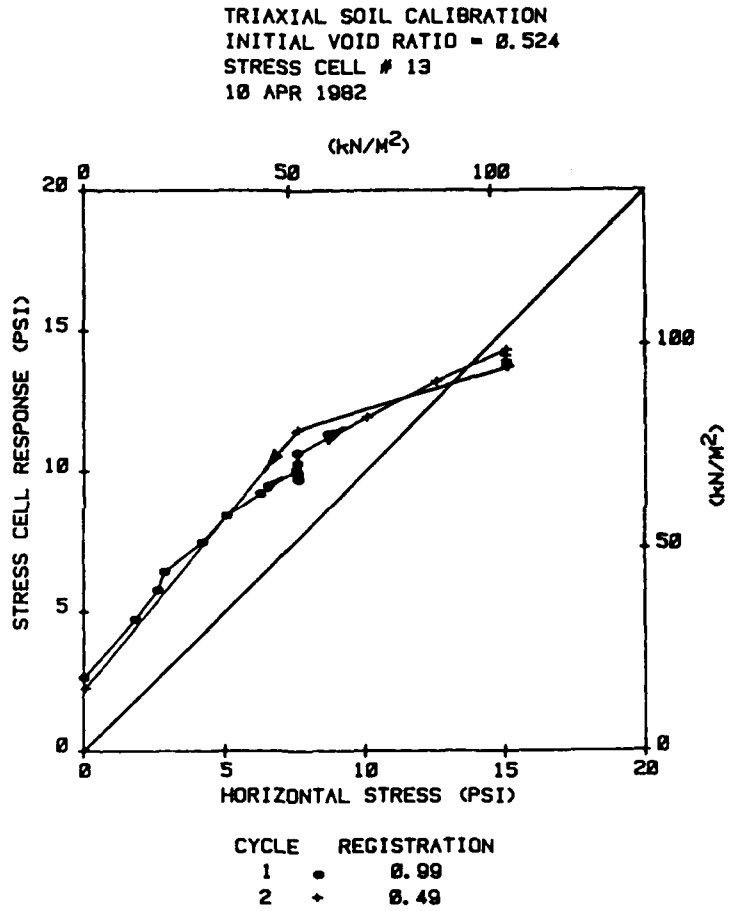

Figure B.47 Triaxial Soil Calibration.

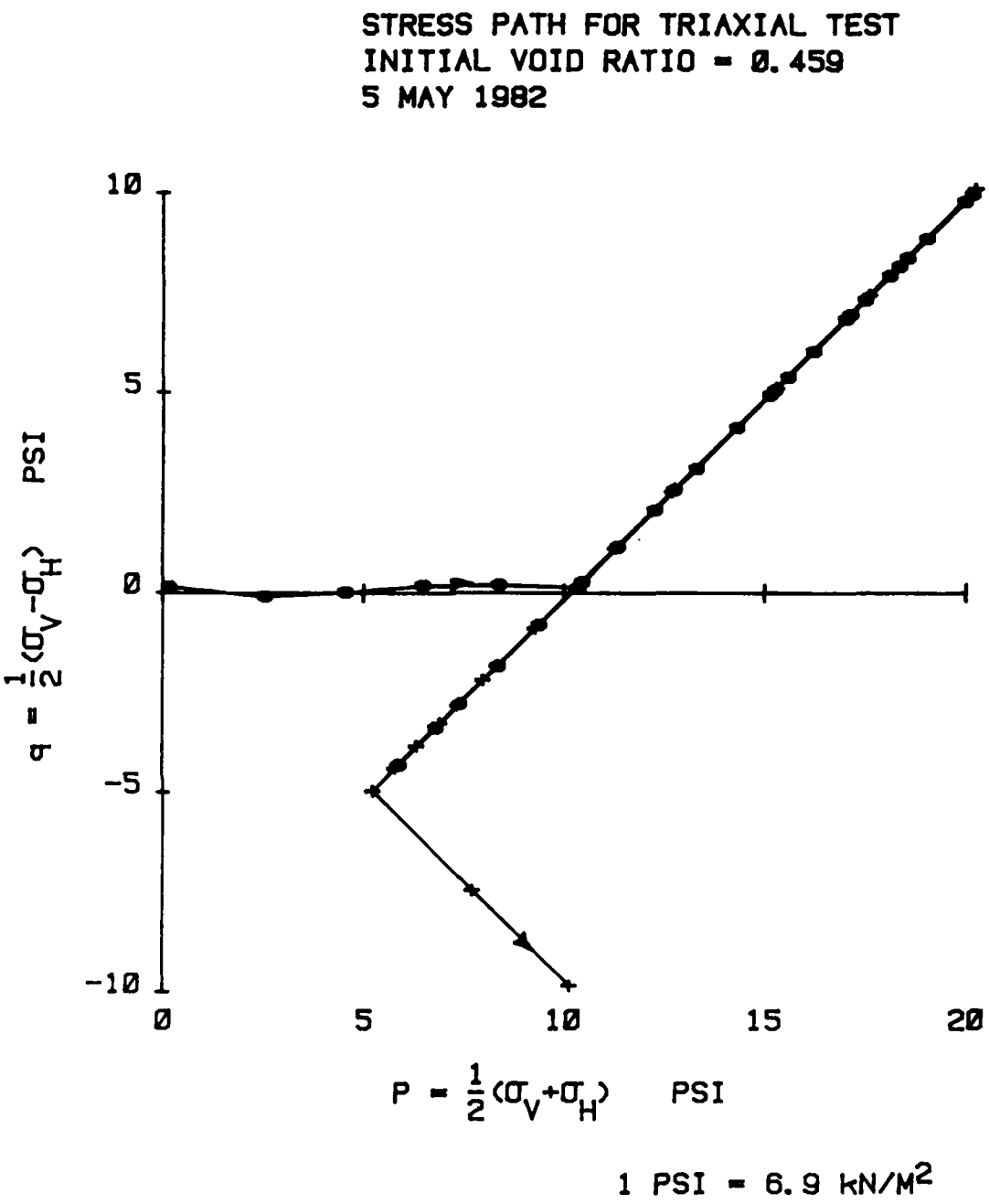

Figure B.48 Triaxial Stress Path.

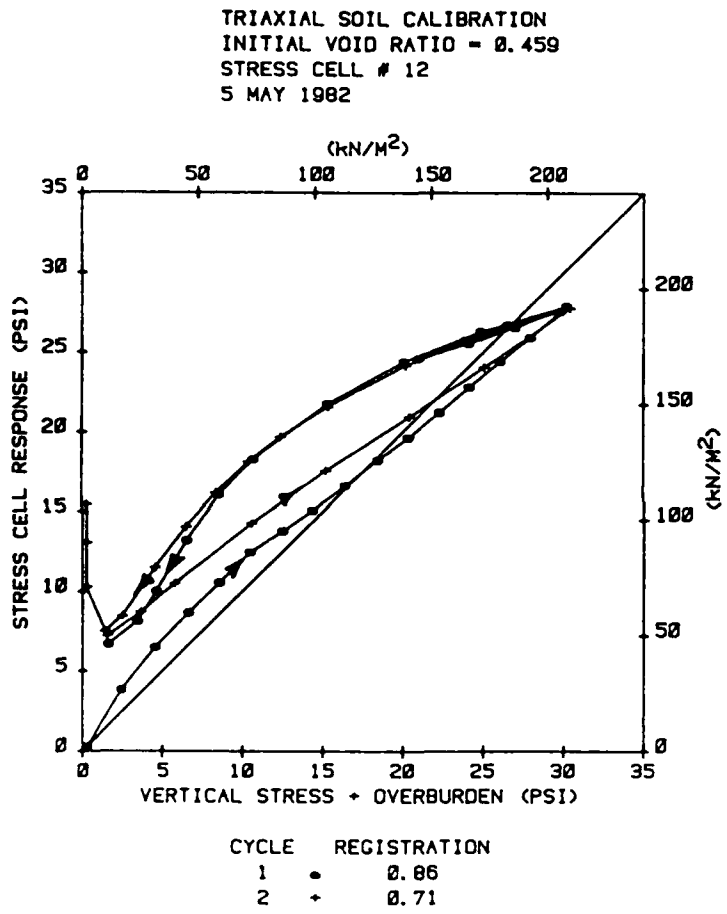

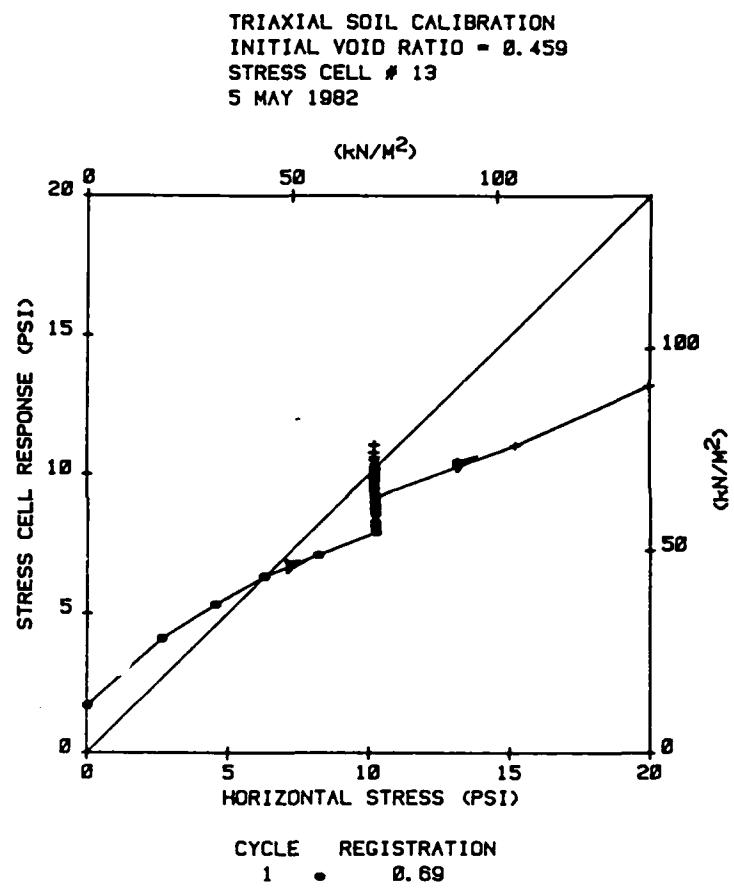

Figure B.49 Triaxial Soil Calibration.

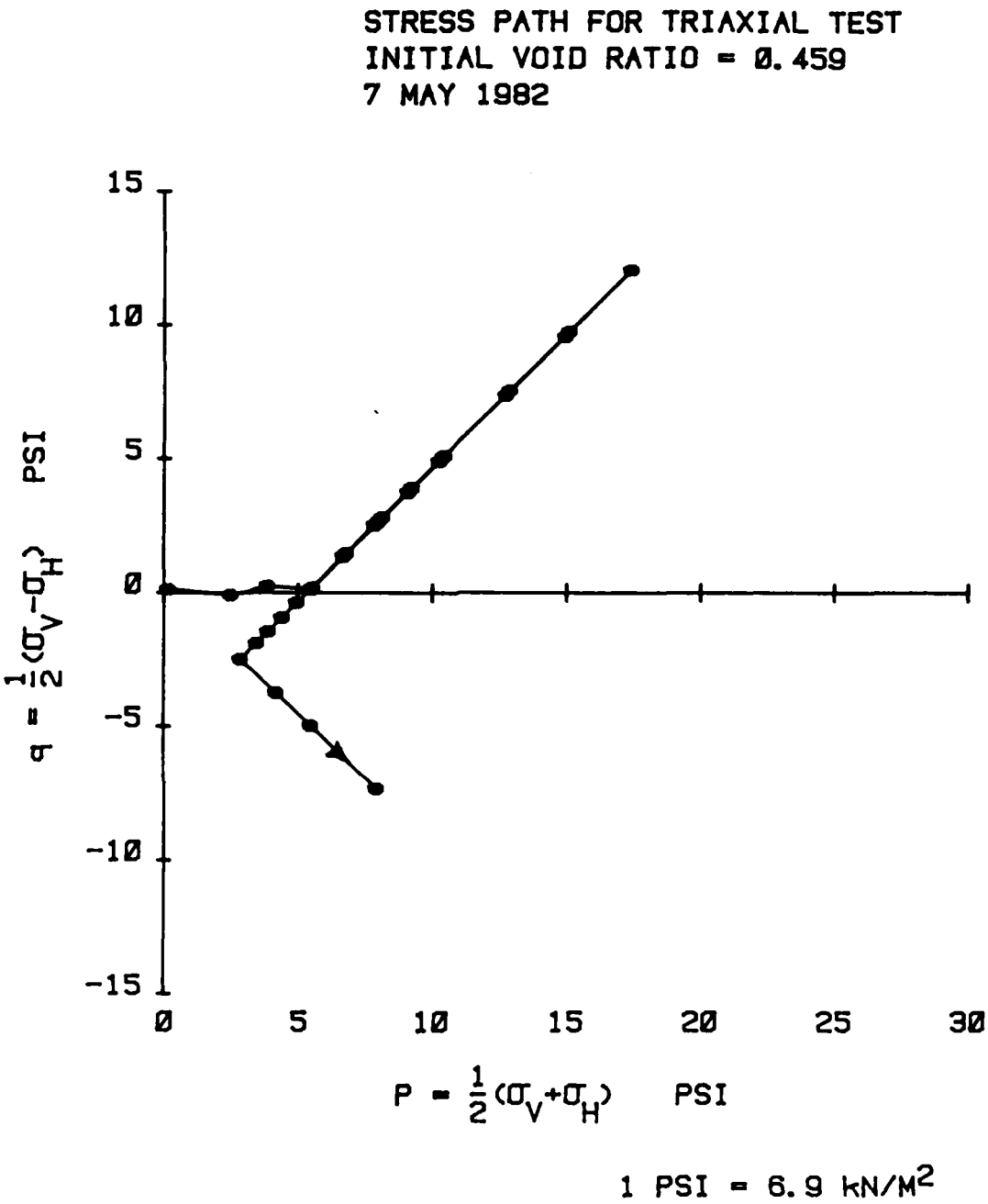

Figure B.50 Triaxial Stress Path.

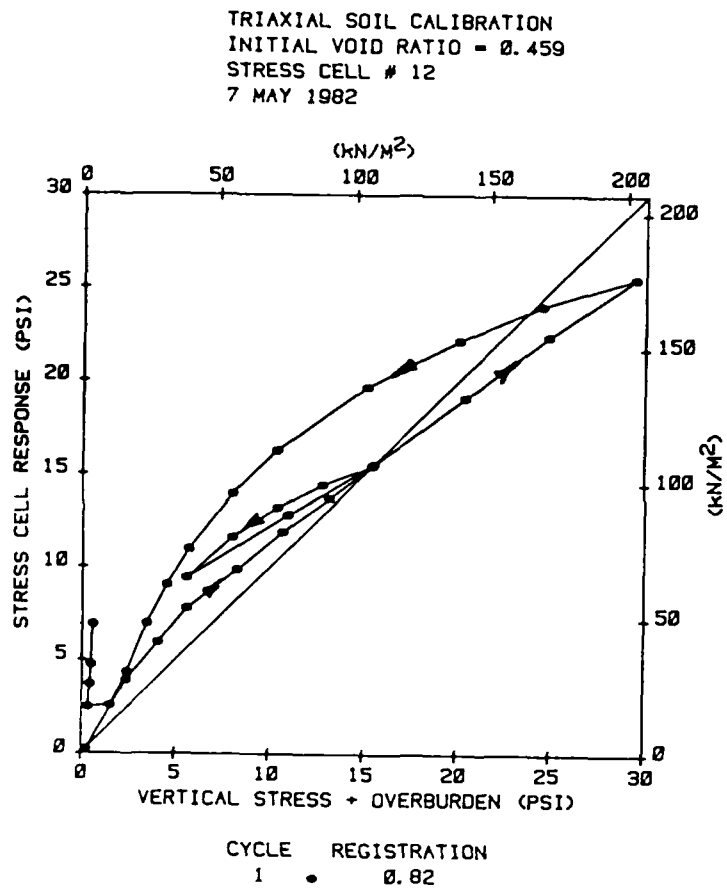

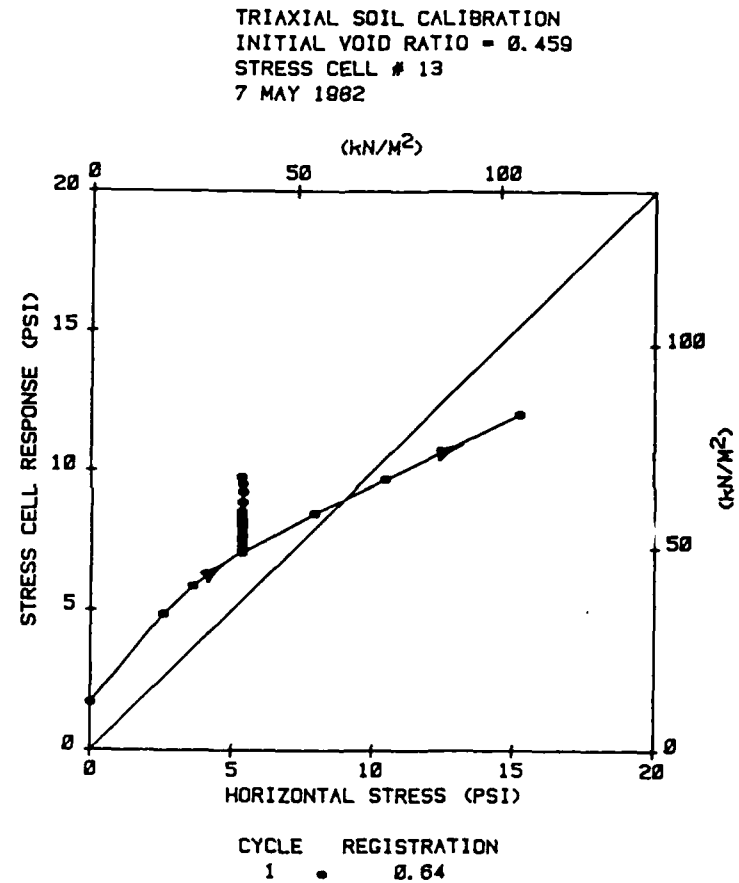

Figure B.51 Triaxial Soil Calibration.

APPENDIX C

K_o TESTING OF FILTER SAND

Figures C.1 through C.17 show the coefficient of horizontal soil stress, K_o, for filter sand as determined by the use of the K_o belt in the soil calibration chamber. The tests were performed as described in Section 5.3. The lateral air pressure was applied independently of the vertical air pressure as necessary to maintain a condition of zero lateral strain on the eleven inch (27.9 mm) diameter sample. The strain was measured by maintaining a constant output from the gages on the thin stainless steel belt around the sample. None of the results in this appendix were obtained from stress cell readings. These K_o measurements were made as an independent check on the lateral stress for the K_o condition. The alternative to these independent stress measurements was to use one of many available empirical formulas for K_o to estimate the lateral stress.

The following figures show the K_o values for loading and unloading cycles for different ranges of applied vertical stress and for different initial void ratios of the filter sand. The unloading results from each K_o test are replotted as the log K_o versus the log of the overconsolidation ratio, OCR. The slope of this log-log plot is nearly a constant for each test and is replotted as the alpha, α,

value on each figure. The K_o value at an overconsolidation ratio of 1.0 was determined by dividing the lateral stress necessary to balance the K_o belt by the peak vertical stress for each cycle of loading. Although the tangent K_o values upon initial loading were usually a constant over a wide range of stress levels, only the value at peak stress was reported on each figure. The alpha values were determined using a least squares linear regression program on the data, not including those data points which showed a decrease in K_o at low vertical stress levels where the soil may have failed upon unloading.

Figure No.	Initial Void Ratio	Cycle No.	Maximum Vertical Stress (psi)	K_o	α
C.1	0.735(P)	1	12	0.32	0.48
		2	13	0.29	0.42
C.2	0.692(P)	1	31	0.28	0.64
		2	30	0.27	0.69
C.3	0.528(C)	1	33	0.17	0.75
C.4	0.678(P)	1	21	0.26	0.45
		2	30	0.27	0.42
		3	31	0.26	0.43
C.5	0.735(P)	1	11	0.23	0.31
		2	21	0.25	0.36
		3	31	0.26	0.40
		4	70	0.28	0.41
C.6	0.678(S)	5	16	0.23	0.38
		6	30	0.24	0.38
C.7	0.548(C)	1	11	0.21	0.72
		2	20	0.17	0.74
		3	30	0.16	0.72
		4	11	0.23	0.67
C.8	0.668(P)	1	11	0.22	0.44
		2	11	0.22	0.45
		3	21	0.24	0.44
		4	32	0.26	0.44
C.9	0.530(V)	1	11	0.33	0.81
		2	20	0.30	0.66
		3	32	0.29	0.63
C.10	0.722(P)	1	11	0.36	0.30
C.11	0.736(P)	1	11	0.42	0.31
		2	21	0.44	0.34
		3	31	0.42	0.33
C.12	0.624(V)	1	11	0.51	0.70
		2	21	0.52	0.72
		3	31	0.56	0.72

Table C.1 Summary of K_o Tests on Filter Sand.

Figure No.	Initial Void Ratio	Cycle No.	Maximum Vertical Stress (psi)	K_o	α
C.13	0.548(V)	1	11	0.23	0.28
		2	21	0.25	0.23
		3	31	0.26	0.30
C.14	0.765(P)	1	11	0.38	0.28
		2	20	0.41	0.29
		3	30	0.42	0.27
C.15	0.524(V)	1	11	0.23	0.76
		2	21	0.22	0.54
		3	31	0.22	0.55
C.16	0.474(C)	1	10	0.38	0.75
		2	20	0.33	0.63
		3	30	0.30	0.57
C.17	0.459(C)	1	10	0.30	0.63
		2	20	0.28	0.60
		3	30	0.27	0.60

Placement Method
P = Pluviation
C = Compaction
S = Static
V = Vibration

Table C.1 Cont. Summary of K_o Tests on Filter Sand.

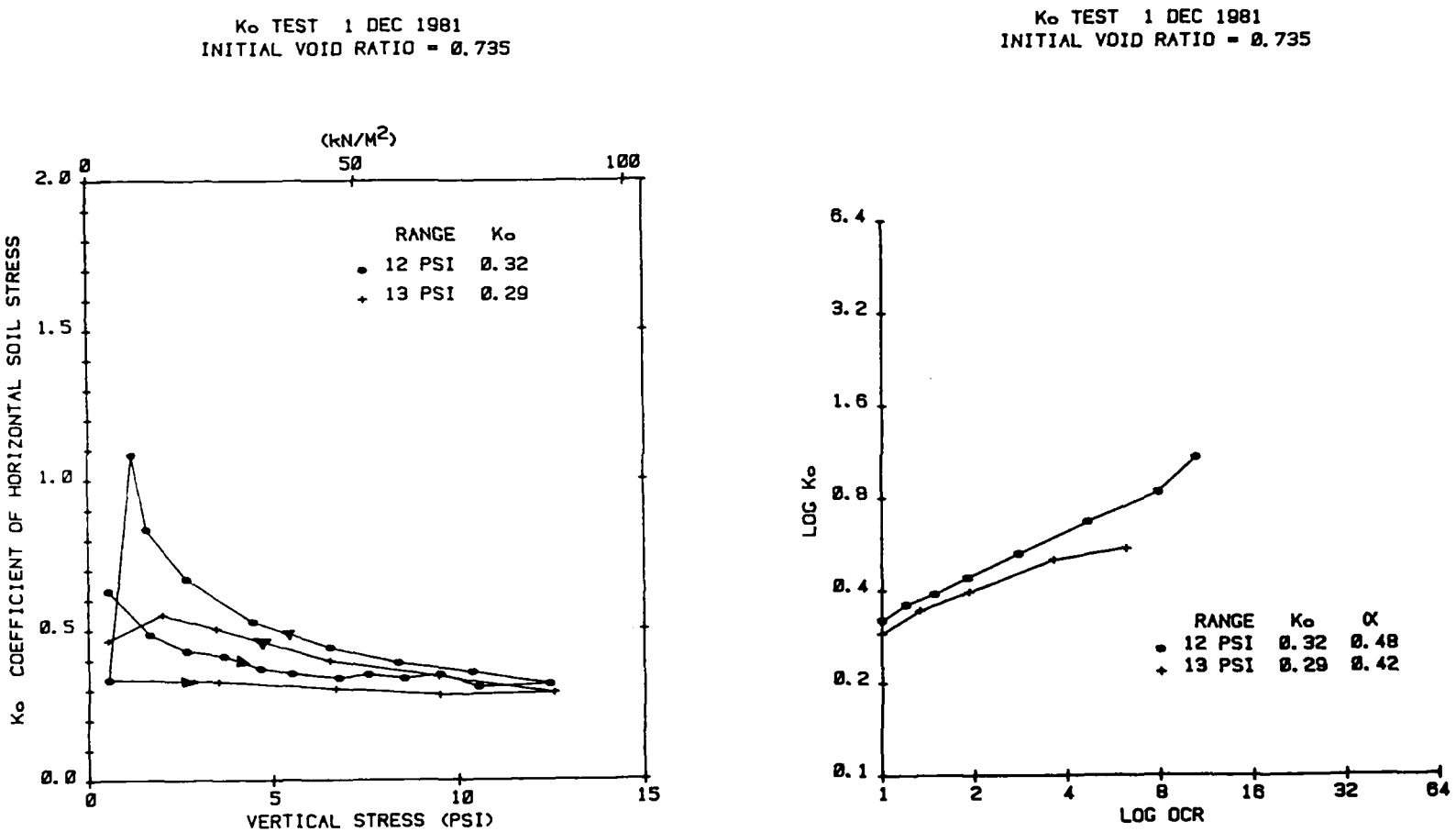

Figure C.1 K_o Testing of Filter Sand.

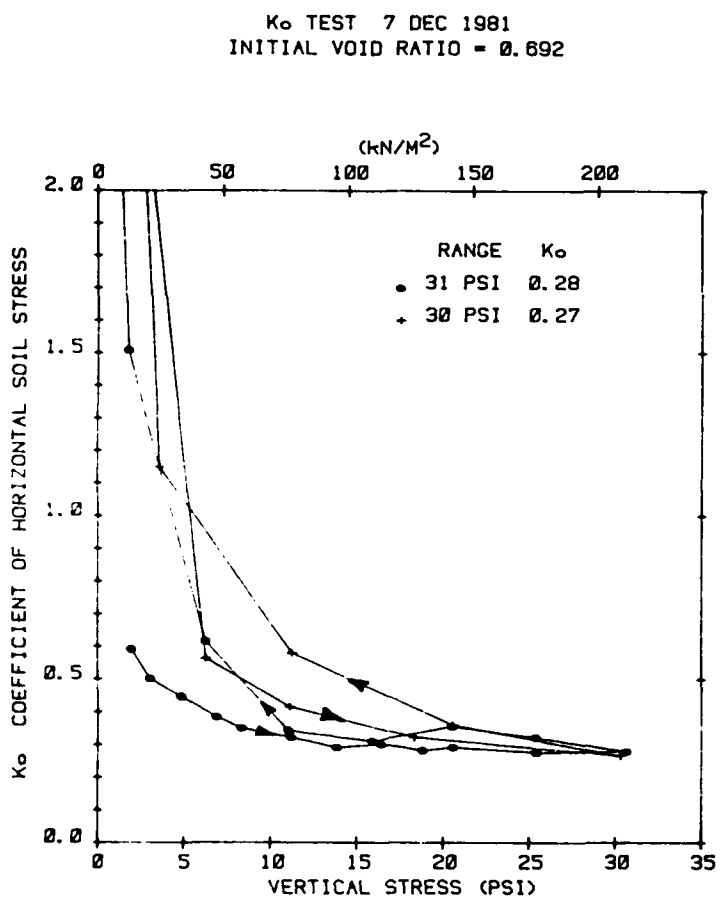

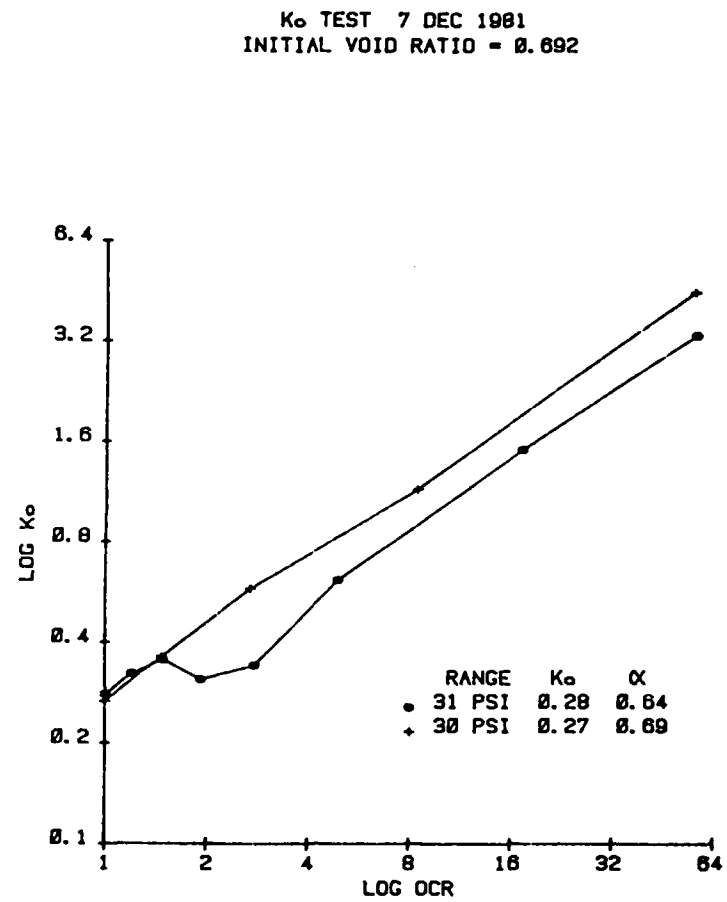

Figure C.2 K_o Testing of Filter Sand.

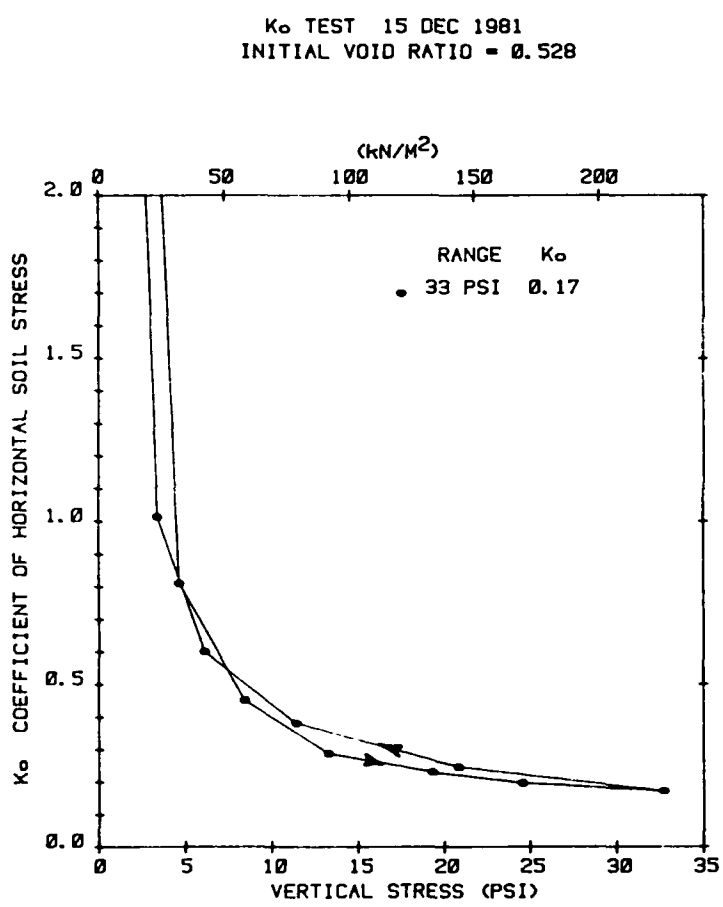

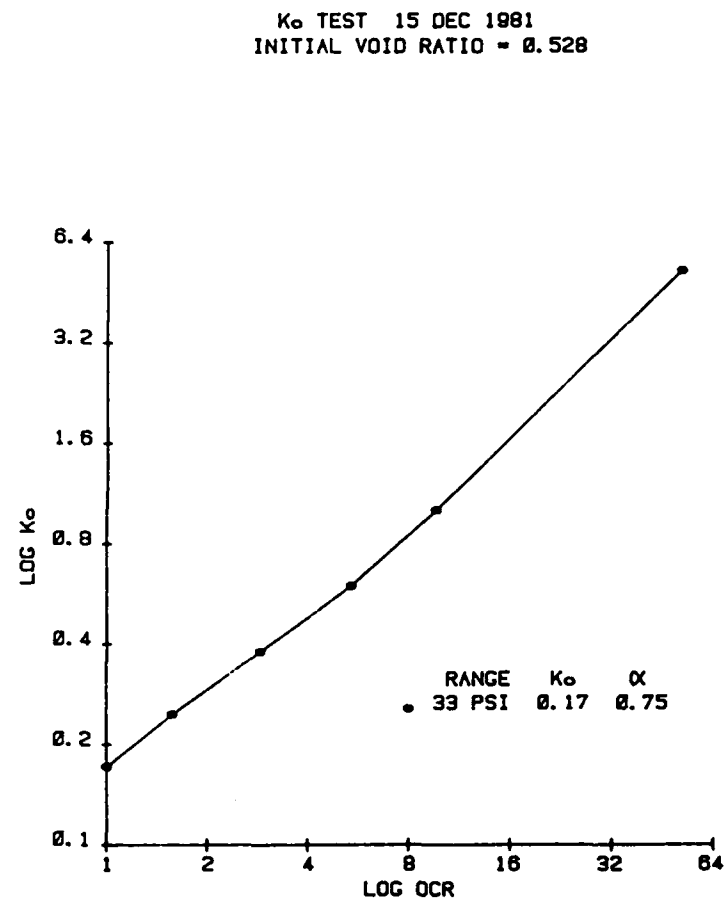

Figure C.3 K_o Testing of Filter Sand.

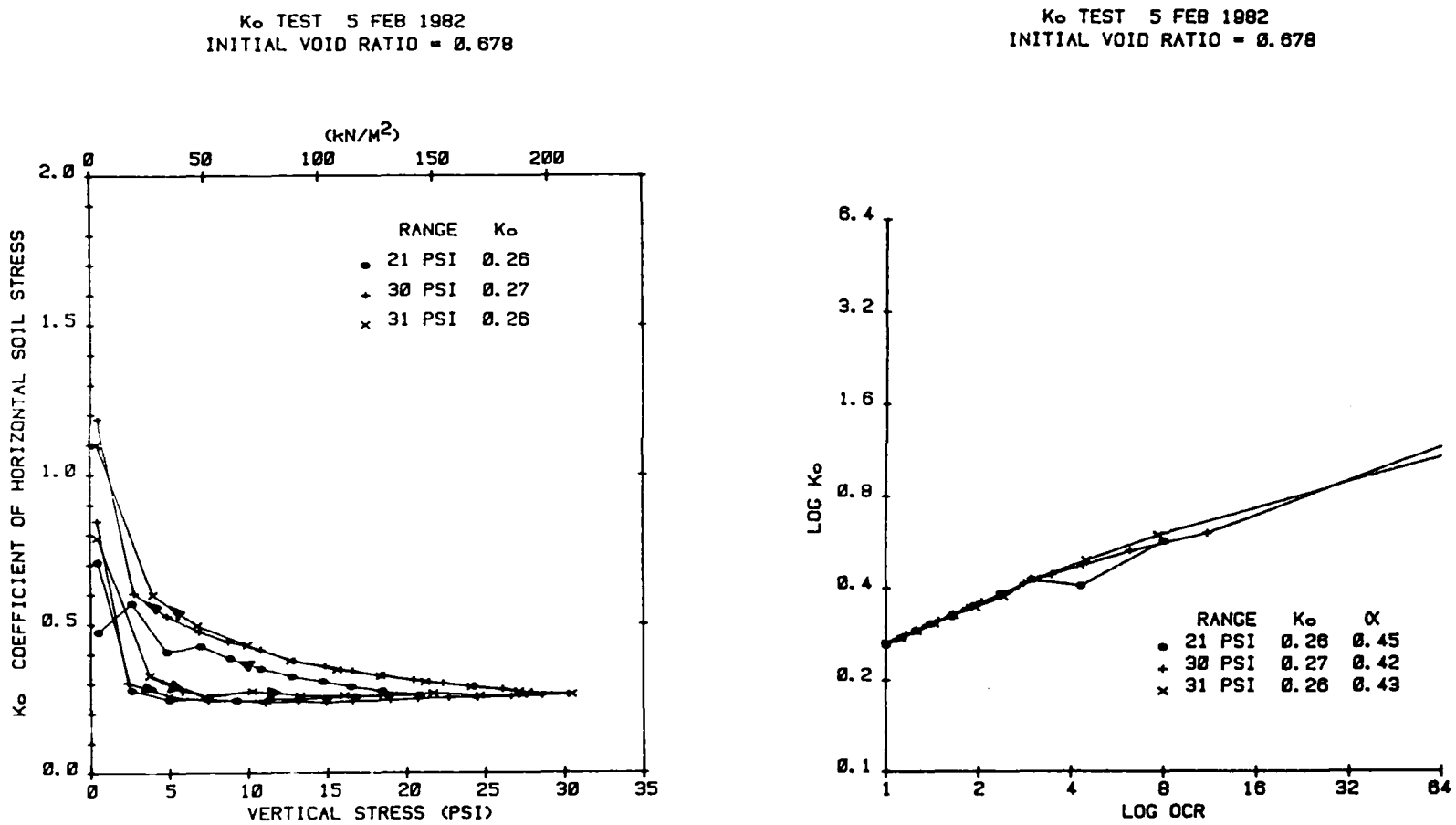

Figure C.4 K_o Testing of Filter Sand.

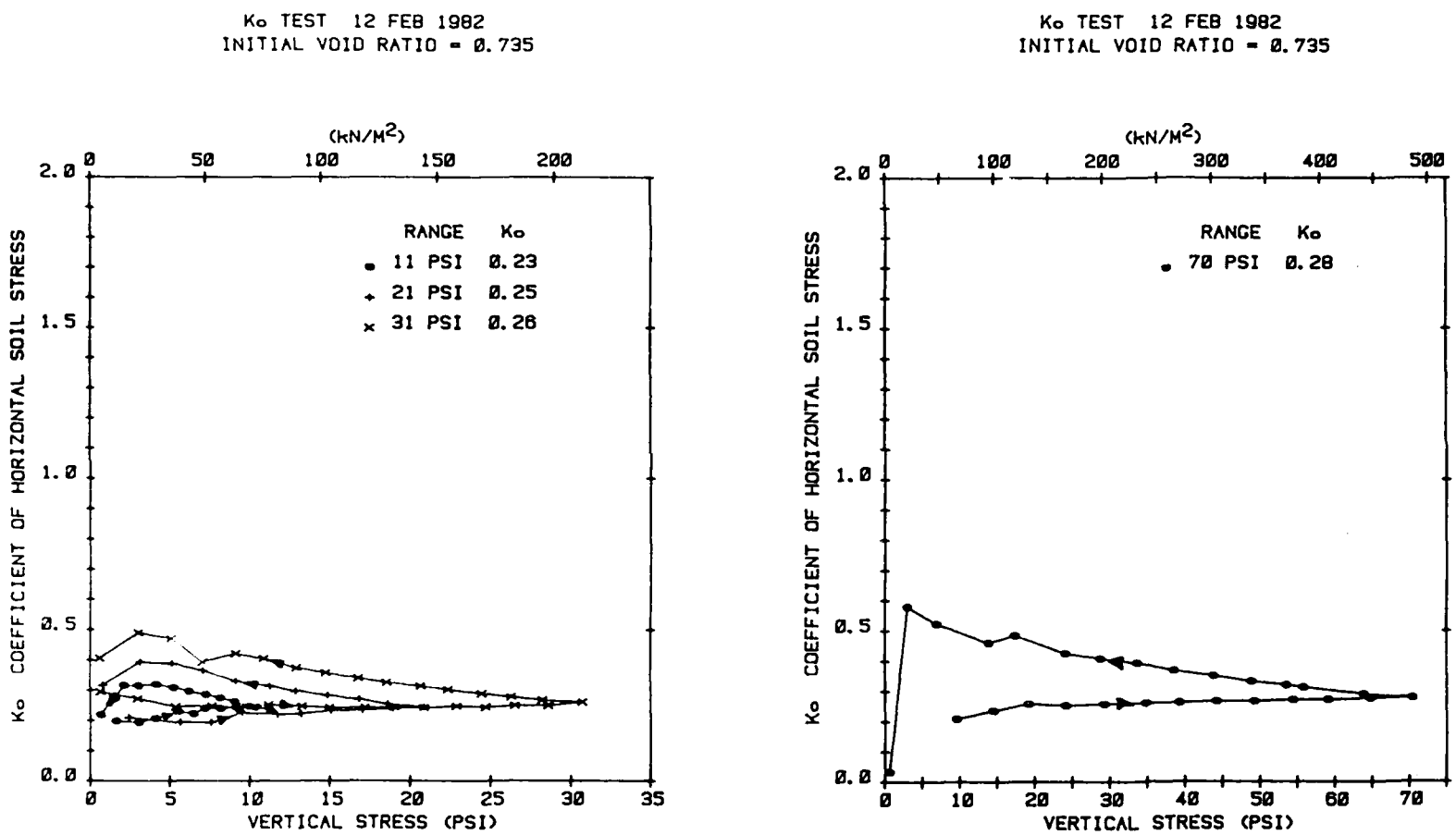

Figure C.5 K_o Testing of Filter Sand.

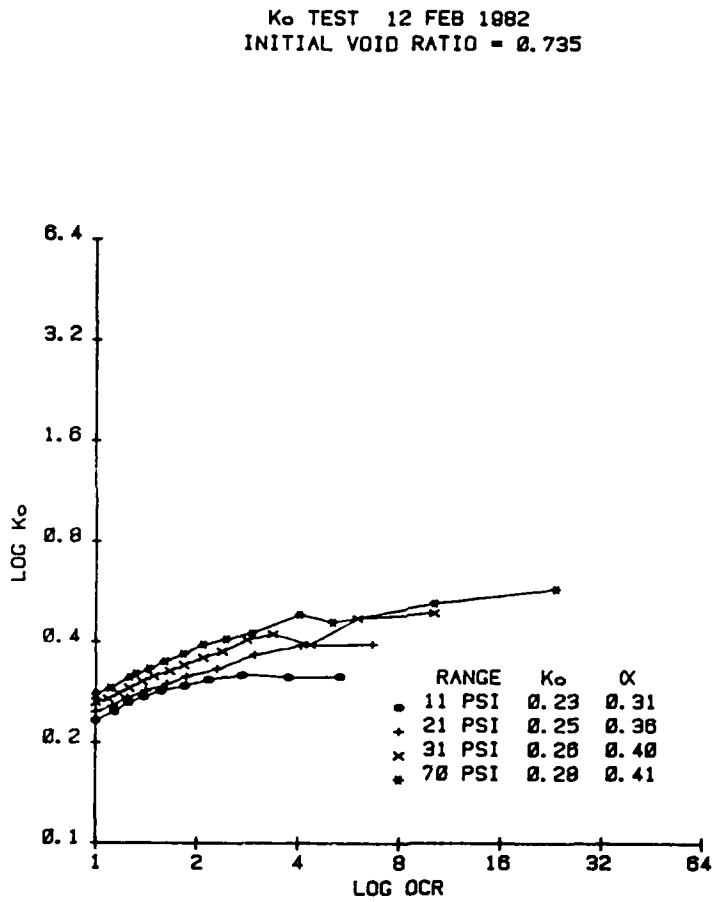

Figure C.5 Cont. K_o Testing of Filter Sand.

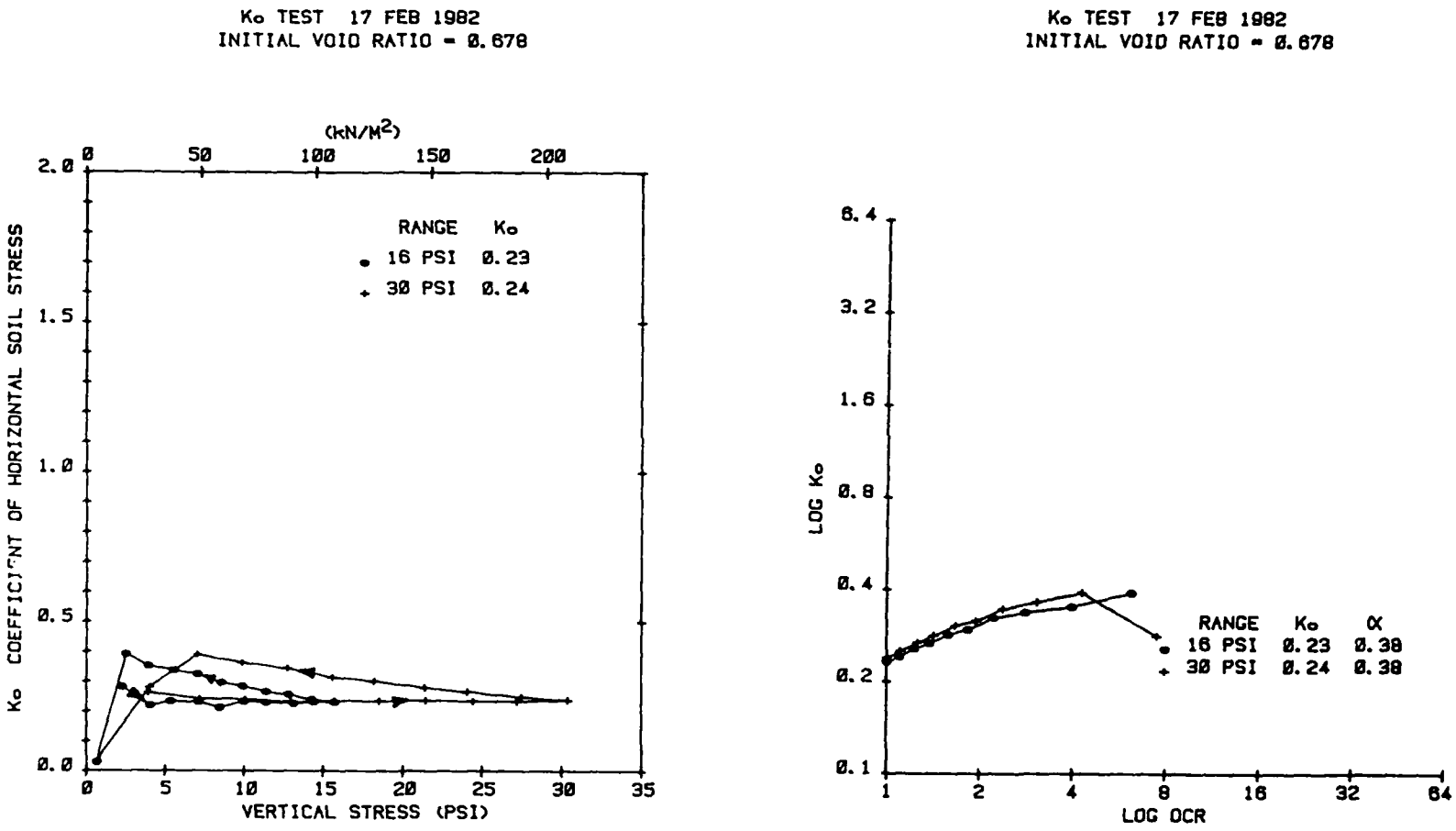

Figure C.6 K_o Testing of Filter Sand.

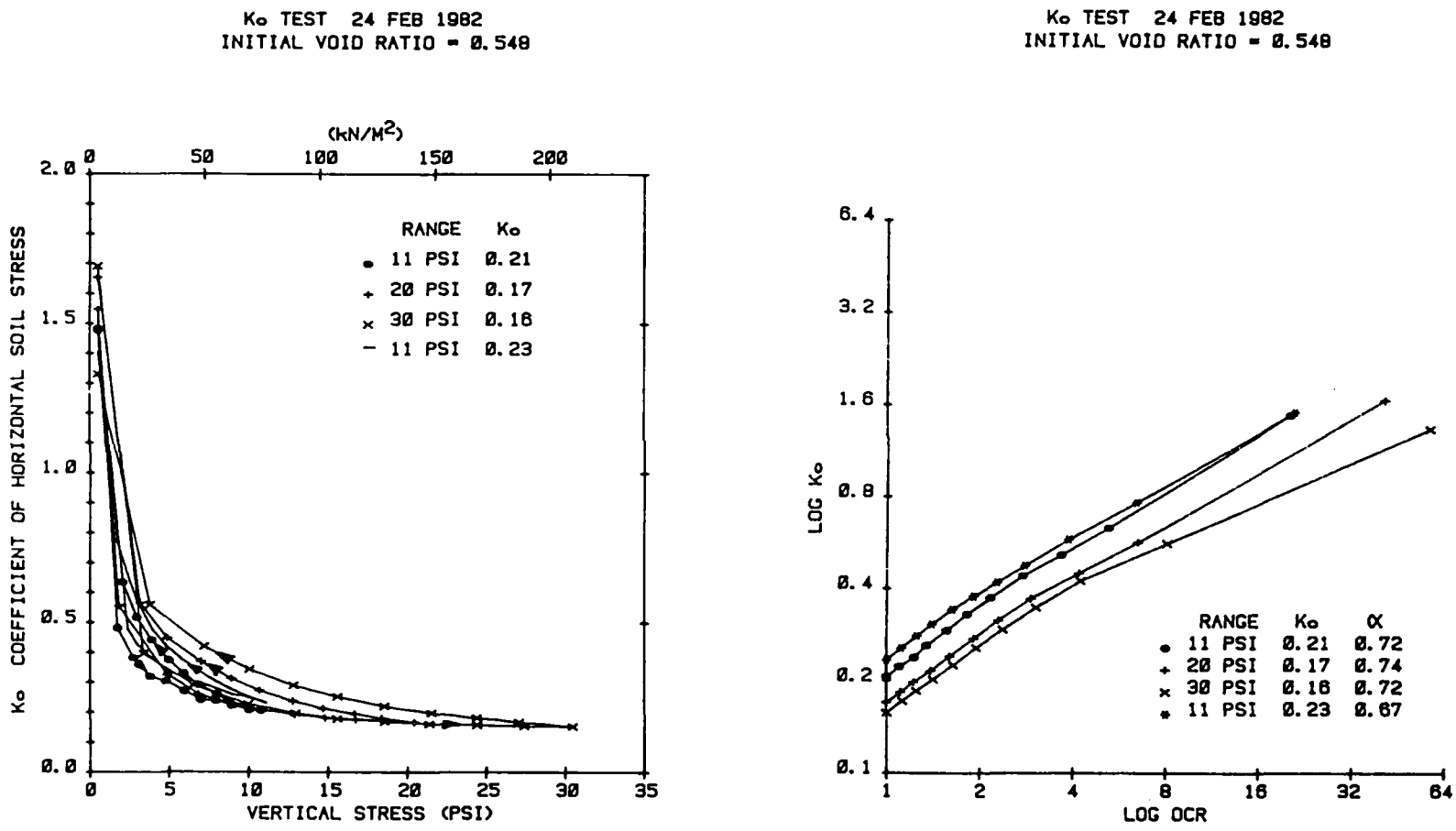

Figure C.7 K_o Testing of Filter Sand.

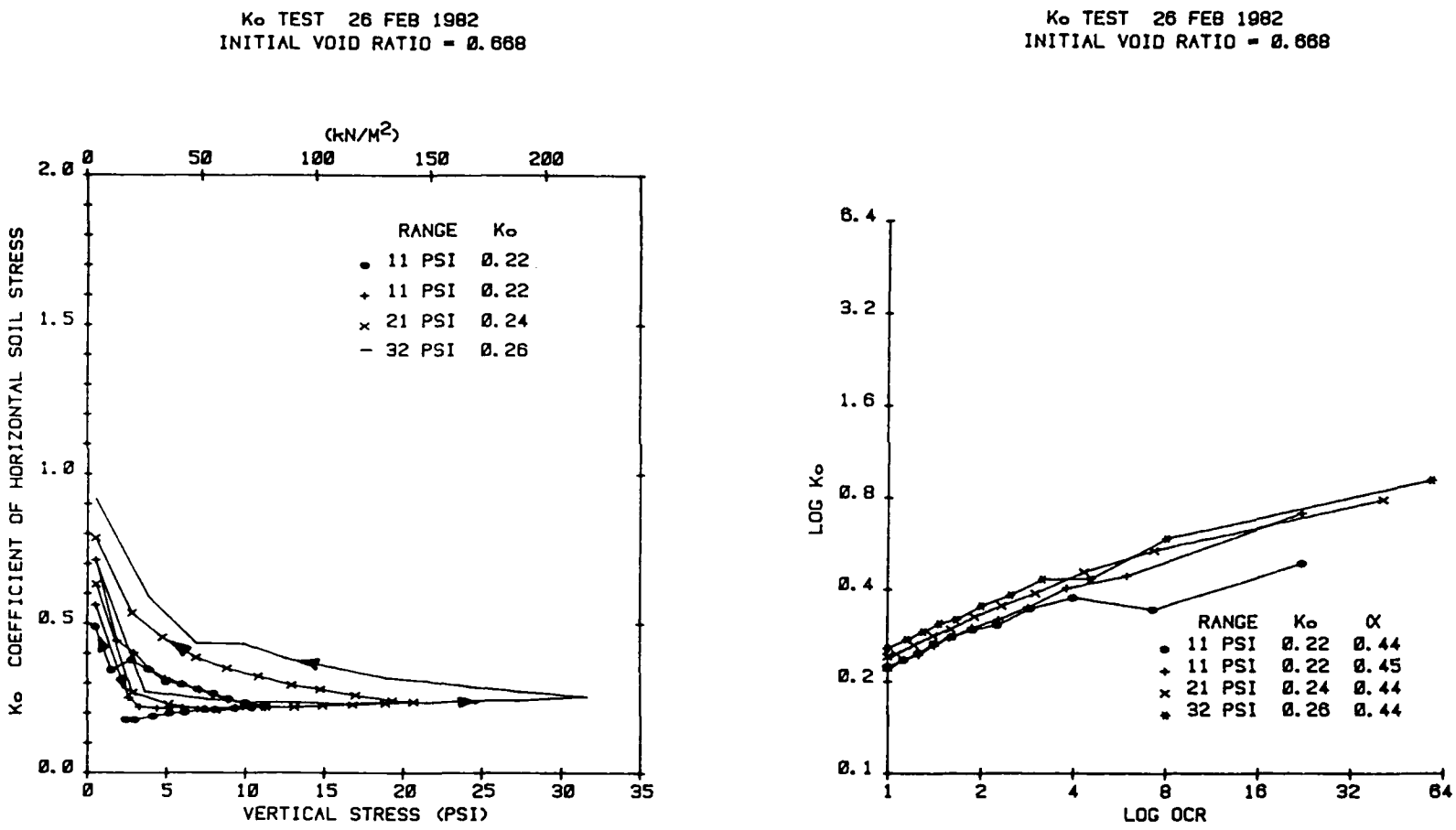

Figure C.8 K_o Testing of Filter Sand.

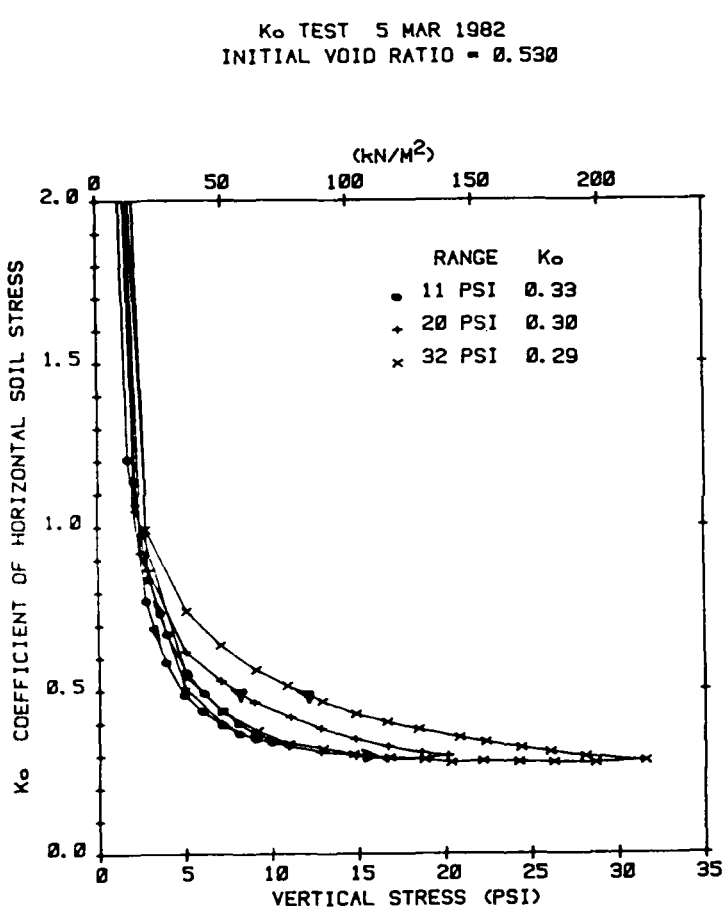

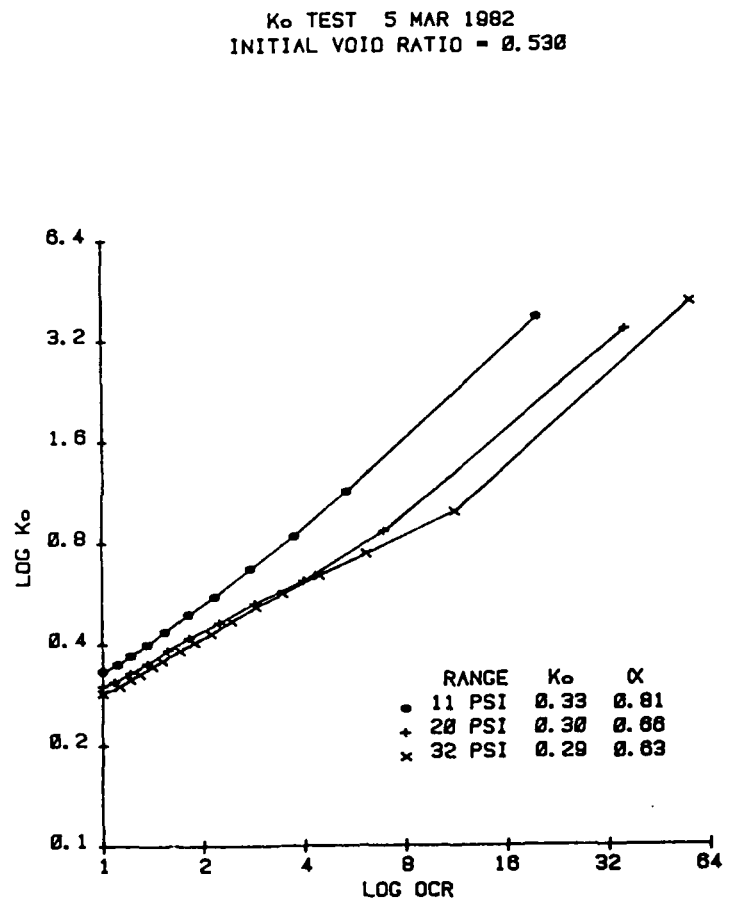

Figure C.9 K_o Testing of Filter Sand.

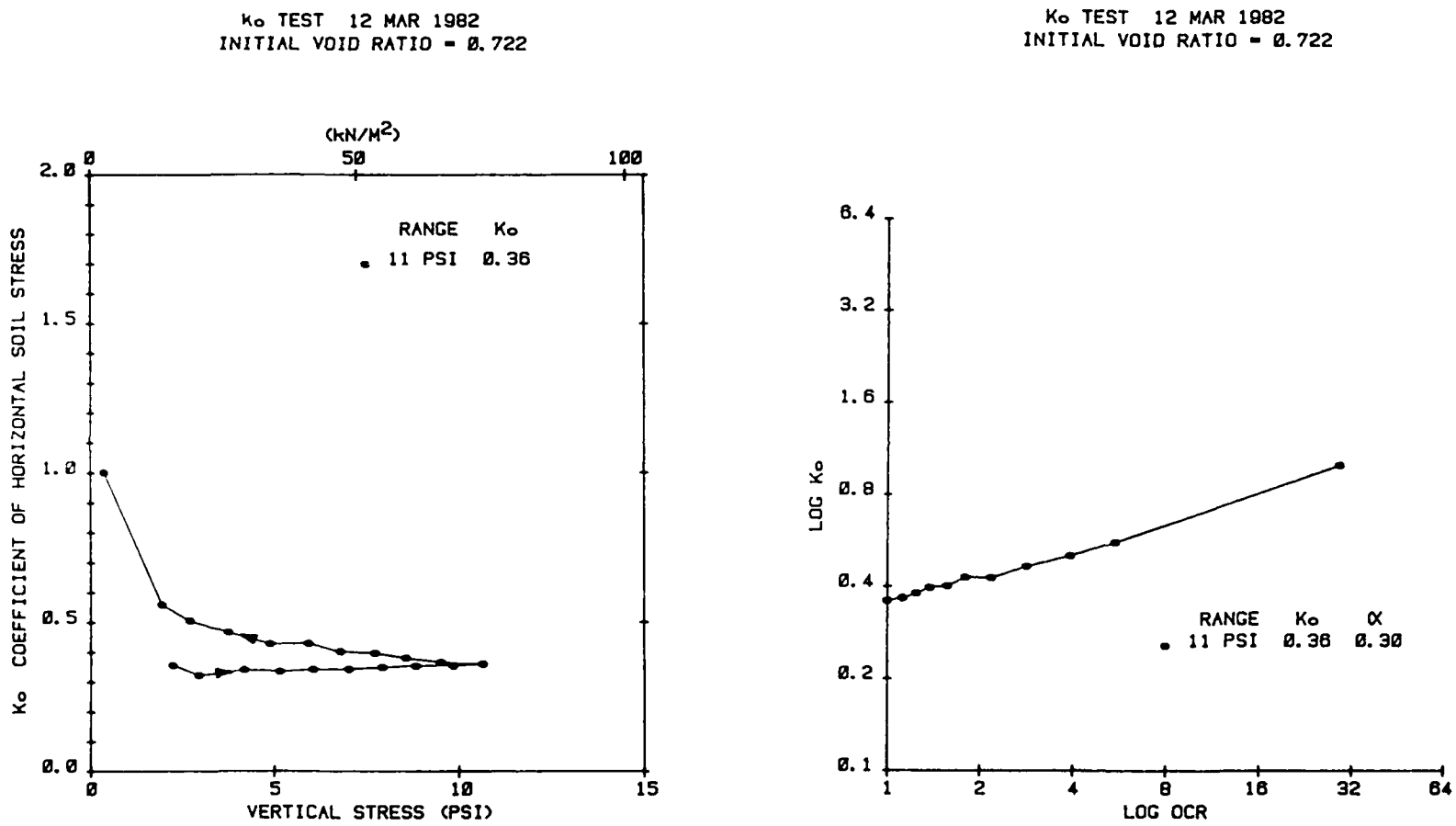

Figure C.10 K_o Testing of Filter Sand.

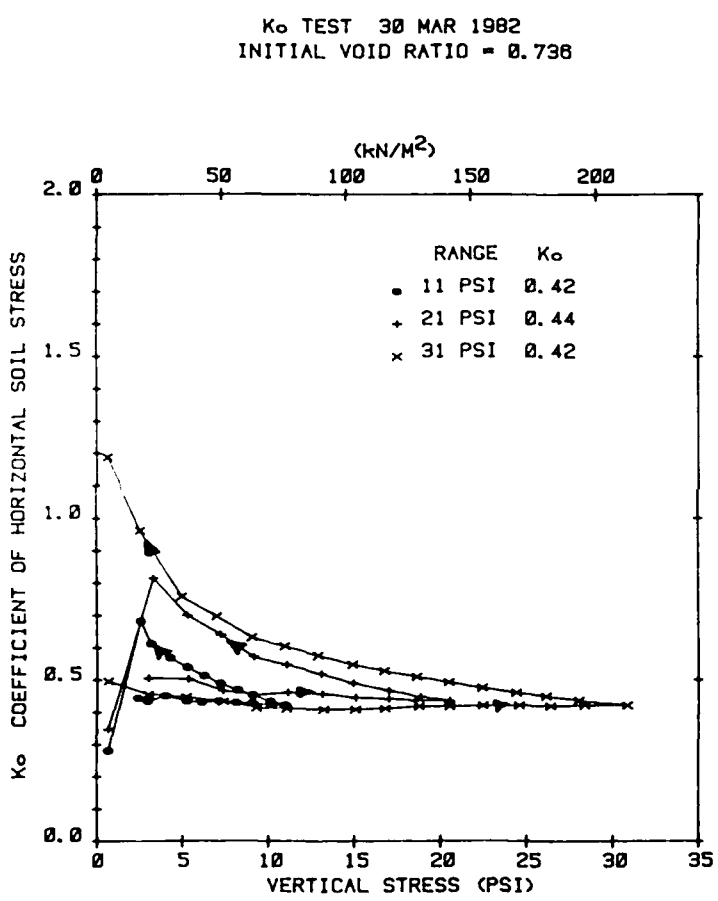

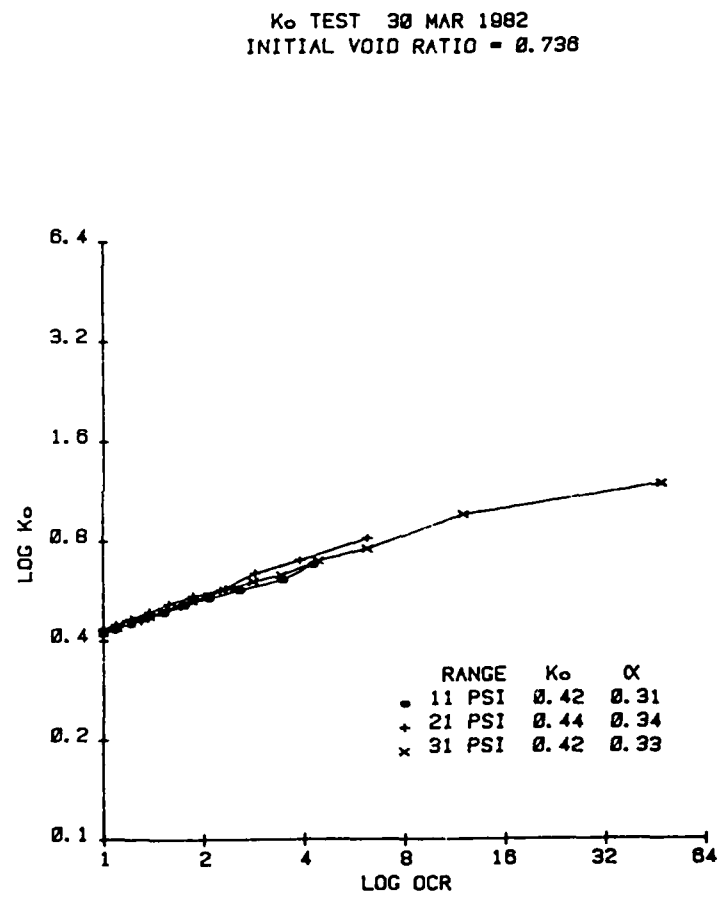

Figure C.11 K_o Testing of Filter Sand.

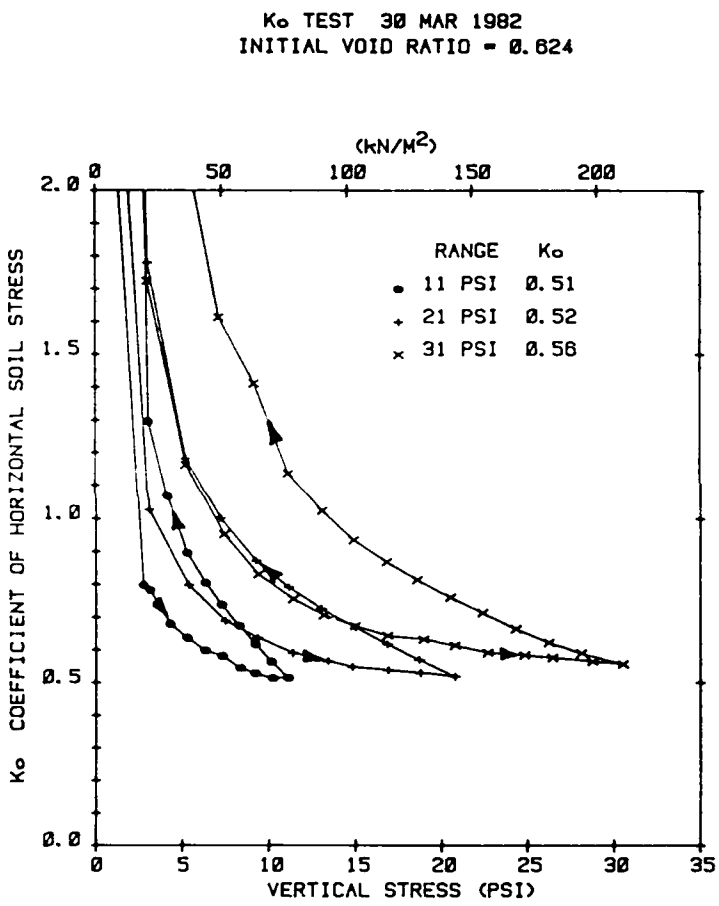

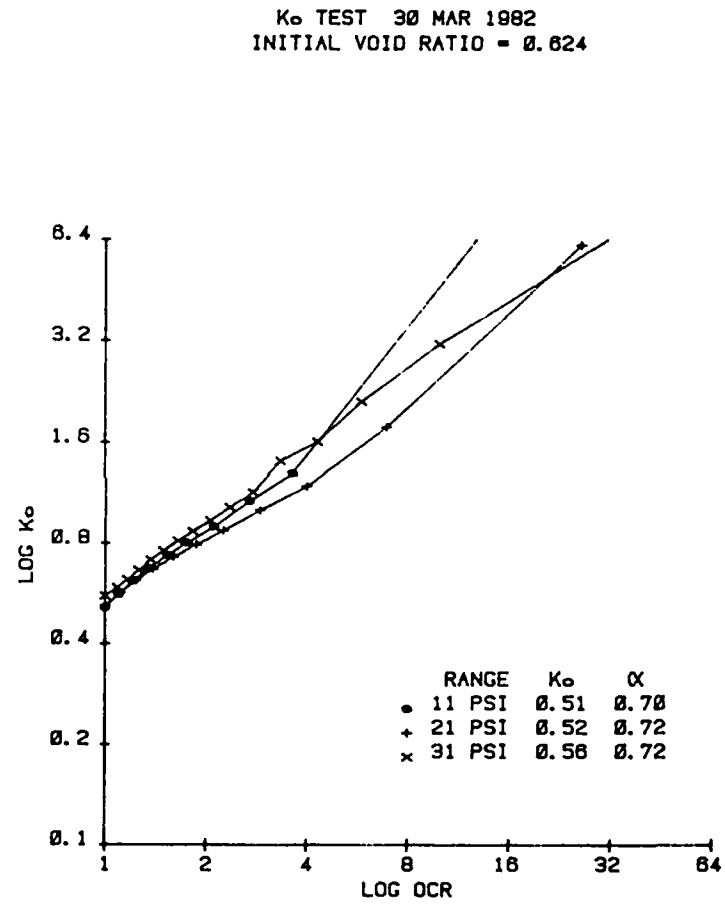

Figure C.12 K_o Testing of Filter Sand.

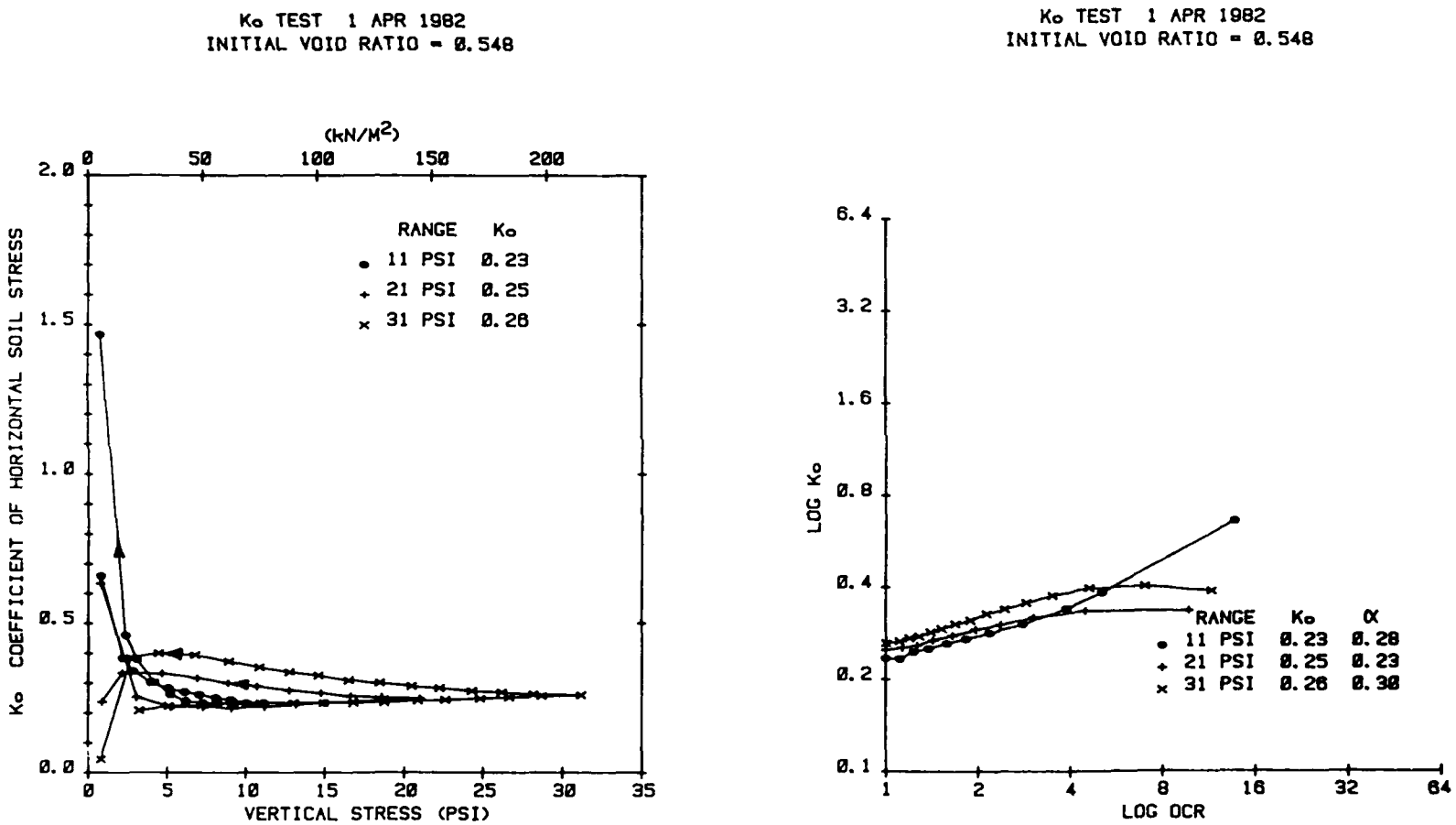

Figure C.13 K_o Testing of Filter Sand.

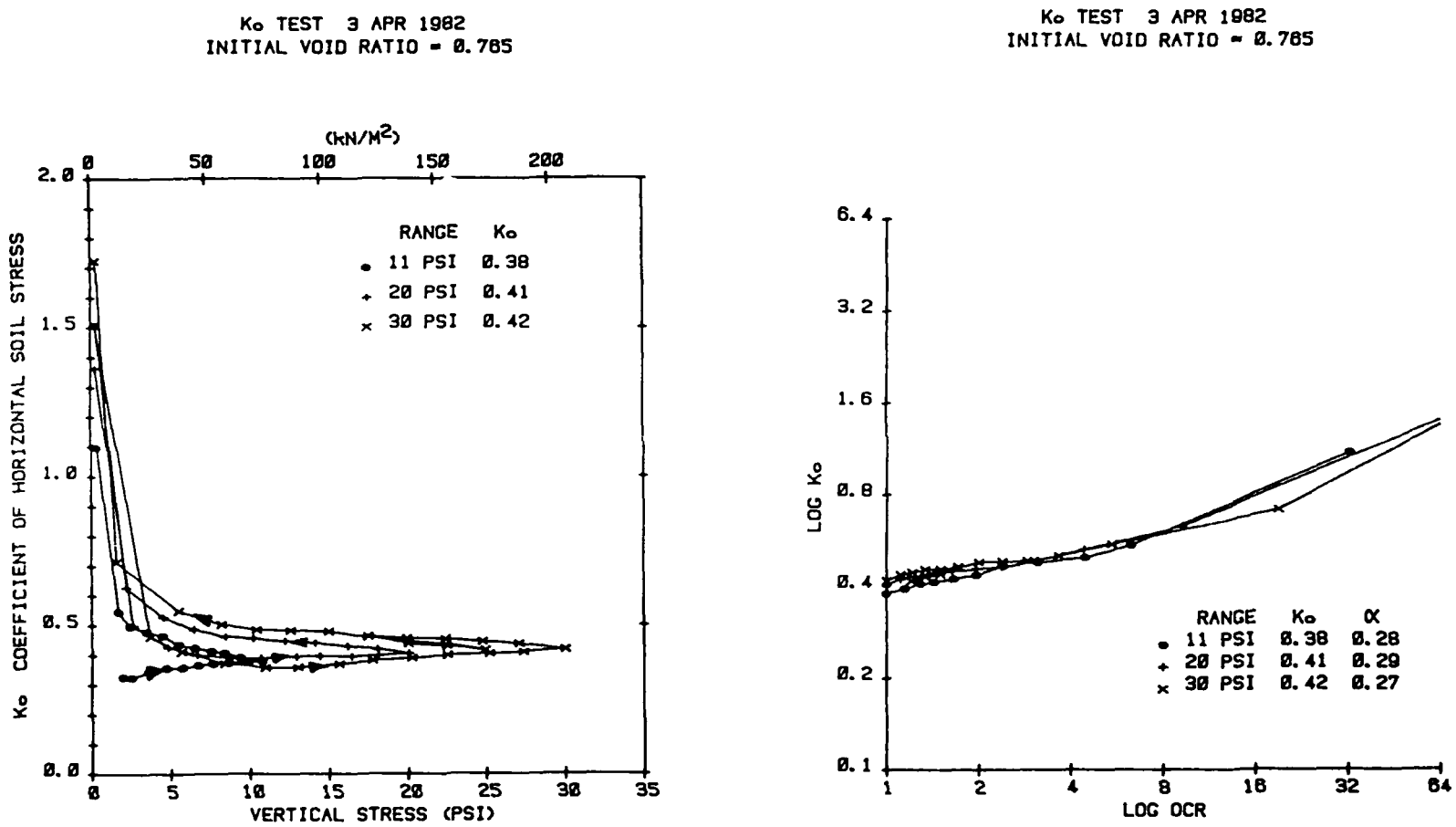

Figure C.14 K_o Testing of Filter Sand.

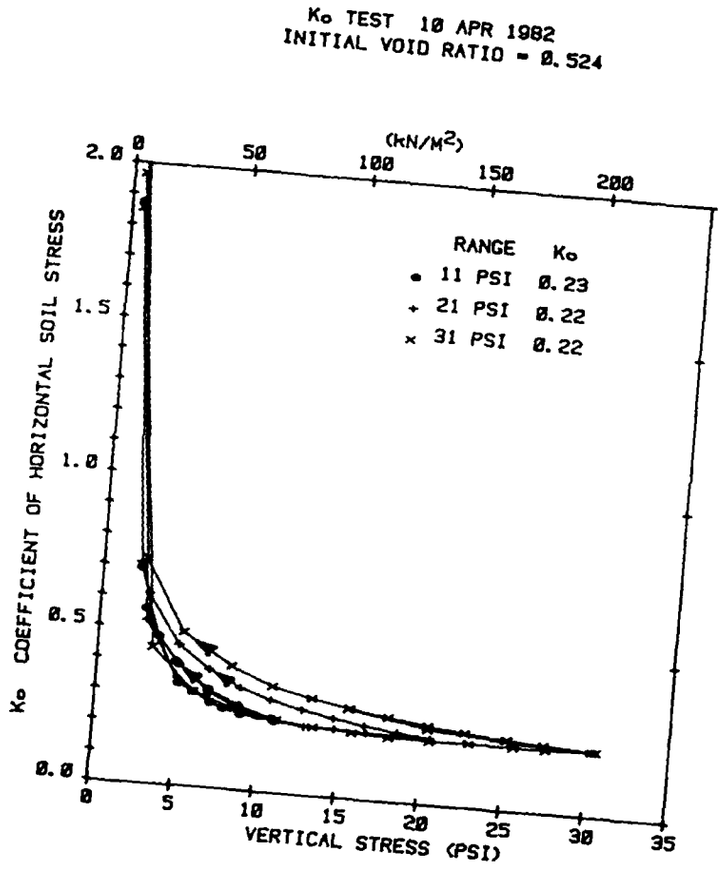

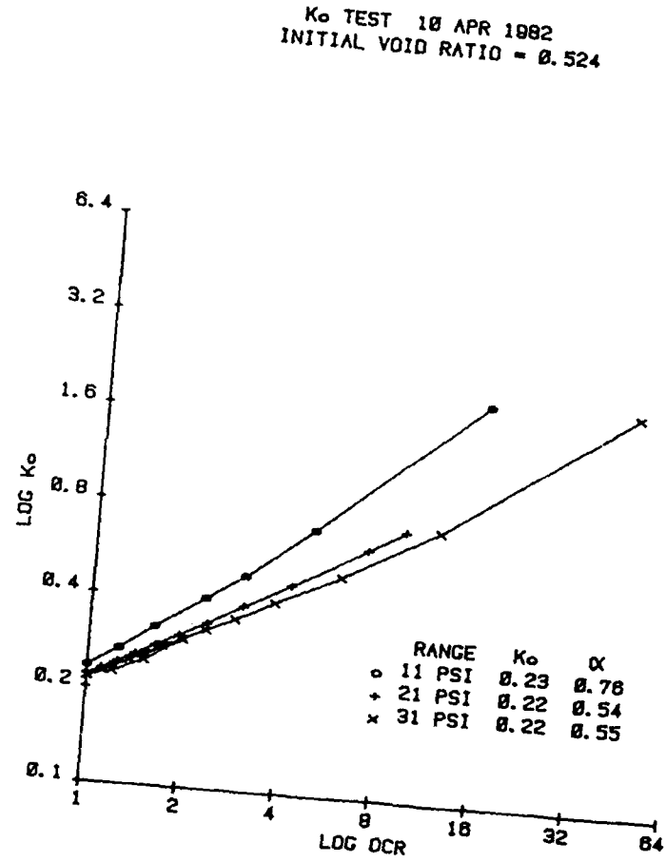

Figure C.15 K_o Testing of Filter Sand.

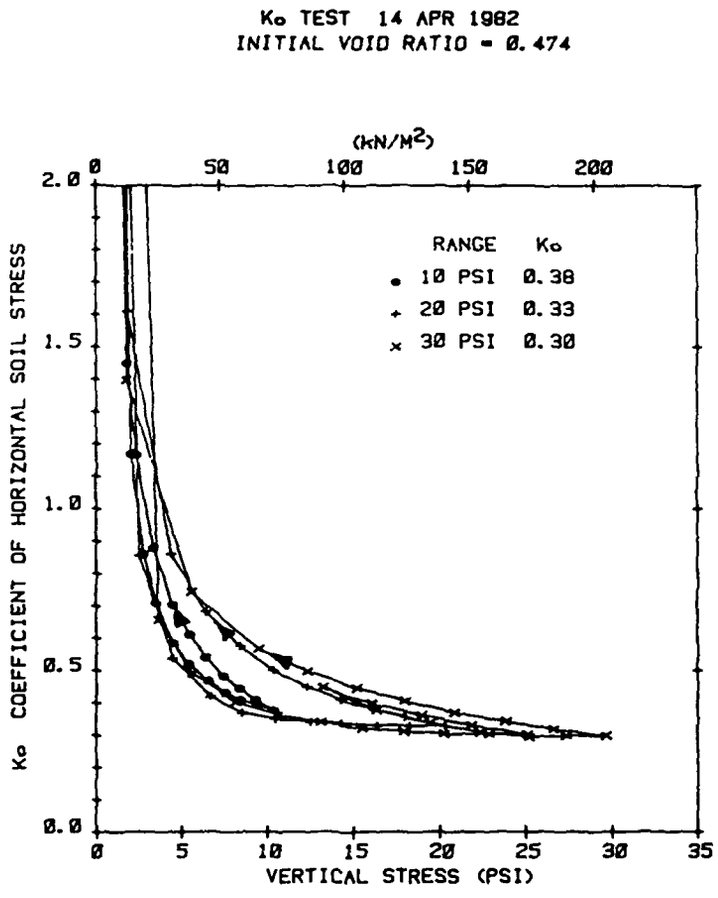

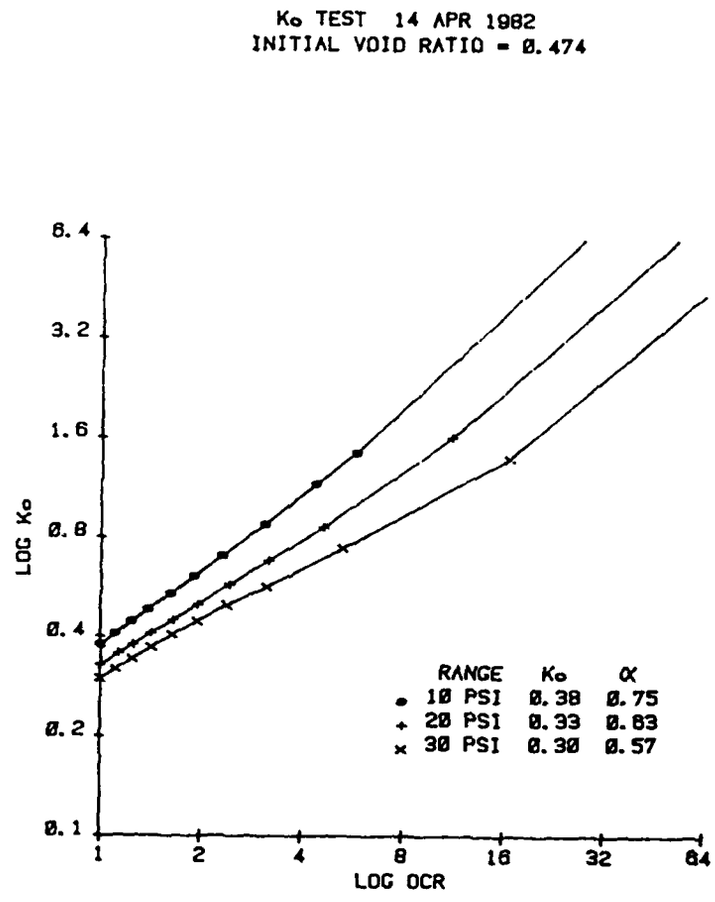

Figure C.16 K_o Testing of Filter Sand.

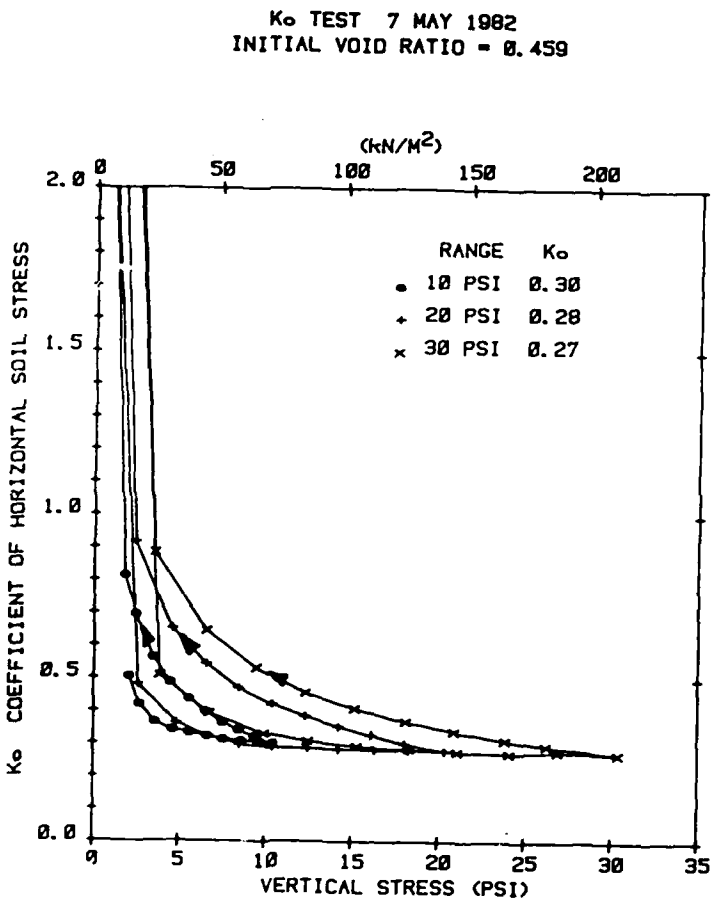

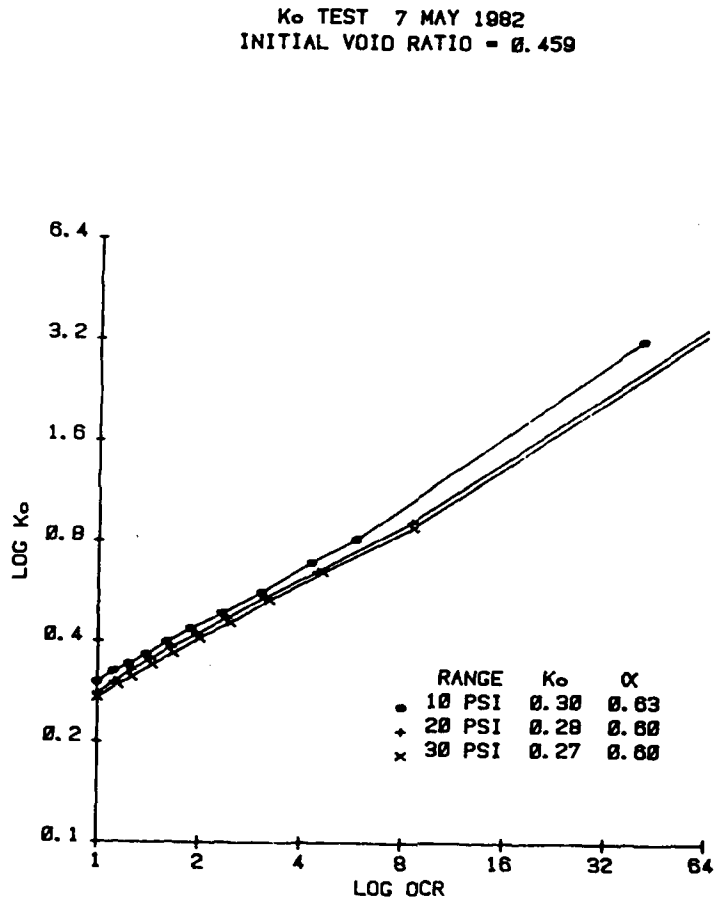

Figure C.17 K_o Testing of Filter Sand.

APPENDIX D

CONSTANT VOLUME DIRECT SHEAR TESTS

Figures D.1 through D.15 show the results of direct shear tests run at constant volume as described in Section 5.5. The normal force on the soil was varied during shear to maintain a constant height and therefore a constant volume sample. The normal stress was calculated by using a corrected area throughout the test. Figures D.1 through D.7 are for a two inch (50.75 mm) high sample and Figures D.8 through D.15 are for a 1.3 inch (33.02 mm) high sample. The purpose for running tests with different thicknesses was to determine if the thickness had a direct influence on the required shear force at failure. The test results are summarized in Table D.1.

Figure No.	Initial Void Ratio	Initial Height (mm)	Initial Normal Stress (psi)	Peak Friction ϕ_{max}	Peak Friction Disp. (mm)	Peak Normal Stress ϕ	Peak Normal Stress Disp. (mm)	Maximum Normal Stress (psi)
D.1	0.61	50.75	2.42	43.2	1.2	34.6	4.5	15.3
D.2	0.57	"	"	46.2	0.9	36.5	4.5	29.8
D.3	0.55	"	"	44.0	0.6	37.5	6.5	71.0
D.4	0.54	"	"	44.6	0.9	38.1	4.2	36.4
D.5	0.53	"	"	42.8	0.5	38.9	4.8	58.8
D.6	0.52	"	"	44.9	0.7	38.7	5.5	91.8
D.7	0.49	"	"	42.1	6.0	37.6	8.0	172.1
D.8	0.61	33.02	"	41.9	1.6	36.2	5.5	32.8
D.9	0.60	"	"	48.2	0.6	36.6	6.0	73.3
D.10	0.55	"	"	43.8	0.9	36.4	6.0	62.8
D.11	0.52	"	"	46.7	0.7	37.6	6.0	46.5
D.12	0.61	"	10.34	40.2	1.5	36.0	4.5	24.5
D.13	0.56	"	"	41.5	1.3	36.1	6.5	50.2
D.14	0.53	"	"	42.5	2.5	38.2	6.5	87.1
D.15	0.52	"	15.61	42.8	3.0	36.4	7.0	91.1

Table D.1 Summary of Constant Volume Direct Shear Tests on Filter Sand.

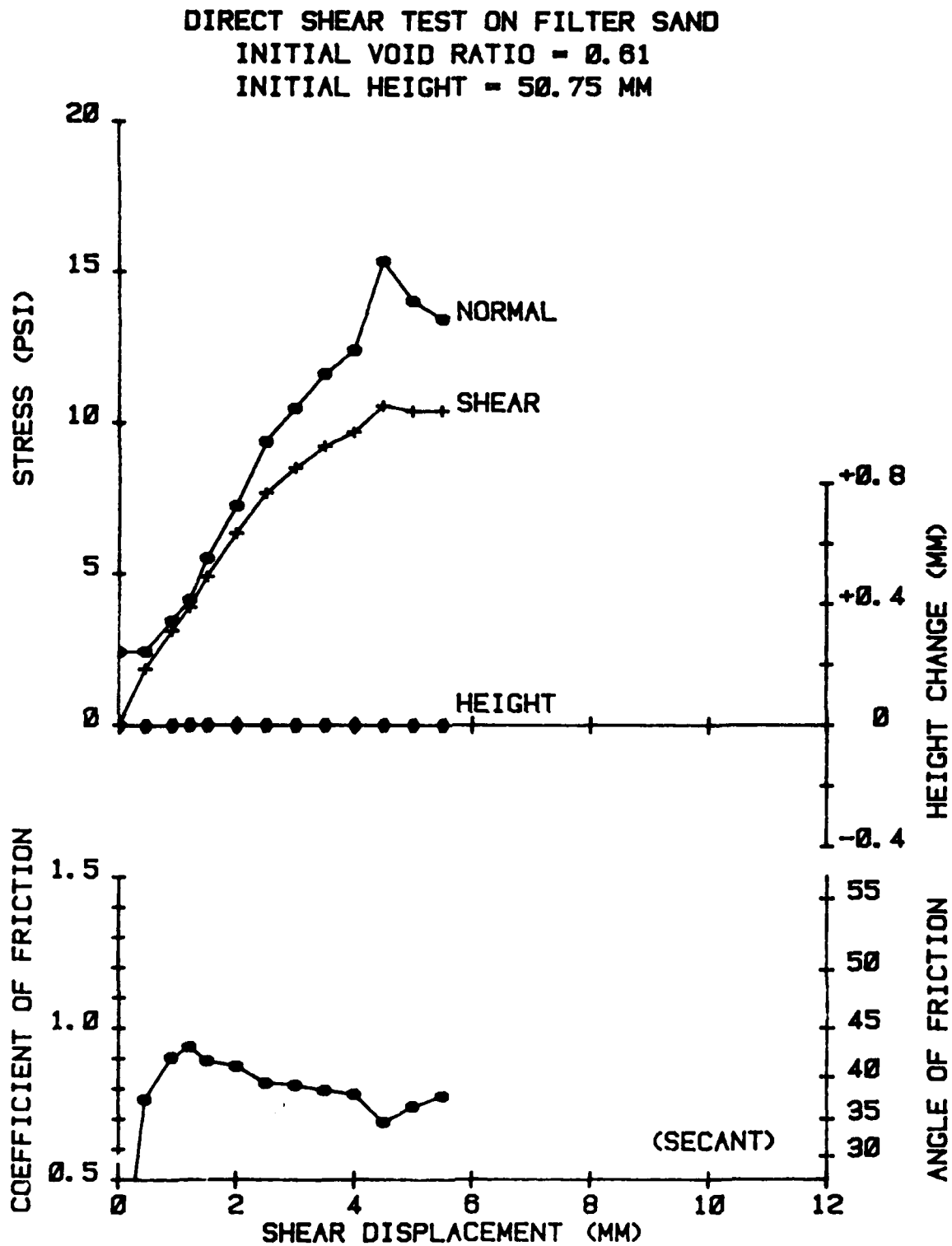

Figure D.1 Constant Volume Direct Shear Test.

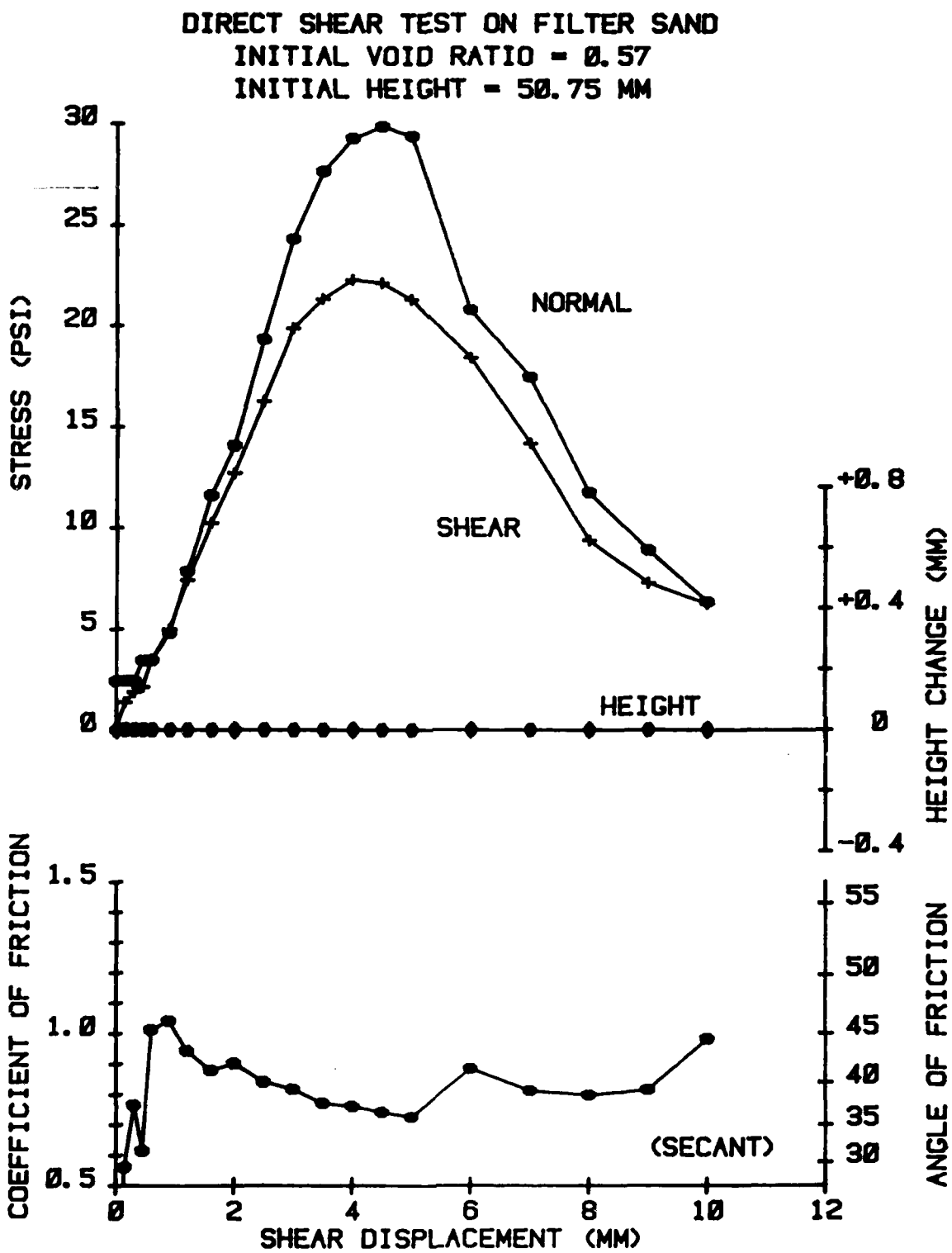

Figure D.2 Constant Volume Direct Shear Test.

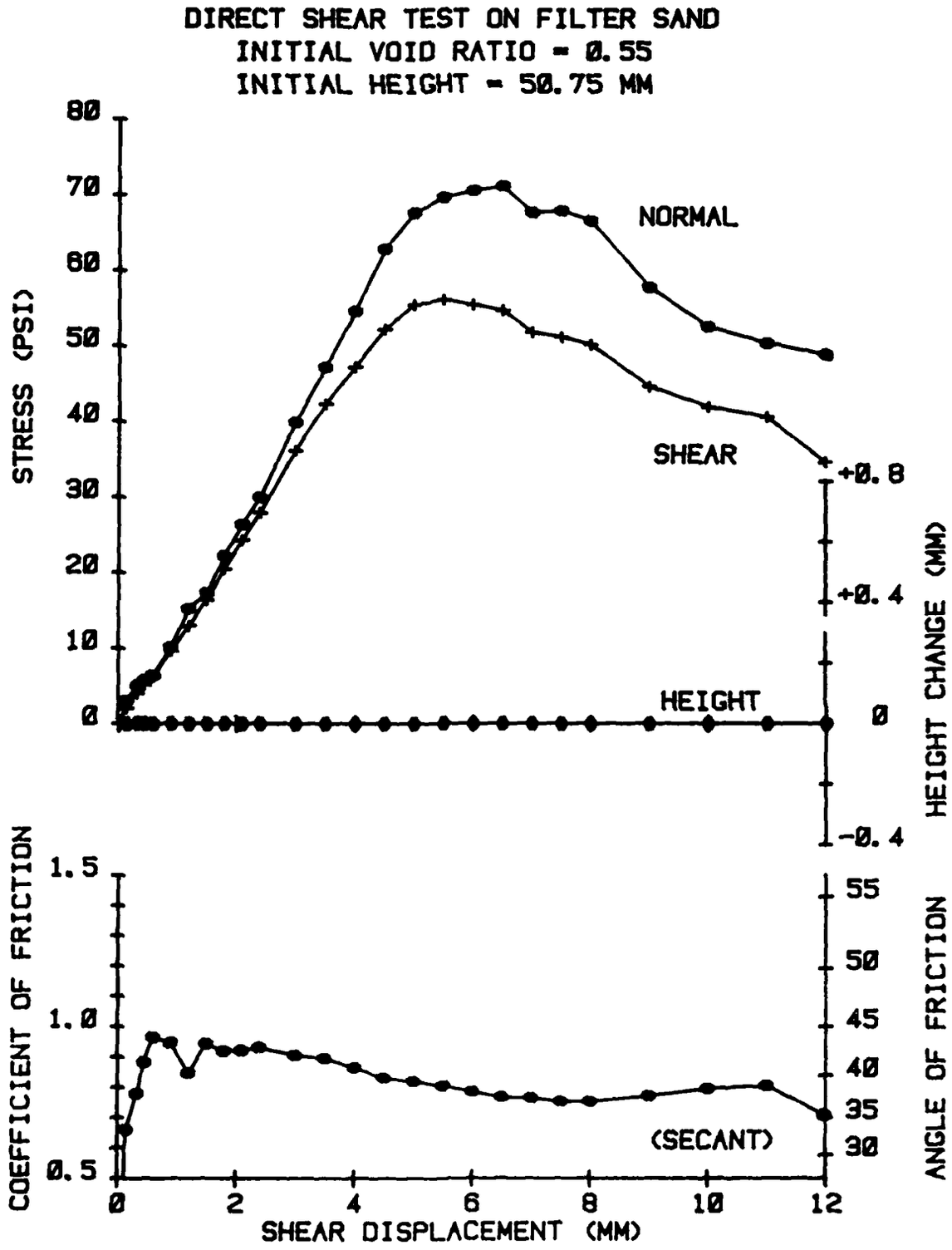

Figure D.3 Constant Volume Direct Shear Test.

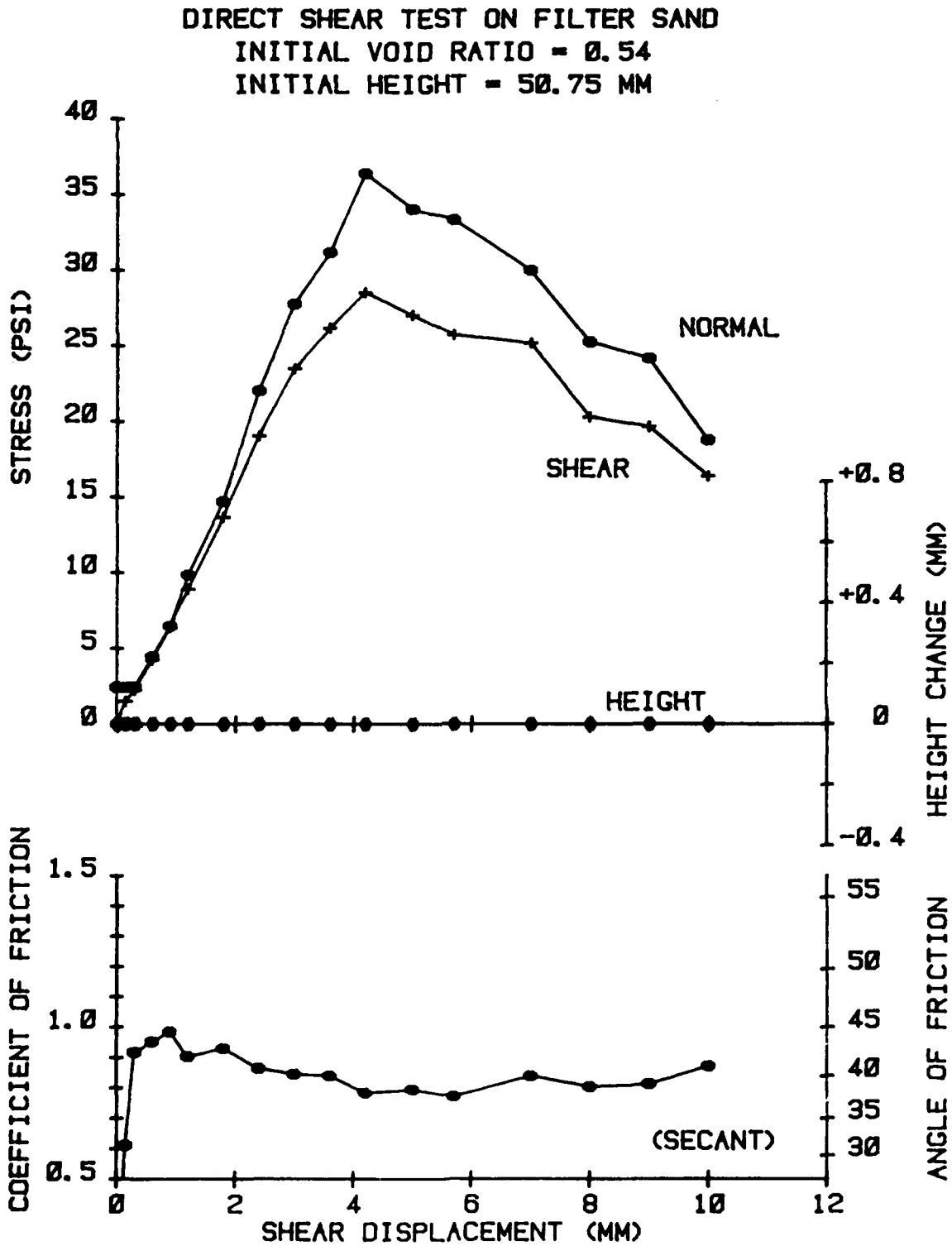

Figure D.4 Constant Volume Direct Shear Test.

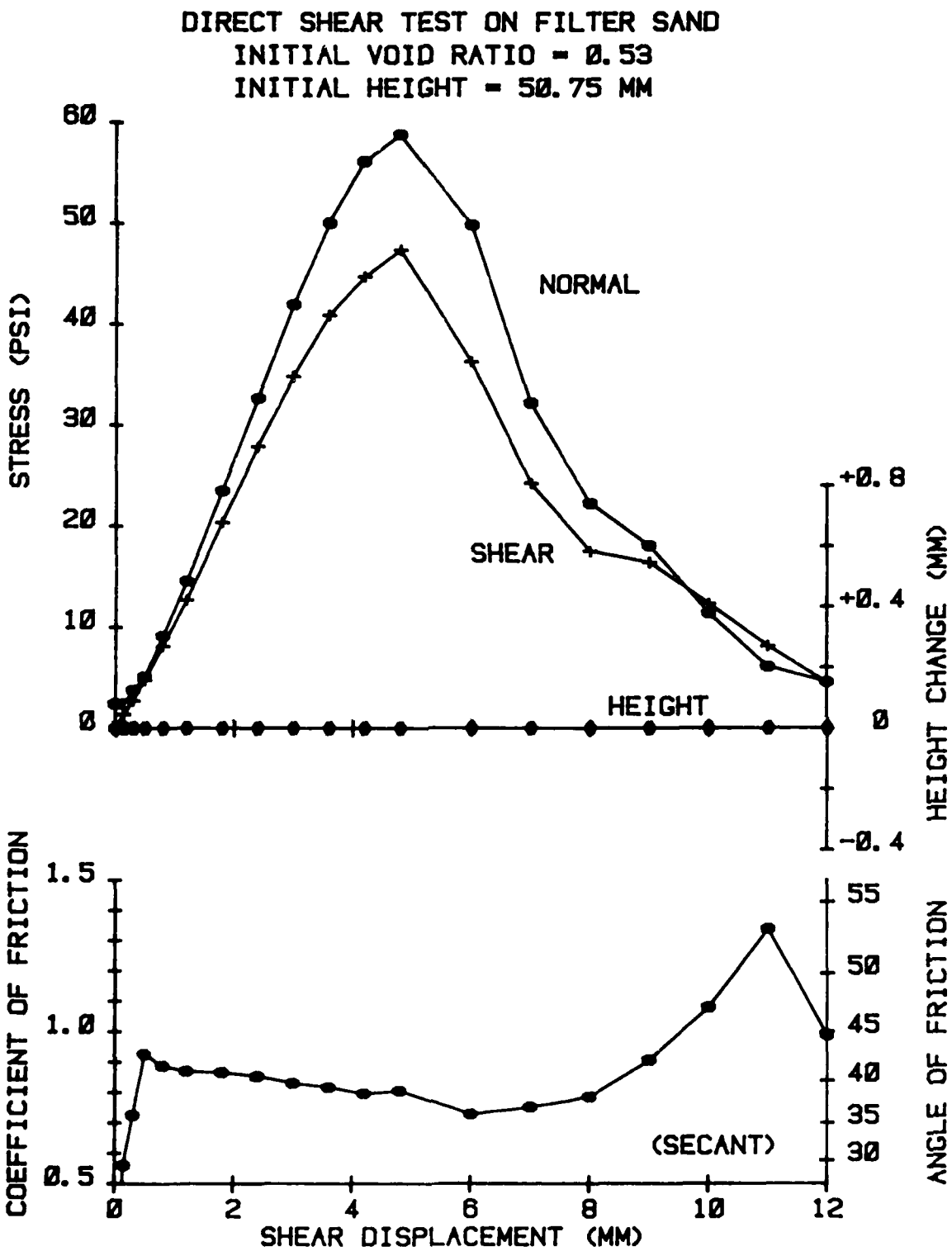

Figure D.5 Constant Volume Direct Shear Test.

AD-A126 948 LABORATORY DETERMINATION OF HORIZONTAL STRESS IN COHESIONLESS SOIL(U) AIR FORCE INST OF TECH WRIGHT-PATTERSON AFB OH S C BOYCE 1983 4/4

UNCLASSIFIED AFIT/CI/NR-83-4T F/G 8/13 NL

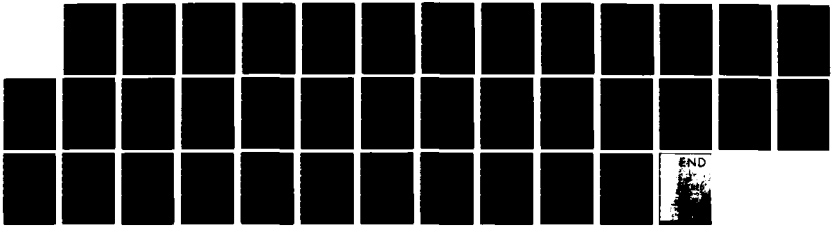

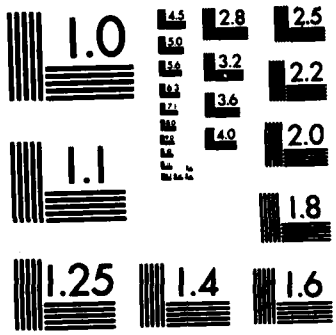

MICROCOPY RESOLUTION TEST CHART
NATIONAL BUREAU OF STANDARDS-1963-A

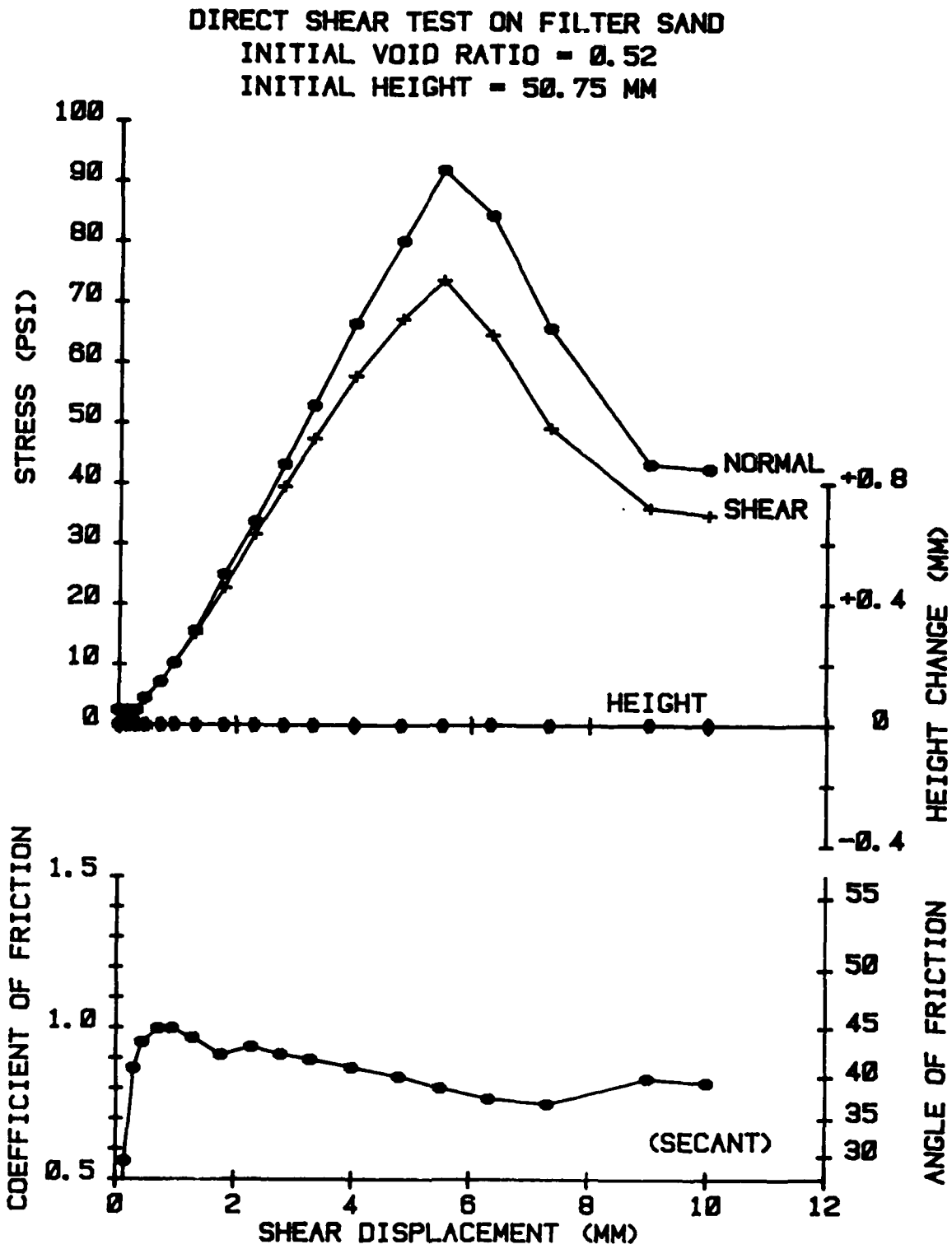

Figure D.6 Constant Volume Direct Shear Test.

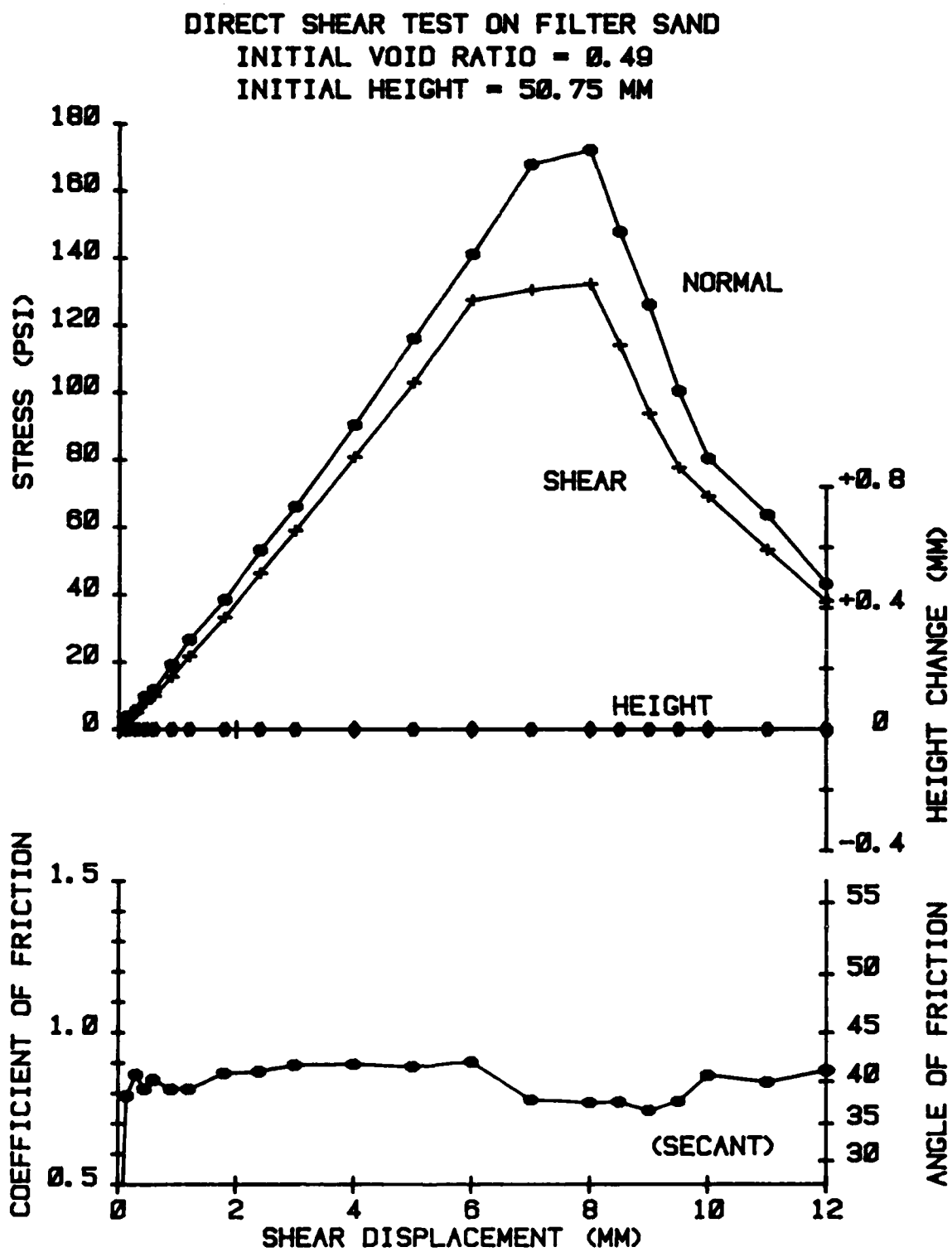

Figure D.7 Constant Volume Direct Shear Test.

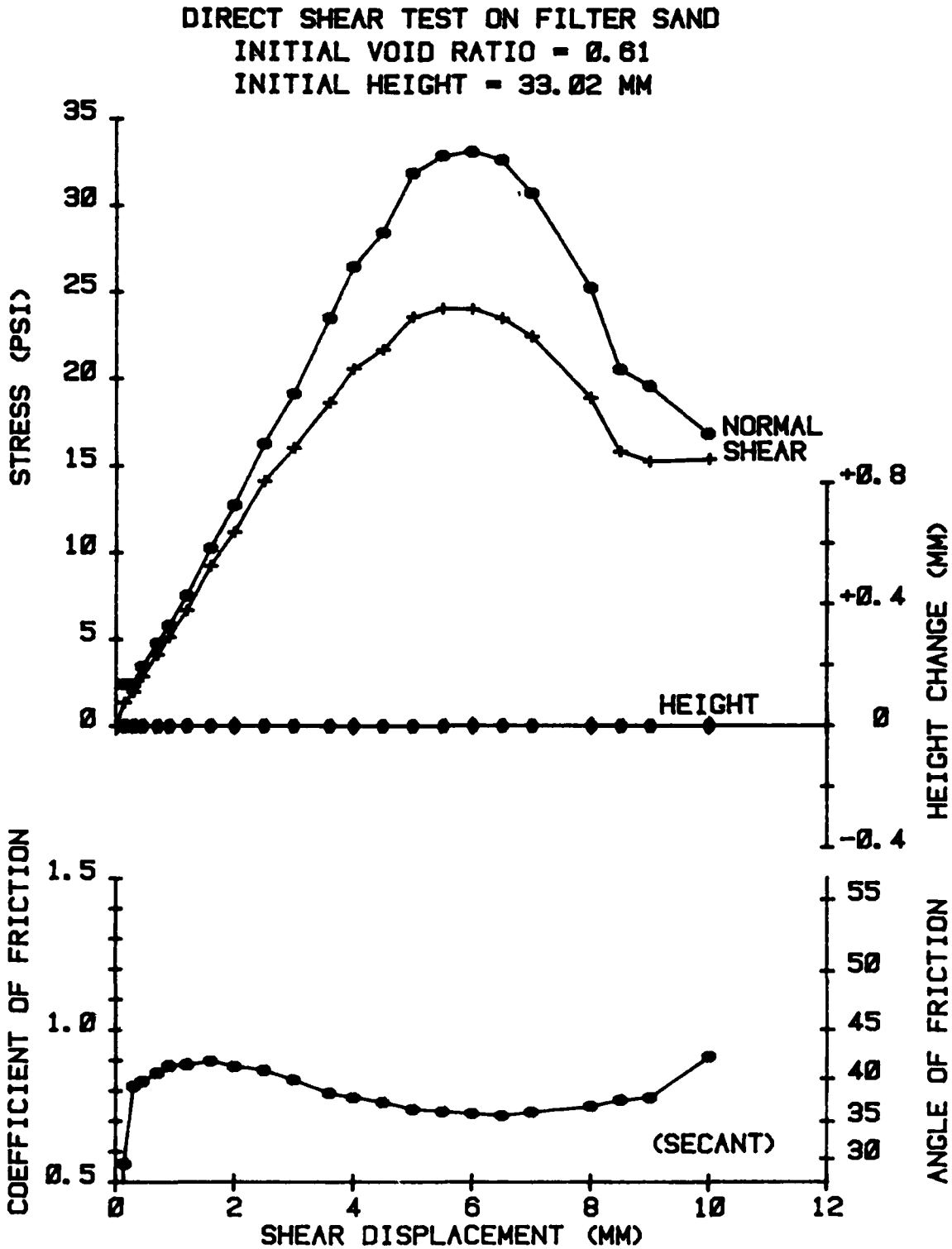

Figure D.8 Constant Volume Direct Shear Test.

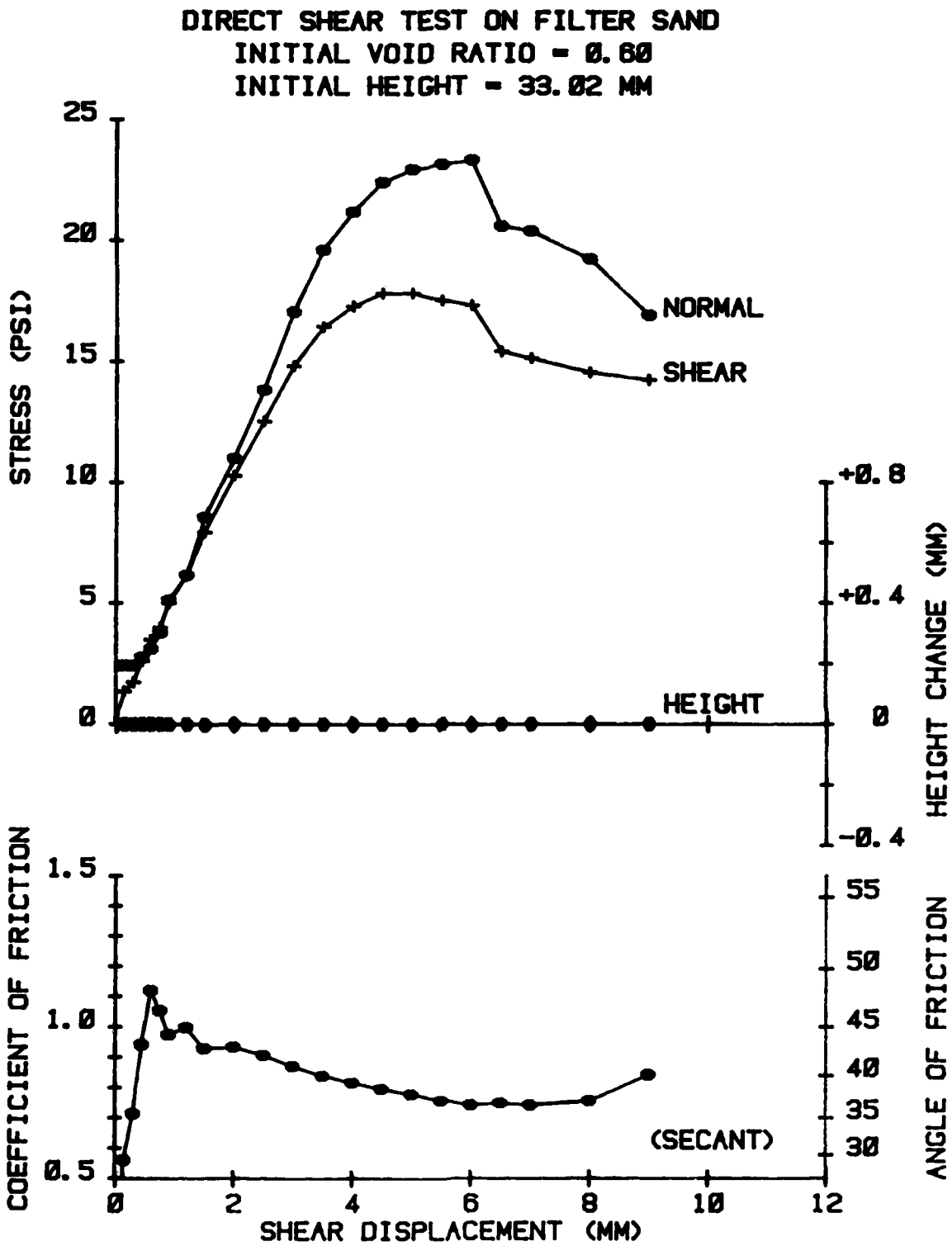

Figure D.9 Constant Volume Direct Shear Test.

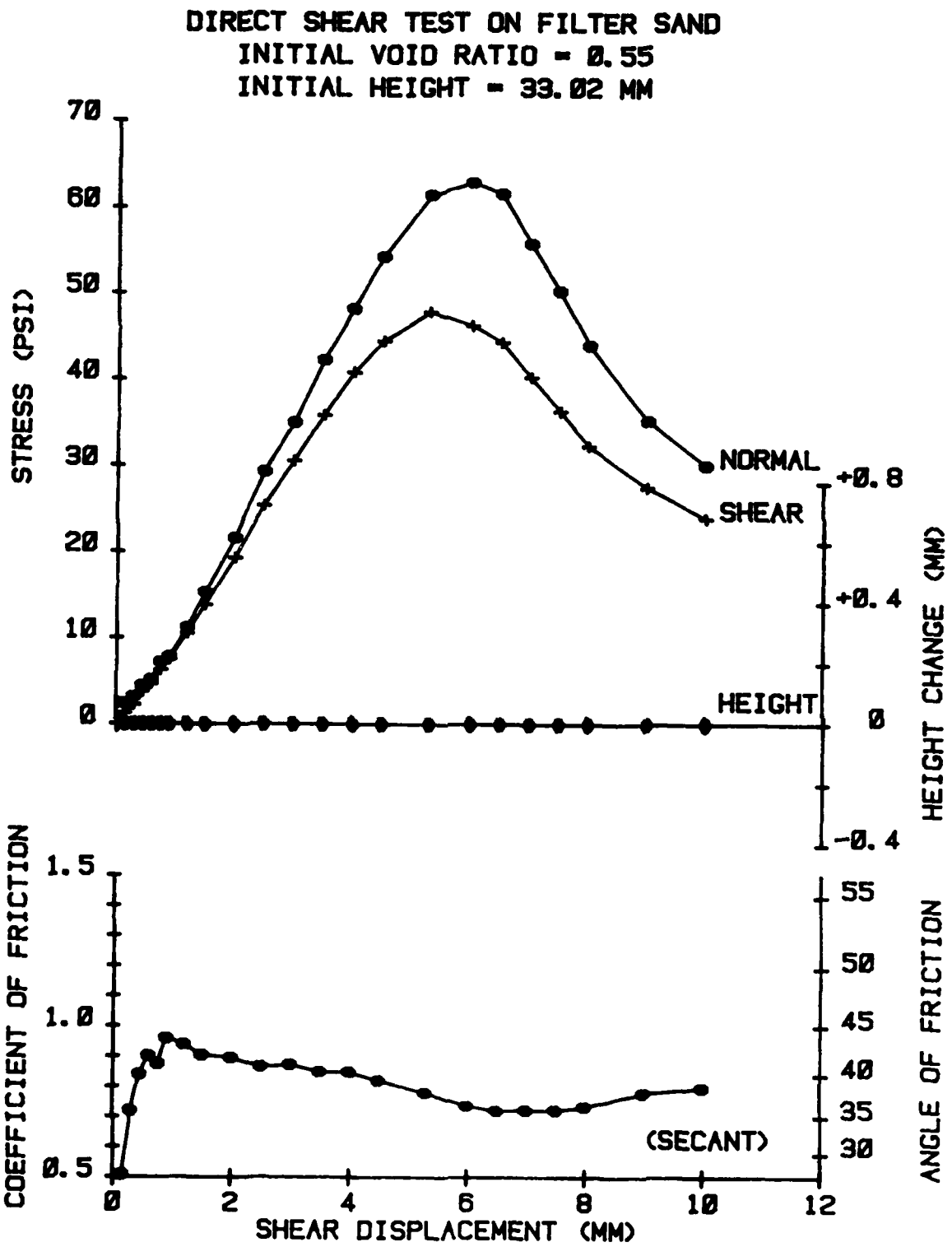

Figure D.10 Constant Volume Direct Shear Test.

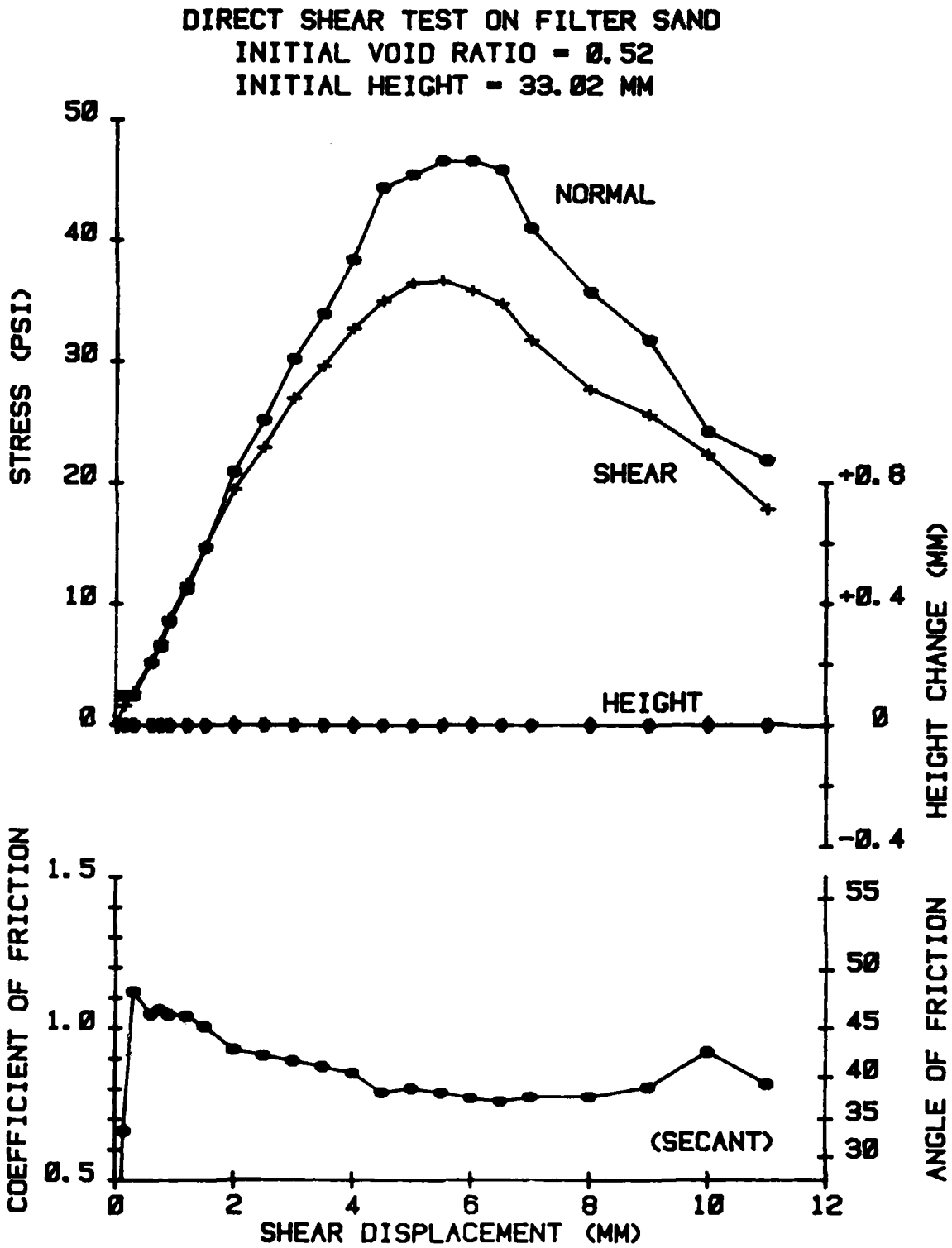

Figure D.11 Constant Volume Direct Shear Test.

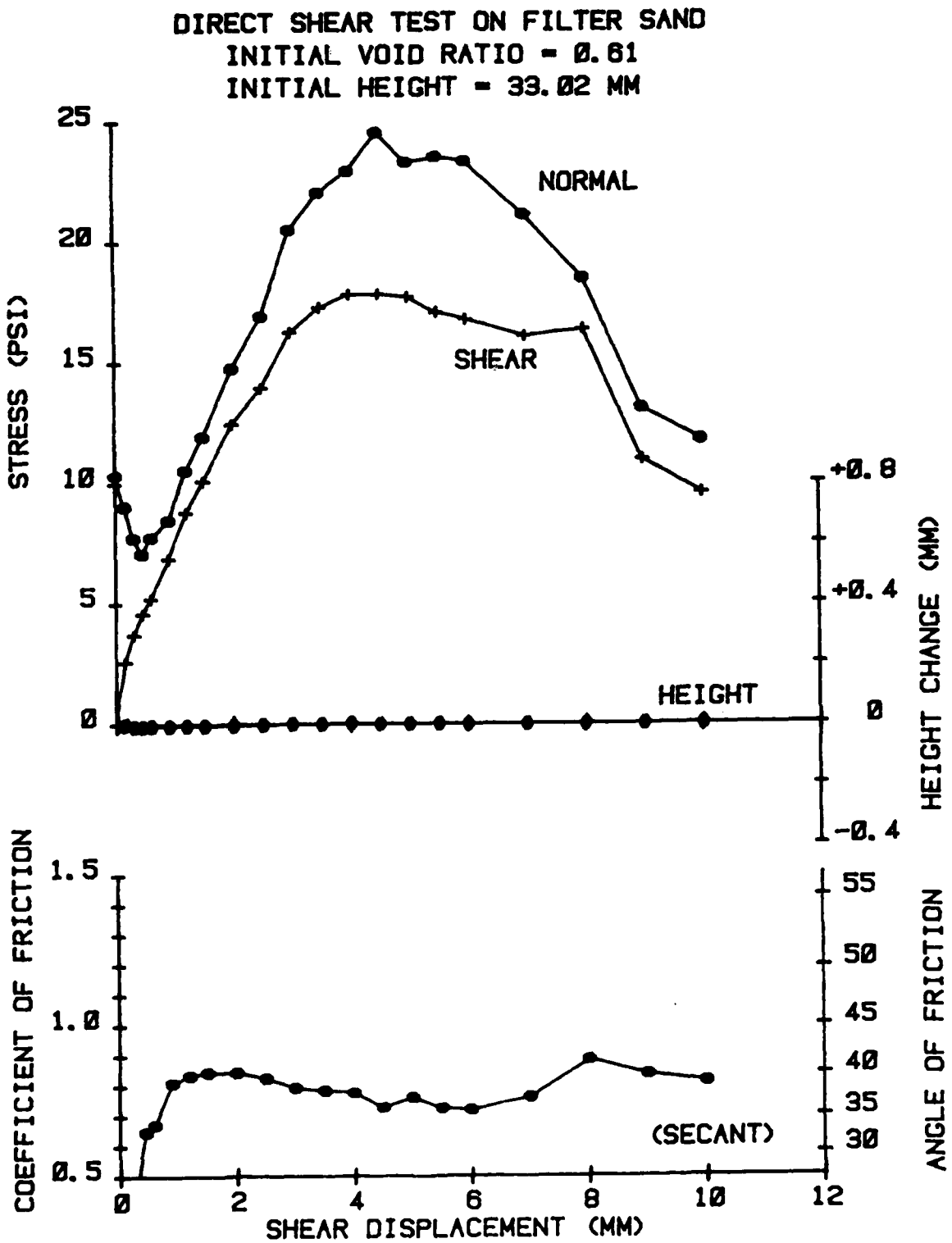

Figure D.12 Constant Volume Direct Shear Test.

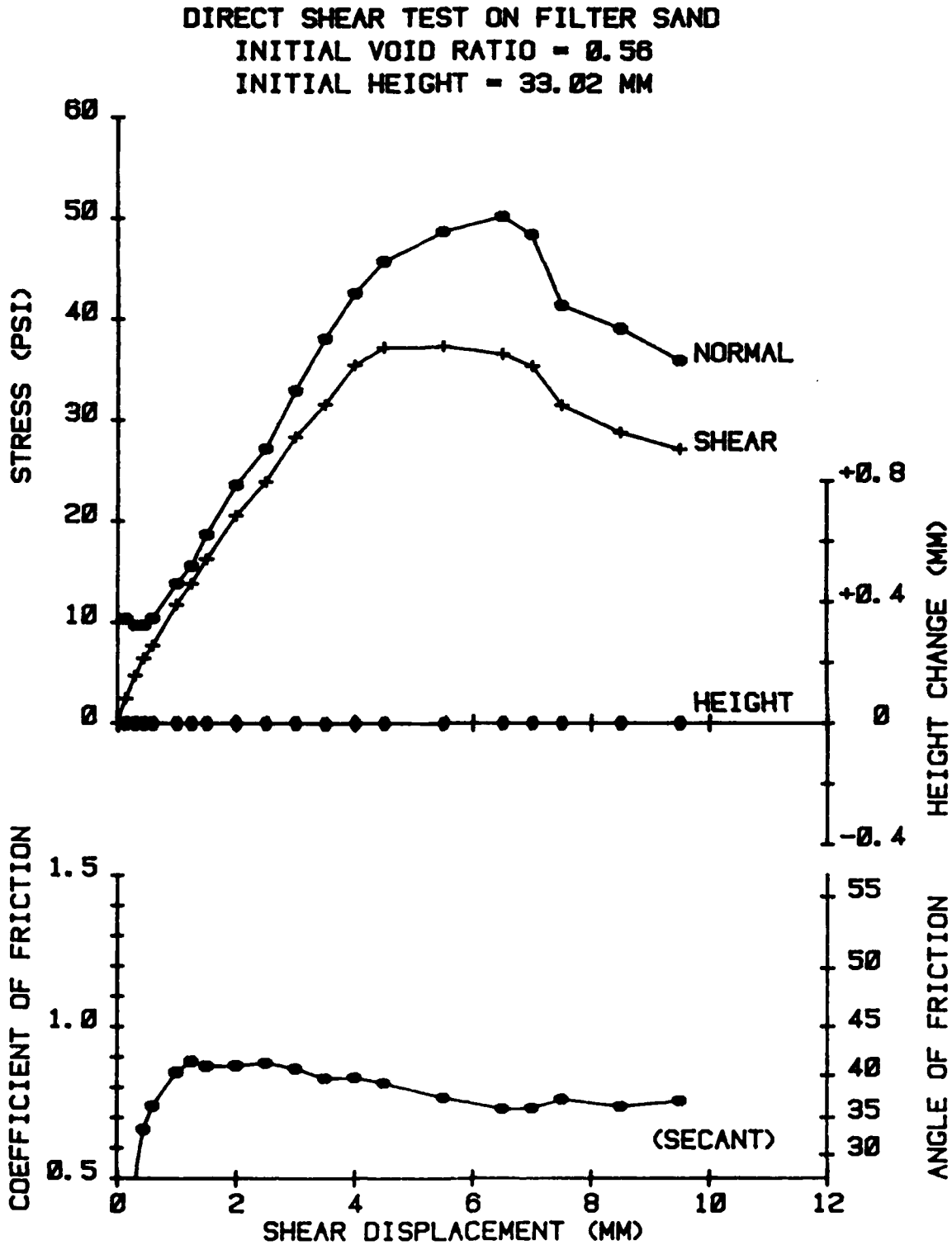

Figure D.13 Constant Volume Direct Shear Test.

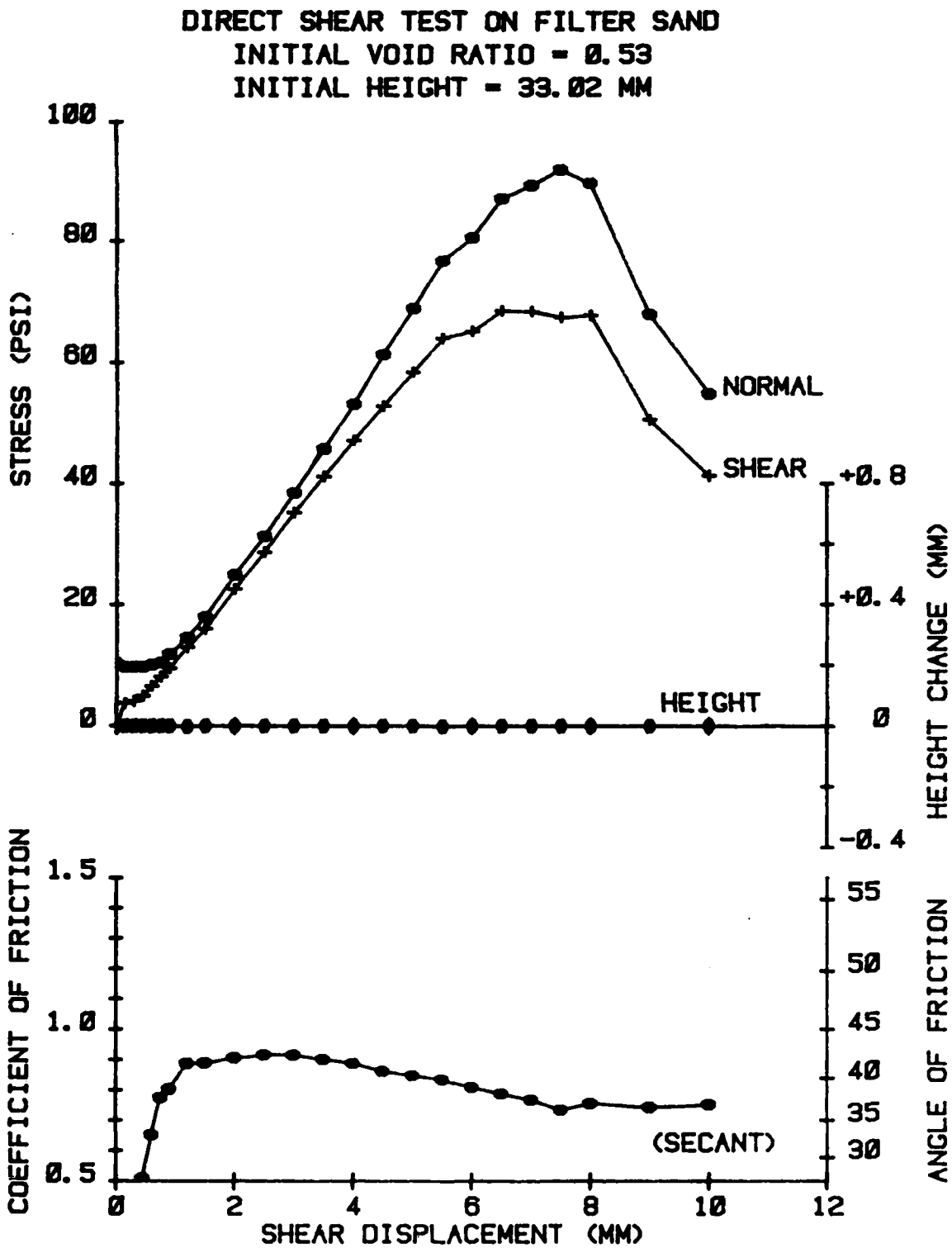

Figure D.14 Constant Volume Direct Shear Test.

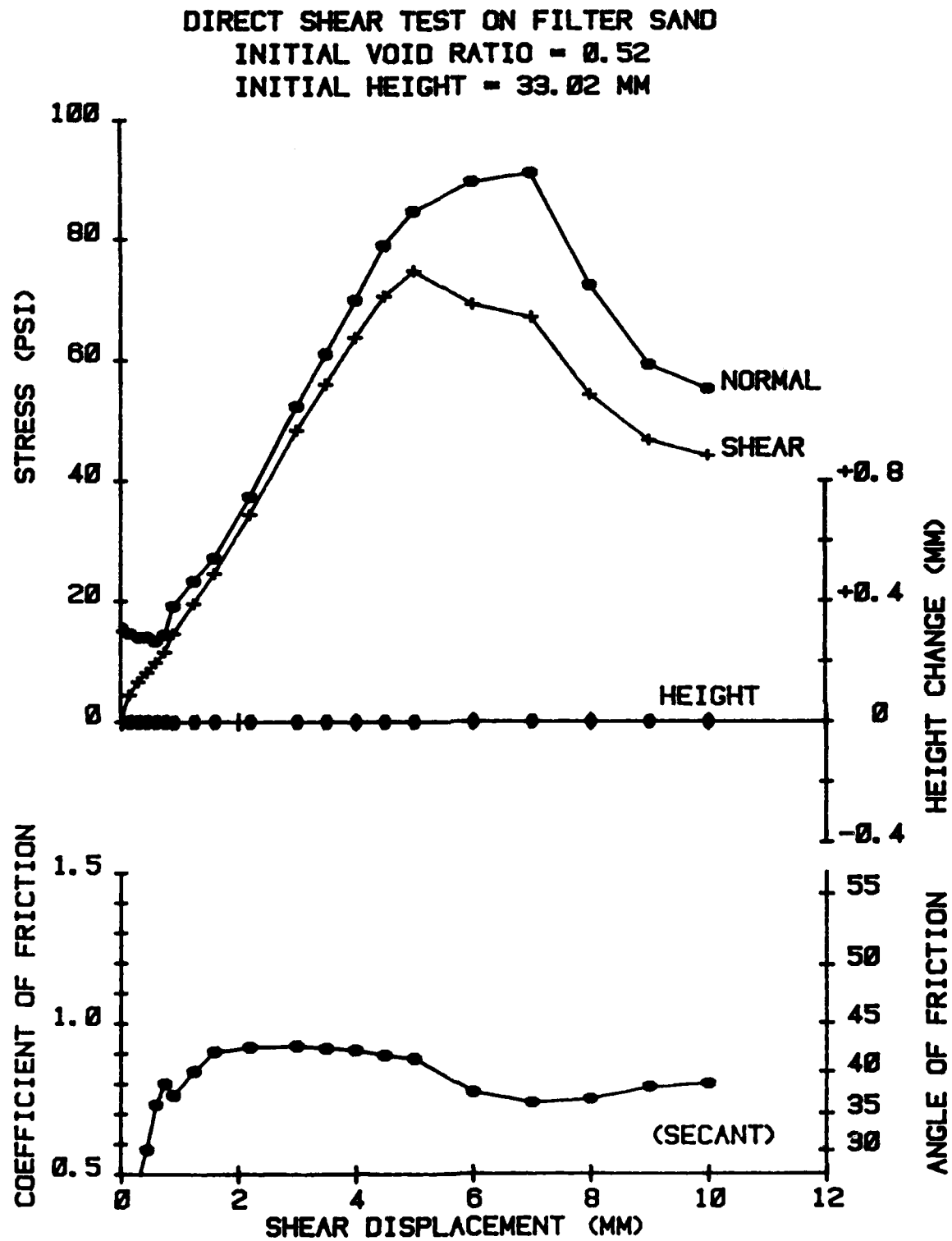

Figure D.15 Constant Volume Direct Shear Test.

APPENDIX E

INTERPRETATION OF PULLOUT TESTS

Figures E.1 through E.20 show the response of the Cornell Stress Cells during the drilled shaft pullout tests in dense filter sand as performed by Stewart and Kulhawy (1981). The sign of the output change during the loading phase of each test has been reversed to show the actual stress cell response. The change in response during pullout of the shaft in the loose and medium dense tests is so small as to be neglected. Only the dense tests described in Table E.1 which were instrumented and recorded are included. Each figure is broken into three phases: Fill, Construction and Loading. The Fill phase is the placement and compaction of the filter sand in six inch lifts. The Construction phase is the casing load test, concreting, removal of the casing and concrete curing. No scale for the Construction phase was given. The Loading phase is the pullout of the shaft in equal increments between loads as recorded in Table J.8 through Table J.10 of Stewart and Kulhawy (1981). In test number 12, Figures E.15 to E.20, no shaft pullout was performed but the casing results are included.

Test No.	Figure No.	Shaft Size d (in)	Shaft Size L (ft)	Initial Void Ratio
9	E.1-E.6	6	7.5	0.475
10	E.7-E.10	6	2.5	0.478
11	E.11-E.14	12	2.5	0.484
12	E.15-E.20	6	5.0	0.487

d = diameter
L = Length
1 in = 25.4 mm
1 ft = 304.8 mm

Table E.1 Description of Shaft Pullout Tests (Stewart and Kulhawy, 1981).

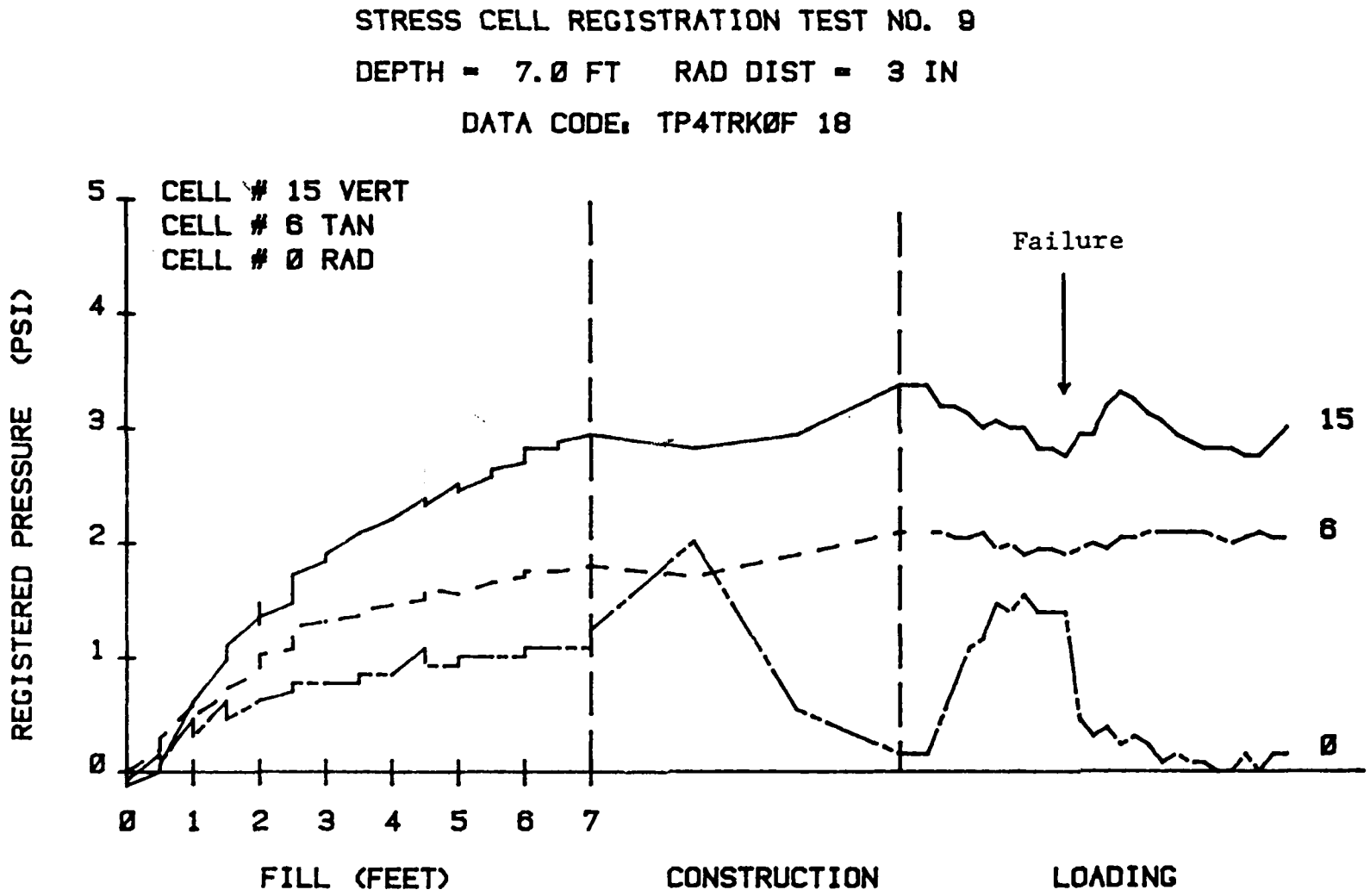

Figure E.1 Stress Cell Response During Pullout Test.

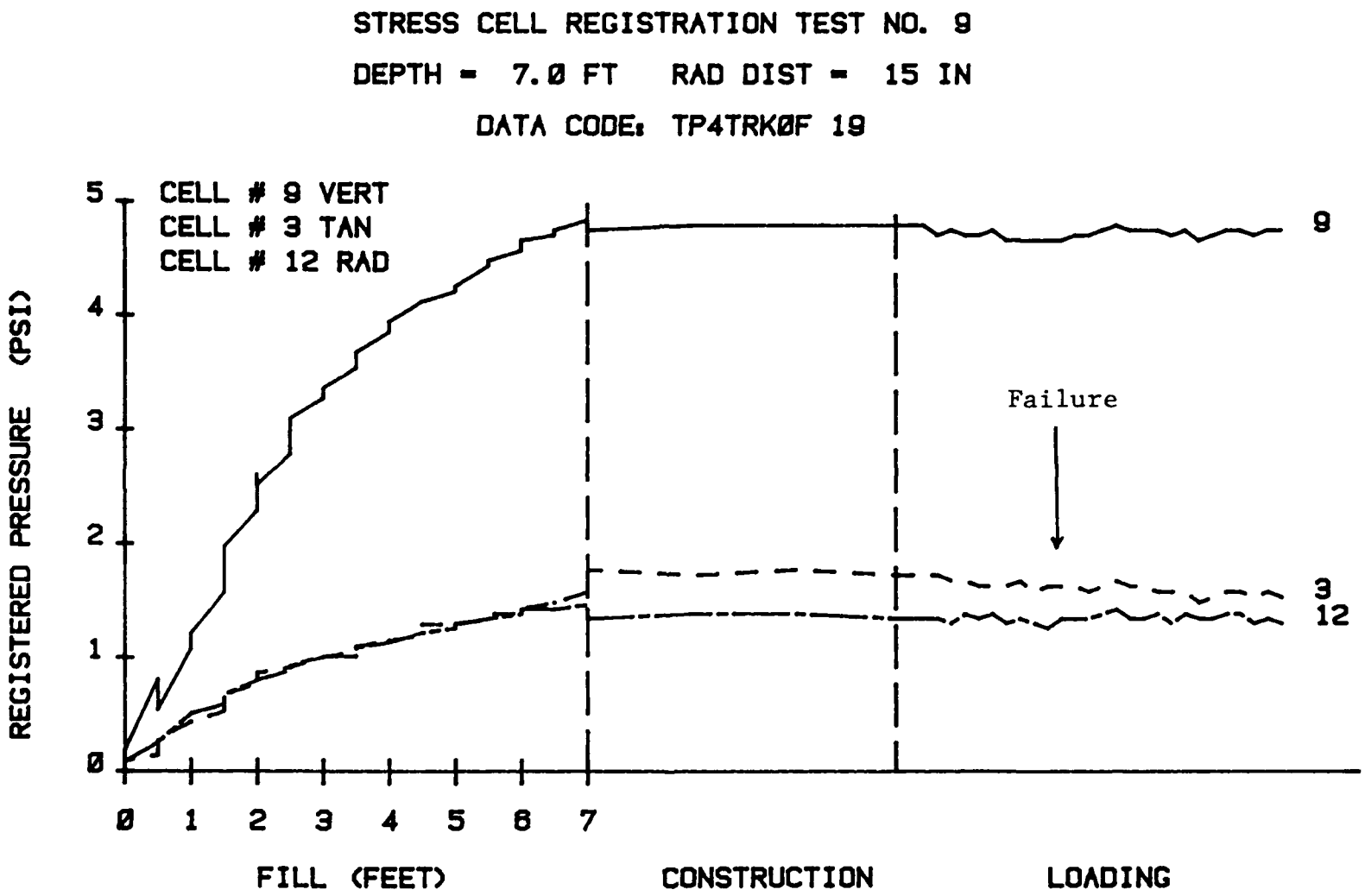

Figure E.2 Stress Cell Response During Pullout Test.

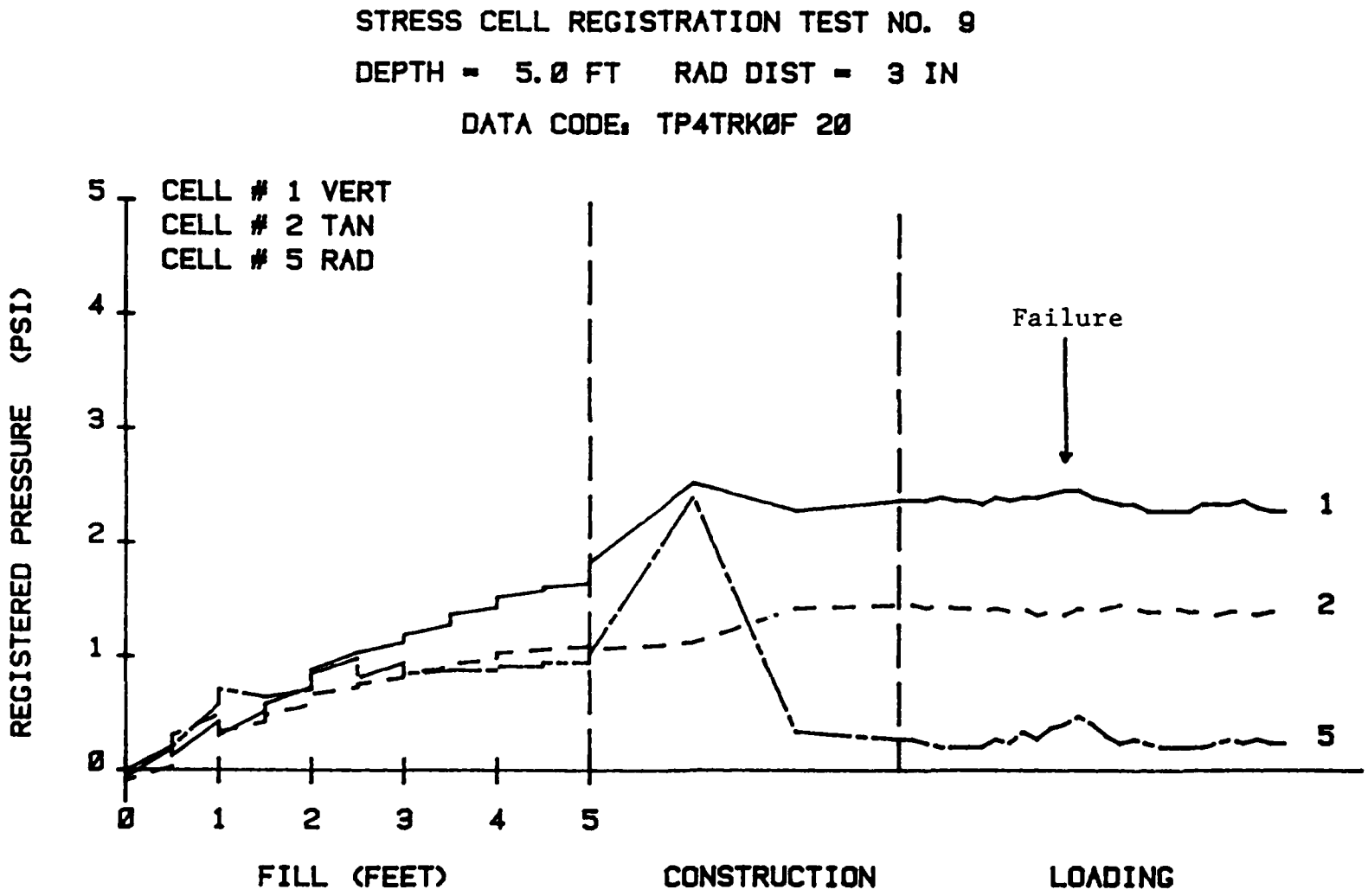

Figure E.3 Stress Cell Response During Pullout Test.

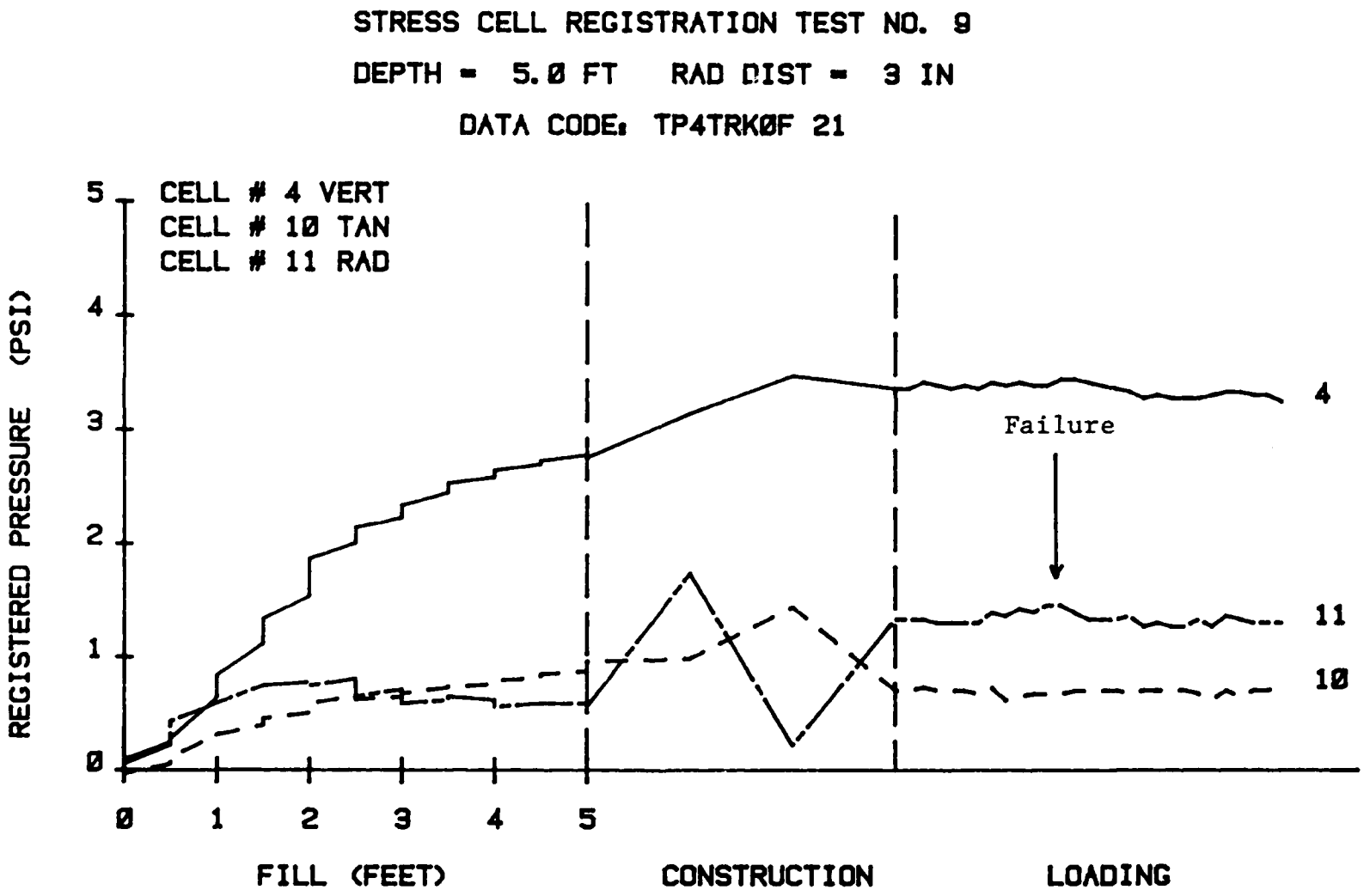

Figure E.4 Stress Cell Response During Pullout Test.

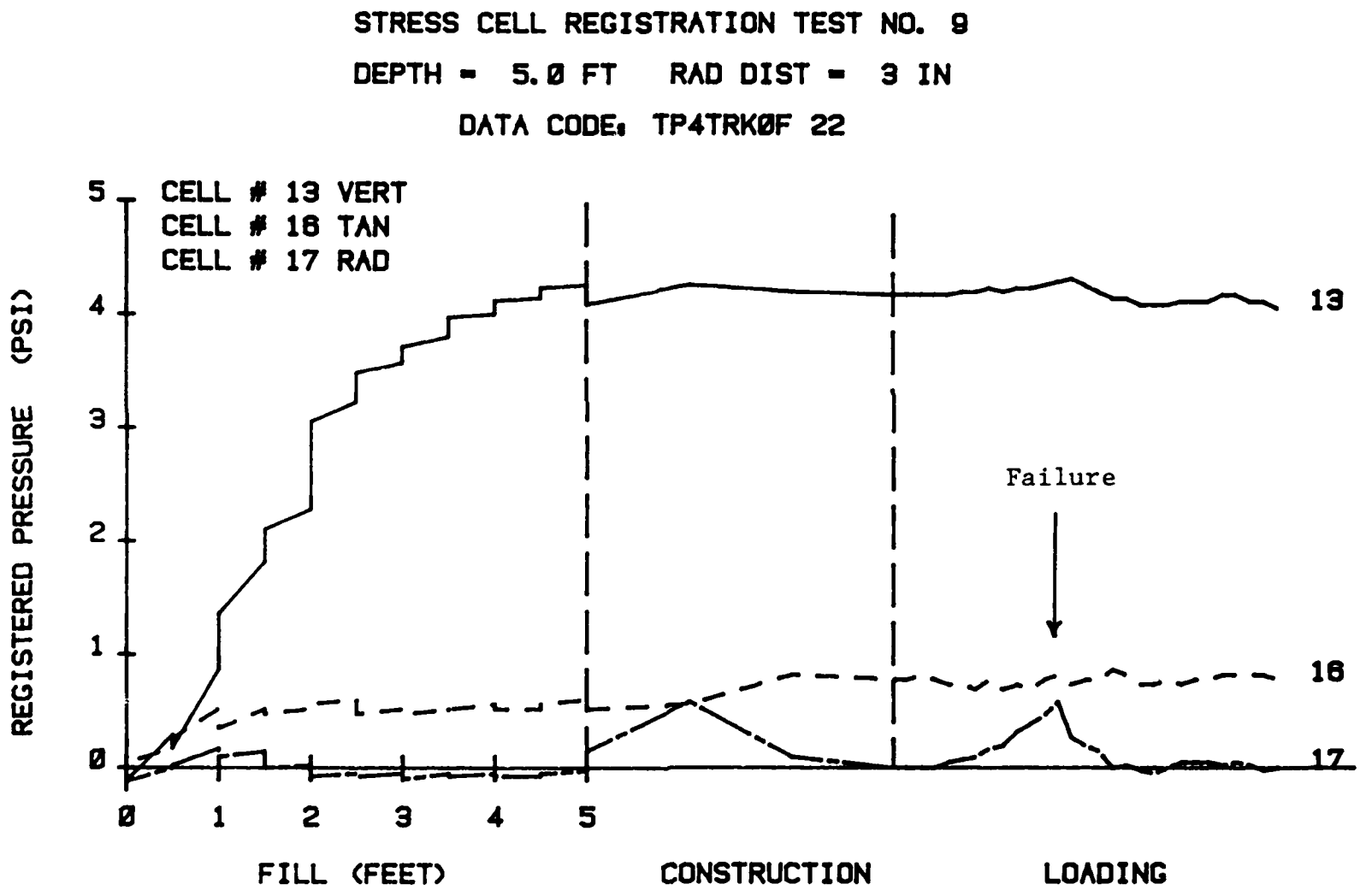

Figure E.5 Stress Cell Response During Pullout Test.

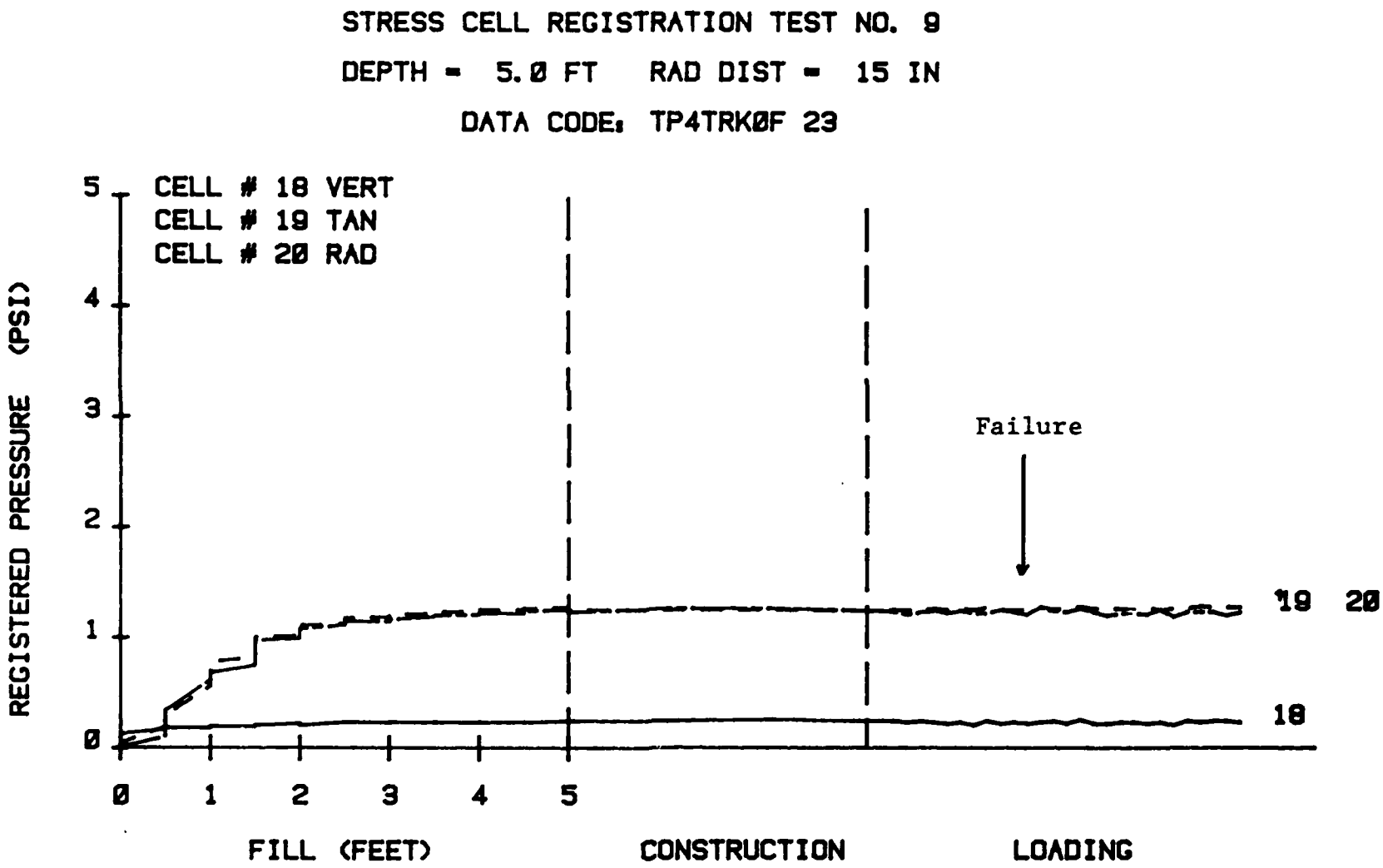

Figure E.6 Stress Cell Response During Pullout Test.

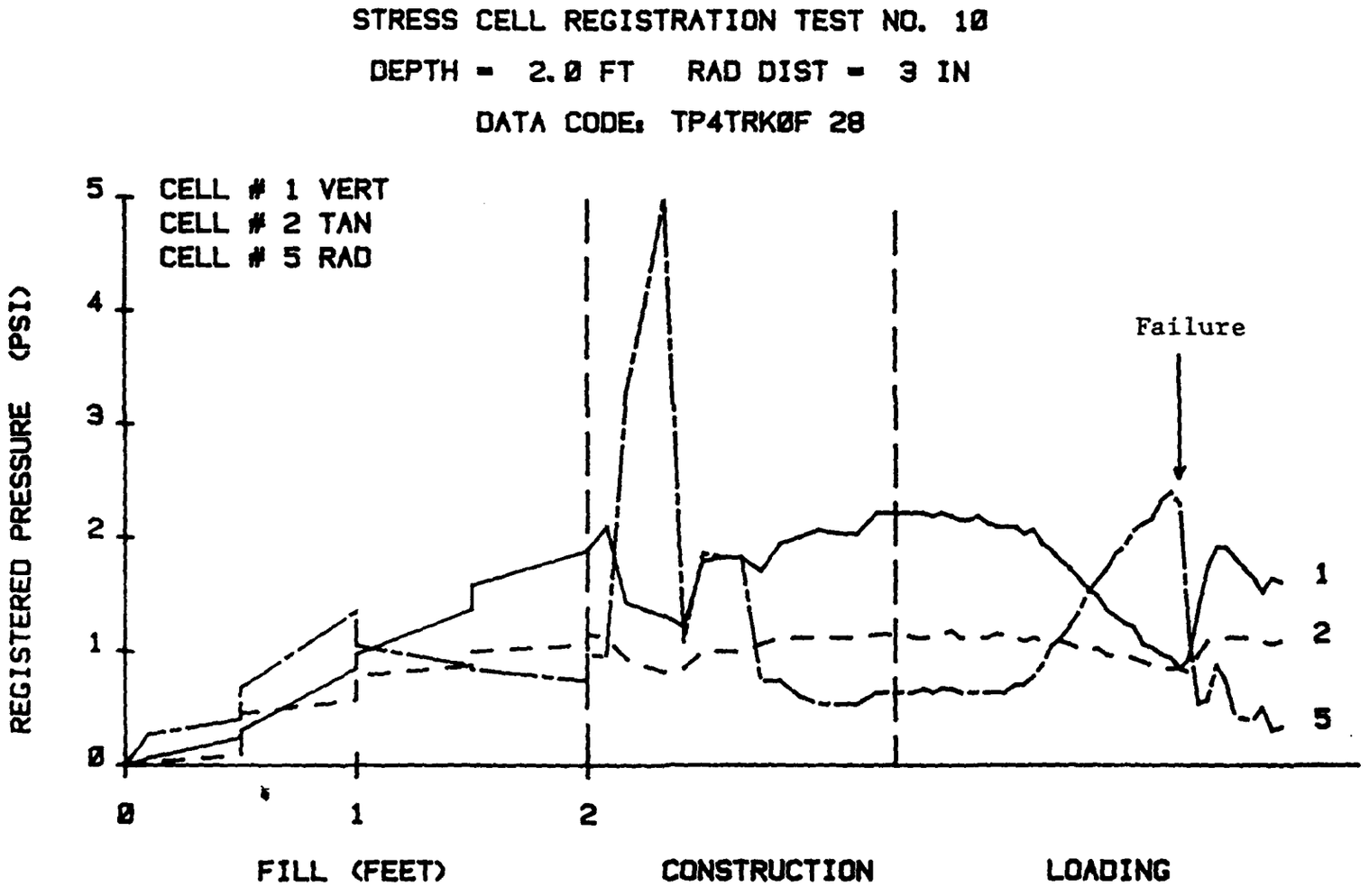

Figure E.7 Stress Cell Response During Pullout Test.

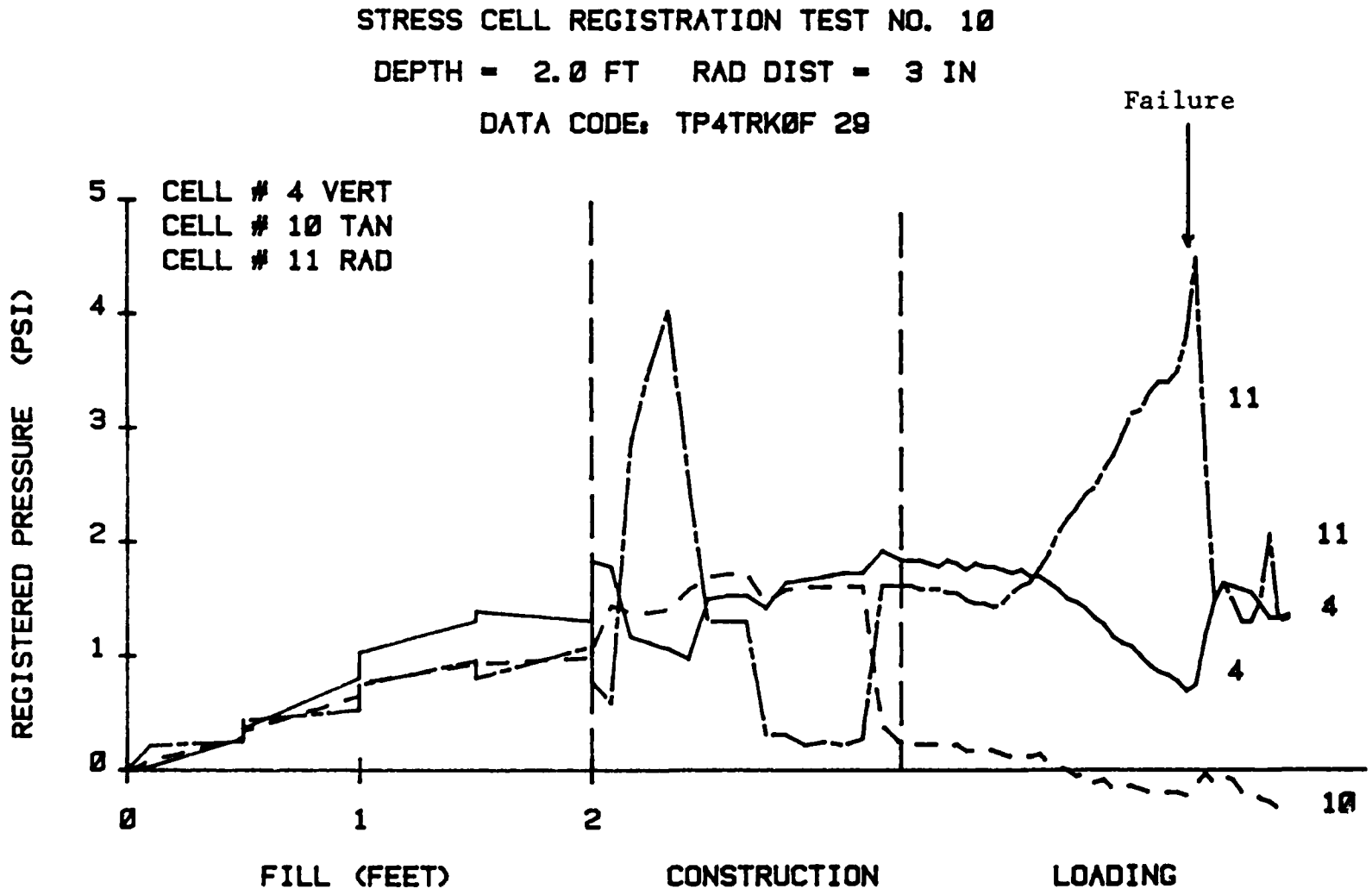

Figure E.8 Stress Cell Response During Pullout Test.

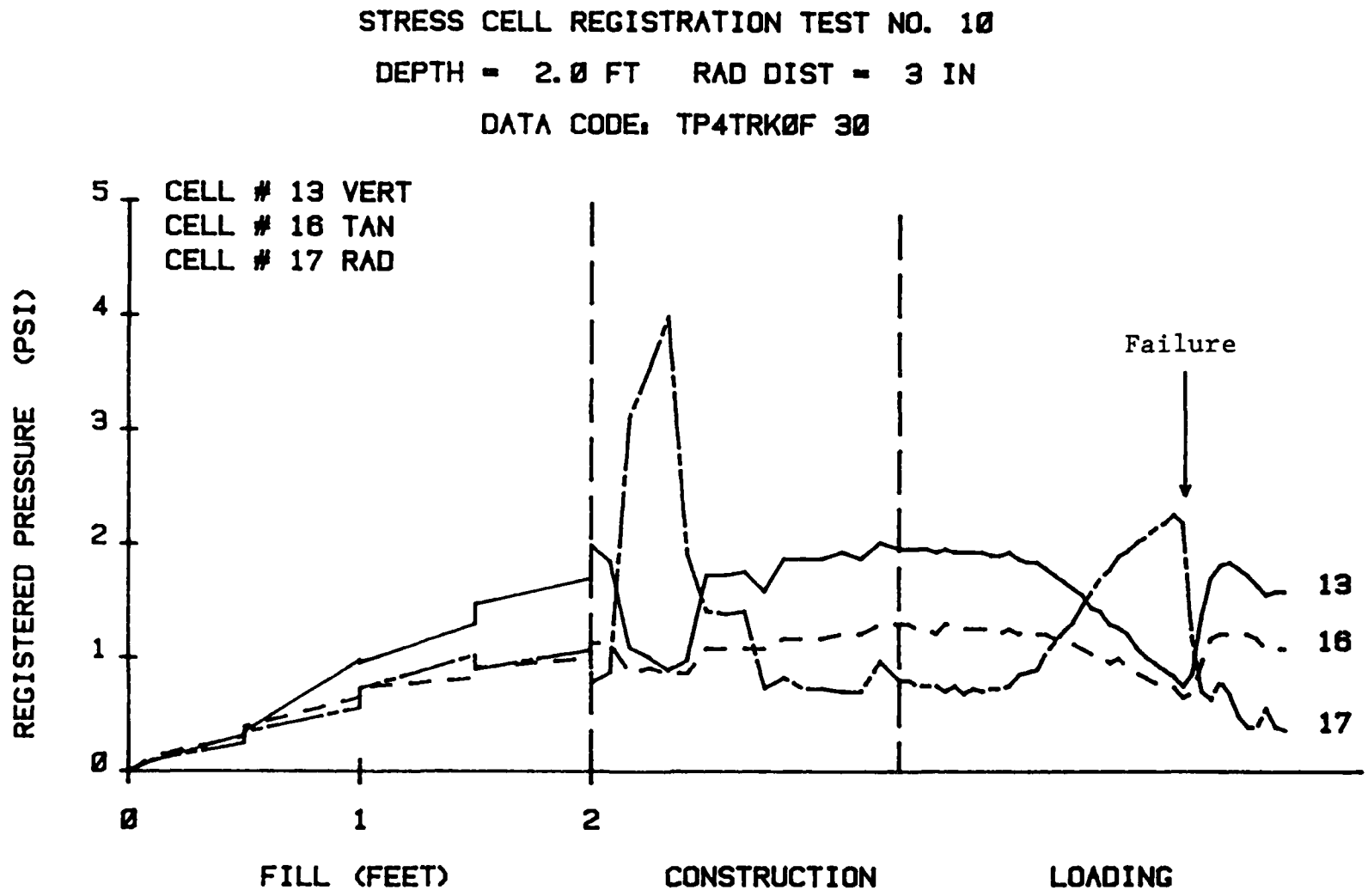

Figure E.9 Stress Cell Response During Pullout Test.

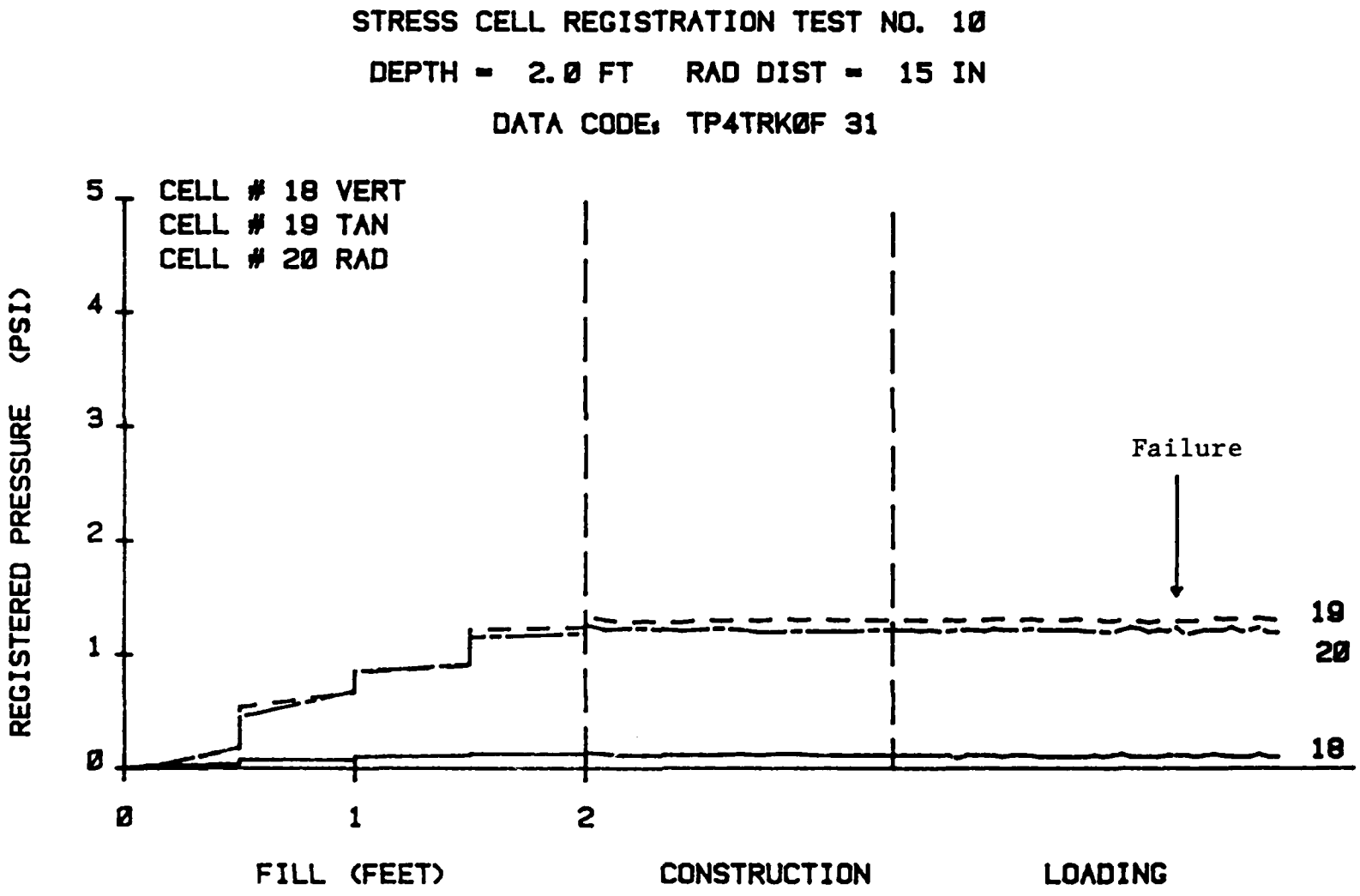

Figure E.10 Stress Cell Response During Pullout Test.

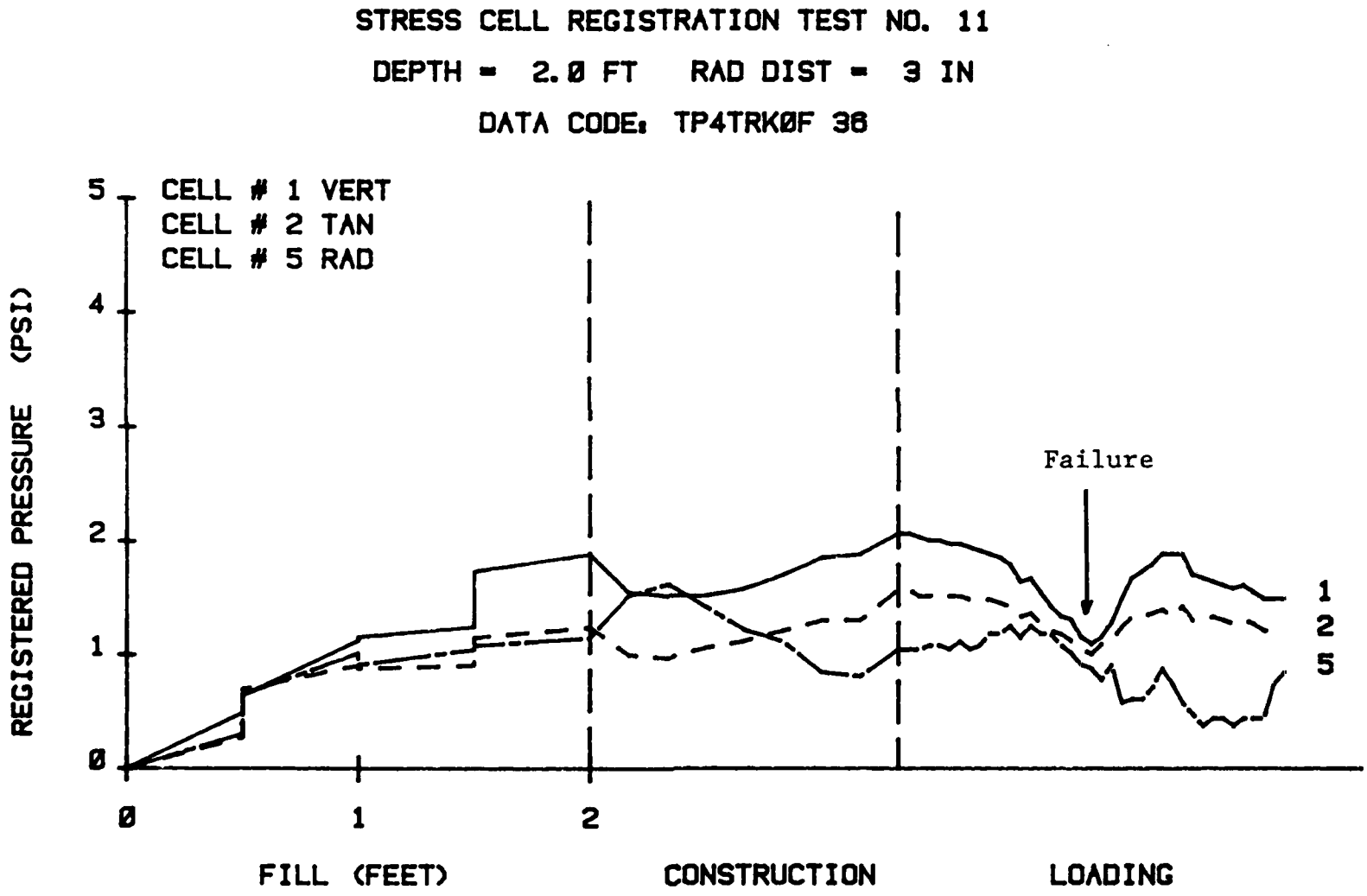

Figure E.11 Stress Cell Response During Pullout Test.

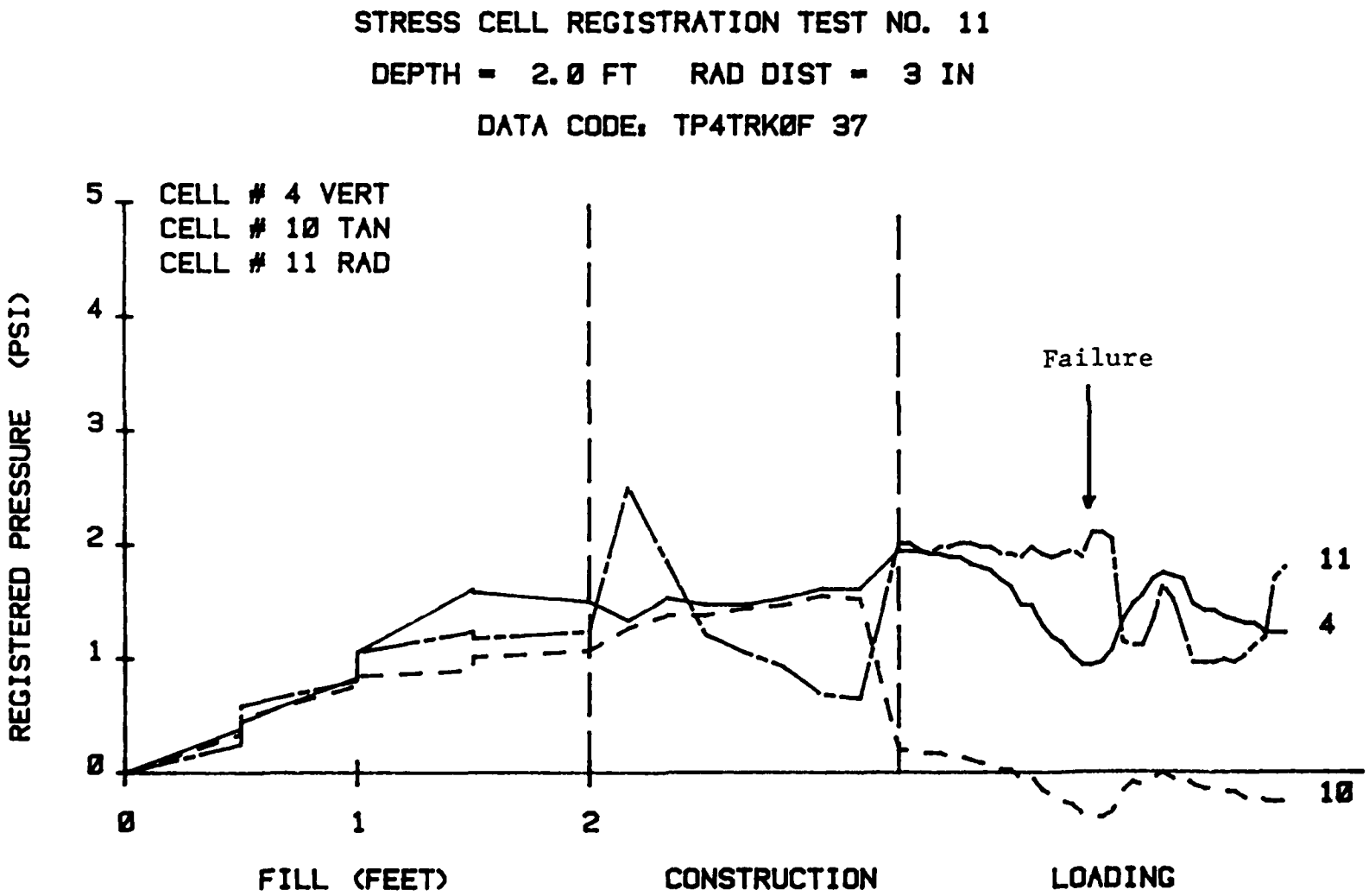

Figure E.12 Stress Cell Response During Pullout Test.

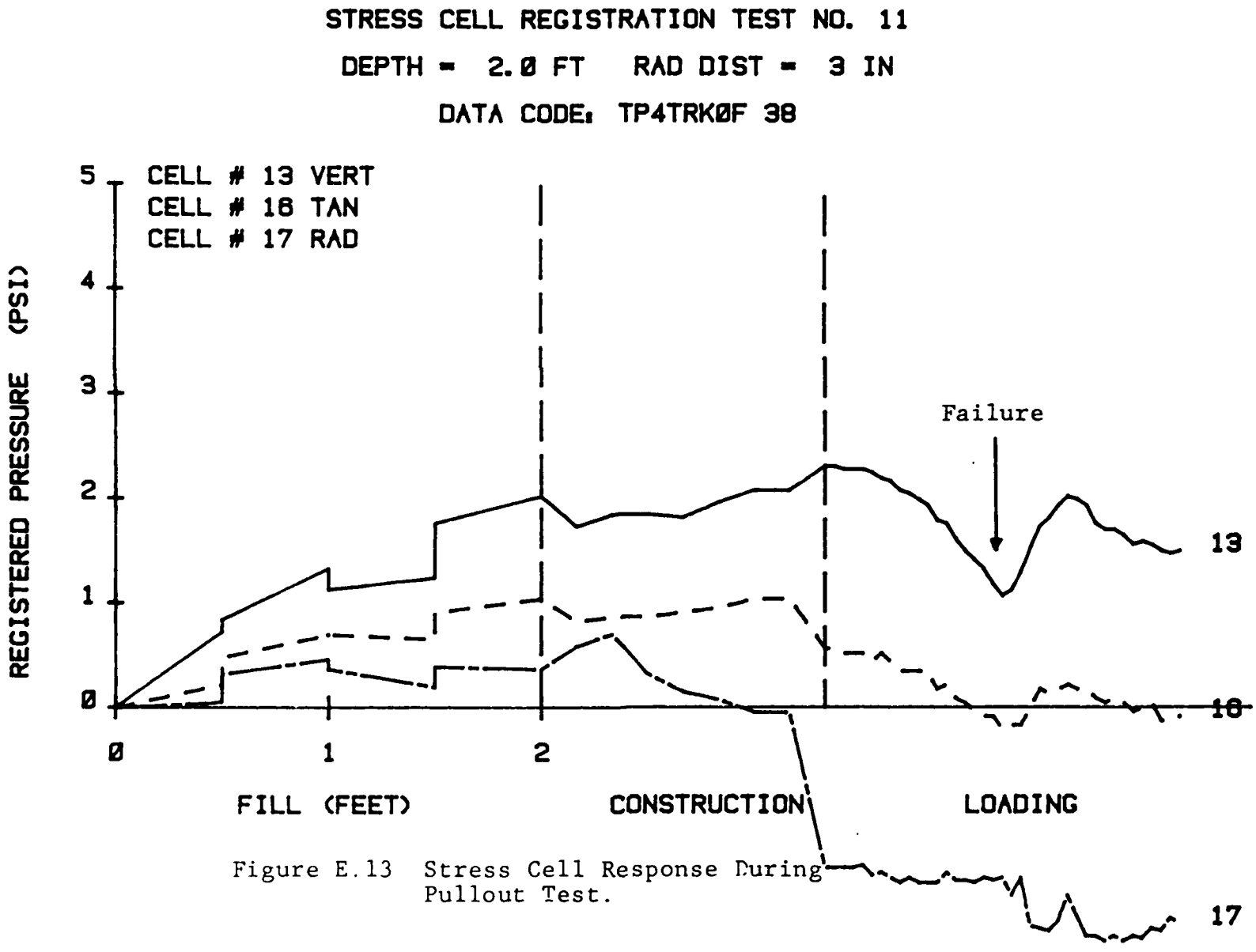

Figure E.13 Stress Cell Response During Pullout Test.

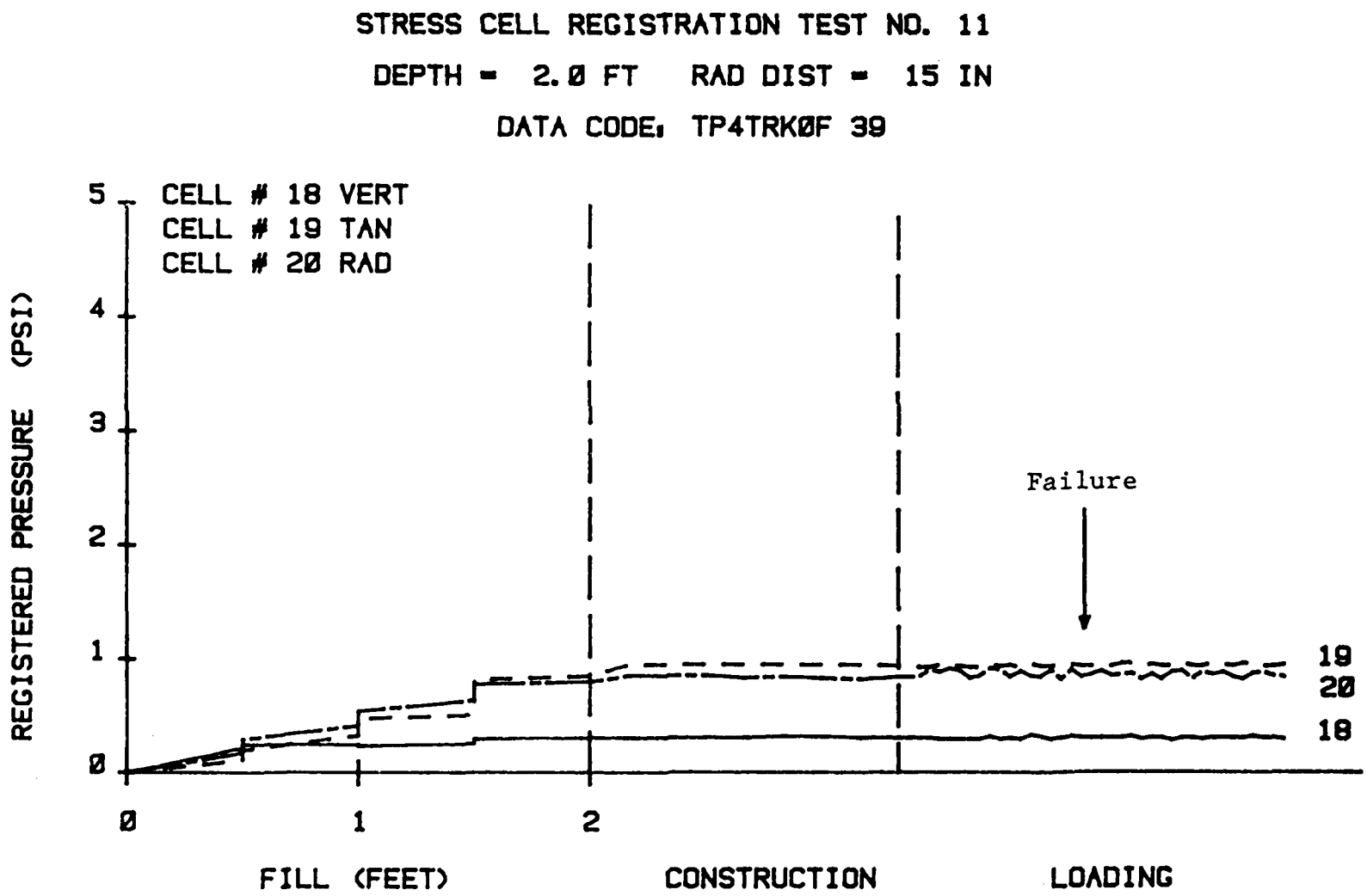

Figure E.14 Stress Cell Response During Pullout Test.

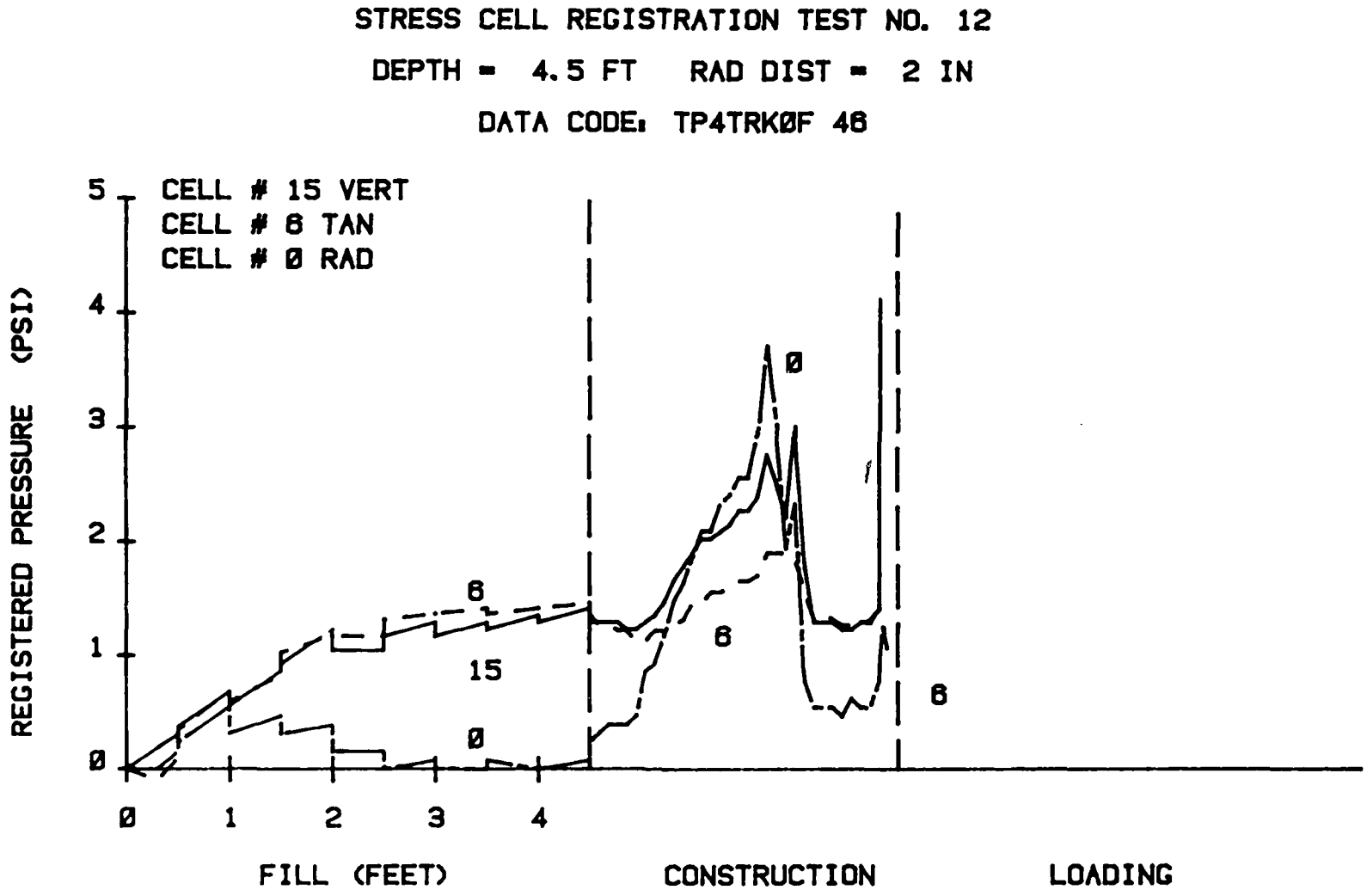

Figure E.15 Stress Cell Response During Pullout Test.

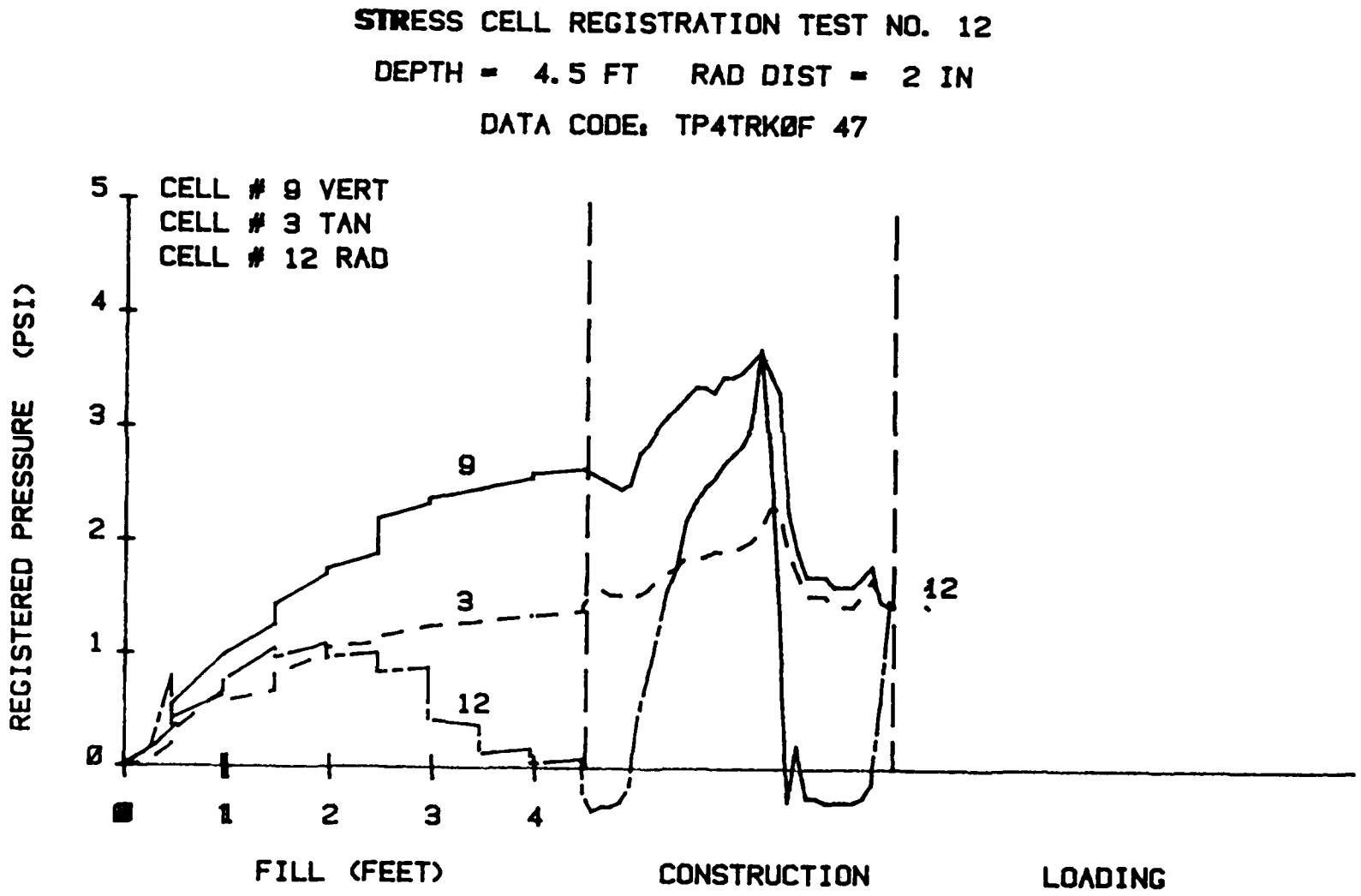

Figure E.16 Stress Cell Response During Pullout Test.

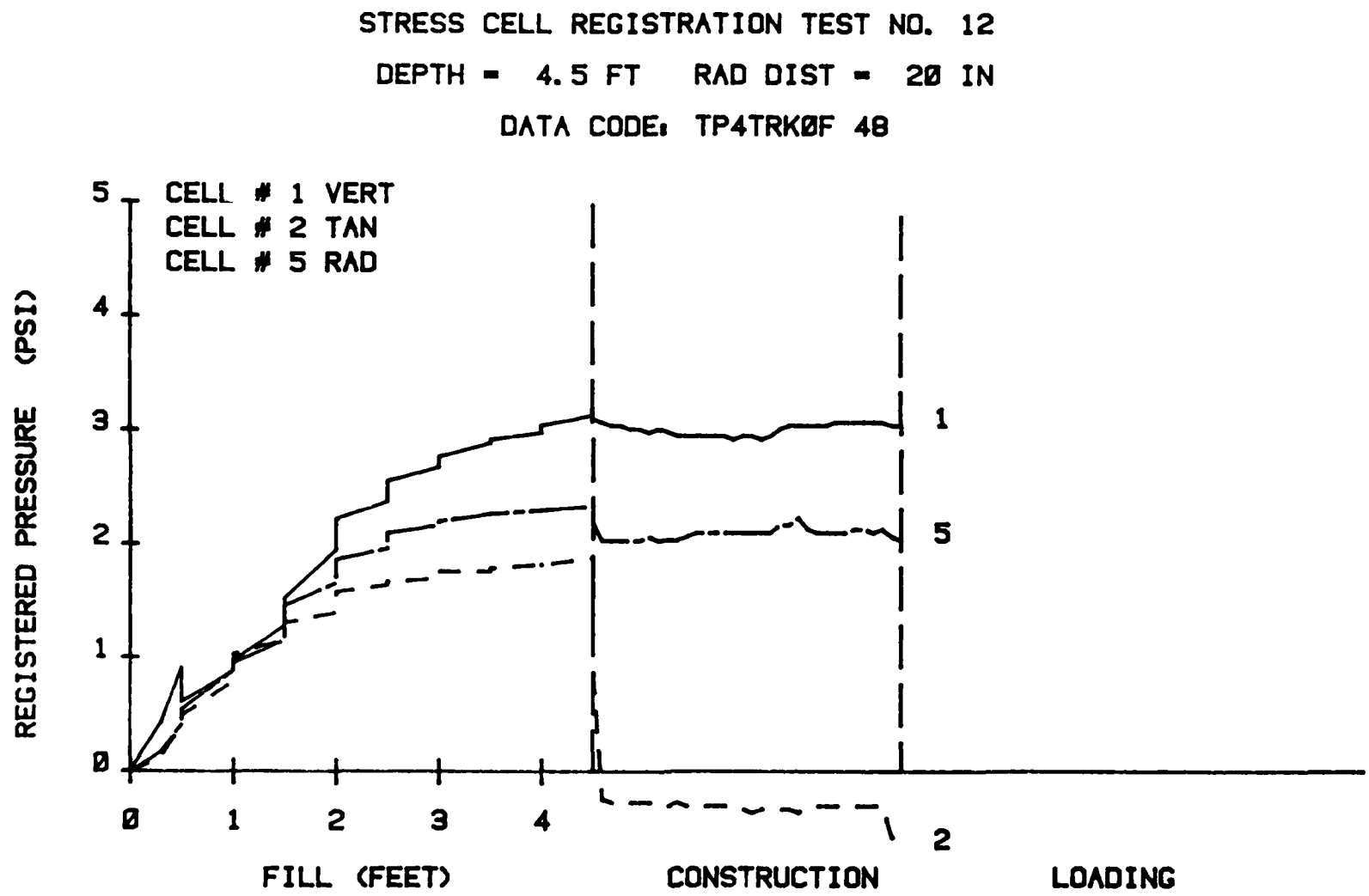

Figure E.17 Stress Cell Response During Pullout Test.

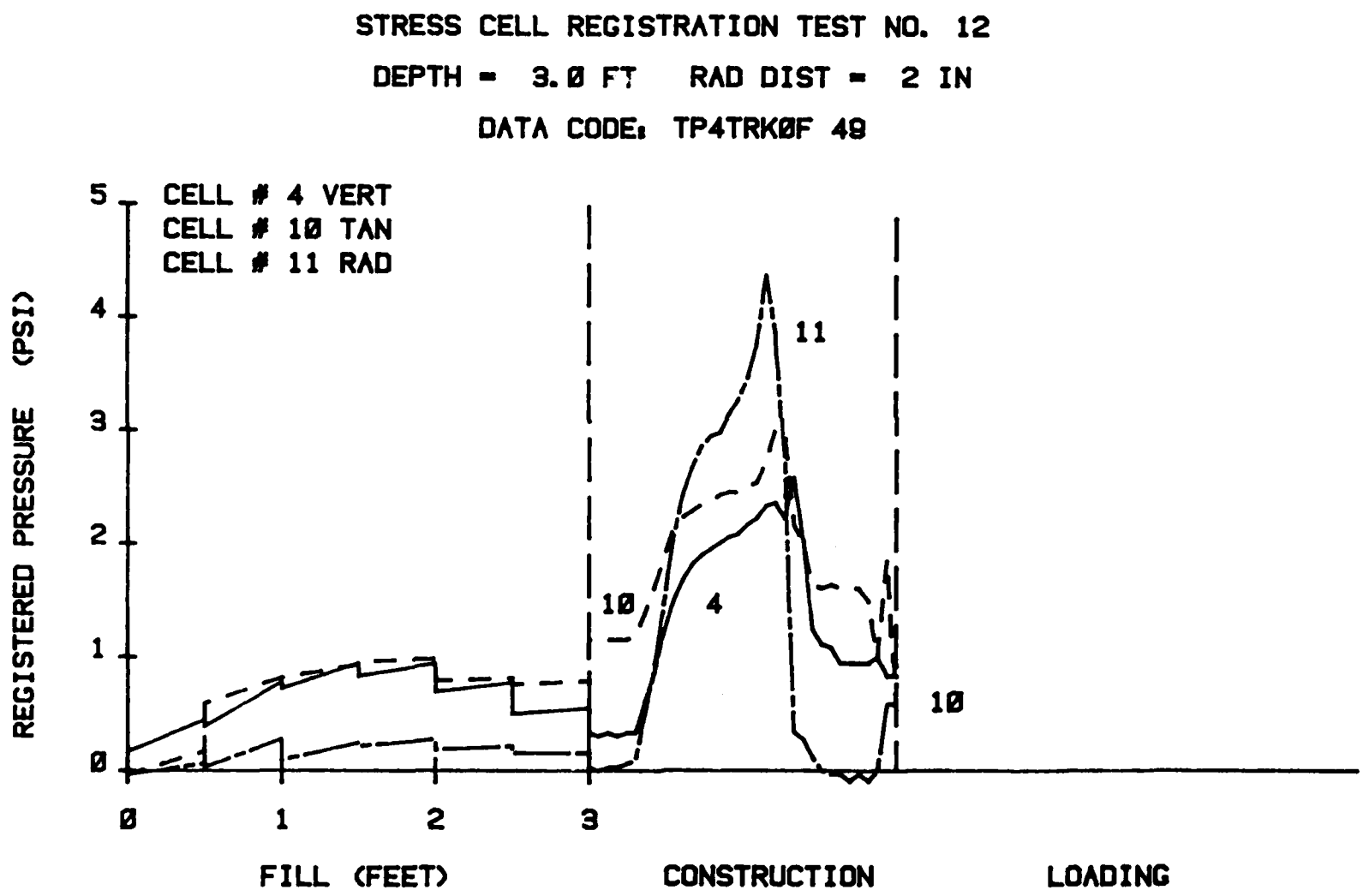

Figure E.18 Stress Cell Response During Pullout Test.

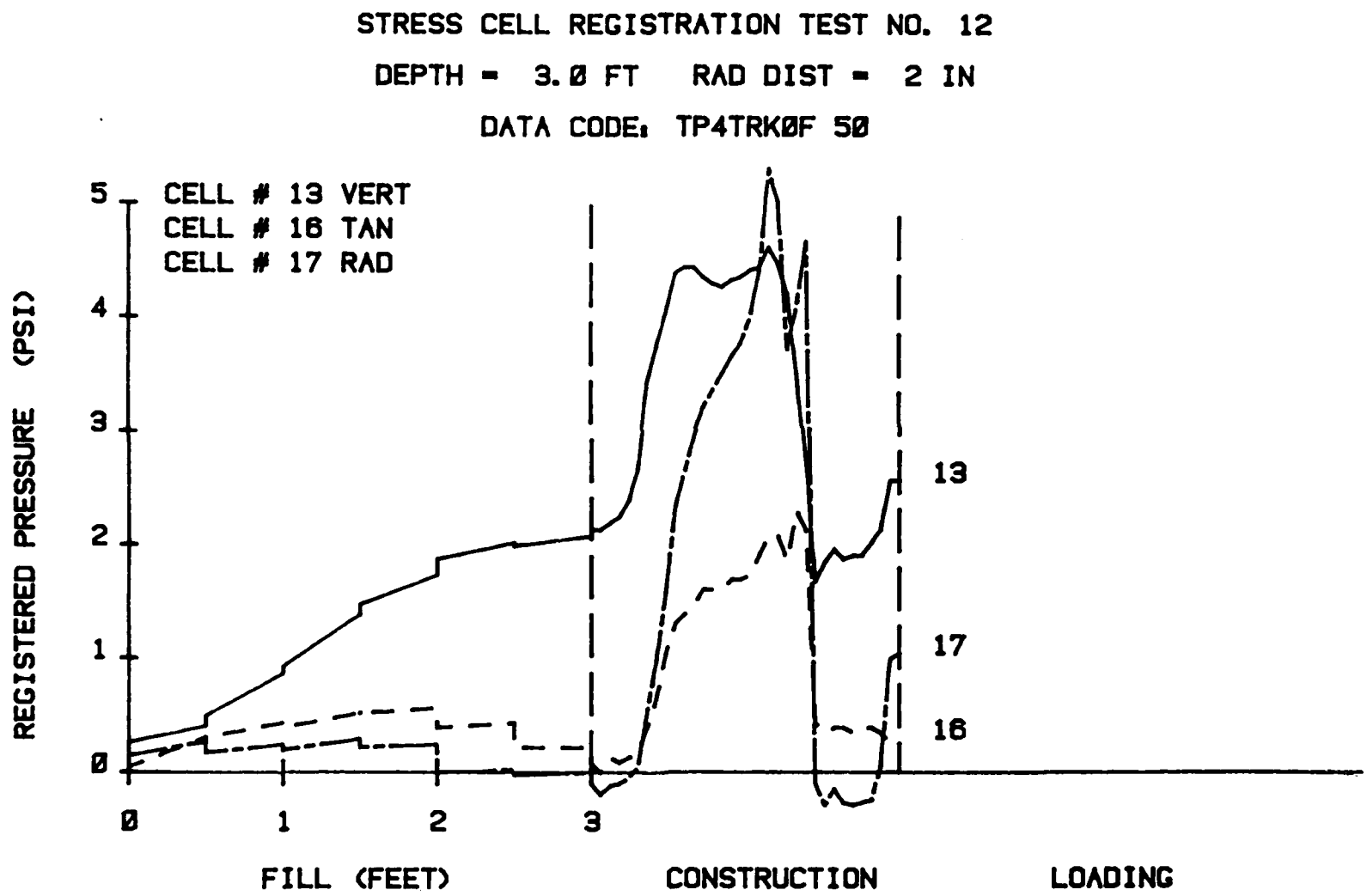

Figure E.19 Stress Cell Response During Pullout Test.

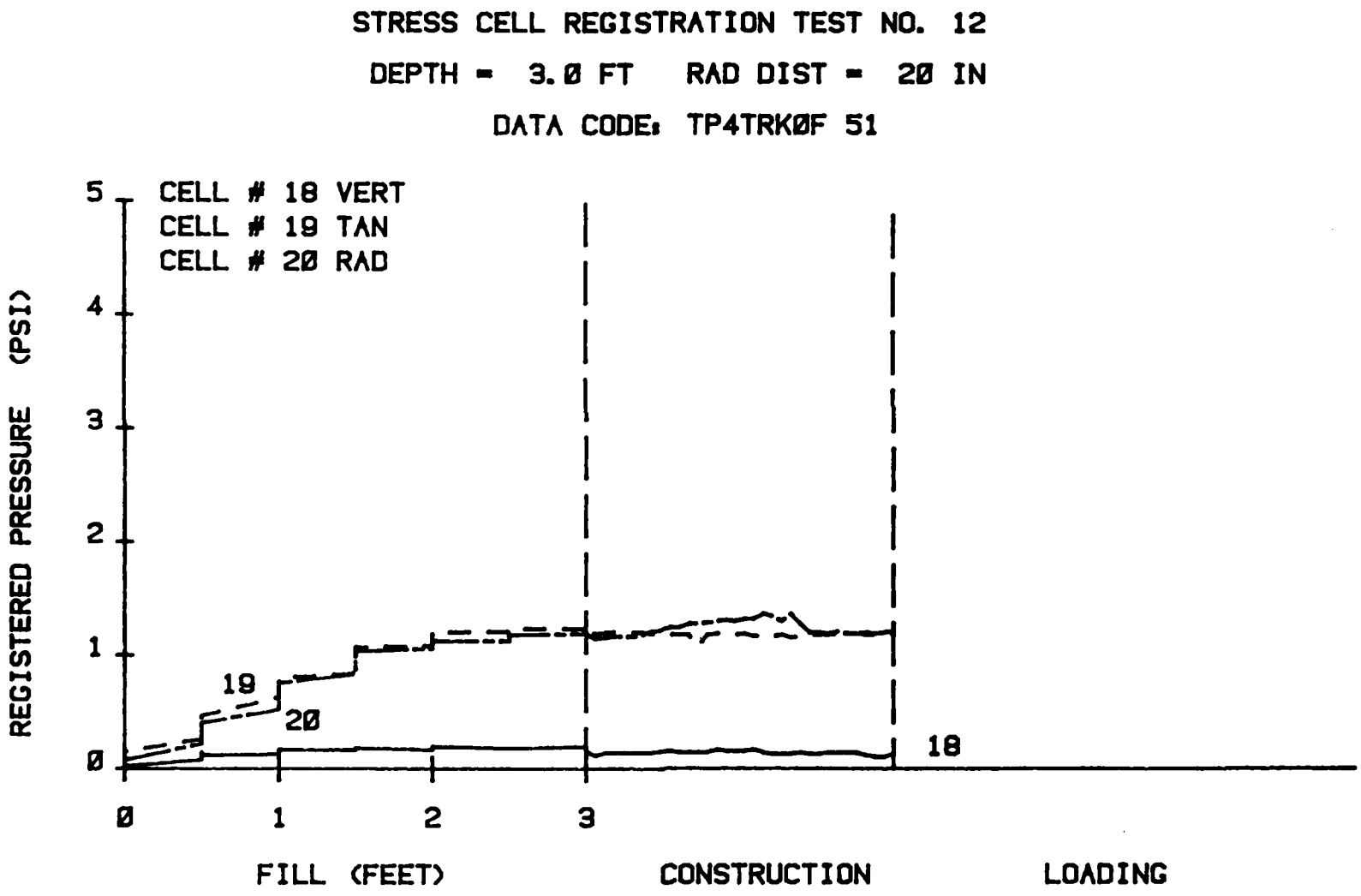

Figure E.20 Stress Cell Response During Pullout Test.

APPENDIX F

MEASUREMENT OF THE VARIATION IN UNIT WEIGHT BY FREEZING

If there is a measurable variation in unit weight of the soil near a stress cell, the effects of pocket action could be evaluated. Should the soil surrounding the stress cell, immediately over the diaphragm, have a lower unit weight than the rest of the soil mass then the cell should underregister. If the soil immediately around the stress cell had a higher unit weight, then the cell should over-register. Although there is no reason to believe that there should be a significant variation in unit weight of the soil around a stress cell in samples prepared by pluviation or vibration, a variation might exist because of compaction of the soil in lifts. The effects of the stress cell on the unit weight of soil placed by any of these techniques is unknown.

In an effort to measure the variation in unit weight of sand around the stress cell, a partially saturated sample was frozen and dissected. The sampling of cohesionless soil by freezing is a relatively new method and is not fully developed. Walberg (1978) reports on his tests on sand that "No significant effect from freezing on . . . specimen density . . . could be established for the sands tested." Marcuson and Franklin (1979), Mitchell, Guzikowski and Villet (1978) and Yoshini, Hatamaka and Hiroshi (1978) all

report success with sampling and testing of cohesionless soils by freezing.

An air dried sample was prepared in a six inch diameter, eight inch high (152.4 by 203.2 mm) California Bearing Ratio mold by compaction in lifts very similar to the method used in the soil calibration tests of the stress cell. The unit weight of the dry sample was determined by weighing the mold before and after filling with soil and dividing by the mold volume. This gross unit weight was used as the overall average for comparison with other unit weight measurements. The sample was saturated by placing the mold slowly in a tub of water and allowing the water to saturate the sample through the bottom porous stone until the top of the sample appeared wet. The sample was then removed from the water, covered loosely and allowed to drain vertically for twenty four hours. The sample was frozen by placing it in a freezer at -10°C. No measurable deformation occurred at the surface of the sample because of freezing. Saturated samples may be frozen without affecting the density or structure of the soil if they are frozen in one direction only or frozen quickly enough to prevent formation of ice lenses (Mitchell, Guzikowski and Villet, 1978). No ice lenses were discovered in any of the samples prepared for this study.

The frozen soil was removed from the steel mold by running water over the mold to thaw quickly a thin layer of

soil nearest the mold. The cylinder of frozen soil was then removed from the mold and brushed lightly to remove any loose soil and returned to the freezer. When the sample was again chilled, it was sliced into discs approximately one half inch (12.5 mm) thick on a band saw. The frozen sample was handled only with gloved hands to reduce thawing from body heat and was returned to the freezer between each step to keep it frozen. The thin discs of frozen soil were either broken by hand or cut on the band saw into smaller pieces. Neither the ends of the cylindrical sample or the outermost edges of any disc were used for the unit weight measurements. The volume of each small piece was determined by a method similar to that recommmended for the shrinkage limit test by Lambe (1951). The frozen piece of soil was submerged into a full bowl of mercury, chilled to -10°C to prevent the sample from thawing. The displaced mercury was collected in a second bowl and weighed to determine the volume. The still frozen piece of soil was removed from the mercury and placed into a tare for oven drying. The dry weight of the soil divided by the volume of displaced mercury gave the dry unit weight of the soil.

It was hoped that this procedure would allow any variation in the soil unit weight around the stress cell to be measured. However there was a large systematic error and an unacceptably large random error in the unit weight measurements as shown in Table F.1. The large systematic

TEST #	1	2	3
Gross Unit Weight (pcf)	113.2	119.1	115.0
Number of Measurements	21	21	20
Average Unit Weight (pcf)	102.0	103.6	102.5
Minimum Unit Weight (pcf)	92.0	95.3	93.6
Maximum Unit Weight (pcf)	107.5	108.0	108.1
Standard Deviation (pcf)	4.1	2.3	2.6

Note: 1 pcf = 16.01 kg/m^3

Table F.1 Unit Weight of Filter Sand Determined From Frozen Samples.

error is shown by the difference between the gross unit weight and the average unit weight. This systematic error is believed to be caused by disturbance of the dense sand along the saw cuts. The sample preparation resulted in a thawing and loosening of the sand grains nearest the saw cut. With small samples necessary to measure the unit weight variations across a 1.75 inch (44.5 mm) diameter stress cell, the specific surface increases with decreasing sample size and a large systematic error is produced. A much smaller error would be produced on larger samples or on finer grained soil, neither of which was possible for this application on filter sand. The sample preparation could also be improved by using a diamond cutting saw and using the saw in a walk-in freezer maintained at -5°C as recommended by Baker (1976).

The random error could be from the variation in sample size, 2500 to 8500 mm^3, and therefore variation in the specific surface as mentioned earlier or from differences in thawing effects between individual pieces, sample preparation technique, or actual variation of the unit weight of the soil. Since the factors could not be sorted out and the random error was quite large as shown in Table F.1, the measurement of the variation in unit weight around a stress cell was considered unsatisfactory. Improved sample preparation techniques and facilities could significantly improve the results of unit weight determination by freezing and could be a suitable topic for further research.

END

FILMED

5-83

DTIC